Chapter 5

Vacuum UV radiation-driven processes

Tünde Alapi, Krisztina Schrantz, Eszter Arany and Zsuzsanna Kozmér

5.1 FUNDAMENTAL PRINCIPLES OF VACUUM UV PROCESSES

Vacuum ultraviolet (VUV) photolysis is one of the Advanced Oxidation Processes (AOPs) for the elimination of pollutants from water and air. The ultraviolet (UV) radiation below 200 nm was named VUV in 1893 by the German physicist Victor Schumann, because it is strongly absorbed by air. The electromagnetic spectrum of UV radiation is defined most broadly as 10–400 nm and is subdivided into a number of spectral ranges (http://spacewx.com/solar_spectrum.html). The VUV radiation covers the spectral range from 100 to 200 nm. The photochemistry in the VUV spectral domain focuses on the region between 140–200 nm.

5.1.1 VUV radiation sources for water treatment

In photo-initiated AOP applications, such as VUV photolysis, the lamp type determines the process effectiveness. There are two types of light sources commonly used in VUV photolysis: the low-pressure mercury vapor (LP) lamps and the excimer lamps.

The spectral radiation from low-pressure mercury plasma (wherein the optimum pressure of mercury is approximately 1 Pa) is dominated by the two Hg resonance lines at 253.7 nm and 184.9 nm. The 253.7 nm line represents 85% of the total emitted UV intensity. The intensity of 184.9 nm line relative to 253.7 nm radiation (quoted as 100%) decreases to 8% through the quartz sleeve for a conventional LP lamp (Masschelein, 2002) (Figure 5.1). These lamps are often called "ozone (O_3) producing UV lamps" *via* absorption of 184.9 nm radiation by O_2. The photo-initiated decomposition of the generated O_3 takes place ($\varepsilon_{O_3,\,254\,nm} = 2952\ M^{-1}\ cm^{-1}$, $\Phi_{230-280\,nm}$ ($^{\bullet}O^{\bullet}$) = 1.0 (Atkinson *et al.* 2004)) simultaneously.

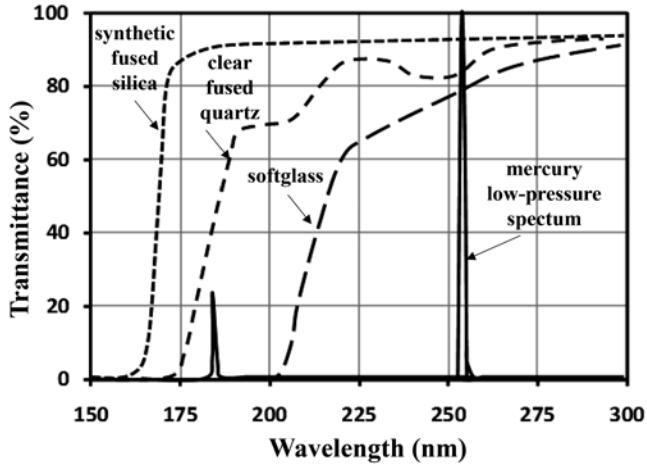

Figure 5.1 Transmittance of different quartz glass types and relative spectral emittance from a low-pressure mercury lamp. Reprinted with permission from Schalk *et al.* (2005).

The optimum operating temperature of these lamps is 40 °C. Lower temperatures result in partial condensation of mercury vapors on the lamp envelope. At temperatures above 40 °C, the self-absorption by the mercury vapors increases. Therefore, the UV output of the lamp is temperature-dependent. The lineal power density (electrical power per unit arc length) is typically between 0.3 and 0.6 W cm^{-1} and the total UV output is in the 0.2 to 0.3 W(UV) cm^{-1} range, which means that the UV efficiency (the ratio of UV output to the electrical input) is between 25% and 35%. The energy losses are mainly in the form of heat (Masschelein, 2002; Schalk *et al.* 2005).

Typically, the LP amalgam lamps use the mercury/indium amalgam, which reaches the optimum mercury vapor pressure at wall temperatures close to 100 °C. Thus, a higher fraction of electrical power is used, and their UV output is less dependent on the ambient temperature (Van der Pol & Krijnen, 2005).

LP lamps require warm-up time in order to reach 90% of their full UV output after the start-up. The solarization of lamp quartz envelope results in loss of transmission at 184.9 nm, which could be as much as 50% after 700 h (Masschelein, 2002). Another reason for the aging is the UV absorbing mercury oxide layer which forms on the inner wall surface of the lamp. This layer stems from a reaction of mercury ions with O_2 in the quartz glass, resulting in a decline of UV output over the long course of operation. Al_2O_3-based protective coatings are commonly used to diminish this effect and to extend the lamp lifetime up to 16000 h (Voronov *et al.* 2003). By combining the high transmittance quartz material, the amalgam lamp, and the long life technology, an optimized lamp with high specific output at 184.9 nm can be achieved.

The LP lamps are available in both "O_3-free" and "O_3 producing" versions depending on the quartz quality of lamp envelope. Ordinary quartz, which is produced by fusing natural quartz, has low transmittance below 200 nm and contains metallic impurities such as Al and Ti. Synthetic fused silica can be made from Si-rich chemical precursor, usually through a continuous process which involves flame oxidation of volatile Si compounds to SiO_2 and thermal fusion of the resulting dust. The transmittance of natural fused quartz is only ~50% at 184.9 nm as compared to ~90% transmittance of synthetic fused silica (Schalk *et al.* 2005; Witzke, 2001) (Figure 5.1).

LP lamps are usually cylindrical, but flat lamp technology is also marketed by Hereaus. These light sources are readily available at comparatively low cost, and their emission spectra are well established and

quantified. Several light source manufacturers produce and distribute a large variety of "O_3 producing" or VUV/UV LP lamps; e.g., SEN, Japan (http://www.senlights.com/), Jelight, USA (http://www.jelight.com/), LightTech, USA (http://www.light-sources.com/).

LP lamps are used worldwide to disinfect, sanitize, and oxidize water, as well as to reduce total organic carbon (TOC) and chlorine/chloramines in water for specific applications. The combination of 184.9 nm and 253.7 nm radiation is necessary for photooxidation of organic compounds and simultaneous sterilization of water. The LP lamps with high purity silica sleeves are used in O_3 generators (http://www.jelight.com/ozone-generator.html). The same lamps are used in the UVOX system (http://www.uvox.com/en/choice-of-right-uvox-system.html), which combines the disinfecting effect of UV light with the oxidizing effect of O_3 and hydroxyl radicals (HO•) in one single system for water treatment. Besides water treatment and disinfection, the VUV/UV LP lamps are used in several other applications, e.g., surface cleaning and modification, photo chemical vapor deposition, ionization, deletion of IC memory, light source of measuring instruments, etc.

Excimer and exciplex light sources based on the formation of noble gas and halogen excimers, or rare gas/halogen exciplex represent a relatively novel lamp generation. They have been developed in the last few decades and became the most important incoherent sources, which can operate over a wide range of wavelengths both in the UV and the VUV spectral regions (Figure 5.2). Their operation is based on the formation of excited dimers.

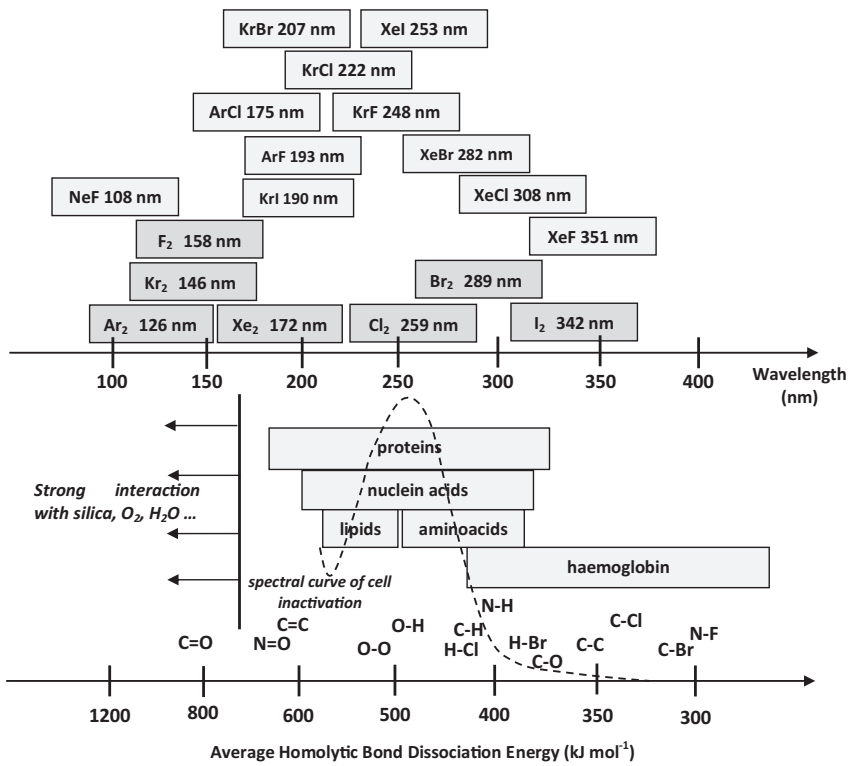

Figure 5.2 Emission wavelengths of common excimer and noble gas/halogen exciplex lamps, absorption bands of biological molecules, microbial pathogen inactivation spectral range, and chemical bond dissociation energies.

The term excimer (excited state dimer) is, strictly speaking, limited to cases in which both components of the dimer are the same atom or molecule. The term exciplex refers to the heterodimeric case; however, common usage expands excimer to cover exciplex. The spectrum of rare gas and halogen gas excimer lamp radiation is characterized by an intense narrow emission band (Eliasson & Kogelschatz, 1988; Gellert & Kogelschatz, 1991; Oppenländer, 2003), therefore these lamps are usually called "*quasi*-monochromatic light sources". The half-width of the spectral emission bands of these light sources depends mainly on the type of gas and excitation conditions.

A noble gas excimer VUV source based on electron beam excitation was first described by Wieser *et al.* (1997). Recently, several types of excimer lamps are built using various types of excitation (Kitamura *et al.* 2004; Lomaev *et al.* 2006b; Sosnin *et al.* 2002; Sosnin *et al.* 2011b), among which the capacitive-discharge (CD) and dielectric-barrier discharge (DBD) are the most attractive ones. Information on excimer lamp technology and potential use of excimers in large scale industrial applications are extensively covered in the literature (Kogelschatz, 1990, 2003, 2012; Kogelschatz *et al.* 2000; Kogelschatz *et al.* 1997; Lomaev *et al.* 2003; Lomaev *et al.* 2006b; Sosnin *et al.* 2006).

In general, the fixed geometry of most of the available lamps limits the flexibility in the reactor design. However, the novel incoherent excimer sources present the advantage that their design is independent of the electrode configuration (Kogelschatz, 1990, 2003; Oppenländer & Sosnin, 2005). Several publications are available on the detailed optimization of working parameters (optimal pressure, gas composition, excitation method and various parameters, e.g., voltage pulse shape, excitation pulse repetition rate and power supplies) (Kogelschatz, 1990, 2004; Kogelschatz *et al.* 2000; Lomaev *et al.* 2003; Lomaev *et al.* 2012; Lomaev *et al.* 2006b; Oppenländer, 2007; Oppenländer & Sosnin, 2005; Oppenländer *et al.* 2005; Sosnin *et al.* 2006; Tarasenko *et al.* 1999).

Xenon excimer (Xe_2*) lamps are the most studied VUV light sources and are widely used in research related to water purification. In order to generate excimer molecules, high energy electrons are required to generate excited state noble gas atoms. Noble gases can be exposed to extremely high electrical power densities, when energized electrons collide with noble gas atoms, and as a result, ionized species and excited states are formed. The short-lived (ns) excimer molecule (e.g., Xe_2*) is formed in a three-body reaction involving the excited state of rare gas atom (e.g., Xe*), and atoms in the ground state (e.g., Xe), where the third collision partner takes away the energy excess of the excimer. The photons are emitted from the excited dimer (excimer) with the formation of two noble gas atoms in the ground state (Figure 5.3). Since the excimer molecule structure is different from that of noble gas atoms and there is no excimer ground state, there is no self-absorption of the emitted radiation. The energy excess dissipated by ions is lost energy as that is not sufficient to generate excimers (Zvereva & Gerasimov, 2001). The Xe_2* decays with emission of radiation peaking at 172 nm, with the half-width of the spectral emission band of 14 nm (Braslavsky, 2007). About 70–80% of the radiation power of an excimer lamp is concentrated in this single emission band (Eliasson & Kogelschatz, 1991).

Theoretically, under optimal conditions 80% of the discharge power can be converted to VUV radiation of Xe_2* (Kogelschatz, 2003, 2012). In practice, the typical radiant power efficiency of Xe_2* lamps is about 40% (Avdeev *et al.* 2008; Gerasimov *et al.* 2006; Lomaev *et al.* 2003; Lomaev *et al.* 2006a; Lomaev *et al.* 2012; Lomaev *et al.* 2006b; Tarasenko *et al.* 1999; Zhang & Boyd, 2000). Pulsed Xe_2* lamps may have up to 40% efficiency (Carman & Mildren, 2003). Beleznai *et al.* (2008) performed theoretical and experimental studies on a dielectric barrier Xe discharge lamp and achieved an overall VUV output efficiency of 66.8%, of which 47.2% was at 172 nm. The other emitted radiation were at 147 nm (2.4%) and 150 nm (17.2%). In addition to the Xe_2* lamps, Lomaev *et al.* (2006b) investigated the windowless Kr_2* and Xe_2* excimer lamps, and reported radiation efficiencies of 25% for Kr_2* (146 nm) and 45% for Xe_2* (172 nm), respectively. Ar_2* lamps were also investigated by Elsner *et al.* (2006) and Baricholo *et al.* (2011).

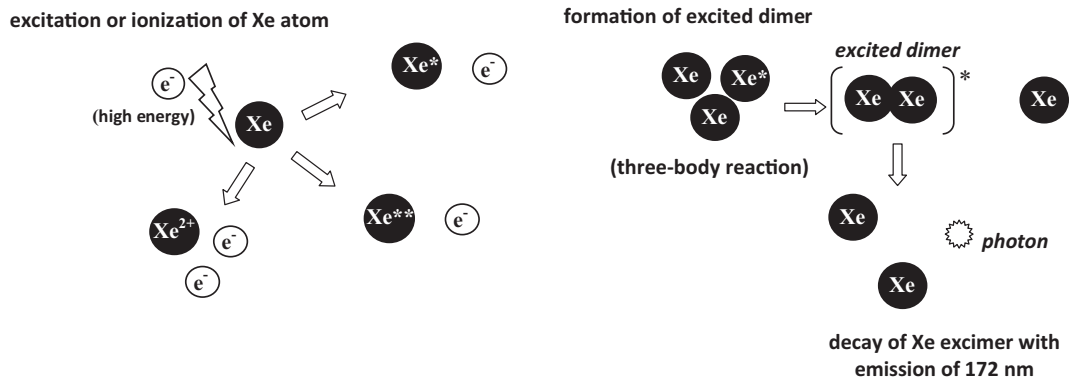

Figure 5.3 Main processes for the formation and decay of Xe_2*.

The average output power density of excimer lamps usually does not exceed 50 mW cm^{-2}. The excitation power and the radiation power density can be enhanced by using two-barrier excilamps (Erofeev *et al.* 2010; Lomaev *et al.* 2008). The average radiation power densities for one- and two-barrier excilamps were found to be 20–30 and ~40 mW cm^{-2}, respectively (Lomaev *et al.* 2008). A high-power sealed-off DBD Xe_2* lamp having output power density of 120 mW cm^{-2} was designed, constructed, and tested by Lomaev *et al.* (2003).

Volkova and Gerasimov (1997) and Gerasimov *et al.* (2000, 2002) studied the emission spectra of a mixture of Kr and Xe and showed that small additions of Xe led to excitation and simultaneous deactivation of molecules of the basic Kr gas. The redistribution of emission energy was accompanied by a nonlinear amplification of radiation near 147 nm. Further investigations were made with binary Xe–X and Kr–Y mixtures (X is He, Ne, Ar, or Kr; Y is He, Ne, or Ar). The emission bands investigated are related to electronic transitions in heteronuclear dimers (Gerasimov *et al.* 2003).

The extremely narrow radiation line at 121.6 nm is due to the transition of a H atom (Lyman-line) and can be obtained in He or Ne gas with traces (less than 0.1%) of H_2 with an energy efficiency of about 10% (Yan *et al.* 2002; Yan & Gupta, 2003). The spectrum, optical power, stability and efficiency of this light source were also investigated in Yan *et al.*'s works. Traces of water (0.02%) in Ar-filled lamp led to an efficient and selective excitation of the O—H band. Shuaibov *et al.* (2012) investigated the energy transfer from Ar to H_2O. The emission maxima are at 297.6 and 308.9 nm in the UV region, and at 156.0, 180.3, and 186.0 nm in the VUV region.

A wide variety of both excimer and exciplex lamps are available (Figure 5.2). Noble gas- and halogen excimer lamps (Avdeev *et al.* 2008) and noble gas/halogen exciplex lamps were also extensively investigated (Kogelschatz, 2012; Lomaev *et al.* 2012; Lomaev *et al.* 2007; Tarasenko *et al.* 1999). Among all, the most commonly investigated are KrCl* (Erofeev *et al.* 2010; Shuaibov *et al.* 2013; Sosnin *et al.* 2011a; Sosnin *et al.* 2015a; Sosnin *et al.* 2015b; Zhuang *et al.* 2010), XeCl* (Avtaeva *et al.* 2013; Baadj *et al.* 2013), and XeBr* (Lomaev *et al.* 2012) lamps with emission at 222, 308, and 282 nm, respectively. Typically, 5–18% of radiant efficiency is reached. KrCl* is formed in Kr gas in the presence of 1% chlorine donor ($C1_2$, HC1 or CCl_4 (Shuaibov *et al.* 2013)). Zhuang *et al.* (2010) investigated the effect of gas composition and pressure, and the maximum efficiency of the 222 nm radiation was found to be 9.2% for a KrCl* filled with Kr (198 mbar) and Cl_2 (2 mbar). Other excimer light sources have been investigated in laboratory studies, e.g., excimers radiating in the visible range,

multi-wavelength excimer sources, etc. Internal phosphor coatings were used to convert the 172 nm radiation of the Xe_2* to near UV or visible one (Beleznai *et al.* 2006; Beleznai *et al.* 2008; Malinin, 2006). This is the basis of mercury-free fluorescent lamps and of flat plasma-display panels with a large screen.

Zhang and Boyd (2000) compared the lifetime of 172, 222, and 308 nm excimer lamps, as well as the overall efficiency, stability and output fluctuations. The Xe_2* lamp caused the formation of "color centers" in the Suprasil quartz, which reduced the intensity transmitted through quartz by 22% during the first 60 hours of operation. In contrast, 100% of the original UV intensity output through the quartz of the 222 and 308 nm lamps was still maintained after up to 4000 h operating time. The fluctuation of the average radiation power of these air-cooled excimer lamps were found to be only 2–5% (Lomaev *et al.* 2003; Zhang & Boyd, 2000).

Efficient lamp operation requires an envelope material with a high transmittance in the VUV spectral range and resistance to high energy radiation. The photo-induced generation of "color centers" in quartz glass is due to various defects. Extrinsic defects are mainly trace impurities. Intrinsic defects are always generated as a result of thermal effect during the production process and are present as equilibrium or frozen-in defects. These are network imperfections, such as two-fold and three-fold coordinated Si atoms, Si to Si bonds, O deficiency centers, non-bridging O atoms, interstitial O atoms and interstitial O_2. Additionally, there are technology-related defects. For example, in quartz glass fused in an atmosphere containing H_2, the typical defects are hydride (SiH), hydroxyl (OH) and free hydrogen. These defects are also present in synthetic fused silica. Other technology-related defects are halogen atoms, e.g., Cl and F, which are often used for OH removal in order to produce dry synthetic fused silica. In dry fused silica, Si—Cl or Si—F bonds, as well as interstitial Cl and F, may be present. Schreiber *et al.* (2005) investigated the colorization and radiation resistance of quartz glass for VUV lamps. Synthetic fused silica containing 250 ppm OH and quartz glass fused from cultured crystals were identified as the best materials for 172 nm VUV applications.

The short wavelength of Ar_2* radiation (126 nm) requires special windows (e.g., CaF_2, MgF_2, LiF) which are expensive and available only in small sizes. To circumvent this problem, open discharge configurations, called as "windowless excimer lamps" were designed by Kogelschatz (1992). An open windowless excilamp capable of operating on Ar_2* (126 nm), Kr_2* (146 nm), and Xe_2* (172 nm) was described by Lomaev *et al.* (2006a).

There are several benefits of excimer lamps, such as high average specific power of either VUV or UV radiation, high energy of emitting photons, quasi-monochromatic radiation, high spectral power density, absence of visible and IR radiation, low heating of radiating surface (cold lamps), no fixed geometry, no warm up time, etc. The availability of multiple-wavelength UV radiation by simultaneous excitation of several kinds of working excimer molecules is also possible. Finally, excimer lamps based on noble gases are non-hazardous and are much more environmentally friendly than mercury vapor lamps.

As shown in Figure 5.2, the VUV radiation can break most of the chemical bonds. VUV excimer lamps emit at short wavelengths, and their high energy radiation is generally used for large scale surface modifications, including low-temperature oxidation, deposition of metal patterns on heat sensitive substrates, photochemical polymerization and cleaning (dry cleaning). Ar_2* lamps are mainly used in photolithography. These VUV excimer lamps also have great potential as light or ionization sources in analytical instrumentation. Xe-based fluorescent excimer lamps used as mercury-free image processing lamps in scanners and in copy machines are manufactured by different companies, such as Ushio and Osram (Kogelschatz, 2012). VUV and UV excimer lamps are an alternative to conventional light sources used for UV disinfection, as the spectral curve of cell inactivation shows in the Figure 5.2. Excimer

lamps have great potential in medical research and applications, e.g., phototherapy (psoriasis), wavelength-selective drug phototoxicity testing (Oppenländer, 1994, 1996). Detailed information on excimer lamps and their applications can be found in the published literature (Kogelschatz, 2012; Lomaev *et al.* 2012; Oppenländer & Schwarzwälder, 2002; Oppenländer & Sosnin, 2005; Sosnin *et al.* 2006).

A wide variety of excimer (Ar_2*, Kr_2* and Xe_2*) and exciplex (KrCl*, XeCl*, XeBr*) lamps are already commercially available. Osram (http://www.osram.com/osram_com/), Ushio (http://www.ushio.com/) and Hamamatsu (http://www.hamamatsu.com/) are the major manufacturers. The mostly applied light source at lab-scale is the XERADEX Xe_2* lamp from Osram. This light source does not require cooling in normal operation, has no startup time, the switching cycle is unlimited and the estimated lifetime is 2500 h. The VUV output at 172 nm is 40 mW cm^{-2} and can be enhanced with active cooling to 80 mW cm^{-2}. The lamp wattage is 60–300 W and the nominal VUV efficiency at 172 nm is 40% (http://www.osram.com/osram_com/).

5.1.2 VUV irradiation of water

5.1.2.1 VUV photolysis of pure water

The VUV photolysis is mainly used and investigated for the elimination and mineralization of various pollutants in aqueous solutions. Organic and inorganic molecules or ions have relatively high absorption coefficients in the VUV region. However in aqueous solutions, the VUV radiation is absorbed almost exclusively by water when its concentration (55.5 mol L^{-1}) substantially exceeds those of the dissolved compounds. Figure 5.4 is a compilation of water absorption coefficients determined at 25 °C (Barrett & Baxendale, 1960; Barrett & Mansell, 1960; Halmann & Platzner, 1965; Kröckel & Schmidt, 2014; Querry *et al.* 1978; Segelstein, 1981; Weeks *et al.* 1963). The absorption coefficients and the photolysis quantum yield of water were found dependent on the radiation wavelength in the 140–200 nm region.

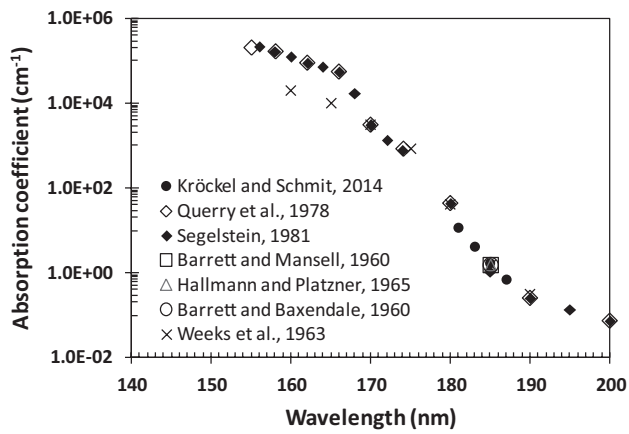

Figure 5.4 Absorption coefficients of pure water determined at 25°C.

The absorption coefficient of water at 184.9 nm was found to be 1.46–1.80 cm^{-1} (Barrett & Mansell, 1960; Halmann & Platzner, 1965; Kröckel & Schmidt, 2014; Weeks *et al.* 1963) at 25 °C. The latest value

reported by Kröckel and Schmidt (2014) was 1.62 cm^{-1}. In this work, a linear dependence of the absorption coefficient at 187 nm on the temperature (10 to 30 °C) was observed (e.g., 0.45 cm^{-1} at 10 °C to 0.67 cm^{-1} at 30 °C). The absorption coefficient of water at 172 nm is 550 cm^{-1}. Consequently, the penetration depth of VUV radiation through the water layer is within a few millimeters for 184.9 nm, or a fraction of a millimeter for 172 nm (Heit & Braun, 1996, 1997). Absorption of the VUV radiation results in the homolysis and photochemical ionization of water molecules (5.1 and 5.2).

$$H_2O + h\nu(<190\,\text{nm}) \rightarrow H^{\bullet} + HO^{\bullet} \tag{5.1}$$

$$H_2O + h\nu(<200\,\text{nm}) \rightarrow [e^-, H_2O^+] + H_2O \rightarrow [e^-, H_2O^+] + (H_2O) \rightarrow e_{aq}^- + HO^{\bullet} + H_3O^+ \tag{5.2}$$

As shown in Figure 5.5, the quantum yield of water homolysis is wavelength-dependent.

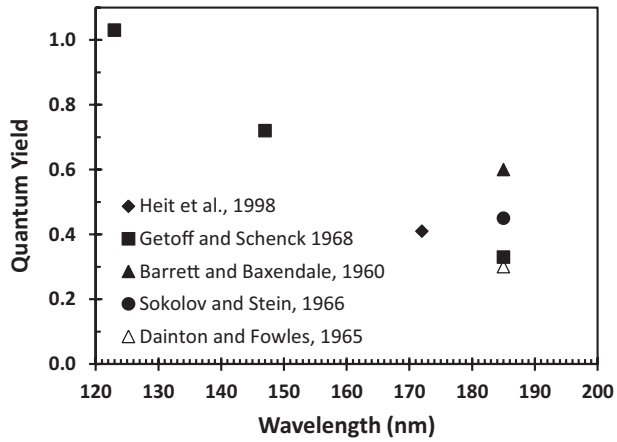

Figure 5.5 Quantum yield of pure water photolysis.

Table 5.1 compiles the literature data on water photolysis and the corresponding $HO^{\bullet}$, H atom ($H^{\bullet}$), and hydrated electron (e_{aq}^-) quantum yields at 172 and 184.9 nm. The threshold energy for the water homolysis is between 6.41 and 6.71 eV (Nikogosyan & Görner, 1992).

The VUV irradiation of water leads primarily to $H^{\bullet}$ and $HO^{\bullet}$. Since e_{aq}^- concentrations are very low, in general, the contribution of e_{aq}^- reactions to overall mechanisms in VUV systems is rather small. $\Phi(e_{aq}^-)$ depends slightly on pH and it was observed to increase in alkaline solutions of pH > 9 due to the contribution of the reaction of $H^{\bullet}$ with HO^- (5.3) (Gonzalez *et al.* 2004).

$$HO^- + H^{\bullet} \rightarrow H_2O + e_{aq}^- \tag{5.3}$$

Inversely, $\Phi(e_{aq}^-)$ decreases drastically in solutions of pH < 4, as e_{aq}^- is scavenged by H_3O^+ (5.4) (Gonzalez *et al.* 2004).

$$H^+ + e_{aq}^- \rightarrow H^{\bullet} \qquad k = 2.2 \times 10^{10}\ \text{L mol}^{-1}\ \text{s}^{-1}\ \text{(Gonzalez } et\ al.\ \text{2004)} \tag{5.4}$$

Table 5.1 Quantum yields of homolysis and ionization of water determined at 172 nm using Xe_2* lamp and 184.9 nm using LP lamp.

	Quantum Yield $H_2O + h\nu$(<190 nm) $\rightarrow H^\bullet + HO^\bullet$	**Quantum Yield $H_2O + h\nu$(<200 nm) $\rightarrow e_{aq}^- + HO^\bullet + H_3O^+$**	**Reference**
172 nm	0.42		Heit *et al.* (1998)
184.9 nm	0.33	0.045	Getoff and Schenck (1968)
	0.6		Barrett and Baxendale (1960)
	0.45		Sokolov and Stein (1966)
	0.3		Dainton and Fowles (1965)

Moreover, the reaction of e_{aq}^- with $HO^\bullet$ results in a much more stable HO^-, increasing the water pH (5.5).

$$e_{aq}^- + HO^\bullet \rightarrow HO^- \qquad k = 3\times10^{10}\ \text{L mol}^{-1}\ \text{s}^{-1}\ \text{(Gonzalez } \textit{et al.}\ \text{2004)} \tag{5.5}$$

In strong alkaline solution (pH > 12.7), the reaction of the conjugated base of $HO^\bullet$ ($O^{\bullet-}$) with dissolved O_2 (DO) yields significant amounts of ozonide radical anion ($O_3^{\bullet-}$) (5.6 and 5.7), which is a source of $HO^\bullet$ (reactions 5.8 and 5.9) (Gonzalez *et al.* 2004; Hayon & McGarvey, 1967; Martire & Gonzalez, 2001).

$$HO^\bullet + HO^- \rightarrow H_2O + O^{\bullet-} \qquad pK_a = 11.9\ \text{(Gonzalez } \textit{et al.}\ \text{2004)} \tag{5.6}$$

$$O^{\bullet-} + O_2 \rightarrow O_3^{\bullet-} \qquad k = 3.5\times10^{3}\ \text{L mol}^{-1}\ \text{s}^{-1}\ \text{(Gonzalez } \textit{et al.}\ \text{2004)} \tag{5.7}$$

$$O_3^{\bullet-} + H^+ \rightarrow H_2O + HO_3^\bullet \qquad pK_a = 8.2\ \text{(Gonzalez } \textit{et al.}\ \text{2004)} \tag{5.8}$$

$$HO_3^\bullet \rightarrow O_2 + HO^\bullet \tag{5.9}$$

The primary radicals ($H^\bullet$ and $HO^\bullet$) are formed in a solvent cage (Thomsen *et al.* 1999), where the recombination is favored (László *et al.* 1998). That explains the quantum yield lower than unity. $H^\bullet$ and $HO^\bullet$ that escape from the "cage" are able to initiate a series of diffusion controlled reactions. Their self-recombination can result in H_2O_2, H_2 and H_2O (5.10–5.12).

$$2HO^\bullet \rightarrow H_2O_2 \quad k = 4\times10^{9} - 2.0\times10^{10}\ \text{L mol}^{-1}\ \text{s}^{-1}\ \text{(Buxton } \textit{et al.}\ \text{1988; Gonzalez } \textit{et al.}\ \text{2004)} \tag{5.10}$$

$$2H^\bullet \rightarrow H_2 \quad k = 1.0\times10^{10}\ \text{L mol}^{-1}\ \text{s}^{-1}\ \text{(Buxton } \textit{et al.}\ \text{1988; Gonzalez } \textit{et al.}\ \text{2004)} \tag{5.11}$$

$$HO^\bullet + H^\bullet \rightarrow H_2O \quad k = 2.4\times10^{9}\ \text{L mol}^{-1}\ \text{s}^{-1}\ \text{(Buxton } \textit{et al.}\ \text{1988; Gonzalez } \textit{et al.}\ \text{2004)} \tag{5.12}$$

The DO changes the radical reactions. The reaction of O_2 with $H^\bullet$ (5.14) reduces greatly the probability of recombination of $H^\bullet$ and $HO^\bullet$, and as a consequence, the concentration of $HO^\bullet$ increases while the concentration of $H^\bullet$ is drastically reduced. László and Dombi (2002) studied the oxidizing and reducing properties of the $H^\bullet$ and $HO^\bullet$ in aqueous solutions of $[Fe(CN)_6]^{4-}$ and $[Fe(CN)_6]^{3-}$ exposed to 172 nm radiation. In O_2-free solutions, there was no significant difference between the rate of oxidation of $[Fe(CN)_6]^{4-}$ and reduction of $[Fe(CN)_6]^{3-}$. However, in the presence of DO, the rate of oxidation of $[Fe(CN)_6]^{4-}$ increased considerably and the rate of $[Fe(CN)_6]^{3-}$ reduction was significantly suppressed, probably because O_2 scavenges e_{aq}^- and $H^\bullet$ to yield $O_2^{\bullet-}$ and its conjugated acid $HO_2^\bullet$, respectively (5.13–5.15).

$$O_2 + e_{aq}^- \rightarrow O_2^{\bullet-} \qquad k = 2\times10^{10}\ \text{L mol}^{-1}\ \text{s}^{-1}\ \text{(Buxton } \textit{et al.}\ \text{1988; Gonzalez } \textit{et al.}\ \text{2004)} \tag{5.13}$$

$$H^\bullet + O_2 \rightarrow HO_2^\bullet \qquad k = 2.1\times10^{10}\ \text{L mol}^{-1}\ \text{s}^{-1}\ \text{(Buxton } \textit{et al.}\ \text{1988)} \tag{5.14}$$

$$HO_2^\bullet + H_2O \rightleftharpoons H_3O^+ + O_2^{\bullet-} \qquad pK_a = 4.8\ \text{(Bielski } \textit{et al.}\ \text{1985)} \tag{5.15}$$

In the presence of DO, H_2O_2 is mostly formed through the disproportionation reaction of $HO_2^\bullet$/$O_2^{\bullet-}$ (5.16).

$$O_2^{\bullet-} + HO_2^\bullet + H_2O \rightarrow O_2 + H_2O_2 + HO^- \qquad k = 9.7\times10^{7}\ \text{L mol}^{-1}\ \text{s}^{-1}\ \text{(Buxton } \textit{et al.}\ \text{1988)} \tag{5.16}$$

The rate constant of reaction 5.16 is pH-dependent (Bielski *et al.* 1985), with a maximum value at pH ≈ pK_a.

During the VUV photolysis of O_2-free pure water, negligible amount of H_2O_2 is formed. In the presence of DO, the H_2O_2 concentration increases, mostly through the disproportionation reaction 5.16. Organic compounds, such as oxalic acid, aromatic compounds, formic acid and methanol (Arany *et al.* 2012; Azrague *et al.* 2005; Imoberdorf & Mohseni, 2011; Robl *et al.* 2012) substantially increase the concentration of H_2O_2 in the presence of DO. The results reported by Azrague *et al.* (2005) show a steep increase of the concentration of H_2O_2, up to a maximum corresponding to approx. 25% conversion of oxalic acid. With diminishing the substrate concentration, the concentration of H_2O_2 decreased to the concentration determined in pure water. Imoberdorf and Mohseni (2011) used formic acid as the model compound, and showed that H_2O_2 concentration increased until approx. 75% conversion of the organic substrate was reached. Robl *et al.* (2012) confirmed the enhanced production of H_2O_2 in aqueous solutions of methanol. During the oxidative transformation of organic pollutants, the formation and accumulation of $HO_2^\bullet$ is possible through the reactions of organic peroxyl radicals. Consequently, the increase of H_2O_2 concentration observed in these studies (Alapi & Dombi, 2007; Azrague *et al.* 2005; Robl *et al.* 2012) is explained by the enhanced concentration of the $HO_2^\bullet$/$O_2^{\bullet-}$ formed during the oxidative degradation mechanisms of the organic compounds.

5.1.2.2 Heterogeneity of the VUV-irradiated aqueous solutions

The inhomogeneity of VUV-irradiated systems is mainly due to the low penetration depth of the VUV radiation. Water homolysis with the formation of primary reactive species ($HO^\bullet$, $H^\bullet$, e_{aq}^-) takes place within a thin liquid layer. The short-lived (<10 μs, (Hoigné, 1998)) primary radicals cannot diffuse far outside the irradiated volume, thus, all their bimolecular reactions take place within this photoreaction zone (Figure 5.6).

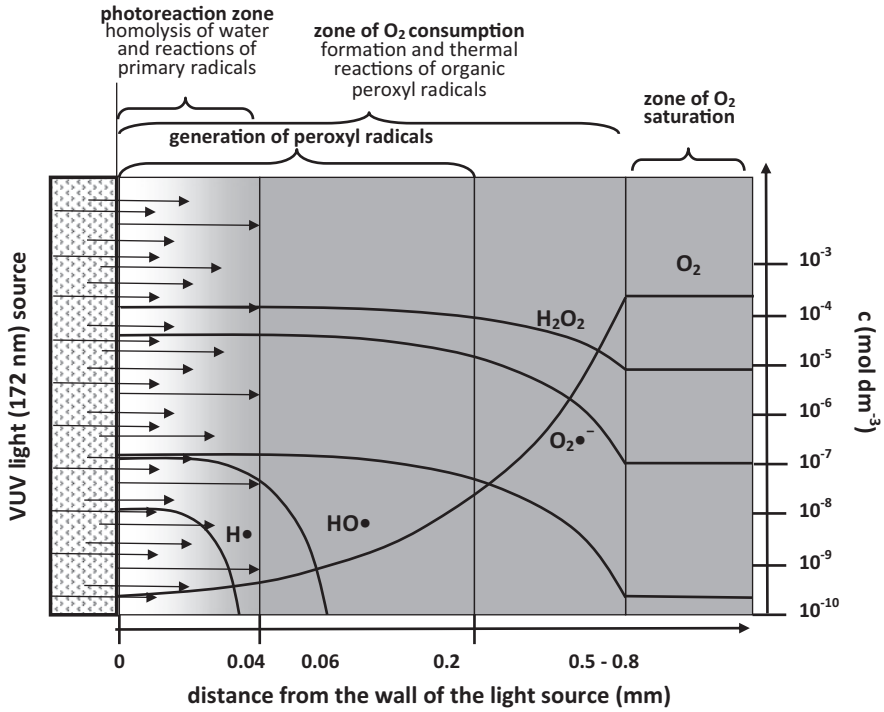

Figure 5.6 Heterogeneity of the VUV-irradiated aqueous solutions (the figure is based on data and figures presented by Heit and Braun (1996, 1997), László (2001), and Oppenländer (2003)).

In a solution containing DO, $H^{\bullet}$ and e_{aq}^{-} are trapped by DO, consequently the transformation of the organic substances is initiated mainly by the reactions with $HO^{\bullet}$. The formed carbon-centered radicals are also trapped by DO, which results in DO depletion in the photoreaction zone. The DO depletion was verified in a well-designed experiment by Heit and Braun (1996) where the DO concentration profile was determined as a function of the radial distance from the Xe_2* lamp surface. The results confirmed the existence of a thin (0.036 mm) photoreaction zone, which is characterized by diffusion controlled reactions of the short-lived primary radicals. The addition of DO to the $H^{\bullet}$ and carbon-centered radicals creates the zone of O_2 consumption, which is outside the irradiated zone. The degree of DO depletion depended on the concentration of the organic substrate and photon flux, and slightly depended on the flow rate of aqueous solution. Within the zone of O_2 consumption the reactions of peroxyl radicals dominate. In contrast to the short lived primary radicals, $HO_2^{\bullet}/O_2^{\bullet-}$ and organic peroxyl radicals have longer lifetimes, which allows their diffusion into the "dark" zone, up to a maximum distance of about 0.5 mm from the surface of the Xe_2* lamp.

The heterogeneity of VUV-irradiated solutions can be mitigated by using high flow rates which generate radial mixing and turbulent flow conditions (Dobrovic *et al.* 2007) enhancing the mass transfer to the photoreaction zone, thus increasing the oxidation and mineralization rates of contaminants. The combination of VUV photolysis and electrolysis with DO generation at the anode close to the irradiated zone enhanced the rate of oxidation and mineralization of benzoic acid (Wörner *et al.* 2003). Tasaki *et al.* (2009) investigated the effect of O_2 microbubbles both in UV (253.7 nm) and VUV/UV (184.9/253.7 nm)-irradiated solutions of methyl

orange. The rate of mineralization is controlled by the diffusion of DO from the non-irradiated bulk to the photoreaction zone. The use of ceramic gassing units or the injection of O_2 or air through a porous glass plate prevented the DO depletion in the VUV-irradiated zone (Han *et al.* 2004; Oppenländer *et al.* 2005).

5.2 KINETICS AND REACTION MODELING

5.2.1 Reactions and role of primary and secondary formed reactive species

In VUV-irradiated aqueous solutions, the primary formed reactive species are $HO^{\bullet}$, $H^{\bullet}$ and e_{aq}^{-}. An excellent compilation of rate constants for the reactions of these species with a wide range of chemical compounds can be found in Buxton *et al.* (1988).

The e_{aq}^{-} is a strong reducing agent. In reactions with halogenated organic compounds, the e_{aq}^{-} acts as a nucleophile, with halide ions as reaction products. This reaction is particularly relevant to the removal of perhalogenated saturated hydrocarbons, compounds unreactive toward the $HO^{\bullet}$ (Gonzalez *et al.* 2004; Oppenländer & Schwarzwälder, 2002).

The $H^{\bullet}$ is the conjugated acid of e_{aq}^{-} with a reduction potential of –2.3 V (Buxton *et al.* 1988). This species reacts by H-abstraction with saturated organic compounds, or addition to double bonds in reactions with unsaturated compounds.

The $HO^{\bullet}$ is by far the most important reactive species in the VUV-irradiated aqueous solutions, particularly in the presence of DO. The rate constants of $HO^{\bullet}$ reactions with organic and inorganic compounds extend over several orders of magnitude, most of which approach the diffusion controlled limits ($10^9 - 10^{10}$ L mol^{-1} s^{-1}).

Despite the fact that $HO^{\bullet}$ is considered a highly reactive and unselective oxidant, one observes a significant selectivity in the H-abstraction reactions with the structural properties of the substrate. Hydroxyl radical reacts with unsaturated compounds by electrophilic addition to π-electron-rich moieties, such as the unsaturated double or triple bonds. $HO^{\bullet}$ is also involved in e^{-} transfer reactions, typically with the inorganic compounds. The most common reaction of the aromatic structures with $HO^{\bullet}$ is the addition to the aromatic ring, while e^{-} transfer and H-abstraction from the side chain generally occur less frequently. In general, the rate constants for the $HO^{\bullet}$ addition reactions are larger than those for H-abstraction. $HO^{\bullet}$ is a strong electrophile and the addition occurs preferentially to the negatively polarized sites. Most of $HO^{\bullet}$ reactions with the organic compounds result in carbon-centered radicals.

In DO-free solutions the carbon-centered radicals are involved in a series of reactions including combination and disproportionation reactions. In the presence of DO, the carbon-centered radicals are converted to peroxyl radicals *via* diffusion-controlled reactions (von Sonntag & Schuchmann, 1991). Detailed information on the formation and fate of peroxyl radicals in aqueous solutions can be found in von Sonntag and Schuchmann (1997).

The reactivity of $HO_2^{\bullet}$ and $O_2^{\bullet-}$ is much lower than that of $HO^{\bullet}$ and $H^{\bullet}$ (Bielski *et al.* 1985); the reaction rate constants for $HO_2^{\bullet}$ and $O_2^{\bullet-}$ radicals with phenol were reported as 2.7×10^3 L mol^{-1} s^{-1} (Kozmér *et al.* 2014) and 5.8×10^2 L mol^{-1} s^{-1} (Tsujimoto *et al.* 1993), respectively. However, if present at high concentrations, these species may contribute to the degradation of organic contaminants (Alapi & Dombi, 2007; Arany *et al.* 2015; Kozmér *et al.* 2014). One typical reaction of $HO_2^{\bullet}$ and $O_2^{\bullet-}$ is the addition to aromatic rings (Getoff, 1996). The $O_2^{\bullet-}$ can also participate in e^{-} transfer reactions, which can be very fast (e.g., reduction of quinones). During the mineralization process of target compounds, the organic peroxyl radical reactions (e.g., Russell mechanism (von Sonntag & Schuchmann, 1997)) yield $HO_2^{\bullet}$ and $O_2^{\bullet-}$. Consequently, the concentration of $HO_2^{\bullet}$ and $O_2^{\bullet-}$ is highly enhanced in VUV-irradiated DO-containing solutions of organic compounds.

In 172 nm- or 184.9/253.7 nm -irradiated systems, DO could have either an accelerating or an inhibitory effect on chemical degradation rates. Studies have reported increased transformation rates (Gonzalez & Braun, 1996; Han *et al.* 2004; Quici *et al.* 2008; Szabó *et al.* 2011), and efficient mineralization of the organic carbon (Arany *et al.* 2015; Gonzalez & Braun, 1996; Han *et al.* 2004; Oppenländer *et al.* 2005) in the presence of DO. Gonzales *et al.*'s studies (1994, 1995) showed that the photodegradation rates (172 nm) of atrazine and 3-amino-5-methylisoxazole did not depend on DO concentration, and higher mineralization yields were obtained in O_2-free than in oxygenated conditions.

5.2.2 Kinetics and mechanistic modeling of VUV AOP

The VUV transformation of contaminants is initiated by second-order kinetics reactions with the radicals generated during the VUV photolysis of water (5.1 and 5.2). At a constant photon flux, the reactive radicals approach *quasi*-steady state concentrations; consequently, the degradation rate is usually described by a *pseudo*-first-order kinetics.

The modeling of the VUV process is complicated mainly because of the heterogeneity of the medium caused by the short penetration depth of the VUV radiation in water (see in Section 5.1.2.2). Furthermore, some of the species are formed *in situ* as a result of light-dependent reactions, while others are formed by subsequent light-independent reactions. Moreover, the reactivity and lifetime of the reactive species are very different.

Gonzalez and Braun (1995) developed a kinetic model that considers 12 different species and a total of 28 elementary reactions. Later, Gonzalez *et al.* (2004) used methanol as a model compound and investigated its oxidation mechanism taking into account 27 different species and 54 elementary reactions.

László (2001) modeled the concentrations of radicals and formation of H_2O_2 in 172 nm irradiated water. The concentration profiles of $H^\bullet$, $HO^\bullet$, $HO_2^\bullet$, $O_2^{\bullet-}$ and H_2O_2, as a function of the radial distance from the Xe_2* lamp surface were computed, and were found in agreement with those reported by Heit and Braun (1997). $H^\bullet$ and $HO^\bullet$ were found to be present only within the 0.03 mm and 0.07 mm water layer, respectively, while the concentrations of the $HO_2^\bullet$, $O_2^{\bullet-}$ and H_2O_2 reached steady-state conditions at 0.5 mm from the lamp surface. The author demonstrated a good agreement between the model predictions and experimental results on H_2O_2 formation in a mixed batch reactor.

Zvereva (2010) modeled the concentrations of the products of liquid water decomposition under 172 nm VUV radiation. The author considered a continuous irradiation, and modeled the kinetics over 10^{-2} s time intervals; the diffusion of primary formed reactive species was neglected. The concentrations of $H^\bullet$, $HO^\bullet$, and e_{aq}^- were calculated based on the quantum yields of their formation and local (spatial) light intensity. The model was used to estimate the rate of decomposition of polychlorinated biphenyls through the reaction with $HO^\bullet$.

Imoberdorf and Mohseni (2011) examined the VUV AOP for environmental contaminant destruction in laboratory-scale reactors using chemical probes. Formic acid was selected as a simple molecule to develop and to validate a kinetic model for the VUV (184.9 nm)/UV (253.7 nm) AOP in a single lamp annular flow-through reactor operated in a batch mode. The kinetic model included the water photochemistry, photolysis of formic acid and of H_2O_2 which was formed during the VUV irradiation, and the radical reactions occurring in the solution. The kinetic model was combined with the radiation model solved using the Monte Carlo method, which allowed the calculation of local (spatial) rate of photon absorption based on the photon flow propagation through the reactor volume and optical characteristics of the solution. The experimental and modeling data showed zero-order kinetics for VUV-radiation driven degradation of formic acid, which indicated limited availability of $HO^\bullet$ in the reaction system. The model was extended to H_2O_2/VUV and H_2O_2/UV AOPs, and good agreement was observed between the experimental and simulated data (Imoberdorf & Mohseni, 2011).

In another study, Imoberdorf and Mohseni (2012) reported the kinetics of VUV/UV degradation of pesticide 2,4-D (2,4-dichlorophenoxyacetic acid) in ultrapure water and in raw surface water samples collected from three different sites in British Columbia, Canada. The model equations, mass balances, and radial radiation profiles for the 184.9 nm and 253.7 nm radiation are provided, along with the experimental patterns of 2,4-D and of the identified degradation by-products. In a study dedicated to the degradation of natural organic matter (NOM), Imoberdorf and Mohseni (2011) determined an overall quantum efficiency of 0.10 for NOM degradation by VUV photolysis at 50% TOC reduction.

Recently, Bagheri and Mohseni (2015b) developed and validated experimentally a comprehensive computational fluid dynamics (CFD) model, incorporating flow hydrodynamics, 184.9 nm and 253.7 nm radiation propagation, and a comprehensive kinetic scheme. The authors monitored the phototransformation of atrazine and found that the VUV/UV process performance depends strongly on the flow characteristics inside the photoreactor. Similar observations were reported in a study on the impact of turbulence and mixing on the performance of VUV/UV-AOPs (Bagheri & Mohseni, 2015a). *para*-Chlorobenzoic acid was used as a probe compound, and the electrical energy-per-order (E_{EO}) as the process performance metric. Baffles were inserted in order to enhance the mixing inside the UV reactor. The treatment efficacy of the VUV/UV process displays much stronger correlation with the extent of mixing than in the case of UV/H_2O_2 process. The enhanced mixing and vortexes ("circulation zones"), due to the presence of baffles, resulted in up to 50% reduction in the energy cost associated with the VUV/UV treatment, whereas no significant impact on the E_{EO} was observed for the UV/H_2O_2 (5 mg L^{-1}) process.

A novel mechanistic model that describes the VUV photolysis in an annular photoreactor with either 172 nm or 184.9 nm (in combination with 253.7 nm, with and without added H_2O_2) was published by Crapulli *et al.* (2014). The study showed that, depending on the reactor characteristics and operating conditions, the reaction zone during the 172 nm-VUV process could be more than one order of magnitude deeper than the photon penetration layer. The model confirmed that short-lived $HO^\bullet$ were present at a radial distance far beyond the radiation penetration depth. The kinetic simulations showed that the presence of $HO^\bullet$ at unexpected long radial distances from the lamp surface is the effect of non-linear behavior of the complex reaction kinetics.

5.3 VACUUM UV RADIATION FOR WATER REMEDIATION

5.3.1 VUV for removal of specific compounds

Over the past two decades, the VUV treatment of contaminated water has been investigated extensively. These studies regarded transformation yields of specific compounds, mineralization of chemical pollutants, by-product formation, and prediction of mechanistic pathways.

5.3.1.1 Aliphatic and chlorinated volatile organic compounds

In DO-containing aqueous solutions, the transformation of non-halogenated aliphatic compounds is initiated primarily by $HO^\bullet$ *via* H-abstraction or addition to unsaturated bonds. The VUV (172 nm) and VUV (184.9 nm)/UV (253.7 nm) treatment of methanol in water was investigated in detail by Heit *et al.* (1998) and Gonzalez *et al.* (2004) (Figure 5.7). The attack of $HO^\bullet$ ($k_{methanol,\ HO^\bullet} = 9.7 \times 10^8$ L mol^{-1} s^{-1} (Heit *et al.* 1998)) or $H^\bullet$ ($k_{methanol,\ H^\bullet} = 2.6 \times 10^6$ L mol^{-1} s^{-1} (Heit *et al.* 1998)) leads almost solely to the formation of hydroxymethyl radicals ($HOCH_2^\bullet$) (Gonzalez *et al.* 2004). The reaction mechanism involving these radicals is determined by the presence or the absence of O_2.

Oppenländer and Gliese (2000) investigated and compared the rates of the 172 nm radiation-initiated transformation and mineralization of twenty organic micropollutants of various structures, including C_1 to C_8 alcohols; the initial TOC content (40–50 ppm) was similar for all compounds. The mineralization

rates of aromatic C_6 compounds were faster than that for the C_6 saturated alcohol, and Cl-substitution on the aromatic ring had an activating effect. The efficiency of TOC removal decreased with the increase of the number of C atoms in the alcohol series.

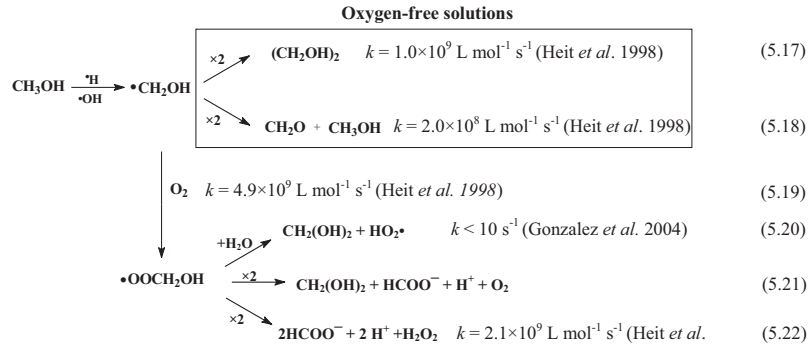

Figure 5.7 Simplified VUV-induced degradation mechanism of methanol in aqueous solution. Rate constants taken from Heit *et al.* (1998) and Gonzalez *et al.* (2004).

Chlorinated methanes, such as CCl_4 ($k_{CCl_4,{}^{\bullet}OH} < 10^5$ L mol^{-1} s^{-1}) and $CHCl_3$ react slowly with HO$^{\bullet}$ and H$^{\bullet}$, whereas their reaction with e_{aq}^- is almost diffusion controlled. The degradation of highly halogenated compounds is slowed down in the presence of O_2 (see reaction 5.13).

$$CCl_4 + e_{aq}^- \rightarrow {}^{\bullet}CCl_3 + Cl^- \qquad k = 3\times10^{10}\ \text{L mol}^{-1}\ \text{s}^{-1}\ \text{(Gonzalez } \textit{et al.}\ 2004) \tag{5.23}$$

$$CHCl_3 + HO^{\bullet} \rightarrow {}^{\bullet}CCl_3 + H_2O \qquad k = 5\times10^{7}\ \text{L mol}^{-1}\ \text{s}^{-1}\ \text{(Gonzalez } \textit{et al.}\ 2004) \tag{5.24}$$

$$CHCl_3 + H^{\bullet} \rightarrow {}^{\bullet}CCl_3 + H_2 \qquad k = 1.1\times10^{7}\ \text{L mol}^{-1}\ \text{s}^{-1}\ \text{(Gonzalez } \textit{et al.}\ 2004) \tag{5.25}$$

$$CHCl_3 + e_{aq}^- \rightarrow {}^{\bullet}CHCl_2 + Cl^- \qquad k = 3\times10^{10}\ \text{L mol}^{-1}\ \text{s}^{-1}\ \text{(Gonzalez } \textit{et al.}\ 2004) \tag{5.26}$$

More than 93% of the organic chlorine from $CHCl_3$ is released as Cl^- upon 172 nm exposure in the presence of DO, indicating that the $^{\bullet}CCl_3$ reactions lead to the formation of HCl and CO_2 (Gonzalez *et al.* 2004).

Trichloroethene (TCE), tetrachloroethene (PCE), and 1,2-dichloroethene (DCE) are volatile organic compounds (VOCs), which, along with their metabolites such as vinyl chloride or trichloroacetic acid are toxic and regulated in drinking water (Weissflog *et al.* 2004). Groundwater contaminated with TCE, DCE and PCE can be treated with the 172 nm radiation (Baum & Oppenländer, 1995). The addition of HO$^{\bullet}$, H$^{\bullet}$ and e_{aq}^- to the unsaturated bonds initiates the degradation process (5.27–5.29).

$$Cl_2C{=}CCl_2 + HO^{\bullet} \rightarrow Cl_2(OH)C{-}C^{\bullet}Cl_2 \qquad k = 4.9\times10^{8}\ \text{L mol}^{-1}\ \text{s}^{-1}\ \text{(Getoff, 1990)} \tag{5.27}$$

$$Cl_2C{=}CCl_2 + H^{\bullet} \rightarrow Cl_2HC{-}C^{\bullet}Cl_2 \qquad k = 5\times10^{9}\ \text{L mol}^{-1}\ \text{s}^{-1}\ \text{(Getoff, 1990)} \tag{5.28}$$

$$Cl_2C{=}CCl_2 + e_{aq}^- \rightarrow Cl_2C_5C^{\bullet}Cl + Cl^- \qquad k = 4.2\times10^{10}\ \text{L mol}^{-1}\ \text{s}^{-1}\ \text{(Getoff, 1990)} \tag{5.29}$$

The carbon-centered radical $Cl_2(OH)C{-}C^{\bullet}Cl_2$ reacts with DO at diffusion-controlled rates, and undergoes further decomposition to aldehydes and carboxylic acids. 1,1,2-trichloroethane (1,1,2-TCA) was found as a by-product of the DCE degradation (Baum & Oppenländer, 1995; Gonzalez *et al.* 2004). Direct photolysis of PCE, TCE, DCE, 1,1,1-TCA, 1,1,2-TCA, $CHCl_3$ and CCl_4 in VUV (184.9 nm)/UV (253.7 nm)-irradiated aqueous solution was discussed by Shirayama *et al.* (2001). The degradation rates of these chlorinated hydrocarbons increased in the absence of DO. The photolysis at 253.7 nm was not efficient in the case of chlorinated methanes, whereas TCE and PCE were easily degraded. The absorption of 184.9 nm radiation initiated the transformation of chlorinated ethanes and methanes *via* dissociation of C–Cl bonds. The negative impact of DO was attributed to the DO competition for the 184.9 nm photons with the chlorinated compounds (Shirayama *et al.* 2001). Wang *et al.* (2014) stated that the competition between DO and organics for VUV photons is not significant, and that the radiation scattering by the O_2 bubbles is negligible in the reactor. Most likely, the negative impact of DO on the degradation rates of the chlorinated compounds is related to the e_{aq}^- scavenging by DO. Gu *et al.* (2013) did not detect any organic intermediates during the VUV/UV treatment of TCE, PCE, and TCA aqueous solutions.

5.3.1.2 Perfluorinated organic compounds

The perfluorinated compounds (PFCs) are persistent organo-fluorine environmental contaminants given their resistance toward biodegradation and oxidation. Perfluorooctanoic acid (PFOA), perfluorodecanoic acid (PFDeA) and perfluorooctanesulfonic acid (PFOS) were quantified in human and marine biota plasma and liver tissue, in water sources, sediments, domestic sludge, and even in the remote Arctic region. Data from animal studies indicate that PFOA can cause several types of tumors and neonatal death, and may affect the immune and endocrine systems (Steenland *et al.* 2010). Because of their high stability and virtually no reactivity towards $HO^{\bullet}$, PFC elimination from water sources with AOPs is not possible.

Studies concerning VUV (172 nm) and VUV (184.9 nm)/UV (253.7 nm) treatment of perfluorinated compounds suggest that the reaction with e_{aq}^- (reduction process) and, to some extent, VUV photolysis represent the mechanistic pathways for the degradation of these compounds. PFOA, PFDeA and PFOS can be degraded by the 184.9 nm radiation, but cannot be removed by the 253.7 nm radiation (Cao *et al.* 2010; Chen *et al.* 2007; Giri *et al.* 2011a; Giri *et al.* 2012; Jin & Zhang, 2015; Wang *et al.* 2010a; Wang & Zhang, 2014). Chen *et al.* (2007) hypothesized that the direct VUV photolysis of PFCs results in photo-Kolbe decarboxylation. Hydrolysis of generated radical ($C_7F_{15}^{\bullet}$) occurs with formation of a shorter chain PFC, i.e., prefluoroheptanoic acid (Chen *et al.* 2007; Wang & Zhang, 2014). Shorter-chain perfluorocarboxylic acids are formed consecutively with a stepwise loss of CF_2 units (Chen *et al.* 2007).

Wang and Zhang (2014) studied the effect of pH and DO on PFOA decomposition under 184.9/253.7 nm irradiation. In the presence of DO, the efficiency of PFOA degradation decreased as the pH was increased from 4.5 to 12.0. In DO-free solutions, the increase of pH enhanced the degradation rate. The authors concluded that in the absence of DO, in acidic and neutral solutions, PFOA degrades primarily *via* direct VUV photolysis, whereas in alkaline conditions the reaction with e_{aq}^- is the major degradation pathway. The role of e_{aq}^--initiated transformation of PFCs in DO-free slightly alkaline solutions was also postulated by Jin and Zhang (2015). Other studies (Cao *et al.* 2010; Wang *et al.* 2010a) confirmed the role of e_{aq}^- in PFC degradation in the VUV process. Detailed investigation of the PFOA decomposition by the VUV (184.9 nm)/UV (253.7 nm) process was reported in a series of publications by (Giri *et al.* 2011a; Giri *et al.* 2011b; Giri *et al.* 2012). The impact of pH, initial concentration, and water quality (Giri *et al.* 2012) and the matrix effect (Giri *et al.* 2011b) on PFOA removal are discussed. Defluorination efficiency in river water and wastewater treatment plant effluent was negligible, due to the strong e_{aq}^- scavenging capacity of water constituents other than PFOA.

5.3.1.3 Aromatic compounds

Phenol is often used as a model compound for the investigation of the efficiency of various AOPs. The VUV degradation of phenol is initiated by $HO^{\bullet}$ and $H^{\bullet}$ reactions at diffusion controlled rates ($k_{phenol,\ HO^{\bullet}} = 8.4 \times 10^9$ L mol^{-1} s^{-1} (Bonin *et al.* 2007), $k_{phenol,\ H^{\bullet}} = 1.7 \times 10^9$ L mol^{-1} s^{-1} (Buxton *et al.* 1988)) yielding dihydroxy-cyclohexadienyl ($DHCD^{\bullet}$) and hydroxyl-cyclohexadienyl ($HCD^{\bullet}$) radicals, respectively. Dimerization and dismutation reactions of these radicals result in bicyclohexadienes, dihydroxybenzenes/cyclohexadiens and phenol (Gonzalez *et al.* 2004). Further transformations of the aromatic radicals can result ring-opening products, and finally CO_2 and H_2O (Gonzalez *et al.* 2004). Huang *et al.* (2013) studied the transformation of 4-*tert*-octylphenol by the 184.9/253.7 nm radiation. The degradation occurs *via* both direct photolysis (C—C bond cleavage) yielding phenol, and $HO^{\bullet}$-based oxidation with the formation of 4-*tert*-octylcatechol.

Chlorophenols represent another environmentally relevant group of pollutants. 2,4-Dichlorophenol is an industrial intermediate product of chlorophenoxy herbicides (Wild *et al.* 1993). Efficient photomineralization of chlorophenols was achieved with a Xe_2* lamp, converting organically bound Cl atoms to Cl^- (Baum & Oppenländer, 1995; Jakob *et al.* 1993). The Cl-substitution on the aromatic ring exerts an activating effect towards $HO^{\bullet}$ addition, accelerating the rate of mineralization, which was found to be lower of 4-chlorophenol and 2,4-dichlorophenol than that of phenol (Oppenländer & Gliese, 2000).

The treatment of 4-chloro-3,5-dinitrobenzoic acid (CDNBA) with 172 nm or 184.9/253.7 nm radiation released Cl^- and NO_2^- at a rate similar to that of substrate depletion. NO_2^- was efficiently oxidized to NO_3^-, which was further reduced to NH_4^+ in the presence of organic matter *via* $H^{\bullet}/e_{aq}^-$ initiated reactions (Lopez *et al.* 2000). No aromatic intermediates were detected, which led to the conclusion that the ring opening followed the reactions of carbon-centered radicals with DO. The rates of transformation and mineralization of CDNBA were slightly slower under the VUV/UV process using a LP lamp than using the 172 nm VUV treatment, most probably due to the difference in the $HO^{\bullet}$ yield at the two wavelengths (Lopez *et al.* 2000).

5.3.1.4 Pesticides

The stability and mobility of various pesticides result in the pollution of soil, surface waters and groundwater, which induce long-term effects on living organisms. Many pesticides have been proven endocrine disruptors in fish, amphibians, birds, reptiles, laboratory rats and even humans. Over twenty pesticides are regulated in drinking water by the US EPA with maximum contaminant levels (MCLs) anywhere from 0.2 μg L^{-1} (lindane) to 0.5 mg L^{-1} (picrolam), whereas under the European Union regulations, the total concentration of pesticides and their metabolites in drinking water should not exceed 0.5 μg L^{-1}, while the concentration of any one pesticide may not exceed 0.1 μg L^{-1}.

Atrazine (2-chloro-4-ethylamino-6-isopropylamino-*s*-triazine) is one of the most widely used *s*-triazine herbicides. Pulse radiolysis studies indicated that in DO-free solutions, atrazine degradation occurred mostly *via* reaction with e_{aq}^-, with other mechanistic pathways involving $HO^{\bullet}$ and $H^{\bullet}$ (Khan *et al.* 2015). Gonzales *et al.* (1994) examined the mineralization of atrazine in aqueous solutions exposed to the 172 nm radiation, and observed two different stages in TOC decay. During the first stage, TOC was removed rapidly and the kinetics was independent on the oxygen level (same rates in argon-, air-, and O_2-saturated solutions). Approximately two-thirds into the mineralization process, the TOC removal reached a plateau under all studied conditions indicating that non-degradable products were formed; the plateau was reached faster in the presence of oxygen than in argon-saturated solutions. Atrazine was degraded to various products, among which the stable, non-degradable cyanuric acid. The conversion yields of atrazine to cyanuric acid were found oxygen dependent, and reported as 10%, 30%, and 50%, in

argon-, air-, and O_2-saturated conditions, respectively. This study showed that mineralization of atrazine to CO_2 and inorganic nitrogen-products *via* 172 nm radiation does not necessarily require the presence of DO and other mechanistic routes involving reducing species are involved.

A similar effect was observed in the 172 nm initiated degradation of 3-amino-5-methylisoxazole (Gonzalez *et al.* 1995). Cyanide was a degradation product of 3-amino-5-methylisoxazole and it was completely removed *via* $HO^{\bullet}$ reaction. Using a theoretical approach, Liu (2014) confirmed the resistance to oxidative treatment of cyanuric acid, which was attributed to the electron deficiency of the triazine ring. Dechlorination and hydroxylation were reported as the main reactions involving the *s*-triazine ring, and the degradation intermediates were assessed as less toxic than the parent pollutants (Gonzalez *et al.* 1994; Khan *et al.* 2014; Khan *et al.* 2015).

2,4-Dichlorophenol and H_2O_2 were detected as by-products of VUV degradation of herbicide 2,4-dichlorophenoxyacetic acid (Imoberdorf & Mohseni, 2012). Moussavi *et al.* (2014) evaluated the performance of UV (253.7 nm) and VUV (184.9 nm)/UV (253.7 nm) processes for the degradation of diazinon. At the optimum pH (5 for UV, 9 for VUV/UV), the transformation rate was two orders of magnitude higher in the presence of the 184.9 nm radiation.

5.3.1.5 Pharmaceuticals

Pharmaceuticals and personal care products (PPCPs) belong to the group of emerging contaminants detected in surface waters, groundwater and even in drinking waters, and were proven to cause adverse effects on the aquatic species, and could impact human health.

Kim and Tanaka (2009) studied the 253.7 nm and 184.9/253.7 nm degradation of 30 PPCPs commonly found in surface water. At a dose of ~230 mJ cm^{-2} approx. 3% (theophylline) to 100% (diclofenac), and ~15% (clarithromycin) to 100% (diclofenac) removals were observed under UV and VUV/UV irradiation, respectively. The PPCP degradation rates were on average 1.4 times faster for the VUV/UV than UV process. It was concluded that some PPCPs containing amide bonds (e.g., cyclophosphamide) were highly resistant to photodegradation at 253.7 nm, whereas at 184.9 nm the removal rates increased considerably. The results proved that the 184.9 nm radiation enhances the oxidative transformation, but the contribution of the $HO^{\bullet}$-initiated degradation to the overall rate depends on the initial concentrations of PPCPs, and their molar absorption coefficients and quantum yields at 253.7 nm (Szabó *et al.* 2011). Direct UV photolysis was found to dominate during the VUV/UV decomposition of ketoprofen and diclofenac, whereas 184.9 nm radiation accelerated the transformation rate of ibuprofen. DO enhanced the rate of decay of ibuprofen, but had no effect on ketoprofen removal yield, in either UV or VUV/UV-irradiated solutions (Szabó *et al.* 2011). However, DO enhanced the rate of mineralization. Arany *et al.* (2013) have reported that DO has no significant effect on the transformation rate of naproxen at 253.7 nm, while it decreases the removal efficiency for the 172 nm or 184.9 nm/253.7 nm processes. Only the 172 nm irradiation was found to be able to completely mineralize naproxen. Degradation of ibuprofen, ketoprofen, naproxen, and diclofenac under VUV (172 nm) exposure is initiated by H-abstraction, $HO^{\bullet}/H^{\bullet}$-addition and decarboxylation reactions. DO enhances significantly the TOC removal rate for each pollutant (Arany *et al.* 2015).

5.3.1.6 Other water contaminants

Alkylphenols are endocrine disrupting chemicals often detected in surface waters in the concentration range of 1.0×10^{-3}–1.0 μg L^{-1}. The transformation rate of 4-*tert*-octylphenol (presumably the most powerful estrogenic compound among alkylphenols (Routledge & Sumpter, 1997)) was much larger upon exposure to 184.9 nm/253.7 nm combined radiation than that to 253.7 nm radiation alone. The C—C bond

cleavage *via* absorption at 184.9 nm was proposed to occur, although direct photolysis at 184.9 nm is likely of a minor importance relative to the HO•-initiated reactions (Huang *et al.* 2013).

Taste and odor-causing compounds (e.g., geosmin (*trans*-1,10-dimethyl-*trans*-9-decalol) and 2-methylisoborneol (MIB)), although non-toxic, impact the aesthetics of drinking water. Currently, there are several full-scale installations in the world using the UV/H_2O_2 process to treat these compounds in drinking water sources impacted by the seasonal algal blooming. The combination of 184.9 nm and 253.7 nm radiation (with or without simultaneous generation of O_3) led to efficient removal of these compounds (Kutschera *et al.* 2009; Zoschke *et al.* 2012).

1,4-Dioxane is a persistent, potentially carcinogenic chemical, widely used as a stabilizing agent and solvent, and is reported as an impurity of surfactants in many household detergents. 1,4-Dioxane, geosmin and MIB were efficiently degraded using VUV/UV treatment, photocatalysis, and the combination of these processes. The degradation rates followed the order geosmin > MIB > 1,4-dioxane, which is consistent with their reactivity toward the HO•.

Anatoxin-a is a potent neurotoxin produced by freshwater cyanobacteria during the algal blooming seasons. The degradation rate of anatoxin-a at 172 nm was significantly slower in natural water containing 3.94 mg L^{-1} dissolved organic carbon (DOC) and in synthetic water with 6.63 mg L^{-1} DOC than in pure water, given the strong competition for the HO• from the water matrix components (Afzal *et al.* 2010).

The VUV/UV radiation can transform non-biodegradable textile dyes into biodegradable oxidized intermediates, thus enhancing their elimination in a VUV-biofiltration combined treatment (Al-Momani *et al.* 2002).

Arsenic (As) is a carcinogenic water pollutant released from soil into the groundwater during weathering of arsenic-containing minerals. The maximum contaminant level of arsenic in drinking water is regulated at 10 μg L^{-1} by the US EPA (https://www3.epa.gov/). Arsenic removal techniques are based on adsorption, oxidation, and coagulation/precipitation. As(V) is better removed by these methods than As(III). As(III) was oxidized more efficiently in the VUV/UV (184.9/253.7 nm) treatment than by the UV/H_2O_2, photo-Fenton, or photocatalytic AOPs (Yoon *et al.* 2008). In all these processes, HO• is the oxidizing species of As(III), with a minor contribution of molecular oxidation by H_2O_2 generated *in situ* in alkaline solutions (pH > 9). The addition of Fe(III) or H_2O_2 increased the efficiency of As(III) oxidation due to the additionally generated HO• and Fe(IV) species in the presence of 253.7 nm radiation. The presence of humic acids (7.5–15 mg L^{-1}) did not affect significantly the As(III) oxidation efficiency. The combination of the VUV/UV process with adsorption onto activated alumina or with coagulation/precipitation using $FeCl_3$ were found to be effective strategies for As removal (Yoon *et al.* 2008).

5.3.2 VUV in combination with other treatment technologies

5.3.2.1 VUV and VUV/UV in combination with H_2O_2

The molar absorption coefficients of H_2O_2 at 172 nm and 184.9 nm ($\varepsilon_{172\,nm} = 782$ L mol^{-1} cm^{-1} (Schürgers & Welge, 1968) and $\varepsilon_{184.9\,nm} = 297$ L mol^{-1} cm^{-1} (Weeks *et al.* 1963)) exceed those of water ($\varepsilon_{172\,nm} = 9.9$ L mol^{-1} cm^{-1} (Heit & Braun, 1996; Heit *et al.* 1998) and $\varepsilon_{184.9\,nm} = 0.04$ L mol^{-1} cm^{-1} (Weeks *et al.* 1963)). However, water is the major VUV light absorbing compound in aqueous solutions of H_2O_2. Upon absorption of VUV radiation, H_2O_2 undergoes photolysis with HO• formation (5.30).

$$H_2O_2 + h\nu(<300\ nm) \rightarrow 2HO^{\bullet} \quad (5.30)$$

In aqueous solution, the quantum yield of HO• formation (reaction 5.30) is 1.11 ± 0.07 (Goldstein *et al.* (2007), which also exceeds that from water (0.42 (172 nm) and 0.33 (184.9 nm)). Although H_2O_2 is a weak

absorber of the 253.7 nm radiation, the addition of H_2O_2 to water exposed to VUV/UV radiation increases the overall $HO^{\bullet}$ yield.

The VUV (184.9 nm)/UV (253.7 nm)/H_2O_2 process was found more effective for clofibric acid degradation than UV (253.7 nm), VUV/UV, and UV (253.7 nm)/H_2O_2 processes (Li *et al.* 2011). Simonsen *et al.* (2013) demonstrated a synergistic effect of the VUV (184.9 nm)/UV (253.7 nm)/H_2O_2 process in degradation of *para*-nitrosodimethylaniline.

The efficiency of VUV/UV process for 1,4-dioxane removal increased upon addition of increasing H_2O_2 concentration. The VUV/UV/H_2O_2 process in the presence of 1 mg/L H_2O_2 was found to be more effective than the UV/H_2O_2 process. Increasing the H_2O_2 concentration to 5.0 mg L^{-1} reduced the difference between the transformation rates determined for VUV/UV/H_2O_2 and UV/H_2O_2 processes (Matsushita *et al.* 2015). The degradation rates of nitrobenzene upon exposure to 172 nm radiation increased upon addition of H_2O_2 up to an optimal H_2O_2:nitrobenzene initial concentration ratio of 7:1; above this ratio, the excess of H_2O_2 competed with nitrobenzene for the $HO^{\bullet}$ decreasing the transformation rate (Li *et al.* 2006).

Reverse osmosis concentrate (ROC) of a municipal wastewater secondary effluent was effectively treated with the UV/H_2O_2 process and, with even a better performance, with the VUV/UV/H_2O_2 process. The highly conjugated compounds of ROC characterized by low biodegradability were efficiently fragmented and oxidized by $HO^{\bullet}$, thus increasing their biodegradability and mineralization (Liu *et al.* 2011).

5.3.2.2 VUV and VUV/UV in combination with photocatalysis

Titanium dioxide (TiO_2) is the commonly used photocatalyst, either in suspension or immobilized on solid surfaces. Because the VUV light is absorbed in a very thin water layer, the TiO_2 particles can be excited by the VUV radiation only within this layer. In VUV/UV process using LP lamp, the excitation of photocatalyst can occur also over a longer path length through the suspension *via* the absorption of 253.7 nm radiation. However, in a 1.00 g L^{-1} TiO_2 containing suspension, the 253.7 nm radiation is absorbed within less than 2 mm.

The VUV (184.9 nm)/UV (253.7 nm) or VUV (172 nm) radiation were found more effective for the degradation of organic pollutants than the UV (253.7 nm)/TiO_2 process (Dombi *et al.* 2002; Han *et al.* 2004; Matsushita *et al.* 2015; Wang *et al.* 2014). The addition of TiO_2 to the VUV/UV-irradiated solutions slightly enhanced the transformation rates of various pollutants and accelerated the rate of mineralization. No synergism was observed between the VUV/UV process and photocatalysis when the distance between the sheet with immobilized TiO_2 and the lamp was large, e.g., 3.5 cm (Matsushita *et al.* 2015) or 1.5 cm (Han *et al.* 2004).

The VUV/UV/TiO_2 process efficiency can be increased upon addition of H_2O_2. Although the performance of this combination was better than those of the VUV/UV or VUV/UV/TiO_2 processes, it was worse than that of the VUV/UV/H_2O_2 process, most likely because the TiO_2 in suspension competes strongly with H_2O_2 for the photons, and has a lower $HO^{\bullet}$ yield (~0.05) than H_2O_2 photolysis (~1.0) (Shen & Liao, 2007).

The VUV (172 nm, 7.2 mW cm^{-2})/TiO_2 process was also found to be more effective in transformation of phenol than the UV (253.7 nm, 10 mW cm^{-2})/TiO_2, UV (310–380 nm, 4 mW cm^{-2})/TiO_2 or VUV (172 nm) processes (Ochiai *et al.* 2013a; Ochiai *et al.* 2013b).

5.3.2.3 VUV and VUV/UV in combination with ozone

Ozone is unstable in water, and its degradation rate depends on various factors, including pH and water composition. O_3 absorbs the UV radiation with large absorption coefficient at 253.7 nm (3300 M^{-1} cm^{-1}, (Reisz *et al.*)). $HO^{\bullet}$ is one of reactive species formed through O_3 photolysis. VUV photolysis of O_2 in gas phase

enables *in situ* photochemical generation of O_3. Consequently, the reactor configuration gives possibility for the combination of VUV, VUV/UV or UV photolysis and ozonation without external ozone generator.

The combination of 172 nm or 184.9 nm/253.7 nm radiation with ozonation was studied using one light source for the photochemical generation of O_3 from O_2 in the gas phase. Hashem *et al.* (1997) used this technique for VUV (172 nm)/O_3 treatment of 4-chlorophenol in laboratory water. Zoschke *et al.* (2014) used the *in situ*-generated O_3 in combination with the VUV (184.9 nm)/UV (253.7 nm) radiation to study the degradation of geosmin and MIB.

The combination of 184.9 nm/253.7 nm radiation with ozonation was more efficient for the NOM mineralization than the individual VUV/UV, UV/O_3, O_3 or direct UV (253.7 nm) processes (Ratpukdi *et al.* 2010). Synergistic effects were observed at pH 7 and 9, but not at pH 11; increased biodegradability of treated water was also observed. Synergistic was also observed during the degradation of organophosphoric acid triesters (OPEs) by the VUV (184.9 nm)/UV (253.7 nm)/O_3 at pH 7.5 as compared to the sequential application of the individual processes (Echigo *et al.* 1996). The efficiency of this combination was reported to increase with the increasing concentration of O_3. This combined process was also more effective than the O_3/H_2O_2 process in distilled water, but only at low OPE concentrations. Treatment of 20 mg L^{-1} OPE exhibited similar efficiencies for the two processes in pure water, whereas the treatment of a solid waste landfill effluent indicated a slightly higher efficiency for the O_3/H_2O_2 process than for the VUV/UV/O_3 combination. This was explained in terms of the negative impact of NO_3^- on the performance of VUV/UV process.

5.4 WATER QUALITY IMPACT ON VACUUM UV PROCESS PERFORMANCE AND BY-PRODUCT FORMATION

5.4.1 The effect of inorganic ions

The inorganic ions are known to impact the VUV process performance. Thus, when designing a VUV process for water remediation, it is important to know the water matrix composition, including the concentrations of ions such as NO_2^-, NO_3^-, Cl^-, CO_3^{2-}, HCO_3^-, SO_4^{2-}, HPO_4^{2-} and $H_2PO_4^-$. Some of these ions, e.g., NO_2^- and CO_3^{2-} are highly reactive toward the $HO^\bullet$. The rate constants for the reactions of many inorganic ions with $HO^\bullet$ are available in the published literature (Buxton *et al.* 1988). The majority of inorganic ions present in natural waters are orders of magnitude less reactive than the organic pollutants towards the $HO^\bullet$, such that the impact of those ions on the contaminant treatment performance becomes significant only at large concentrations.

At low pH (< 3), Cl^- becomes a significant $HO^\bullet$ scavenger, reducing the efficiency of the VUV process. The reaction of Cl^- with $HO^\bullet$ results in the formation of $Cl^\bullet$ *via* the decomposition of $HOCl^{\bullet-}$, an unstable intermediate. $Cl^\bullet$ is highly reactive toward organic compounds and could increase the adsorbable organic halogen (AOX) level of water (Oppenländer, 2003). An inhibitory effect of Cl^- (1 mmol L^{-1} and 100 mmol L^{-1}) on the transformation of 1,1,1-trichloroethane in VUV/UV-irradiated solution was observed by Gu *et al.* (2013).

The HCO_3^- or CO_3^{2-} can compete for $HO^\bullet$ especially in high alkalinity waters. The reactions of HCO_3^- and CO_3^{2-} with $HO^\bullet$ are electron transfer reactions. The $HO^\bullet$ scavenging by CO_3^{2-} becomes significant mainly at pH > 10.5, where CO_3^{2-} is the predominant carbonate species ($k_{HO^\bullet, carbonate} = 3.9 \times 10^8$ L mol^{-1} s^{-1} (Buxton *et al.* 1988)).

Although the photolysis at 172 nm radiation of SO_4^{2-}, HPO_4^{2-} and $H_2PO_4^-$ yields highly reactive and selective radicals, i.e., $SO_4^{\bullet-}$, $HPO_4^{\bullet-}$ and $H_2PO_4^\bullet$, respectively, this process is insignificant relative to water photolysis, due to the high molar absorption coefficient of water at $\lambda < 175$ nm. In aqueous solutions containing less than 10^{-2} mol L^{-1} of dissolved organic compounds with molar absorption coefficients

of ~6×10^3 mol L^{-1} cm^{-1}, the water photolysis is the dominant process in the VUV-based treatment ($\lambda < 200$ nm) (Gonzalez *et al.* 2004).

The VUV (172 nm) water photolysis in the presence of nitrate (NO_3^-) and nitrite ions (NO_2^-) is a very complex reaction system. It involves 16 N-containing species and 64 reactions, where NO_2^- is generated from NO_3^- and *vice versa*, yielding N_2O and N_2 as final products. Due to the small rate constant of the reaction of NO_3^- with $HO^\bullet$ (see 5.31), NO_3^- reacts preferentially with reducing species (reactions 5.32 and 5.33) and it competes efficiently for e_{aq}^- with DO. Nitrite is an intermediate product of NO_3^- photolysis which reacts at diffusion controlled rates with all primary radicals of water VUV photolysis (Gonzalez & Braun, 1995) (reactions 5.34–5.36).

$$NO_3^- + HO^\bullet \rightarrow NO_3^\bullet + HO^- \qquad k < 1\times10^5 \text{ L mol}^{-1} \text{ s}^{-1} \text{ (Gonzalez \& Braun, 1995)} \tag{5.31}$$

$$NO_3^- + H^\bullet \rightarrow NO_3H^{\bullet-} \qquad k = 2.4\times10^7 \text{ L mol}^{-1} \text{ s}^{-1} \text{ (Gonzalez \& Braun, 1995)} \tag{5.32}$$

$$NO_3^- + e_{aq}^- \rightarrow NO_3^{\bullet 2-} \qquad k = 1\times10^{10} \text{ L mol}^{-1} \text{ s}^{-1} \text{ (Gonzalez \& Braun, 1995)} \tag{5.33}$$

$$NO_2^- + HO^\bullet \rightarrow NO_3H^{\bullet-} \qquad k = 2.5\times10^9 \text{ L mol}^{-1} \text{ s}^{-1} \text{ (Gonzalez \& Braun, 1995)} \tag{5.34}$$

$$NO_2^- + e_{aq}^- \rightarrow NO_2^{\bullet 2-} \qquad k = 6\times10^9 \text{ L mol}^{-1} \text{ s}^{-1} \text{ (Gonzalez \& Braun, 1995)} \tag{5.35}$$

$$NO_2^- + H^\bullet \rightarrow NO_2H^{\bullet-} \qquad k = 1\times10^9 \text{ L mol}^{-1} \text{ s}^{-1} \text{ (Gonzalez \& Braun, 1995)} \tag{5.36}$$

It was found that both in the presence and the absence of DO, the N-containing species that form during the 172 nm irradiation of NO_3^--containing solutions ($c_0 = 2.6 \times 10^{-4} - 2.3 \times 10^{-3}$ mol L^{-1}) promote the transformation and mineralization of phenol (Gonzalez & Braun, 1996). An excellent description on the mechanistic pathways and dynamics of inorganic N-species in VUV-irradiated systems as well as their impact on contaminant treatment efficiency are given in Gonzales *et al.*'s review (2004).

NO_2^- is not a common water constituent but it could be generated *in situ via* NO_3^- photolysis particularly with medium-pressure lamps and 184.9 nm radiation. Therefore, its contribution to the overall $HO^\bullet$ water demand should be anticipated and properly accounted for in VUV- and medium-pressure lamp-based AOP applications. In VUV (172 nm)/O_3 and/or VUV (184.9 nm)/UV (253.7 nm)/O_3 combined processes, NO_2^- is rapidly removed through the reaction with O_3 (Kutschera *et al.* 2009; Zoschke *et al.* 2012).

5.4.2 The effect of dissolved natural organic matter (NOM)

Studies conducted on the potential application of VUV (184.9 nm)/UV (253.7 nm) radiation as a pretreatment step to biological filtration of drinking water proved that the VUV/UV process increases the biodegradability and mineralizes NOM to a greater extent than the UV (253.7 nm) radiation alone (Buchanan *et al.* 2006; Buchanan *et al.* 2005; Ratpukdi *et al.* 2010; Thomson *et al.* 2002). The enhanced biodegradability of VUV/UV-irradiated NOM in water samples was attributed to the sequential breakdown of high molecular weight, conjugated compounds in the hydrophobic acidic NOM fractions to generate biodegradable, charged (hydrophilic) and neutral (hydrophilic) structures. Low molecular weight, hydrophilic neutral fractions of NOM however, were refractory to photo-oxidation but more amenable by biological filtration than the hydrophobic fractions (Buchanan *et al.* 2005).

Xing *et al.* (2015) investigated UV (253.7 nm) and VUV (184.9 nm)/UV (253.7 nm) photolysis as pre- and post-treatment of coking wastewater and compared the effect of processes on TOC, COD, BOI, NH_4^+ and NO_2^- concentration, total-nitrogen content, biodegradability and toxicity of the treated water samples.

It was demonstrated that the combination of UV or VUV radiation with O_3 was more effective at the decomposition of high molecular weight compounds than ozonation alone. The combined processes are effective in the mineralization of hydrophobic neutral and acidic fractions of NOM. The oxidized residue mainly consisted of hydrophilic neutral NOM, which is more biodegradable than the original NOM (Ratpukdi *et al.* 2010). Thus, VUV/UV photooxidation or its combination with other oxidants followed by biological treatment appears to be a promising approach to NOM removal (Matilainen & Sillanpää, 2010; Zoschke *et al.* 2014).

The NOM removal during the pre-treatment steps of water is desirable particularly in water treatment scenarios which require contaminant removal *via* $HO^\bullet$-based processes. It is well known that humic and fulvic acids, as well as other NOM constituents are both $HO^\bullet$ scavengers and UV light absorbing species. The negative impact of water matrix constituents on the efficiency of VUV/UV process is well represented in the published literature (Imoberdorf & Mohseni, 2012; Kutschera *et al.* 2009; Li *et al.* 2009; Li *et al.* 2011).

5.4.3 Effect of pH

The effect of pH on the yield of primary radicals ($HO^\bullet$, $H^\bullet$ and e_{aq}^-) and on their subsequent reactions was discussed briefly in Section 5.1.2. The reaction rate constants of the protonated and deprotonated forms of the target compounds as well as of pH-dependent structures of NOM constituents with $HO^\bullet$ and other reactive species could be different. The pH also affects the HCO_3^-/CO_3^{2-}concentration ratio in water, which consequently affects the contribution of these species to the $HO^\bullet$ water background demand. Therefore, the effect of pH on the VUV-irradiated aqueous solutions is complex.

Quici *et al.* (2008) investigated the pH effect on the 172 nm-irradiated solutions of citric acid and gallic acid. The removal of citric acid at pH 3.4 was faster than at pH 11, which was explained as due to a lower steady-state concentration of $HO^\bullet$ at pH 11 ($pK_{a(HO^\bullet)} = 11.9$ (Gonzalez *et al.* 2004)) than at pH 3.4, and to the lower reactivity of citrate ion toward $O^{\bullet-}$ than toward $HO^\bullet$. Additionally, the coulombic repulsion between the ionized species and $O^{\bullet-}$ at high pH decreases the degradation rate of the substrate. Gallic acid (pK_a values of 4.44, 8.45, and 10.05) degradation rate was not significantly affected by pH within the 2.5–7.5 pH range, despite the difference between the reported $HO^\bullet$ rate constants for the fully protonated (6.4×10^9 L mol^{-1} s^{-1} at pH 0) and monoprotonated form (1.1×10^{10} L mol^{-1} s^{-1} at pH 6.8) of gallic acid (Dwibedy *et al.* 1999).

The degradation efficiency of 4-*tert*-octylphenol (4-OP) with the 253.7 nm radiation was significantly higher in alkaline media than under acidic conditions (pH 3 or 6) (Huang *et al.* 2013), which could be due to a larger molar absorption coefficient at 254 nm of 4-OP ionized form than that of non-ionized form. The $HO^\bullet/O^{\bullet-}$ speciation as a function of pH, as well as the pH-dependent oxidation potential of $HO^\bullet$ are factors to be considered during the assessment of the VUV/UV for water contaminant treatment (Huang *et al.* 2013). The oxidation potential of $HO^\bullet$ was reported as 2.59 V at pH 0 and 2.18 V at pH 7, while that of $O^{\bullet-}$ is 1.64 V at pH 14 (Koppenol & Liebman, 1984).

The degradation rates of 1,4-dioxane, geosmin, and MIB in buffered dechlorinated tap water treated with VUV/UV and VUV/UV/TiO_2 processes were reported to decrease with the increase of pH in the 5.5–8.0 range (Matsushita *et al.* 2015), effect attributed to the pH-dependent speciation of carbonate ions and their reactivity with $^\bullet OH$. Formation and accumulation of H_2O_2 in VUV light irradiated DO containing solutions is mainly due to the pH-dependent disproportionation reactions of $HO_2^\bullet/O_2^{\bullet-}$ (Arany *et al.* 2012;

Azrague *et al.* 2005; Robl *et al.* 2012). Given that $pK_a(HO_2^{\bullet}) = 4.8$, higher H_2O_2 concentrations formed through the $HO_2^{\bullet}$ disproportion reaction are expected at pH < 6 than at neutral and alkaline pH.

5.4.4 By-product formation during the VUV process and their removal through biological activated carbon filtration

5.4.4.1 Chlorination disinfection by-products (DBPs)

Buchanan *et al.* (2006) and Matsushita *et al.* (2015) have studied the THM formation potential as a result of NOM and 1,4-dioxane treatment with VUV/UV radiation, respectively. The applied UV doses were several times larger than those used in full-scale AOP applications. The authors observed that VUV/UV doses lower than 10 J cm^{-2} decreased the THM formation potential, particularly for chloroform, dibromochloro- and bromodichloromethanes (Matsushita *et al.* 2015). At doses of 30–40 J cm^{-2}, the THM formation potential increased, which was attributed to the halogenation of low molecular weight compounds generated from the high molecular weight NOM constituents. Although the total THM formation potential decreased upon VUV/UV treatment, a linear increase in bromoform formation was observed. Bromoform formation was associated only with the treatment of the hydrophilic fraction of NOM. The major species accounting for the THM formation potential were characterized as chlorinated hydrophobic compounds. The superiority of the VUV/UV treatment over UV photolysis on the reduction of THM formation potential was demonstrated (Buchanan *et al.* 2006; Matsushita *et al.* 2015).

The nine HAAs (i.e., monochloroacetic, dichloroacetic, trichloroacetic, monobromoacetic, dibromoacetic, tribromoacetic, bromochloroacetic, dibromochloroacetic and bromodichloroacetic acids) are potentially genotoxic and carcinogenic. The HAA formation potential on VUV/UV-treated 1,4-dioxane and NOM was found nearly constant at doses lower than 32 J cm^{-2} and decreased upon exposure to doses ≥ 48 J cm^{-2}. In contrast, the UV photolysis caused no significant change in the HAA formation potential. Most of the HAAs were chlorinated compounds, but significant concentrations of brominated HAAs were also observed (Buchanan *et al.* 2006; Matsushita *et al.* 2015).

Biological activated carbon (BAC) filtration is a well-established, widely implemented process in water treatment. BAC removes effectively the biodegradable fraction of DOC, a vast range of water micropollutants, inorganic species, and toxic as well as genotoxic compounds.

The combination of VUV/UV treatment with BAC or granular activated carbon (GAC) filtration reduced significantly the THM and HAA formation potentials, which was explained by the ability of BAC to remove the hydrophilic biodegradable compounds, including carbonyl and carboxylic compounds, generated through VUV-induced degradation of hydrophobic fraction of NOM (Buchanan *et al.* 2008; Matsushita *et al.* 2015).

5.4.4.2 Aldehydes, nitrite and H_2O_2

The low-molecular weight compounds such as aldehydes and carboxylic acids are assimilable organic carbon and are responsible for the biofilm growth in the water distribution network and on filtration membranes used in water treatment. The VUV/UV treatment of NO_3^--containing waters generates NO_2^-. Exposure to NO_2^- may cause methaemoglobinaemia in infants and mutations in mammalian cells. H_2O_2 formed during the VUV water photolysis in the presence of DO should be removed from the treated water prior to use or discharge. H_2O_2 reacts with chlorine and consequently increases the chlorine demand in the water disinfection process. The concentration of H_2O_2 formed in solutions treated with VUV/UV process exceeds that formed during the UV (253.7 nm) irradiation (Buchanan *et al.* 2006; Matsushita *et al.* 2015).

Matsushita *et al.* (2015) showed that the chlorination and VUV/UV treatment of raw water from Lake Hakucho and raw groundwater generated formaldehyde, glyoxal, and formaldehyde-forming compounds from NOM. These compounds were efficiently removed by the subsequent BAC or GAC treatment. Imoberdorf and Mohseni (2014) reported that VUV/UV doses in the range of 1–3 J cm^{-2} increased the aldehyde levels, which were reduced upon extended treatment (> 4 J cm^{-2}).

The VUV/UV/BAC or VUV/UV/GAC processes removed NO_2^- and H_2O_2 from the VUV/UV treated waters (Buchanan *et al.* 2006, 2008; Matsushita *et al.* 2015). The NO_2^- concentration in VUV/O_3 or VUV/UV/O_3 treated water was below the detection limit (Kutschera *et al.* 2009; Zoschke *et al.* 2012).

5.4.4.3 Bromate

Although the efficiency of the VUV or VUV/UV processes could be significantly increased in the presence of O_3, the application of the combined processes raises concerns over bromate (BrO_3^-) formation. In the VUV/UV/O_3 process, the oxidation of Br^- by O_3 *via* $HO^\bullet$-based mechanism yields BrO_3^-. Bromate absorbs the VUV radiation and is converted back to Br^-. When the UV (253.7 nm) or VUV (184.9 nm)/UV (253.7 nm) photolysis and the ozonation of bromide-containing water were performed in the same reactor and sufficient time was allowed for BrO_3^- reduction by the VUV/UV light, the measured BrO_3^- concentrations in the treated water were 6 times lower for the VUV/UV/O_3 process than those observed for the UV/O_3 process at pH 9 (Ratpukdi *et al.* 2011). An opposite outcome was found in a system configuration where ozonation and photolysis were performed separately, in two reactors, with a short VUV/UV treatment time (Collivignarelli & Sorlini, 2004). Since the increase of the lamp electrical power, O_3 concentration, and pH results in both the increase of BrO_3^- concentration and DOC removal, the optimization of these factors is required to control the BrO_3^- formation and to maximize the pollutant removal efficiency (Ratpukdi *et al.* 2011).

5.5 WATER DISINFECTION

An advantage of UV-based oxidation processes is the simultaneous disinfection. The 253.7 nm radiation emitted by the LP lamp causes the inactivation of microorganisms *via* absorption-induced changes in the DNA structure. The disinfection mechanism of the VUV radiation is different than that of UV radiation. In the VUV process, the disinfection is the effect of the radical species which induce surface oxidation at the cell wall, resulting in the cell membrane damage (Wang *et al.* 2010b). Diffusion of $HO^\bullet$ through the damaged membrane creates conditions for radical-induced alteration of biologically active cell constituents (Mamane *et al.* 2007).

Wang *et al.* (2010b) determined the fluence-based rate constants of inactivation of *Bacillus subtilis* spores at 172, 222 and 253.7 nm as 0.0023, 0.122 and 0.069 cm^2 mJ^{-1}, respectively. These results indicated quantitatively that VUV light alone is not satisfactory for water and wastewater disinfection, but the combination of the VUV (184.9 nm) and UV (253.7 nm) radiation emitted by the LP lamps would be effective both at micropollutant removal (AOP process) and microorganism inactivation.

The efficiency of the VUV process depends on the $HO^\bullet$ concentration, which is reduced in the presence of radical scavengers, such as NOM. Liu and Ogden (2010) reported a faster inactivation of *Xanthomonas* species in pure water under VUV (184.9 nm)/UV (253.7 nm) than under UV (253.7 nm) irradiation. Zoschke *et al.* (2012) examined the inactivation of coliforms and *Escherichia coli* under VUV/UV and UV irradiation in drinking water, and observed no significant difference in the results. Similar conclusions were drawn on the inactivation of *Bacillus subtilis* spores. The authors explained the results as an impact of the $HO^\bullet$ scavengers, which makes the contribution of the 184.9 nm radiation to the microorganism inactivation negligible, such that the disinfection is achieved mostly by the 253.7 nm light. Moreover, the regrowth potential after VUV/UV exposure was somewhat higher than after the UV alone due to

the formation of lower molecular weight compounds during the VUV-radical-initiated oxidation of the organics in the water matrix (Zoschke *et al.* 2012).

Ochiai *et al.* (2013a) compared the efficacy of the combination of two AOPs, namely, UV (253.7 nm)/TiO_2-mesh filter/O_3 and VUV (172 nm)/TiO_2-mesh filter at the contaminant removal and waterborne pathogen inactivation. The authors concluded that the VUV/TiO_2 process was more effective at pollutant removal than the UV (253.7 nm)/TiO_2-mesh filter/O_3 but less efficient for *Escherichia coli* inactivation both in laboratory water and in sewage effluents.

5.6 REACTOR/EQUIPMENT DESIGN AND ECONOMIC CONSIDERATIONS

5.6.1 Actinometry for VUV photon flow measurements

In order to design a photoreactor, the incident photon flow must be known. A chemical system that undergoes a light-induced reaction at a certain wavelength, for which the quantum yield is known and the measuring of the reaction rate allows the calculation of the absorbed photon flux, can be used as an actinometer. It has to be simple to use, easy to reproduce and should not require special equipment. The quantum yield of the actinometer reaction should be independent of the reactant concentration and light intensity, and, if any, its temperature dependence should be known.

Gas- and liquid-phase chemical actinometers are used to quantify the incident photon flows of VUV radiation. László *et al.* (1998) determined the radiation power of a Xe_2* lamp (172 nm) by indirect O_2 actinometry, following the O_3 formation from O_2. Model calculations led to a simple correlation between the quantum yield of O_3 formation and the concentrations of O_3 and O_2 at room temperature ($\Phi = 2–1.10\ [O_3]/[O_2]^{1.94}$). This method was also used by Vicente *et al.* (2009) in a cascade reactor system.

Three liquid-phase chemical actinometers are described for 184.9 nm and 172 nm VUV light (Kuhn *et al.* (2004)). Ethanol/water actinometer (Farkas & Hirshberg, 1937), known as Farkas actinometer, is based on gas chromatography (GC) analysis of H_2 formed during ethanol photolysis (184.9 nm) in water. Because of the $\Phi(H_2)$ dependence on ethanol concentration, this method is not used routinely. Adam and Oppenländer (1984) used a reproducible method based on *cis-trans* photo-isomerization of *cis*-cyclooctene to quantify the 184.9 nm radiation. The concentration of *cis*-cyclooctene was followed by GC analysis. Due to the formation of minor degradation products after ~20 min of irradiation, this actinometer was described as suitable only for short irradiation times.

Nowadays methanol is the most commonly used actinometer for VUV radiation. Heit *et al.* (1998) described for the first time the actinometer based on methanol degradation, using a Xe_2* lamp (172 nm). The authors determined the quantum yield for water photolysis from the experimental rate of methanol degradation and the rate of $HO^\bullet$ production. The overall quantum yield of water photolysis ($\Phi(H_2O)$) at 172 nm was found as 0.42 ± 0.04 (Heit *et al.* 1998). This methanol actinometer was calibrated against the *cis*-cyclooctene actinometer. Oppenländer and Schwarzwälder (2002) determined the photon flow emitted from a Xe_2* lamp (172 nm) using methanol photolysis in competition kinetics with water photolysis. The degradation kinetics of methanol was found to depend on its initial concentration. At low concentrations ($< 1 \times 10^{-3}$ mol L^{-1}), methanol degradation follows *pseudo*-first-order kinetics, whereas at high concentrations (0.075–0.250 mol L^{-1}) zero-order kinetics is obeyed ($k_0^{obs.} = 4.9 \pm 0.2 \times 10^{-4}$ mol L^{-1} min^{-1}). Under the latter experimental conditions, the VUV photolysis of methanol occurs concomitantly with water VUV photolysis and the $HO^\bullet$-initiated degradation of methanol increases the $k_0^{obs.}$ values (Heit *et al.* 1998; Oppenländer & Schwarzwälder, 2002). The actinometry must be performed in the same reactor which is used for the photodegradation experiments.

In recent years, alternatives to the methanol actinometry were also developed. For example, diamond-based sensors have been developed and tested over a wide spectral range, from the extreme UV (20 nm)

to the near IR region (2400 nm) (Balducci *et al.* 2005), and showed VUV to UV sensitivity ratios larger than 400 (Bergonzo *et al.* 2000), indicating their solar blindness. This is a consequence of the band-gap energy of diamond (5.5 eV), which corresponds to the 225 nm radiation energy, thus the sensor is essentially sensitive only to radiation carrying higher energies, such as 184.9 nm radiation from LP lamps and 172 nm radiation of Xe_2* lamp. Hayashi *et al.* (2005) demonstrated that the output signals from the diamond sensors are reproducible and stable for more than 500 h continuous irradiation from the Xe_2* lamp. Suzuki *et al.* (2006) reported direct measurement data for 184.9 nm radiation from low-pressure mercury lamps used in VUV/O_3 surface dry cleaning process monitored with diamond-based VUV sensor.

Small photoionization lamps operating in the short-VUV spectral region are used in analytical engineering, particularly in gas analysis devices with ionization detectors. These sources are generally Kr_2* or Xe_2* lamps. Budovich and Il'in (2014) described a method to measure the light intensities of Kr_2* (116.5 nm and 123.6 nm) and Xe_2* (129.6 nm and 147.0 nm) photoionization lamps using a flow ionization total absorption chamber operating at atmospheric pressure. The chamber has no window and radiation is directed into the mixture of vapors of volatile organics (e.g., methane, hexane, and/or isobutylene), O_2 and/or N_2, with known individual concentrations. The photon flux is determined indirectly from the measured ionization current, ionization quantum yield, and the fraction of radiation absorbed by the organics. The method proved to be applicable in the wavelength range of 105–147 nm and photon fluxes of $10^5 - 10^{15}$ photon s^{-1}.

5.6.2 Reactor design

Photochemical reactors can be designed in batch, semi-batch or flow-through configurations. Most often the semi-batch configuration (Figure 5.8) is used to study VUV processes, with the lamp placed at the center of a water-cooled, tubular reactor. The VUV lamps are housed by high purity quartz sleeves, to allow high transmittance of the VUV radiation and to be resistant to solarization.

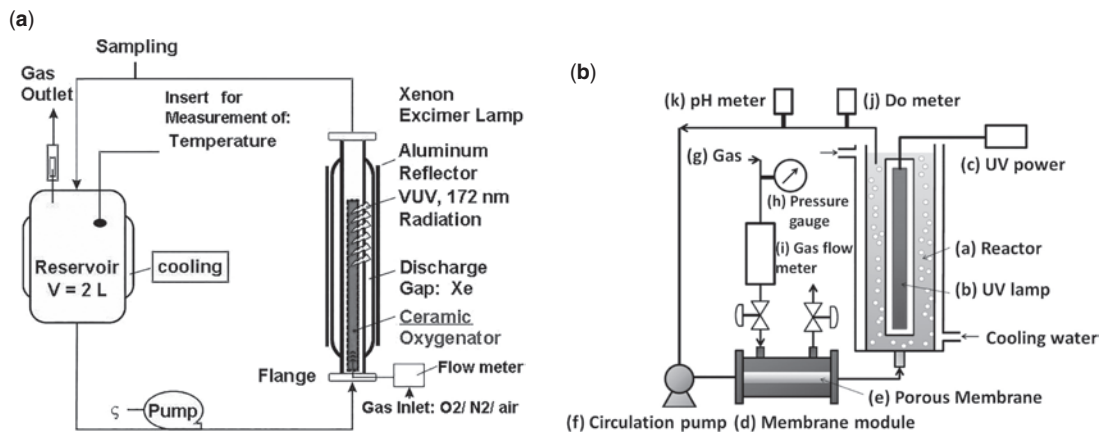

Figure 5.8 (a) Scheme of 100 W photochemical apparatus containing a ceramic gassing unit; (b) Photochemical apparatus containing Shirasu porous glass (SPG) membrane module for microbubble formation. Reprinted with permission from Oppenländer *et al.* (2005) (Fig. 5.8a) and Tasaki *et al.* (2009) (Fig. 5.8b). Copyright Elsevier 2016.

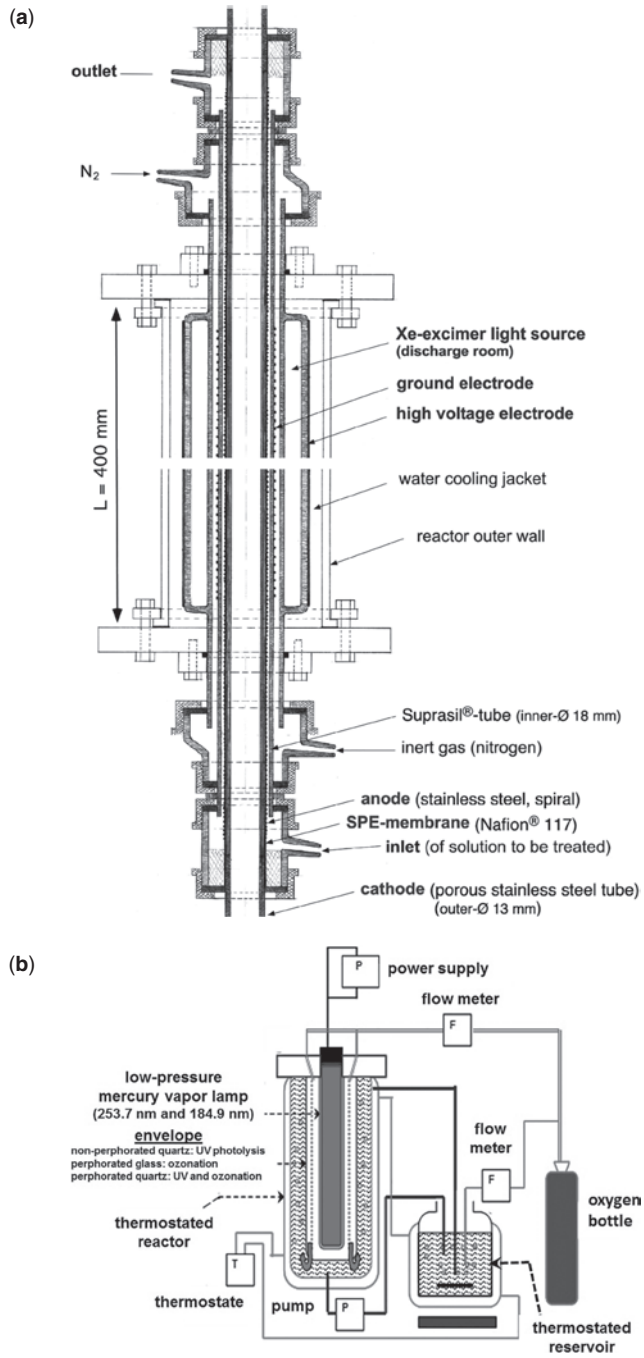

Figure 5.9 (a) Schematic representation of the photochemical reactor combined with electrochemical generation of O_2. Reprinted with permission from Gonzalez *et al.* (2004). Copyright Elsevier 2016. (b) Schematic representation of VUV/UV photochemical reactor with O_3 generation; adapted from Alapi *et al.* (2013).

Completely mixed batch cylindrical vessels are also popular reactor configurations. A typical batch operation requires a chemical storage reservoir and the UV reactor equipped with an O_2 injection port. The reactor chamber is usually surrounded by a cooling jacket.

Given the temperature dependency of the quantum yield of water homolysis, the studies are usually conducted in thermostated reactors. Oppenländer and Xu (2008) demonstrated that the rates of VUV (172 nm)-initiated oxidation and mineralization of methanol in water in a flow-through photoreactor are independent of the water temperature in the 20–50 °C range.

It was shown that the presence of DO has a significant role on the transformation rates of pollutants (Oppenländer *et al.* 2005). Moreover, DO concentration is reduced near to the lamp wall. To reduce the negative effect of the DO demand layer, Han *et al.* (2004) injected O_2 or air through a porous glass plate. This procedure drastically increased the rate of TOC removal. Similarly, Oppenländer *et al.* (2005) used a ceramic oxygenator mounted axially within the Xe_2* lamp, which facilitated the transfer of O_2 directly into the irradiation zone (Figure 5.8a).

Tasaki *et al.* (2009) used uniform-size O_2 microbubbles (average diameter of 5.79 nm) in irradiated solutions of methyl orange (model compound). It was found that the decolorization reaction rate constant in the microbubble system was 2.1 times higher than that in conventional large bubble systems. Photodegradation experiments were conducted with LP lamps (253.7 nm and 184.9/253.7 nm) (Figure 5.8b). The O_2 microbubbles accelerated methyl orange decolorization and TOC reduction rates with 184.9/253.7 nm radiation, but no significant effect was observed on the kinetics for the 253.7 nm radiation.

In situ electrochemical generation of O_2 during the VUV irradiation was experimented by Braun *et al.* (2004) and Wörner *et al.* (2003). This method resulted in fast mineralization of the studied organic compounds. In this case, the mass transfer limitations were overcome *via* electrochemical generation of O_2 within or close to the irradiated volume and with optimum reactor design (Figure 5.9a).

As mentioned briefly earlier in this chapter, VUV radiation emitted from the LP lamps can be used for O_3 generation from O_2 in gas phase. Figure 5.9b shows a reactor configuration where ozone is generated in the air/oxygen atmosphere within the quartz sleeve housing the VUV/UV lamp. The O_3 containing gas is passed through the irradiated solution, where the photolysis of O_3 at 253.7 nm radiation results in $HO^{\bullet}$ formation, such that the conditions for UV/O_3 treatment are created. This reactor configuration was used by Zhao *et al.* (2013) and Alapi *et al.* (2013).

Oppenländer *et al.* (1995) used the combination of 172 nm (VUV) and 222 nm (UV) radiation in a VUV/UV-excimer flow through photoreactor for wastewater treatment. The VUV/UV-excimer "double irradiation" unit consisted of coupled Xe_2* and KrCl* light sources. The results showed more effective photomineralization of organics in this "double radiation" than in single-radiation configuration. The 172 nm irradiation of pure water saturated with either air or O_2, led to *in situ* generation of both H_2O_2 and O_3. Therefore, the VUV/UV-oxidation process in excimer flow-through photoreactor could combine the advantages of multiple photo-oxidation processes (H_2O_2/O_3/UV) without the addition of chemical oxidizing agents.

Alekseev *et al.* (2006) constructed a flow-through reactor suitable for irradiation of gases and solutions at pressures up to 40 atm. They used a sealed single barrier Xe_2* lamp with about 700 cm^2 radiation surface. The mean VUV radiation power was found to be inversely proportional with the lamp temperature.

Dobrovic *et al.* (2007) investigated the effect of Reynolds number on the rate of NOM transformation in a flow-through VUV/UV reactor. In the presence of 184.9 nm radiation (VUV/UV process), the overall degradation rate increased ten-fold and seventeen-fold, at lower and at higher Reynolds numbers, respectively, as compared to the UV (253.7 nm) process under the same flow conditions. This proved that

the hydrodynamic characteristics of the photoreactor are important for the overall energy efficiency of the VUV treatment. Al-Gharabli *et al.* (2016) compared the effect of flow rate on the efficiency of Rhodamine B transformation using either low-pressure mercury lamp or Xe_2* lamp. No flowrate effect was found in the 184.9/253.7 nm tests, whereas the hydrodynamics played a significant role in 172 nm-based tests, which indicates an enhanced mass transfer into the photoreaction zone with increasing flow rate, particularly required for very narrow photoreaction zones as in the case of 172 nm radiation.

Bagheri and Mohseni (2015b) stressed the role of flowrate on the VUV AOP performance, based on the profiles and distribution of $HO^{\bullet}$ in the VUV (184.9 nm)/UV (253.7 nm) reactor. The computed volume-weighted average $HO^{\bullet}$ concentration was two times higher at 0.5 L min^{-1} than at 6.7 L min^{-1}. Higher $HO^{\bullet}$ concentrations are expected at higher UV doses (i.e., lower flowrates), but the flowrate should be optimized such that extensive mixing is achieved. Degradation rates of micropollutants in the VUV/UV photoreactors are limited by mass transfer in the VUV-irradiated photoreaction zone. The extent of mixing and circulation zones was found to be the key parameter controlling the treatment economics and energy-efficiency (Bagheri & Mohseni, 2015a, 2015b).

5.6.3 Economics considerations

The treatment of organic pollutants is an energy-intensive process, thus the use of an appropriate "figure-of-merit" based on the energy input is justified. The largest part of the treatment costs are the electrical energy costs. Bolton *et al.* (2001) proposed two figures-of-merit, i.e., Electric energy per mass (E_{EM}, kWh kg^{-1}), to evaluate process treatment performance for waters containing high concentrations of pollutants (in which case the zero-order kinetics is obeyed) and the Electric energy per order (E_{EO}, kWh m^{-3} $order^{-1}$) to assess process treatment performance for water containing low micropollutant concentrations (in this case *pseudo*-first order kinetics is followed).

Thomson *et al.* (2004) concluded that the removal of NOM from highly colored surface water by the VUV/UV process is not economically feasible, as an electrical energy dose of 290 kWh m^{-3} was required to reduce the DOC by one order of magnitude. Puspita *et al.* (2011) compared the E_{EO} values for the removal of humic acids from wastewater through the UV (253.7 nm) and VUV/UV (184.9/253.7 nm) processes, with and without the addition of H_2O_2. Under the studied water quality and operating conditions, the determined E_{EO} values (kWh m^{-3} $order^{-1}$) followed the order: 29 (UV) > 15 (VUV/UV) > 5 (UV/H_2O_2 (16 mg L^{-1})) = 5 (VUV/UV/H_2O_2 (16 mg L^{-1})) > 2.5 (UV/H_2O_2 (32 mg L^{-1})).

Andreozzi *et al.* (1999) stated that an E_{EO} of 2.5 kWh m^{-3} $order^{-1}$ would be acceptable for practical treatment of organic micropollutants in water. Matsushita *et al.* (2015) investigated the efficacy of a series of AOPs for the degradation of 1,4-dioxane, geosmin, and MIB in water and found that under the experimental conditions used in that study the process efficiency followed the order: UV/TiO_2 < VUV/UV < VUV/UV/TiO_2. All these processes were assessed as economically feasible, with the best performance determined for the VUV/UV and VUV/UV/TiO_2 AOPs, whose E_{EO} values were lower than 1 kWh m^{-3} $order^{-1}$.

Zoschke *et al.* (2012) calculated the E_{EO} values for the degradation of geosmin and MIB under VUV (184.9 nm)/UV (253.7 nm) irradiation, and compared them with those obtained for the UV/O_3 and UV/H_2O_2 processes. In ultrapure water, all treatments yielded E_{EO} values close or below 1 kWh m^{-3} $order^{-1}$ for both pollutants. In raw water from drinking water reservoir (Saxony, Germany) both pollutants could be removed at ~1.5, ~0.5 and ~3.5 kWh m^{-3} $order^{-1}$ for the VUV/UV, UV/O_3 and UV/H_2O_2 processes, respectively. The O_3 dose in these experiments was 0.9 mg min^{-1}, and O_3 was generated by silent electric discharge. It was also shown, that the E_{EO} values decreased with increasing O_3 dose, and leveled off below 1 kWh m^{-3} $order^{-1}$ at O_3 dosages above 1 mg min^{-1}.

Afzal *et al.* (2010) reported the degradation of the algal toxin anatoxin-a (as fumarate salt) in pure, natural, and synthetic waters using the VUV (172 nm) and UV (253.7 nm)/H_2O_2 treatments. The results showed that an UV dose of ~200 mJ cm^{-2} was sufficient to achieve more than 70% degradation of anatoxin-a with $HO^{\bullet}$-based AOPs (172 nm VUV and UV (253.7 nm)/H_2O_2 (30 mg L^{-1})), whereas an UV (medium-pressure lamp, 200–300 nm range) dose of 1285 mJ cm^{-2} was needed to degrade 88% of 0.6 mg L^{-1} anatoxin-a by direct photolysis.

Bagheri and Mohseni (2015b) used a validated computer model to optimize the energy-efficiency of the VUV/UV process for a variety of reactor configurations. E_{EO}, $HO^{\bullet}$ concentration, and delivered UV and VUV dose distributions were included in the model. The mixing and circulation zones were recognized as key parameters in controlling the treatment economics and energy-efficiency of the VUV/UV process. The authors used a computer-aided reactor design with baffle insertion to control good mixing and circulation zones inside the reactor, which led to up to 72% reduction in the total electrical energy requirement for atrazine degradation *via* VUV/UV treatment. The theoretical predictions were validated experimentally for the optimized reactor/baffle configuration.

5.7 APPLICATIONS OF VACUUM UV LIGHT SOURCES

5.7.1 Applications in instrumental chemical analysis

The instrumentation for TOC analysis in water samples commonly uses the VUV radiation for water photolysis as a means of $HO^{\bullet}$ generation. The process mineralizes the organic carbon present in the water to CO_2 (http://www.lfe.de/en/process-water-analysis/toc-810). Satou *et al.* (2013) used a home-made lamp-pass-through photoreactor with a built-in narrow (2 mm inner diameter) reaction tube passing through a 40 W VUV (184.9 nm)/UV (253.7 nm) LP lamp, for the mineralization of DOM in river water. This "reagent-free" photoreactor was also suitable for TOC analysis of river-water samples. The detection limit was determined as 6.2 μg $C \cdot L^{-1}$ using potassium hydrogen phthalate as a standard compound.

Liquid chromatographs with organic carbon – organic nitrogen detection (LC-OCD-OND) used for the identification and quantification of NOM fractions are equipped with VUV (184.9 nm)/UV (253.7 nm) lamps. The VUV/UV lamp is placed in the so-called Graentzel thin-film reactor which has a light shielded (for inorganic carbon, IC) and a light exposed (for organic carbon, OC) section. For detailed description on the process principle the reader is referred to the manufacturer website (http://www.doc-labor.de/OCD.html). The LC-OCD/OND instruments are widely employed in drinking water, wastewater, and marine water characterization, as well as in steam condensate analysis in power plants. They are also routinely used in analytical laboratories in chemical, pharmaceutical, and semiconductor industry.

Incoherent VUV excimer light is also used for single photon ionization (SPI) in time-of-flight mass spectrometers (TOF-MS). Most common light sources in these instruments are based either on brilliant (focused) lasers, which are expensive, or on conventional VUV deuterium lamps, which have low output. The rare gas excimer VUV lamps do not emit brilliant radiation, therefore they are not suitable for this application without further modification. Muhlberger *et al.* (2002) generated compact brilliant VUV light using electron beam excitation of dense rare gases through a thin ceramic foil window. This novel VUV light source was then coupled to a compact and mobile TOF-MS. This device can be adapted for analytical application or monitoring purposes. Chen *et al.* (2014) designed a *quasi*-trapping chemical ionization (QT-CI) source with a commercial VUV 10.6 eV Kr_2* for time-of-flight mass spectrometry. The use of Kr_2* lamp improved the sensitivity and extended the range of ionizable molecules with ionization potential higher than 10.6 eV.

VUV Analytics Inc. (http://www.vuvanalytics.com/) developed a new VUV/UV absorption detector for gas chromatography, which acquires data from ~120 nm to 240 nm. Chemical compounds eluting from the gas chromatograph column enter a heated transfer line. At the end of the transfer line, a makeup flow of carrier gas is introduced, which carries the analyte into the flow cell irradiated by a deuterium lamp. The eluted components absorb light resulting in reduced transmission and a detectable signal. This detector (Vapor Generation Accessory, VGA-100) has claimed the distinguished "Best New Analytical Instrument" award at the Gulf Coast Conference in 2014, emerging from the competitive market of the World's newest scientific instruments.

An application of a KrCl* lamp (222 nm) and a conventional LP lamp (184.9 nm/253.7 nm) was described by Matter *et al.* (1994). They examined how the ionization of the combustion aerosols depends on the electric power of the lamps and on the irradiation time, and showed that particles from different sources (petrol engine, diesel engine, cigarette smoke) can be differentiated by measuring the photocurrent. The advantage of the exciplex lamp is the possibility to rapidly switching off and on, eliminating the time delay in the measurements. This system could be made more compact by the miniaturization of the exciplex lamp (http://www.epa.gov/ordntrnt/ORD/NRMRL/archive-etv/pubs/01_vs_ecochem_pas2000.pdf). These instruments can be used in the field of pollution detection like the analysis of indoor and outdoor air quality or quantification of combustion aerosols, and in air conditioning or fire alarm systems.

Ellipsometers are used for investigating the dielectric properties (complex refractive index or dielectric function) of thin films. This technique has found applications in many different fields, from semiconductor physics to microelectronics and biology, from basic research to industrial applications. The VUV-VASE® spectroscopic ellipsometer is the standard in optical characterization of materials used in lithography applications. Equipped with deuterium, Xe_2* and tungsten halogen lamps, it covers the spectral range from 140 nm up to 1700 nm (http://www.jawoollam.com/vuv_home.html).

VUV Resonance Fluorescence CO Instrument (VUV-CO) was developed as a commercial version of the instrument described by Gerbig *et al.* (1999). It quantitatively determines airborne CO using resonant fluorescent (RF) discharge gas lamp emitting in the VUV range. The narrow emission band centered at 151 nm is achieved using an optical filter and CO fluorescence is detected by photon counting. The instrument was integrated into the HAIS O_3 instrument used within the NASA Airborne Science Program (https://airbornescience.nasa.gov/instrument/VUV-CO).

A new method for explosives detection based on the field asymmetric ion mobility spectrometry (FAIMS) and ionization by an Ar_2* (126 nm) emitter has been developed jointly with a portable detector by Chistyakov *et al.* (2014). Vapor of explosives are introduced into the ionization region containing the Ar_2* lamp. The ions are separated based on their relative mobility. A varying compensation voltage (CV) is applied generating spectra of ion current as a function of CV.

5.7.2 Ultrapure water production

Ultrapure water (UPW) production is one of the most important industrial applications of the VUV process. UPW with strict quality specifications is used in semiconductor, solar photovoltaic, pharmaceutical, and power generation industries, as well as in research laboratories. Point of use (POU) treatment is often applied in critical tool applications such as immersion lithography. Typically wafer manufacture uses ~5500 m^3 city water per day to produce UPW, which is only used once before becoming waste. Recycling rinse water from the semiconductor manufacturing processes has been encouraged. Also, given the increasing water and wastewater treatment costs, the recovery and reuse of spent UPW is currently being investigated (Yazdani, 2016).

UPW is treated to the highest purity from all types of contamination, including organic and inorganic compounds, dissolved and particulate matter, volatiles and non-volatiles, reactive and/or inert species, dissolved gases and bacteria. Treatment steps include gross filtration for large particulate removal, carbon filtration, water softening, reverse osmosis (RO), VUV/UV process for TOC reduction and disinfection, ion exchange or electrodeionization, heat exchange and finally, filtration or ultrafiltration. Depending on the required water quality, UPW treatment plants often also feature degassing, microfiltration, and ultrafiltration (Figure 5.10).

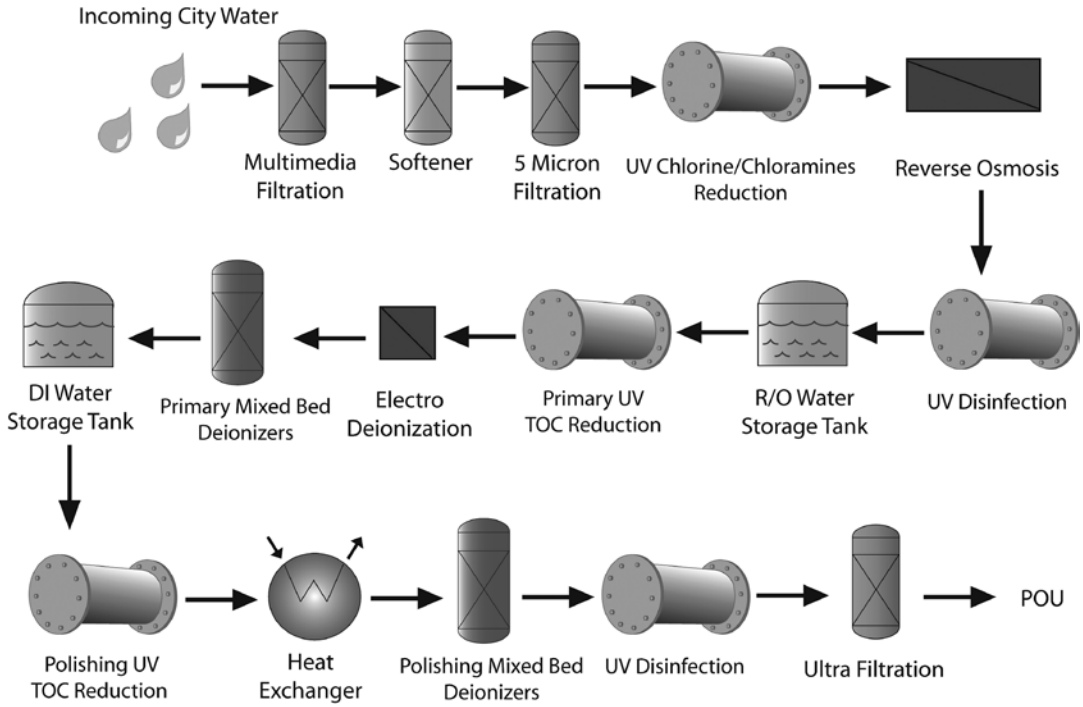

Figure 5.10 Microelectronics water treatment process (courtesy of Aquafine Corporation, Valencia, CA).

The biofilm potentially formed onto RO membranes causes operational problems such as decrease in the membrane water flux, and increased operating pressure. Bohus *et al.* (2010) conducted microbiological investigations at an industrial UPW treatment plant and found that most of the identified bacteria could contribute to microbial-induced corrosion of semiconductor industry products.

Particles, which can cause defects in photolithography products, are controlled through filtration and ultrafiltration. TOC contributes to bacterial proliferation by providing nutrients and, in severe cases, leaves unwanted residues on products and product lines. Water entering the UPW purification system can contain TOC levels between 0.7–15 mg/L (ppm). Removal of TOC requires activated carbon filtration, RO, intermediate oxidation processes, and finally the VUV/UV process to decrease it typically below 1 μg/L (ppb), preferably below 0.5 ppb. Elimination of metallic and anionic (mainly silica) contaminants by ion exchange or electrodeionization and dissolved gases (O_2, O_3 and CO_2) is also required.

Typically, city water feed containing several unwanted contaminants and chlorine as a disinfectant is taken through a series of purification steps depending on the UPW specifications. UPW systems generally consist of

three subsystems, i.e., pretreatment, primary treatment, and polishing. Pretreatment produces purified water by using multimedia filtration and ultrafiltration to remove suspended solids and to reduce turbidity, as well as activated carbon for chlorine removal and organic loading reduction. Commercially available activated carbon can effectively remove large non-polar molecules, but shows low removal efficiency for low molecular weight neutral compounds, such as isopropyl alcohol (IPA) and acetone; acetone is the IPA oxidation by-product. Among the most difficult-to-treat compounds in UPW production are urea, trihalomethanes, and low molecular weight neutral compounds, such as acetone. The elimination of chloroform and bromoform is important in minimizing the TOC level. The efficiency of RO followed by UV disinfection can be enhanced by increasing the pH, which results in improved rejection rate of both organics and boron.

The primary treatment (see Figure 5.10) for residual TOC reduction is based on the VUV/UV process, with or without oxidant addition (e.g., sodium persulfate or H_2O_2). Persulfate use is limited as both persulfate residual and sulfate are UPW ionic contaminants. The VUV/UV process efficiency is impacted by suspended solids (light shadowing effect), the presence of Fe^{2+} and Mn^{2+}, which are limited to 0.3 ppm and 0.05 ppm, respectively, to avoid discoloration of quartz housing the VUV/UV lamps, turbidity, and lamp sleeve fouling. Still, the advantages of VUV/UV primary treatment far outweigh these limitations (http://www.prudentialtechgy.com/data/TOC-reduction-article-JD.pdf). Gareth and Avijit (2003) discussed the removal of THMs, particularly of chloroform which was found in RO permeate, and showed the role of 184.9 nm radiation in $CHCl_3$ removal. Another option is the use of heat exchangers, which enable the gas transfer membranes to extract the volatile organics formed, thus reducing residual TOC level. During the primary treatment step, IPA is very efficiently degraded to acetone.

Polishing system established for the final treatment steps (VUV/UV photolysis for TOC reduction, heat exchange, deionization, final disinfection by UV light and ultrafiltration) includes a recirculation and distribution system in order to maintain stable and high quality UPW. High quality UPW is characterized by high resistivity, typically ~18 MΩ cm. When the TOC is less than 1 ppm and the water is saturated with O_2, the VUV/UV process is effective at oxidizing the organics to CO_2. TOC level below 0.5 ppb can be reached using VUV/UV lamps having high output at 184.9 nm (Baas, 2003). Mineralization of TOC results in resistivity drop and ionization of some organics, therefore a deionizer is also required in the polishing system. The oxidative degradation of organics generates CO_2, which is eliminated by degasifier.

Today, the semiconductor manufacturing processes demand typically < 1 ppb (preferably 0.5 ppb) TOC. Aquafine Corporation, a Trojan Technologies business, manufactures VUV (184.9 nm)/UV (253.7 nm)-lamp based reactors which provide an enhanced, synergistic effect toward the reduction of trace organics and microbial contamination for UPW production. These systems are used in applications for TOC reduction, disinfection, ozone (commonly used in the pre-treatment step, as well as for sanitizing process and re-circulating systems) destruction, and chlorine/chloramines removal. Aquafine Corporation also offers UV/H_2O_2-based advanced oxidation solutions for remediation and reuse of spent rinse water, which translates into significant cost savings to utilities and reduces the waste disposal.

There are increasing requirements for TOC reduction (<100 ppb) in industrial water used at nuclear power plants in order to prevent the formation of corroding acids in the steam used to drive the power generating turbines. The system developed and installed by Aquafine for Frosmark nuclear power plant (Sweden) is operated at 2.7 kW and at flow rate of 58 $m^3\ h^{-1}$ (http://www.aquafineuv.com).

Evoqua introduced a high flow solution specifically for TOC reduction. The Vanox AOP System can consistently reduce TOC to 0.5 ppb and treat seasonal TOC variations in feed water (http://www.evoqua.com). Species, such as urea, THMs, 1,4-dioxane and IPA are efficiently eliminated with this system. The UPW produced by Vanox AOP Systems contains low levels of particles (<100 units/L, 0.05 μm average diameter) and low residual metal levels (<1.0 ng/L (ppt)).

UPW is also extensively used in analytical chemistry and fundamental research. EMD Millipore (Darmstadt, Germany) manufactures a wide range of Milli-Q® water systems producing high quality UPW (Milli-Q water, resistivity > 18 MΩ, < 4 µg/L TOC) using tap water as feed water. The system contains pretreatment units including RO, electrodeionization and UV irradiation for disinfection, and a polishing system. The polishing system contains two VUV (184.9 nm)/UV (253.7 nm) LP lamps. The first is designed for TOC reduction, and the second one is part of the in-line TOC analyzer. The TOC is determined from the difference between the resistivity of the water before and after the VUV/UV photooxidation.

5.8 VACUUM UV AOP – GENERAL CONCLUSIONS

VUV photolysis is a simple and clean method to produce high concentrations of $HO^{\bullet}$ in water without the addition of oxidizing agents. The overall yield of $HO^{\bullet}$ in VUV photolysis of water is much higher than in any other AOPs, because water is the main absorber. However, its application to water treatment is limited, mainly because of the short penetration depth of VUV radiation and inhomogeneity of aqueous VUV systems. Various studies have shown that the irradiation of water by VUV light results in a fast degradation of organic micropollutants and a sequential decomposition of larger NOM structures. Moreover, VUV light sources offer the possibility for the combination of the VUV photolysis with ozonation, when O_3 is photochemically generated from O_2 in the gas phase. Thus, application of external ozone generator can be avoided. Although the VUV photolysis enhances the formation of NO_2^- which is an inorganic by-product of concern in drinking water, the combination of VUV irradiation and O_3 generated by the same lamp enhances the oxidation and disinfection efficiencies of the system and minimizes the formation of NO_2^-.

Currently, the LP lamps with high quality quartz envelopes are used as VUV light sources. Thus, disinfection due to the germicidal effect of UV light and mineralization of organic substances *via* generation of $HO^{\bullet}$ due to the 184.9 nm light can be simultaneously achieved. Moreover, addition of H_2O_2 enhances the efficiency of the VUV/UV process due to the UV photolysis of H_2O_2 to $HO^{\bullet}$.

The VUV excimer lamps offer new opportunities for expanding the VUV AOP applications and develop versatile reactor designs. Excimer lamps have several advantages over mercury vapor-based lamps, among which, they are mercury-free, have high photon flux, sharp emission lines, instant on-off switch without UV power losses, and their geometry can be adapted to various reactor configurations. Further development of VUV excimer lamps opens up new dimensions in water treatment.

Despite current limitations, the VUV AOP could be a viable solution for niche applications, such as on-site treatment of industrial wastewater for biodegradability enhancement, and in small residential equipment for concomitant chemical micropollutant destruction and disinfection, in combination with post-VUV activated carbon filtration.

However, at first, the VUV AOP has to evolve from lab-scale experimentation to full-scale implementation. Among others, research is needed on VUV lamp efficiency enhancement, optimization of photoreactor concepts and design to counter-balance the short VUV radiation penetration depth by optimized hydrodynamics and mass transfer into the photoreaction zone, development of reliable kinetic models for equipment sizing and performance guarantee.

5.9 ACKNOWLEDGEMENTS

The authors would like to thank Prof. Dr. Thomas Oppenländer and Dr. Mihaela Stefan for their valuable contributions to this chapter. Special thanks to Prof. Dr. André Braun and Dr. Masato Kukizaki for providing the high quality diagrams of the VUV reactors used in their works (reproduced with permission from Elsevier as Figure 5.9a and 5.9b in this chapter).

5.10 REFERENCES

Adam W. and Oppenländer T. (1984). Absolute intensity method for the determination of quantum yields in 185 nm photochemistry: application to the azoalkane 2,3-diazabicyclo[2.2.1]hept-2-ene. *Photochemistry and Photobiology*, **39**(6), 719–723.

Afzal A., Oppenländer T., Bolton J. R. and El-Din M. G. (2010). Anatoxin-a degradation by advanced oxidation processes: vacuum-UV at 172 nm, photolysis using medium pressure UV and UV/H_2O_2. *Water Research*, **44**(1), 278–286.

Alapi T. and Dombi A. (2007). Comparative study of the UV and UV/VUV-induced photolysis of phenol in aqueous solution. *Journal of Photochemistry and Photobiology A: Chemistry*, **188**(2–3), 409–418.

Alapi T., Berecz L. and Arany E. (2013). Comparison of the UV-induced photolysis, ozonation, and their combination at the same energy input using a self-devised experimental apparatus. *Ozone Science and Engineering*, **35**(5), 350–358.

Alekseev S. B., Kuvshinov V. A., Lisenko A. A., Lomaev M. I., Orlovskii V. M., Panarin V. A., Rozhdestvenskii E. A., Skakun V. S. and Tarasenko V. F. (2006). A photoreactor on the basis of a Xe_2 excilamp. *Instruments and Experimental Techniques*, **49**(1), 132–134.

Al-Gharabli S., Engesser P., Gera D., Klein S. and Oppenländer T. (2016). Engineering of a highly efficient Xe_2*-excilamp (xenon excimer lamp, λ_{max} = 172 nm, η = 40%) and qualitative comparison to a low-pressure mercury lamp (LP-Hg, λ = 185/254 nm) for water purification. *Chemosphere*, **144**, 811–815.

Al-Momani F., Touraud E., Degorce-Dumas J. R., Roussy J. and Thomas O. (2002). Biodegradability enhancement of textile dyes and textile wastewater by VUV photolysis. *Journal of Photochemistry and Photobiology A: Chemistry*, **153**(1–3), 191–197.

Andreozzi R., Caprio V., Insola A. and Marotta R. (1999). Advanced oxidation processes (AOP) for water purification and recovery. *Catalysis Today*, **53**, 51–59.

Arany E., Oppenländer T., Gajda-Schrantz K. and Dombi A. (2012). Influence of H_2O_2 formed in situ on the photodegradation of ibuprofen and ketoprofen. *Current Physical Chemistry*, **2**(3), 286–293.

Arany E., Szabó R. K., Apáti L., Alapi T., Ilisz I., Mazellier P., Dombi A. and Gajda-Schrantz K. (2013). Degradation of naproxen by UV, VUV photolysis and their combination. *Journal of Hazardous Materials*, **262**, 151–157.

Arany E., Alapi T. and Schrantz K. (2015). Reactive Species against Selected Nonsteroidal Anti-inflammatory Drugs. Lap Lambert Academic Publishing, Saarbrücken, Germany.

Atkinson R., Baulch D. L., Cox R. A., Crowley J. N., Hampson R. F., Hynes R. G., Jenkin M. E., Rossi M. J. and Troe J. (2004). Evaluated kinetic and photochemical data for atmospheric chemistry: volume I gas phase reactions of O_x, HO_x, NO_x and SO_x species. *Atmospheric Chemistry and Physics*, **4**, 1461–1738.

Avdeev S. M., Sosnin É. A., Skakun V. S., Tarasenko V. F. and Schitz D. V. (2008). Two-band emission source based on a three-barrier KrCl-XeBr excilamp. *Technical Physics Letters*, **34**(9), 725–727.

Avtaeva S. V., Sosnin E. A., Saghi B., Panarin V. A. and Rahmani B. (2013). Influence of the chlorine concentration on the radiation efficiency of a XeCl exciplex lamp. *Plasma Physics Reports*, **39**(9), 768–778.

Azrague K., Bonnefille E., Pradines V., Pimienta V., Oliveros E., Maurette M. T. and Benoit-Marquie F. (2005). Hydrogen peroxide evolution during V-UV photolysis of water. *Photochemical & Photobiological Sciences*, **4**(5), 406–408.

Baadj S., Harrache Z. and Belasri A. (2013). Electrical and chemical properties of XeCl* (308 nm) exciplex lamp created by a dielectric barrier discharge. *Plasma Physics Reports*, **39**(12), 1043–1054.

Baas M. (2003). Enhanced 185 nm UV-source to achieve a TOC reduction below 1 ppb. *Ultrapure Water*, **20**, 26–30.

Bagheri M. and Mohseni M. (2015a). Impact of hydrodynamics on pollutant degradation and energy efficiency of VUV/UV and H_2O_2/UV oxidation processes. *Journal of Environmental Management*, **164**, 114–120.

Bagheri M. and Mohseni M. (2015b). A study of enhanced performance of VUV/UV process for the degradation of micropollutants from contaminated water. *Journal of Hazardous Materials*, **294**, 1–8.

Balducci A., Marinellia M., Milani E., Morgada M. E., Tucciarone A. and Verona-Rinati G. (2005). Extreme ultraviolet single-crystal diamond detectors by chemical vapor deposition. *Applied Physics Letters*, **86**(19), 193509.

Baricholo P., Hlatywayo D. J., Von Bergmann H. M., Stehmann T., Rohwer E. G. and Collier M. (2011). Influence of gas discharge parameters on emissions from a dielectric barrier discharge excited argon excimer lamp. *The South African Journal of Science*, **107**(11–12), 46–52.

Barrett J. and Baxendale J. H. (1960). The photolysis of liquid water. *Transactions of the Faraday Society*, **56**, 37–43.

Barrett J. and Mansell A. L. (1960). Ultraviolet absorption spectra of the molecules H_2O, HDO and D_2O. *Nature*, **187**, 138–139.

Baum G. and Oppenländer T. (1995). Vacuum-UV-oxidation of chloroorganic compounds in an excimer flow-through photoreactor. *Chemosphere*, **30**(9), 1781–1790.

Beleznai S., Mihajlik G., Agod A., Maros I., Juhász R., Németh Z., Jakab L. and Richter P. (2006). High-efficiency dielectric barrier Xe discharge lamp: theoretical and experimental investigations. *Journal of Physics D: Applied Physics*, **39**(17), 3777–3787.

Beleznai S., Mihajlik G., Maros I., Balázs L. and Richter P. (2008). Improving the efficiency of a fluorescent Xe dielectric barrier light source using short pulse excitation. *Journal of Physics D: Applied Physics*, **41**(11), 115202.

Bergonzo P., Brambilla A., Tromson D., Mer C., Guizard B. and Foulon F. (2000). Diamond devices as characterisation tools for novel photon sources. *Applied Surface Science*, **154–155**, 179–185.

Bielski B. H. J., Cabelli D. E., Arudi R. L. and Ross A. B. (1985). Reactivity of HO_2/O_2^- radicals in aqueous-solution. *Journal of Physical and Chemical Reference Data*, **14**(4), 1041–1100.

Bolton J. R., Bircher K. G., Tuman W. and Tolman C. A. (2001). Figure-of-merit for the technical developement and application of advanced oxidation technologies for both electric- and solar-driven systems. *Pure and Applied Chemistry*, **73**(4), 627–637.

Bonin J., Janik I., Janik D. and Bartels D. M. (2007). Reaction of the hydroxyl radical with phenol in water up to supercritical conditions. *The Journal of Physical Chemistry A*, **111**(10), 1869–1878.

Braslavsky S. E. (2007). Glossary of terms used in photochemistry, 3rd edition (IUPAC Recommendations 2006). *Pure and Applied Chemistry*, **79**(3), 293–465.

Braun A. M., Pintori I. G., Popp H. P., Wakahata Y. and Worner M. (2004). Technical development of UV-C- and VUV-photochemically induced oxidative degradation processes. *Water Science and Technology*, **49**(4), 235–240.

Buchanan W., Roddick F., Porter N. and Drikas M. (2005). Fractionation of UV and VUV pretreated natural organic matter from drinking water. *Environmental Science & Technology*, **39**(12), 4647–4654.

Buchanan W., Roddick F. and Porter N. (2006). Formation of hazardous by-products resulting from the irradiation of natural organic matter: comparison between UV and VUV irradiation. *Chemosphere*, **63**(7), 1130–1141.

Buchanan W., Roddick F. and Porter N. (2008). Removal of VUV pre-treated natural organic matter by biologically activated carbon columns. *Water Research*, **42**(13), 3335–3342.

Budovich V. L. and Il'in V. P. (2014). Measurements of the intensities of vacuum ultraviolet radiation sources using the flow ionization chamber. *Instruments and Experimental Techniques*, **57**(2), 195–200.

Buxton G. V., Greenstock C. L., Helman W. P. and Ross A. B. (1988). Critical-review of rate constants for reactions of hydrated electrons, hydrogen-atoms and hydroxyl radicals ($\bullet OH/\bullet O^-$) in aqueous-solution. *Journal of Physical and Chemical Reference Data*, **17**(2), 513–886.

Cao M. H., Wang B. B., Yu H. S., Wang L. L., Yuan S. H. and Chen J. (2010). Photochemical decomposition of perfluorooctanoic acid in aqueous periodate with VUV and UV light irradiation. *Journal of Hazardous Materials*, **179**(1–3), 1143–1146.

Carman R. J. and Mildren R. P. (2003). Computer modelling of a short-pulse excited dielectric barrier discharge xenon excimer lamp ($\lambda \sim 172$ nm). *Journal of Physics D: Applied Physics*, **36**(1), 19–33.

Chen J., Zhang P. and Liu J. (2007). Photodegradation of perfluorooctanoic acid by 185 nm vacuum ultraviolet light. *Journal of Environmental Sciences*, **19**(4), 387–390.

Chen P., Hou K., Hua L., Xie Y., Zhao W., Chen W., Chen C. and Li H. (2014). Quasi-trapping chemical ionization source based on a commercial VUV lamp for time-of-flight mass spectrometry. *Analytical Chemistry*, **86**(3), 1332–1336.

Chistyakov A. A., Kotkovskii G. E., Sychev A. V. and Budovich V. L. (2014). An excimer-based FAIMS detector for detection of ultra-low concentration of explosives. Conference: SPIE Defense + Security. Chromdet/Analytical Instruments, Russia.

Collivignarelli C. and Sorlini S. (2004). AOPs with ozone and UV radiation in drinking water: contaminants removal and effects on disinfection byproducts formation. *Water Science and Technology*, **49**(4), 51–56.

Crapulli F., Santoro D., Sasges M. R. and Ray A. K. (2014). Mechanistic modeling of vacuum UV advanced oxidation process in an annular photoreactor. *Water Research*, **64**, 209–225.

Dainton F. S. and Fowles P. (1965). The photolysis of aqueous systems at 1849 Å. I. Solutions containing nitrous oxide. *Proceedings of Royal Society*, **A287**, 295–311.

Dobrovic S., Juretic H. and Ruzinski N. (2007). Photodegradation of natural organic matter in water with UV irradiation at 185 and 254 nm: importance of hydrodynamic conditions on the decomposition rate. *Separation Science and Technology*, **42**(7), 1421–1432.

Dombi A., Ilisz I., László Z. and Wittmann G. (2002). Comparison of ozone-based and other (VUV and TiO_2/UV) radical generation methods in phenol decomposition. *Ozone Science and Engineering*, **24**(1), 49–54.

Dwibedy P., Dey G. R., Naik D. B., Kishore K. and Moorthy P. N. (1999). Pulse radiolysis studies on redox reactions of gallic acid: one electron oxidation of gallic acid by gallic acid OH adduct. *Physical Chemistry Chemical Physics*, **1**(8), 1915–1918.

Echigo S., Yamada H., Matsui S., Kawanishi S. and Shishida K. (1996). Comparison between O_3/VUV, O_3/H_2O_2, VUV and O_3 processes for the decomposition of organophosphoric acid triesters. *Water Science and Technology*, **34**(9), 81–88.

Eliasson B. and Kogelschatz U. (1988). UV excimer radiation from dielectric-barrier discharges. *Applied Physics B-Photo*, **46**(4), 299–303.

Eliasson B. and Kogelschatz U. (1991). Modeling and applications of silent discharge plasmas. *IEEE Transactions on Plasma Science*, **19**(2), 309–323.

Elsner C., Lenk M., Prager L. and Mehnert R. (2006). Windowless argon excimer source for surface modification. *Applied Surface Science*, **252**(10), 3616–3624.

Erofeev M. V., Schitz D. V., Skakun V. S., Sosnin E. A. and Tarasenko V. F. (2010). Compact dielectric barrier discharge excilamps. *Physica Scripta*, **82**(4), 045403.

Farkas L. and Hirshberg Y. (1937). The photochemical decomposition of aliphatic alcohols in aqueous solution. *Journal of the American Chemical Society*, **59**(11), 2450–2453.

Gareth T. and Avijit D. (2003). Removal of trihalomethanes from RO product water using UV 185 nm technology. *Ultrapure Water*, **20**, 18–22.

Gellert B. and Kogelschatz U. (1991). Generation of excimer emission in dielectric barrier discharges. *Applied Physics B-Photo*, **52**(1), 14–21.

Gerasimov G. N., Volkova G. A., Hallin R., Zvereva G. N. and Heikensheld F. (2000). VUV spectrum of the barrier discharge in a krypton-xenon mixture. *Optics and Spectroscopy*, **88**(6), 814–818.

Gerasimov G. N., Krylov B. E., Hallin R., Morozov A. O., Arnesen A. and Heijkenskjold F. (2002). Stimulated emission of inert gas mixtures in the VUV range. *Optics and Spectroscopy*, **92**(2), 290–297.

Gerasimov G. N., Krylov B. E., Hallin R., Morozov A. O., Arnesen A. and Heijkenskjold F. (2003). Vacuum ultraviolet spectra of heteronuclear dimers of inert gases in a direct-current discharge. *Optics and Spectroscopy*, **94**(3), 374–383.

Gerasimov G. N., Krylov B. E., Hallin R. and Arnesen A. (2006). Parameters of VUV radiation from a DC capillary discharge in a mixture of krypton with xenon. *Optics and Spectroscopy*, **100**(6), 825–829.

Gerbig C., Schmitgen S., Kley D., Volz-Thomas A., Dewey K. and Haaks D. (1999). An improved fast-response vacuum-UV resonance fluorescence CO instrument. *Journal of Geophysical Research*, **104**(D1), 1699–1704.

Getoff N. (1990). Decomposition of biological resistant pollutants in water by irradiation. *Radiation Physics and Chemistry*, **35**, 432–439.

Getoff N. (1996). Radiation-induced degradation of water pollutants – state of the art. *Radiation Physics and Chemistry*, **47**(4), 581–593.

Getoff N. and Schenck G. O. (1968). Primary products of liquid water photolysis at 1236 Å, 1470 Å and 1849 Å. *Journal of Photochemistry and Photobiology A: Chemistry*, **8**, 167–178.

Giri R. R., Ozaki H., Morigaki T., Taniguchi S. and Takanami R. (2011a). UV photolysis of perfluorooctanoic acid (PFOA) in dilute aqueous solution. *Water Science and Technology*, **9**, 276–282.

Giri R. R., Ozaki H., Okada T., Takikita S., Taniguchi S. and Takanami R. (2011b). Water matrix effect on UV photodegradation of perfluorooctanoic acid. *Water Science and Technology*, **64**(10), 1980–1986.

Giri R. R., Ozaki H., Okada T., Taniguchi S. and Takanami R. (2012). Factors influencing UV photodecomposition of perfluorooctanoic acid in water. *Chemical Engineering Journal*, **180**, 197–203.

Goldstein S., Aschengrau D., Diamant Y. and Rabani J. (2007). Photolysis of aqueous H_2O_2: quantum yield and applications for polychromatic UV actinometry in photoreactors. *Environmental Science & Technology*, **41**(21), 7486–7490.

Gonzalez M. C. and Braun A. M. (1995). VUV photolysis of aqueous solutions of nitrate and nitrite. *Research on Chemical Intermediates*, **21**, 837–859.

Gonzalez M. C. and Braun A. M. (1996). Vacuum-UV photolysis of aqueous solutions of nitrate: effect of organic matter I. Phenol. *Journal of Photochemistry and Photobiology A: Chemistry*, **93**, 7–19.

Gonzalez M. C., Braun A. M., Prevot A. B. and Pelizzetti E. (1994). Vacuum-ultraviolet (VUV) photolysis of water - mineralization of atrazine. *Chemosphere*, **28**(12), 2121–2127.

Gonzalez M. C., Hashem T. M., Jakob L. and Braun A. M. (1995). Oxidative-degradation of nitrogen-containing organic-compounds – Vacuum-ultraviolet (VUV) photolysis of aqueous-solutions of 3-amino 5-methylisoxazole. *Fresenius J. Anal. Chem.*, **351**(1), 92–97.

Gonzalez M. C., Oliveros E., Worner M. and Braun A. (2004). Vacuum-ultraviolet photolysis of aqueous reaction systems. *Journal of Photochemistry and Photobiology C: Photochemistry Reviews*, **5**(3), 225–246.

Gu X., Lu S., Qiu Z., Sui Q., Banks C. J., Imai T., Lin K. and Luo Q. (2013). Photodegradation performance of 1,1,1-trichloroethane in aqueous solution: in the presence and absence of persulfate. *Chemical Engineering Journal*, **215–216**, 29–35.

Halmann M. and Platzner I. (1965). The photochemistry of phosphorus compounds. Part III. Photolysis of ethyl dihydrogen phosphate in aqueous solution. *Journal of the Chemical Society*, **1440**, 5380–5385.

Han W., Zhang P., Zhu W., Yin J. and Li L. (2004). Photocatalysis of p-chlorobenzoic acid in aqueous solution under irradiation of 254 nm and 185 nm UV light. *Water Research*, **38**(19), 4197–4203.

Hashem T. M., Zirlewagen M. and Braum A. M. (1997). Simultaneous photochemical generation of ozone in the gas phase and photolysis of aqueous reaction systems using one VUV light source. *Water Science and Technology*, **35**(4), 41–48.

Hayashi K., Tachibana T., Kawakami N., Yokota Y., Kobashi K., Ishihara H., Uchida K., Nippashi K. and Matsuoka M. (2005). Diamond sensors durable for continuously monitoring intense vacuum ultraviolet radiation. *The Japanese Journal of Applied Physics*, **44**(10), 7301–7304.

Hayon E. and McGarvey J. J. (1967). Flash photolysis in the vacuum ultraviolet region of $S_2O_4^{2-}$, CO_3^{2-} and OH^- ions in aqueous solutions. *Journal of Physical Chemistry*, **71**(5), 1472–1477.

Heit G. and Braun A. M. (1996). Spatial resolution of oxygen measurements during VUV-photolysis of aqueous systems. *Journal of Information Recording*, **22**(5–6), 543–546.

Heit G. and Braun A. M. (1997). VUV-photolysis of aqueous systems: spatial differentiation between volumes of primary and secondary reactions. *Water Science and Technology*, **35**(4), 25–30.

Heit G., Neuner A., Saugy P. Y. and Braun A. M. (1998). Vacuum-UV (172 nm) actinometry. The quantum yield of the photolysis of water. *The Journal of Physical Chemistry A*, **102**(28), 5551–5561.

Hoigné J. (1998). Chemistry of aqueous ozone and transformation of pollutants by ozonation and advanced oxidation processes, Part C Quality and treatment of drinking water II. In: The Handbook of Environmental Chemistry, J. Hrubec (ed.), Springer, Berlin.

Huang L., Jing H., Cheng Z. and Dong W. (2013). Different photodegradation behavior of 4-tert-octylphenol under UV and VUV irradiation in aqueous solution. *Journal of Photochemistry and Photobiology A: Chemistry*, **251**, 69–77.

Imoberdorf G. and Mohseni M. (2011). Modeling and experimental evaluation of vacuum-UV photoreactors for water treatment. *Chemical Engineering Science*, **66**(6), 1159–1167.

Imoberdorf G. and Mohseni M. (2012). Kinetic study and modeling of the vacuum-UV photoinduced degradation of 2,4-D. *Chemical Engineering Science*, **187**, 114–122.

Imoberdorf G. and Mohseni M. (2014). Comparative study of the effect of vacuum-ultraviolet irradiation on natural organic matter of different sources. *Journal of Environmental Engineering*, **140**(3), 04013016.

Jakob L., Hashem T. M., Bürki S., Guindy N. M. and Braun A. M. (1993). Vacuum-ultraviolet (VUV) photolysis of water: oxidative degradation of 4-chlorophenol. *Journal of Photochemistry and Photobiology A: Chemistry*, **75**(2), 97–103.

Jin L. and Zhang P. (2015). Photochemical decomposition of perfluorooctane sulfonate (PFOS) in an anoxic alkaline solution by 185 nm vacuum ultraviolet. *Chemical Engineering Journal*, **280**, 241–247.

Khan J. A., He X., Shah N. S., Khan H. M., Hapeshi E., Fatta-Kassinos D. and Dionysiou D. D. (2014). Kinetic and mechanism investigation on the photochemical degradation of atrazine with activated H_2O_2, $S_2O_8^{2-}$ and HSO_5^-. *Chemical Engineering Journal*, **252**(0), 393–403.

Khan J. A., Shah N. S., Nawaz S., Ismail M., Rehman F. and Khan H. M. (2015). Role of e_{aq}^-, $^{\bullet}OH$ and $H^{\bullet}$ in radiolytic degradation of atrazine: a kinetic and mechanistic approach. *Journal of Hazardous Materials*, **288**, 147–157.

Kim I. and Tanaka H. (2009). Photodegradation characteristics of PPCPs in water with UV treatment. *Environment International*, **35**(5), 793–802.

Kitamura M., Mitsuka K. and Sato M. A. (2004). Practical high-power excimer lamp excited by a microwave discharge. *Applied Surface Science*, **79–80**, 507–513.

Kogelschatz U. (1990). Silent discharges for the generation of ultraviolet and vacuum ultraviolet excimer radiation. *Pure and Applied Chemistry*, **62**(9), 1667–1674.

Kogelschatz U. (1992). Silent-discharge driven excimer UV sources and their applications. *Applied Surface Science*, **54**, 410–423.

Kogelschatz U. (2003). Dielectric-barrier discharges: their history, discharge physics, and industrial applications. *Plasma Chemistry and Plasma Processing*, **23**(1), 1–46.

Kogelschatz U. (2004). Excimer lamps: history, discharge physics, and industrial applications. Proceedings of the SPIE 5483, Atomic and Molecular Pulsed Lasers V. Bellingham, WA.

Kogelschatz U. (2012). Ultraviolet excimer radiation from nonequilibrium gas discharges and its application in photophysics, photochemistry and photobiology. *Journal of Optical Technology*, **79**(8), 484–493.

Kogelschatz U., Esrom H., Zhang J. Y. and Boyd I. W. (2000). High-intensity sources of incoherent UV and VUV excimer radiation for low-temperature materials processing. *Applied Surface Science*, **168**, 29–36.

Kogelschatz U., Eliasson B. and Egli W. (1997). Dielectric-barrier discharges. Principle and applications. *J. Phys. IV France*, **7**(C4), 47–66.

Koppenol W. H. and Liebman J. F. (1984). The oxidizing nature of the hydroxyl radical – a comparison with the ferryl ion (FeO_2^+). *Journal of Physical Chemistry*, **88**(1), 99–101.

Kozmér Z., Arany E., Alapi T., Takács E., Wojnárovits L. and Dombi A. (2014). Determination of the rate constant of hydroperoxyl radical reaction with phenol. *Radiation Physics and Chemistry*, **102**, 135–138.

Kröckel L. and Schmidt M. A. (2014). Extinction properties of ultrapure water down to deep ultraviolet wavelengths. *Optical Materials Express*, **4**(9), 1932–1942.

Kuhn H. J., Braslavsky S. E. and Schmidt R. (2004). International Union of pure and applied chemistry organic and biomolekular chemistry division subcommittee on photochemistry, Chemical actinometry (IUPAC Technical Report). *Pure and Applied Chemistry*, **76**(12), 2105–2146.

Kutschera K., Bornick H. and Worch E. (2009). Photoinitiated oxidation of geosmin and 2-methylisoborneol by irradiation with 254 nm and 185 nm UV light. *Water Research*, **43**(8), 2224–2232.

László Z. (2001). Application of the VUV Photolysis in the Mineralization of Pollutants of Water. PhD thesis, University of Szeged, Szeged, Hungary.

László Z. and Dombi A. (2002). Oxidation of $[Fe(CN)_6]^{4-}$ and reduction of $[Fe(CN)_6]^{3-}$ in VUV irradiated aqueous solutions. *Chemosphere*, **46**, 491–494.

László Z., Ilisz I., Peintler G. and Dombi A. (1998). VUV intensity measurement of a 172 nm Xe excimer lamp by means of oxygen actinometry. *Ozone Science and Engineering*, **20**(5), 421–432.

Li Q. R., Gu C. Z., Di Y., Yin H. and Zhang J. Y. (2006). Photodegradation of nitrobenzene using 172 nm excimer UV lamp. *Journal of Hazardous Materials*, **133**(1–3), 68–74.

Li W., Lu S., Chen N., Gu X., Qiu Z., Fan J. and Lin K. (2009). Photo-degradation of clofibric acid by ultraviolet light irradiation at 185 nm. *Water Science and Technology*, **60**(11), 2983–2989.

Li W., Lu S., Qiu Z. and Lin K. (2011). UV and VUV photolysis vs. UV/H_2O_2 and VUV/H_2O_2, treatment for removal of clofibric acid from aqueous solution. *Environmental Technology*, **32**(9–10), 1063–1071.

Liu G. Y. (2014). Recalcitrance of cyanuric acid to oxidative degradation by OH radical: theoretical investigation. *RSC Advances*, **4**(70), 37359–37364.

Liu K., Roddick F. A. and Fan L. (2011). Potential of UV/H_2O_2 oxidation for enhancing the biodegradability of municipal reverse osmosis concentrates. *Water Science and Technology*, **63**(11), 2605–2611.

Liu Y. and Ogden K. (2010). Benefits of high energy UV 185 nm light to inactivate bacteria. *Water Science and Technology*, **62**(12), 2776–2782.

Lomaev M. I., Skakun V. S., Sosnin E. A., Tarasenko V. F., Shitts D. V. and Erofeev M. V. (2003). Excilamps: efficient sources of spontaneous UV and VUV radiation. *Physics-Uspekhi*, **46**(2), 193–209.

Lomaev M. I., Skakun V. S., Tarasenko V. F., Shitts D. V. and Lisenko A. A. (2006a). A windowless VUV excilamp. *Technical Physics Letters*, **32**(7), 590–592.

Lomaev M. I., Sosnin E. A., Tarasenko V. F., Shits D. V., Skakun V. S., Erofeev M. V. and Lisenko A. A. (2006b). Capacitive and barrier discharge excilamps and their applications (Review). *Instruments and Experimental Techniques*, **49**(5), 595–616.

Lomaev M. I., Tarasenko V. F. and Schitz D. V. (2007). On the formation of a barrier discharge in excilamps. *Technical Physics*, **52**(8), 1046–1052.

Lomaev M. I., Skakun V. S., Tarasenko V. F. and Schitz D. V. (2008). One- and two-barrier excilamps on xenon dimers operating in the VUV range. *Technical Physics*, **53**(2), 244–248.

Lomaev M. I., Sosnin E. A. and Tarasenko V. F. (2012). Excilamps and their applications (Review). *Quantum Electronics*, **36**(1), 51–97.

Lopez J. L., Einschlag F. S. G., Gonzalez M. C., Capparelli A. L., Oliveros E., Hashem T. M. and Braun A. M. (2000). Hydroxyl radical initiated photodegradation of 4-chloro-3,5-dinitrobenzoic acid in aqueous solution. *Journal of Photochemistry and Photobiology A: Chemistry*, **137**(2–3), 177–184.

Malinin A. N. (2006). An excimer source of visible light. *Instruments and Experimental Techniques*, **49**(1), 96–100.

Mamane H., Shemer H. and Linden K. G. (2007). Inactivation of *E. coli*, *B. subtilis* spores, and MS2, T4, and T7 phage using UV/H_2O_2 advanced oxidation. *Journal of Hazardous Materials*, **146**, 479–486.

Martire D. O. and Gonzalez M. C. (2001). Aqueous phase kinetic studies involving intermediates of environmental interest: phosphate radicals and their reactions with substituted benzenes. *Progress in Reaction Kinetics and Mechanism*, **26**(2–3), 201–218.

Masschelein W. J. (2002). Ultraviolet Light in Water and Wastewater Sanitation. Lewis Publishers. Boca Raton, FL.

Matilainen A. and Sillanpää M. (2010). Removal of natural organic matter from drinking water by advanced oxidation processes - review. *Chemosphere*, **80**, 351–365.

Matsushita T., Hirai S., Ishikawa T., Matsui Y. and Shirasaki N. (2015). Decomposition of 1,4-dioxane by vacuum ultraviolet irradiation: study of economic feasibility and by-product formation. *Process Safety and Environmental Protection*, **94**, 528–541.

Matter D., Burtscher H., Kogelschatz U. and Scherrer L. (1994). Photoemission of combustion aerosols using an excimer UV radiation source. *Staub-Reinhaltung der Luft*, **54**, 163–166.

Moussavi G., Hossaini H., Jafari S. J. and Farokhi M. (2014). Comparing the efficacy of UVC, UVC/ZnO and VUV processes for oxidation of organophosphate pesticides in water. *Journal of Photochemistry and Photobiology A: Chemistry*, **290**, 86–93.

Muhlberger F., Wieser J., Ulrich A. and Zimmermann R. (2002). Single photon ionization (SPI) via incoherent VUV-excimer light: robust and compact time-of-flight mass spectrometer for on-line, real-time process gas analysis. *Analytical Chemistry*, **74**(15), 3790–3801.

Nikogosyan D. N. and Görner H. (1992). Photolysis of aromatic amino acids in aqueous solution by nanosecond 248 and 193 nm laser light. *Journal of Photochemistry and Photobiology B: Biology*, **13**(3–4), 219–234.

Ochiai T., Masuko K., Tago S., Nakano R., Nakata K., Hara M., Nojima Y., Suzuki T., Ikekita M., Morito Y. and Fujishima A. (2013a). Synergistic water-treatment reactors using a TiO_2-modified Ti-mesh filter. *Water*, **5**(3), 1101–1115.

Ochiai T., Masuko K., Tago S., Nakano R., Niitsu Y., Kobayashi G., Horio K., Nakata K., Murakami T., Hara M., Nojima Y., Kurano M., Serizawa I., Suzuki T., Ikekita M., Morito Y. and Fujishima A. (2013b). Development of a hybrid environmental purification unit by using of excimer VUV lamps with TiO_2 coated titanium mesh filter. *Chemical Engineering Journal*, **218**, 327–332.

Oppenländer T. (1994). Novel incoherent excimer UV irradiation units for the application in photochemistry, photobiology/-medicine and for waste water treatment. *European Photochemistry Association Newsletter*, **50**, 2–8.

Oppenländer T. (1996). The contribution of organic photochemistry to investigations of phototoxicity. In: The Photostability of Drugs and Drug Formulations, H. Tonnesen (ed.), Taylor & Francis, London, pp. 217–265.

Oppenländer T. (2003). Photochemical Purification of Water and Air. Wiley-VCH, Weinheim.

Oppenländer T. (2007). Mercury-free sources of VUV/UV radiation: application of modern excimer lamps (excilamps) for water and air treatment. *Journal of Environmental Engineering and Science*, **6**(3), 253–264.

Oppenländer T. and Gliese S. (2000). Mineralization of organic micropollutants (homologous alcohols and phenols) in water by vacuum-UV-oxidation (H_2O-VUV) with an incoherent xenon-excimer lamp at 172 nm. *Chemosphere*, **40**, 15–21.

Oppenländer T. and Schwarzwälder R. (2002). Vacuum-UV oxidation (H_2O-VUV) with a xenon excimer flow-through lamp at 172 nm: use of methanol as actinometer for VUV intensity measurement and as reference compound for OH-radical competition kinetics in aqueous systems. *Journal of Advanced Oxidation Technologies*, **5**(2), 155–163.

Oppenländer T. and Sosnin E. (2005). Mercury-free vacuum-(VUV) and UV excilamps: lamps of the future? *IUVA News*, **7**(4), 16–20.

Oppenländer T. and Xu F. (2008). Temperature effects on the vacuum-UV (VUV)-initiated oxidation and mineralization of organic compounds in aqueous solution using a xenon excimer flow-through photoreactor at 172 nm. *Ozone Science and Engineering*, **30**(1), 99–104.

Oppenländer T., Baum G., Egle W. and Hennig T. (1995). Novel vacuum-UV-(VUV) and UV-excimer flow-through photoreactors for waste water treatment and for wavelength-selective photochemistry. *Proceedings of the Indian Academy of Sciences, Chemical Sciences*, **107**(6), 621–636.

Oppenländer T., Walddorfer C., Burgbacher J., Kiermeier M., Lachner K. and Weinschrott H. (2005). Improved vacuum-UV (VUV)-initiated photomineralization of organic compounds in water with a xenon excimer flow-through photoreactor (Xe_2* lamp, 172 nm) containing an axially centered ceramic oxygenator. *Chemosphere*, **60**(3), 302–309.

Puspita P., Roddick F. A. and Porter N. A. (2011). Decolourisation of secondary effluent by UV-mediated processes. *Chemical Engineering Journal*, **171**(2), 464–473.

Querry M. R., Cary P. G. and Waring R. C. (1978). Split-pulse laser method for measuring attenuation coefficients of transparent liquids: application to deionized filtered water in the visible region. *Applied Optics*, **17**(22), 3587–3592.

Quici N., Litter M. I., Braun A. M. and Oliveros E. (2008). Vacuum-UV-photolysis of aqueous solutions of citric and gallic acids. *Journal of Photochemistry and Photobiology A: Chemistry*, **197**(2–3), 306–312.

Ratpukdi T., Siripattanakul S. and Khan E. (2010). Mineralization and biodegradability enhancement of natural organic matter by ozone-VUV in comparison with ozone, VUV, ozone-UV, and UV: effects of pH and ozone dose. *Water Research*, **44**(11), 3531–3543.

Ratpukdi T., Casey F., DeSutter T. and Khan E. (2011). Bromate formation by ozone-VUV in comparison with ozone and ozone-UV: effects of pH, ozone dose, and VUV power. *Journal of Environmental Engineering*, **137**(3), 187–195.

Reisz E., Schmidt W., Schochmann H.-P. and von Sonntag C. (2003). Photolysis of ozone in aqueous solution in the presence if tertiary butanol. *Environmental Science & Technology*, **37**(9), 1941–1948.

Robl S., Worner M., Maier D. and Braun A. M. (2012). Formation of hydrogen peroxide by VUV-photolysis of water and aqueous solutions with methanol. *Photochemical & Photobiological Sciences*, **11**(6), 1041–1050.

Routledge E. J. and Sumpter J. P. (1997). Structural features of alkylphenolic chemicals associated with estrogenic activity. *The Journal of Biological Chemistry*, **272**(6), 3280–3288.

Satou T., Nakazato T. and Tao H. (2013). Online TOC analysis based on reagent-free oxidation of dissolved organic matter using a mercury lamp-pass-through photoreactor. *Analytical Sciences*, **29**, 233–238.

Schalk S., Adam V., Arnold E., Brieden K., Voronov A. and Witzke H.-D. (2005). UV-lamps for disinfection and advanced oxidation – lamp types, technologies and applications. *IUVA News*, **8**(1), 32–37.

Schreiber A., Kühn B., Arnold E., Schilling F. J. and Witzke H. D. (2005). Radiation resistance of quartz glass for VUV discharge lamps. *Journal of Physics D: Applied Physics*, **38**(17), 3242–3250.

Schürgers M. and Welge K. H. (1968). Absorptionskoeffizient von H_2O_2 und N_2H_4 zwischen 1200 und 2000 Å. *Z. Naturforsch.*, **23a**, 1508–1510.

Segelstein D. J. (1981). The Complex Refractive Index of Water. M.S. thesis, University of Missouri, Kansas City, USA.

Shen Y. S. and Liao B. H. (2007). Study on the treatment of Acid Red 4 wastewaters by a laminar-falling-film-slurry-type VUV photolytic process. *Water Science and Technology*, **55**(12), 13–18.

Shirayama H., Tohezo Y. and Taguchi S. (2001). Photodegradation of chlorinated hydrocarbons in the presence and absence of dissolved oxygen in water. *Water Research*, **35**(8), 1941–1950.

Shuaibov A. K., Minya A. I., Malinin A. N., Homoki Z. T. and Hrytsak R. V. (2012). VUV lamp based on mixtures of inert gases with water molecules pumped by a pulsed-periodic capacitive discharge. *Journal of Applied Spectroscopy*, **78**(6), 867–872.

Shuaibov A. K., Gomoki Z. T., Minya A. I. and Shevera I. V. (2013). Emission characteristics of an ultraviolet emitter based on mixtures of krypton with low-aggressive halogen carriers pumped by a barrier discharge. *Optics and Spectroscopy*, **114**(2), 189–192.

Simonsen M. E., Jensen C. V. and Sogaard E. G. (2013). Comparison of different UV-activated AOP methods. *Journal of Advanced Oxidation Technologies*, **16**(1), 179–187.

Sokolov U. and Stein G. (1996). Photolysis of liquid water at 1849 Å. *Journal of Chemical Physics*, **44**(9), 3329–3337.

Sosnin E. A., Erofeev M. V., Tarasenko V. F. and Shitz D. V. (2002). Capacitive discharge excilamps. *Instruments and Experimental Techniques*, **45**(6), 838–839.

Sosnin E. A., Oppenländer T. and Tarasenko V. F. (2006). Applications of capacitive and barrier discharge excilamps in photoscience. *Journal of Photochemistry and Photobiology C: Photochemistry Reviews*, **7**(4), 145–163.

Sosnin E. A., Avdeev S. M., Panarin V. A., Tarasenko V. F., Pikulev A. A. and Tsvetkov V. V. (2011a). The radiative and thermodynamic processes in DBD driven XeBr and KrBr exciplex lamps. *The European Physical Journal D*, **62**(3), 405–411.

Sosnin E. A., Pikulev A. A. and Tarasenko V. F. (2011b). Optical characteristics of cylindrical exciplex and excimer lamps excited by microwave radiation. *Technical Physics*, **56**(4), 526–530.

Sosnin E. A., Avdeev S. M., Tarasenko V. F., Skakun V. S. and Schitz D. V. (2015a). KrCl barrier-discharge excilamps: energy characteristics and applications (Review). *Instruments and Experimental Techniques*, **58**(3), 309–318.

Sosnin E. A., Korzenev A. N., Avdeev S. M., Volkind D. K., Novakovskii G. S. and Tarasenko V. F. (2015b). Numerical simulation and experimental study of thermal and gas-dynamic processes in barrier-discharge coaxial excilamps. *High Temperature*, **53**(4), 558–563.

Steenland K., Fletcher T. and Savitz D. (2010). Epidemiologic evidence on the health effects of perfluorooctanoic acid (PFOA). *Environmental Health Perspectives*, **118**(8), 1100–1108.

Suzuki F., Ono K., Sakai K. and Hayashi K. (2006). Direct measurement of 185 nm radiation from low-pressure mercury lamps using diamond-based vacuum ultraviolet sensors. *The Japanese Journal of Applied Physics*, **45**(8A), 6484–6485.

Szabó R. K., Megyeri C., Illés E., Gajda-Schrantz K., Mazellier P. and Dombi A. (2011). Phototransformation of ibuprofen and ketoprofen in aqueous solutions. *Chemosphere*, **84**(11), 1658–1663.

Tarasenko V. F., Chernov E. B., Erofeev M. V., Lomaev M. I., Panchenko A. N., Skakun V. S., Sosnin E. A. and Shitz D. V. (1999). UV and VUV excilamps excited by glow, barrier and capacitive discharges. *Applied Physics A*, **69**, 327–329.

Tasaki T., Wada T., Fujimoto K., Kai S., Ohe K., Oshima T., Baba Y. and Kukizaki M. (2009). Degradation of methyl orange using short-wavelength UV irradiation with oxygen microbubbles. *Journal of Hazardous Materials*, **162**(2–3), 1103–1110.

Thomsen C. L., Madsen D., Keiding S. R., Thøgersen J. and Christiansen O. (1999). Two-photon dissociation and ionization of liquid water studied by femtosecond transient absorption spectroscopy. *Journal of Chemical Physics*, **110**(7), 3453–3462.

Thomson J., Roddick F. A. and Drikas M. (2002). Natural organic matter removal by enhanced photo-oxidation using low pressure mercury vapour lamps. *Water Science and Technology*, **2**(5–6), 435–443.

Thomson J., Roddick F. A. and Drikas M. (2004). Vacuum ultraviolet irradiation for naturai organic matter removal. *Journal of Water Supply: Research & Technology*, **53**(4), 196–206.

Tsujimoto Y., Hashizume H. and Yamazaki M. (1993). Superoxide radical scavenging activity of phenolic compounds. *International Journal of Biochemistry*, **25**(4), 491–494.

Van der Pol A. J. H. P. and Krijnen S. (2005). Optimal UV output in different application of low-pressure UV-C lamps. Proceedings of the Third International Congress on Ultraviolet Technologies, International Ultraviolet Association. Whistler, BC, Canada.

Vicente J. S., Gejo J. L., Rothenbacher S., Sarojiniamma S., Gogritchiani E., Worner M., Kasper G. and Braun A. M. (2009). Oxidation of polystyrene aerosols by VUV-photolysis and/or ozone. *Photochemical & Photobiological Sciences*, **8**(7), 944–952.

Volkova G. A. and Gerasimov G. N. (1997). Amplification of $\lambda = 147$ nm radiation from a barrier discharge in a mixture of krypton with xenon. *Quantum Electronics*, **27**(3), 213–216.

von Sonntag C. and Schuchmann H. P. (1991). The elucidation of peroxyl radical reactions in aqueous solution with the help of radiation-chemical methods. *Angewandte Chemie International Edition (England)*, **30**, 1229–1253.

von Sonntag C. and Schuchmann H. P. (1997). Peroxyl Radicals in Aqueous Solutions. John Wiley and Sons, Chichester.

Voronov A., Arnold E. and Roth E. (2003) Long life technology of high power amalgam lamps. Proceedings of the Second International Conference on Ultraviolet Technologies, International Ultraviolet Association. Vienna, Austria.

Wang B. B., Cao M. H., Tan Z. J., Wang L. L., Yuan S. H. and Chen J. (2010a). Photochemical decomposition of perfluorodecanoic acid in aqueous solution with VUV light irradiation. *Journal of Hazardous Materials*, **181**(1–3), 187–192.

Wang D., Oppenländer T., El-Din M. G. and Bolton J. R. (2010b). Comparison of the disinfection effects of vacuum-UV (VUV) and UV light on Bacillus subtilis spores in aqueous suspensions at 172, 222 and 254 nm. *Photochemistry and Photobiology*, **86**(1), 176–181.

Wang J., Yang C., Wang C., Han W. and Zhu W. (2014). Photolytic and photocatalytic degradation of micro pollutants in a tubular reactor and the reaction kinetic models. *Separation and Purification Technology*, **122**, 105–111.

Wang Y. and Zhang P. (2014). Effects of pH on photochemical decomposition of perfluorooctanoic acid in different atmospheres by 185 nm vacuum ultraviolet. *Journal of Environmental Sciences (China)*, **26**(11), 2207–2214.

Weeks J. L., Meaburn G. M. A. C. and Gordon S. (1963). Absorption coefficients of liquid water and aqueous solutions in the far ultraviolet. *Radiation Research*, **19**(3), 559–567.

Weissflog L., Elansky N., Putz E., Krueger G., Lange C. A., Lisitzina L. and Pfennigsdorff A. (2004). Trichloroacetic acid in the vegetation of polluted and remote areas of both hemispheres - Part II: salt lakes as novel sources of natural chlorohydrocarbons. *Atmospheric Environment*, **38**(25), 4197–4204.

Wieser J., Murnick D. E., Ulrich A., Huggins H. A., Liddle A. and Brown W. L. (1997). Vacuum ultraviolet rare gas excimer light source. *Review of Scientific Instruments*, **68**(3), 1360–1364.

Wild S. R., Harrad S. J. and Jones K. C. (1993). Chorophenols in digested UK sewage sludges. *Water Research*, **27**(10), 1527–1534.

Witzke H.-D. (2001) Recent studies on fused quartz and synthetic fused silica for light sources. Proceedings of 9th International Symposium on the Science and Technology of Light Sources. Ithaca, NY, USA.

Wörner M., Eggers J., Nunes M., Schnabel C., Rudolph S., Zegenhagen f., Workman A. and Baum A. M. (2003). Combination of VUV (Vacuum-Ultraviolet)-photolysis and electrolysis for the accelerated mineralization of organic pollutant in aqueous systems. 3rd International Conference on Oxidation Technologies for Water and Wastewater – Special Topic: AOP's for Recycling and Reuse. Clausthal.

Xing R., Zheng Z. and Wen D. (2015). Comparison between UV and VUV photolysis for the pre- and post-treatment of coking wastewater. *Journal of Environmental Sciences (China)*, **29**, 45–50.

Yan J. and Gupta M. C. (2003). High power 121.6 nm radiation source. *Journal of Vacuum Science & Technology B*, **21**(6), 2839–2842.

Yan J., El-Dakrouri A., Laroussi M. and Gupta M. C. (2002). 121.6 nm radiation source for advanced lithography. *Journal of Vacuum Science & Technology B*, **20**(6), 2574–2577.

Yazdani A. (2016). Is POU water recovery and reuse practical in microelectronics fabs? *Ultrapure Water*, 1–3. https://www.ultrapurewater.com/articles/micro/is-pou-water-recovery-and-reuse-practical-in-microelectronics-fabs

Yoon S. H., Lee J. H., Oh S. and Yang J. E. (2008). Photochemical oxidation of As(III) by vacuum-UV lamp irradiation. *Water Research*, **42**(13), 3455–3463.

Zhang J.-W. and Boyd I. W. (2000). Lifetime investigation of excimer UV sources. *Applied Surface Science*, **168**, 296–299.

Zhao G., Lu X., Zhou Y. and Gu Q. (2013). Simultaneous humic acid removal and bromate control by O_3 and UV/O_3 processes. *Chemical Engineering Journal*, **232**, 74–80.

Zhuang X., Han Q., Zhang H., Feng X., Roth M., Rosier O., Zhu S. and Zhang S. (2010). The efficiency of coaxial KrCl* excilamps. *Journal of Physics D: Applied Physics*, **43**(20), 205202.

Zoschke K., Dietrich N., Bornick H. and Worch E. (2012). UV-based advanced oxidation processes for the treatment of odour compounds: efficiency and by-product formation. *Water Research*, **46**(16), 5365–5373.

Zoschke K., Bornick H. and Worch E. (2014). Vacuum-UV radiation at 185 nm in water treatment – A review. *Water Research*, **52**, 131–145.

Zvereva G. N. (2010). Investigation of water decomposition by vacuum ultraviolet radiation. *Optics and Spectroscopy*, **108**(6), 915–922.

Zvereva G. N. and Gerasimov G. N. (2001). Numerical simulation of a barrier discharge in Xe. *Optics and Spectroscopy*, **90**(3), 321–328.

Chapter 9

UV/Chlorine process

Joseph De Laat and Mihaela Stefan

9.1 INTRODUCTION

Since the early 1970s, an increasing number of research studies have been carried out to develop advanced oxidation processes (AOPs) for the degradation of organic pollutants refractory to the oxidants conventionally used in water treatment (chlorine, ozone, chlorine dioxide). AOPs are based on the *in situ* generation of the hydroxyl radical (•OH) which is a powerful oxidant and a highly reactive species with most organic pollutants. After the first studies on Fenton reaction (Fe^{2+}/H_2O_2) for treatment of industrial wastewaters, other advanced oxidation processes have been explored at laboratory- and/or pilot-scale, and full-scale AOPs were implemented at water treatment facilities over the past three decades. Hydroxyl radicals can be produced at room temperature and atmospheric pressure by various processes based on chemical, photochemical, electrochemical or sonochemical reactions (Legrini *et al.* 1993; Oturan & Aaron, 2014). Recently, the UV/Chlorine process has been investigated as an alternative to the UV/H_2O_2 process and was tested at a few water treatment utilities (pilot- or full-scale) for water reuse, drinking water production, or groundwater decontamination.

As mentioned by Allmand *et al.* (1925), the photodecomposition of chlorine in water has been investigated since the 1850s. Buxton and Subhani (1972b) showed that the photodecomposition mechanism of hypochlorite ion is very complex and depends on the irradiation wavelength. Photodecomposition of hypochlorite ion leads to chloride, chlorate, chlorite, and oxygen as end-products and to the *in situ* generation of •OH and Cl• as well as many other unstable intermediates. A few research works performed in the 1970s showed that UV/Cl_2 can oxidize or mineralize completely organic compounds which are resistant to chlorine in the dark and to direct photolysis. These reactions have been demonstrated in the case of ethanol, n-butanol and benzoic acid at pH < 10 and at ~350 nm (Oliver & Carey, 1977), ethylene glycol dimethyl ether and related substrates, acetic and propionic acids at pH > 12 with a high pressure Hg lamp (Ogata *et al.* 1978; Ogata *et al.* 1979), benzoic acid at pH ≥ 12 and $\lambda = 253.7$ nm and $\lambda \geq 350$ nm (Ogata & Tomizawa, 1984), benzoic acid and nitrobenzene at pH 6 and $\lambda \geq 350$ nm (Nowell & Crosby, 1985), 1-chlorobutane, n-octanol and nitrobenzene at sunlight wavelengths (Nowell & Hoigné, 1992b). Since 2005, a few research groups have performed studies to determine quantum yields of photolysis of free chlorine species (HOCl

and ClO^-) at various wavelengths, to examine the effects of various experimental parameters on the rate of photodecomposition of free chlorine, and to evaluate the performance of the UV/Cl_2 process as an AOP.

This chapter will present first the fundamental aspects of the photochemical decomposition of aqueous solutions of free chlorine into $^{\bullet}OH$ and chlorine atoms. The reactivity of chlorine atoms ($Cl^{\bullet}$) and of dichlorine anion radicals ($Cl_2^{\bullet-}$) towards organic and inorganic compounds will then be reviewed. In the last part of this chapter, the recent works on the degradation of organic pollutants by the UV/Cl_2 AOP will be discussed. In this context, pilot-scale and full-scale studies will be emphasized, and the performances of the UV/Cl_2 and UV/H_2O_2 oxidation processes will be compared.

9.2 PHOTODECOMPOSITION OF FREE CHLORINE BY UV LIGHT

9.2.1 Distribution of free chlorine species

The predominant free chlorine species in dilute aqueous solutions are aqueous dichlorine (Cl_2), hypochlorous acid (HOCl) and hypochlorite ion (ClO^-):

$$Cl_2 + H_2O \rightleftharpoons HOCl + H^+ + Cl^- \quad K_d = 3.94 \times 10^{-4}\ M^2 \text{ at } 25°C \text{ and } I = 0 \text{ (Connick \& Chia, 1959)} \tag{9.1}$$

$$HOCl \rightleftharpoons ClO^- + H^+ \quad pK_a = 7.537 \text{ at } 25°C \text{ and } I = 0 \text{ (Morris, 1966)} \tag{9.2}$$

The distribution of Cl_2, HOCl and ClO^- species can be calculated from the disproportionation constant of Cl_2 (K_d) and the pK_a value of HOCl. At a given temperature and zero ionic strength ($I = 0$), K_d and pK_a can be calculated from expressions 9.3 (Connick & Chia, 1959) and 9.4 (Morris, 1966), respectively:

$$\log K_d = -982798/T^2 + 5485.7/T - 10.7484 \text{ at temperatures from 0 to 45°C} \tag{9.3}$$

$$pK_a = 3000/T - 10.0686 + 0.0253T \text{ at temperatures from 0 to 35°C} \tag{9.4}$$

where T is the absolute temperature in Kelvin degrees (0°C = 273.15 K).

The K_d values determined from equation 9.3 vary from 1.45×10^{-4} M^2 at 0°C to 6.09×10^{-4} M^2 at 45°C, and the pK_a values of HOCl calculated from equation 9.4 decrease from 7.825 at 0°C to 7.463 at 35°C. At 25°C and $I = 0$, the values of K_d and pK_a are equal to 3.94×10^{-4} M^2 and 7.537, respectively.

As indicated by reactions 9.1 and 9.2, the distribution of free chlorine species depends on chloride concentration, temperature, and pH; of all, pH is the most impactful parameter. Figure 9.1 presents the distribution patterns of chlorine species calculated at 25°C and for a chloride concentration of 2 mM.

Cl_2 is only present at low pH values (pH < 3). At 25°C, HOCl is the predominant free chlorine species at pH < 7.5, and ClO^- at pH > 7.5. More than 99% of free chlorine is present as HOCl in the pH range of 3–5.5, and as ClO^- at pH > 9.5.

9.2.2 Absorption spectra of free chlorine species in water

HOCl and ClO^- absorb UV light at wavelengths ranging from 200 to 375 nm (Figure 9.2) and therefore, free chlorine can be photolyzed by UV-C light, as well as by the UV-B and UV-A radiation from the solar light (Buxton & Subhani, 1972b; Nowell & Hoigné, 1992a). Molar absorption coefficients (ε) range from 0 to 370 M^{-1} cm^{-1}. Absorption spectra show a maximum absorption band centered at 236 nm for HOCl

($\varepsilon = 101 \pm 2$ M^{-1} cm^{-1}) and at 292 nm for ClO^- ($\varepsilon = 365 \pm 8$ M^{-1} cm^{-1}). The molar absorption coefficients of HOCl and ClO^- at 253.7 nm are equal to 59 ± 1 and 66 ± 1 M^{-1} cm^{-1}, respectively (Feng *et al.* 2007; De Laat & Berne, 2009).

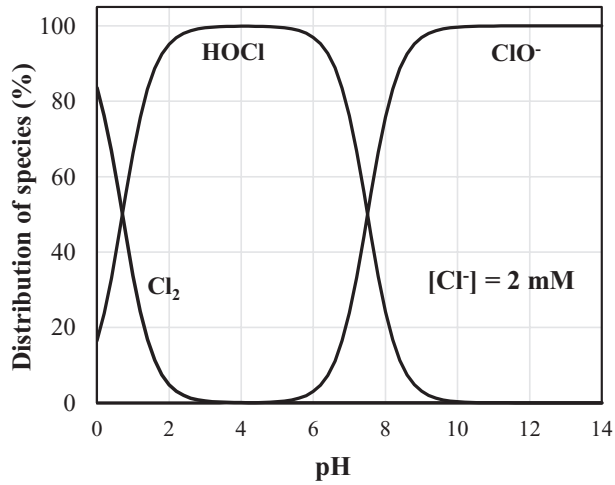

Figure 9.1 Distribution of Cl_2, HOCl and ClO^- in water as a function of pH at 25°C. (Distribution curves calculated for $[Cl^-] = 2$ mM, $K_d = 3.94 \times 10^{-4}$ M^2 and $pK_a = 7.537$; De Laat, 2016).

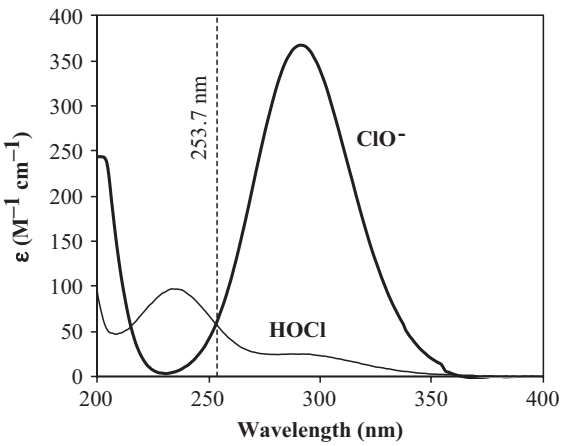

Figure 9.2 UV spectra of HOCl and ClO^- in water (De Laat, 2016).

9.2.3 Radical species, quantum yields and degradation mechanisms of free chlorine

While the photodecomposition of chlorine in water has been investigated since the 1850s (Allmand *et al.* 1925), the potential use of UV/Cl_2 as an AOP has been examined only in the recent years (Watts *et al.* 2007a, b; Jin *et al.* 2011; Sichel *et al.* 2011; Watts *et al.* 2012; Wang *et al.* 2012; Shu *et al.* 2014; Wang *et al.*

2015a). The photodecomposition of chlorine in aqueous solution leads to chloride, chlorate, chlorite, and oxygen as end-products. The yields of these products are both wavelength- and chlorine species-dependent (Buxton & Subhani, 1972b; Cooper *et al.* 2007). Molar yields for the production of chlorate vary from 0.02 to 0.3 mole of chlorate/mole of chlorine decomposed and depend on the irradiation wavelength, pH, and chlorine concentration (Buxton & Subhani, 1972b; Karpel Vel Leitner *et al.* 1992a; Feng *et al.* 2010; Rao *et al.* 2010; Wang *et al.* 2012). Recently, it was also shown that perchlorate can be produced at yields less than 0.01 mole of ClO_4^- per mole of chlorine photodecomposed (Kang *et al.* 2006; Rao *et al.* 2010). All these end-products are formed from complex reactions initiated by the primary photo-products of HOCl or ClO^-; numerous reactive intermediates are also produced.

9.2.3.1 Primary quantum yields of photolysis of hypochlorite ion and hypochlorous acid

From steady-state and flash photolysis experiments on sodium hypochlorite solutions at alkaline pH, Buxton and Subhani (1972b) showed that the primary photoproducts of hypochlorite ion as well as the primary quantum yields of photoproduct formation depend on the irradiation wavelength (Table 9.1). The primary products of photolysis of hypochlorite ion are chloride ion, hydroxyl radicals ($^{\bullet}OH/O^{\bullet-}$, $pK_a = 11.9$; Buxton *et al.* 1988), $Cl^{\bullet}$ and $O(^3P)$ at 253.7, 313 and 365 nm. $O(^1D)$ is also produced at 253.7 nm and 313 nm.

Table 9.1 Primary quantum yields of photodecomposition reactions of hypochlorite ion at pH > 11.5 (Buxton & Subhani, 1972b).

Initiation step	Reaction	253.7 nm	313 nm	365 nm
$ClO^- + h\nu \rightarrow Cl^- + O(^3P)$	9.5	0.074 ± 0.019	0.075 ± 0.015	0.28 ± 0.03
$ClO^- + h\nu \rightarrow Cl^{\bullet} + O^{\bullet-}$	9.6	0.278 ± 0.016	0.127 ± 0.014	0.08 ± 0.02
$ClO^- + h\nu \rightarrow Cl^- + O(^1D)$	9.7	0.133 ± 0.017	0.020 ± 0.015	0

As shown in Table 9.1, the quantum yields of formation of ($^{\bullet}OH/O^{\bullet-}$) and $Cl^{\bullet}$ from ClO^- photolysis markedly decrease when irradiation wavelength increases, e.g., from 0.28 at 253.7 nm to 0.08 at 365 nm.

Similarly, $^{\bullet}OH$, $Cl^{\bullet}$ and oxygen atoms are formed by UV photolysis of HOCl (Kläning *et al.* 1984; Thomsen *et al.* 2001; Herrmann, 2007). $Cl^{\bullet}$ exhibits a strong absorption band in the UV region with a maximum at around 310–320 nm (Figure 9.3) (Kläning & Wolff, 1985; Buxton *et al.* 2000; Thomsen *et al.* 2001). From femtosecond photolysis experiments of HOCl (~1.5 M) at 266 nm, Thomsen *et al.* (2001) showed that HOCl molecules photodissociate within 1 picosecond into $^{\bullet}OH$ and $Cl^{\bullet}$ with a near-unity quantum yield:

$$HOCl \xrightarrow{h\nu} {}^{\bullet}OH + Cl^{\bullet} \tag{9.8}$$

The authors also observed higher yield of $^{\bullet}OH$ than of $Cl^{\bullet}$ because a fraction of $Cl^{\bullet}$ (~10%) reacted with HOCl to form $^{\bullet}OH$ under the experimental conditions used (high HOCl concentration):

$$Cl^{\bullet} + HOCl \rightarrow Cl_2 + {}^{\bullet}OH \tag{9.9}$$

By monitoring the concentrations of photoproducts by ultrafast transient absorption spectroscopy, Thomsen *et al.* (2001) observed that the concentration of $Cl^{\bullet}$ decayed rapidly within 50 ps due to back geminate recombination with $^{\bullet}OH$ within the solvent "cage", to re-form HOCl (Figure 9.4).

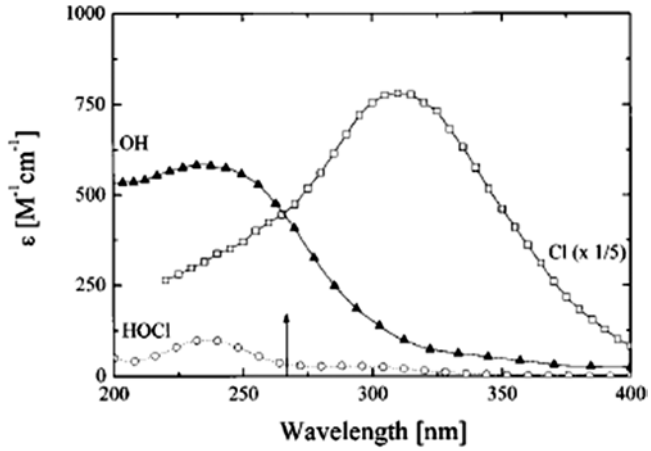

Figure 9.3 Absorption spectra of HOCl, •OH and Cl• (×1/5). Reprinted with permisson from Thomsen *et al.* (2001). Copyright 2016 AIP Publishing.

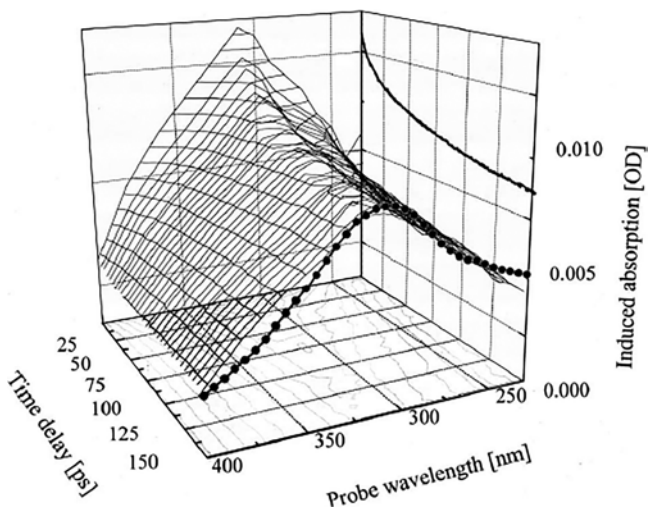

Figure 9.4 Full transient absorption spectrum following photolysis of aqueous HOCl at 266 nm. The steady state spectrum of Cl• is shown in the wavelength-transient absorption plane, and the spectrally integrated dynamics is shown in the time-transient absorption plane. Reprinted with permission from Thomsen *et al.* (2001). Copyright 2016 AIP Publishing.

Under the assumption that the decrease in the absorbance at 340 nm is proportional to the concentration of Cl•, the authors determined the quantum yield of Cl• that escaped recombination from the absorbance values measured at 1 ps and 150 ps, using equation 9.10:

$$\Phi(\mathrm{Cl}^{\bullet}) = \frac{\Delta\mathrm{OD}(t = 150\ \mathrm{ps})}{\Delta\mathrm{OD}(t = 1\ \mathrm{ps})} \tag{9.10}$$

The authors obtained a $\Phi(Cl^{\bullet})$ of 0.55 ± 0.05 at 266 nm. Therefore, the primary quantum yields for HOCl photolysis (Φ(-HOCl) and for $^{\bullet}OH$- and $Cl^{\bullet}$-formation ($\Phi(HO^{\bullet})$ and $\Phi(Cl^{\bullet})$) are equal to 0.55 ± 0.05 at 266 nm.

A lower value has been reported in a more recent study (Herrmann, 2007) from excimer laser photolysis experiments at 248 nm. Experiments were carried at pH 1.5 in O_2-free solutions, with a concentration of chlorine of 4.4×10^{-4} M. Under the experimental conditions used by the authors, the concentrations of HOCl, Cl^-, Cl_2 and Cl_3^- were roughly 4.4×10^{-4}, 4.4×10^{-4}, 2×10^{-5} and 2×10^{-9} M, respectively. The absorption of UV (248 nm) light in the reaction cell by Cl_2 and Cl_3^- could be neglected. The $\Phi(Cl^{\bullet})$ and $\Phi(^{\bullet}OH)$ values (0.25 ± 0.05; Herrmann, 2007) were determined from the initial concentration of $Cl^{\bullet}$ formed through HOCl photolysis at $t = 50$ ns and from the amount of $Cl^{\bullet}$ which has been consumed during the first 50 ns through the reactions with $Cl^{\bullet}$, HOCl, Cl^- and H_2O.

In order to assess the formation of $^{\bullet}OH$ in the free chlorine photolysis process, Nowell and Hoigné (1992b) introduced the 'yield factor' which represents the released $^{\bullet}OH$ per free chlorine photodecomposed, on a molar basis. The authors determined the pH-dependent $^{\bullet}OH$-yield factors in the photodecomposition of free chlorine under simulated solar radiation and at 253.7 nm. At pH 5 and in the absence of scavengers other than the probe compound, the $^{\bullet}OH$ yield factors were determined as 0.85 and 0.70, at 253.7 nm and under simulated solar radiation, respectively; at pH 10, the yield factors were 0.12 and 0.10, respectively.

Watts and Linden (2007a) determined a quantum yield of 1.40 ± 0.18 (253.7 nm) for $^{\bullet}OH$ formation from HOCl photolysis at pH 5, and compared it to the quantum yield of $^{\bullet}OH$ formation ($\Phi_{^{\bullet}OH} \sim 1.0$) in the H_2O_2 photolysis in aqueous solutions. Wang *et al.* (2012) reported $\Phi_{^{\bullet}OH}$ (253.7 nm) = (0.79 ± 0.01) at pH 5, which is larger than that determined by Jin *et al.* (2011), i.e., $\Phi_{^{\bullet}OH} = 0.46 \pm 0.09$. At pH 10, the $^{\bullet}OH$ quantum yield reported by Wang *et al.* (2012) was 1.18 ± 0.12 (253.7 nm), almost twice as large as that determined by Chan *et al.* (2012), $\Phi_{^{\bullet}OH} = 0.61$. Based on the $^{\bullet}OH$ yield factor determined for ClO^- photolysis (0.70 ± 0.02), Chan *et al.* (2012) concluded that 30% of hypochlorite photolysis does not result in OH radicals.

9.2.3.2 Degradation pathways of hypochlorite and hypochlorous acid in organic-free water

Once formed, the primary photoproducts of ClO^- initiate decomposition reactions of ClO^- into unstable transient species ($ClO^{\bullet}$, Cl_2O_2, Cl_2O), secondary oxidants (ClO_2, O_3, H_2O_2) and stable by-products (Cl^-, ClO_2^-, ClO_3^-, ClO_4^- and O_2). The yields of by-products highly depend on the experimental conditions such as irradiation wavelength, pH and concentration of dissolved oxygen.

Table 9.2 lists the quantum yields of byproduct formation as determined by Buxton and Subhani (1972b) in deoxygenated solutions of ClO^-. The main by-products of photodecomposition of ClO^- at 253.7 nm are chloride (~0.82 mol/mol of ClO^-) and chlorate (~0.18 mol/mol of ClO^-). The yields of chloride and chlorate were roughly the same at 308 nm. At 365 nm, the molar yields of chloride, chlorite and chlorate were 0.60, 0.13 and 0.27 mol/mol of ClO^-, respectively.

Buxton and Subhani (1972b) proposed the sequence of reactions listed in table 9.3 to explain the formation of Cl^-, ClO_2^-, ClO_3^-, O_2 and O_3 by photolysis of hypochlorite ion. These reactions are initiated by the primary photo-products of ClO^- (reactions 9.5–9.7 in Table 9.1).

$^{\bullet}OH/O^{\bullet-}$ and $Cl^{\bullet}$ oxidize hypochlorite ion to $ClO^{\bullet}$ (Reactions 9.11–9.13). Dichlorine peroxide (Cl_2O_2 or ClOOCl) produced by the very fast $ClO^{\bullet}$ dimerization (reaction 9.14) decomposes *via* parallel pathways to produce chloride, chlorate and oxygen as stable end-products and chlorite (reactions 9.15–9.18). Chlorite has been detected only in hypochlorite solutions irradiated at 365 nm (Table 9.2). In a more recent study on the photolysis of hypochlorite ($[Cl_{2,T}]_0 \approx 16$–18 mM, initial pH > 10.6) at 253.7, 300,

Table 9.2 Quantum yields of ClO^- photodecomposition and of by-product formation (experimental values) determined by Buxton and Subhani (1992b) at 253.7, 313 and 365 nm.

Conditions	253.7 nm pH 11.5 $[ClO^-] = 1$ mM	313 nm pH 12.0 $[ClO^-] = 1$ mM	365 nm pH 12.1 $[ClO^-] = 7–10$ mM
Φ-ClO^- photodecomposition	0.85 ± 0.02	0.39 ± 0.01	0.60 ± 0.05
Φ-ClO_2^- formation	0	0	0.160 ± 0.005
Φ-ClO_3^- formation	0.15 ± 0.02	0.08 ± 0.02	0.08 ± 0.02
Φ-Cl^- formation	0.70 ± 0.03	0.27 ± 0.02	0.36 ± 0.03
Φ-O_2 formation	0.200 ± 0.005	0.069 ± 0.005	0.04 ± 0.02

Table 9.3 Photodecomposition pathways of hypochlorite ion proposed by Buxton and Subhani (1972a and 1972b).

Reactions		Rate Constants and Comments
$^{\bullet}OH + ClO^- \rightarrow ClO^{\bullet} + OH^-$	9.11	$(9.0 \pm 0.5) \times 10^9$ M^{-1} s^{-1} (Buxton & Subhani, 1972a)
$O^{\bullet-} + ClO^- \rightarrow ClO^{\bullet} + O^{2-}$	9.12	$(2.4 \pm 0.1) \times 10^8$ M^{-1} s^{-1} (Buxton & Subhani, 1972a)
$Cl^{\bullet} + ClO^- \rightarrow ClO^{\bullet} + Cl^-$	9.13	8.2×10^9 M^{-1} s^{-1} (Kläning & Wolff, 1985)
$2\ ClO^{\bullet} \rightleftharpoons Cl_2O_2$	9.14	$2k = 1.5 \times 10^{10}$ M^{-1} s^{-1} (Buxton & Subhani, 1972a)
$Cl_2O_2 + H_2O \rightarrow ClO_2^- + ClO^- + 2\ H^+$	9.15	
$Cl_2O_2 + H_2O \rightarrow Cl^- + O_2 + ClO^- + 2\ H^+$	9.16	$k_{9.15}/k_{9.16} = 1.93 \pm 0.24$ (Buxton & Subhani, 1972b)
$Cl_2O_2 + ClO_2^- \rightarrow ClO_3^- + Cl_2O$	9.17	$k_{9.17}/k_{9.15} = (1.3 \pm 0.6) \times 10^5$ M^{-1} (Buxton & Subhani, 1972b)
$Cl_2O + H_2O \rightleftharpoons 2\ HOCl$	9.18	
$^{\bullet}OH + ClO_2^- \rightarrow ClO_2 + HO^-$	9.19	$(6.3 \pm 0.5) \times 10^9$ M^{-1} s^{-1} (Buxton & Subhani, 1972a)
$O^{\bullet-} + ClO_2^- \rightarrow ClO_2 + O^{2-}$	9.20	$(1.9 \pm 0.1) \times 10^8$ M^{-1} s^{-1} (Buxton & Subhani, 1972a)
$^{\bullet}OH + ClO_3^- \rightarrow$ Products	9.21	$<10^6$ M^{-1} s^{-1} (Buxton & Subhani, 1972a)
$O^{\bullet-} + ClO_3^- \rightarrow$ Products	9.22	$<10^6$ M^{-1} s^{-1} (Buxton & Subhani, 1972a)
$O(^1D) + H_2O \rightarrow H_2O_2$	9.23	$O(^1D)$ only produced at $\lambda = 313$ and 253.7 nm
$ClO^- + H_2O_2 \rightarrow O_2 + Cl^- + H_2O$	9.24	
$O(^3P) + ClO^- \rightarrow ClO_2^-$	9.25	
$O(^3P) + ClO^- \rightarrow Cl^- + O_2$	9.26	$k_{9.26}/k_{9.25} = 0.17 \pm 0.09$ (Buxton & Subhani, 1972b)
$O(^3P) + ClO_2^- \rightarrow ClO_3^-$	9.27	
$O(^3P) + ClO_2^- \rightarrow Cl^- + O_2 + O(^3P)$	9.28	$k_{9.28}/k_{9.27} = 1.50 \pm 0.27$ (Buxton & Subhani, 1972b)
$O(^3P) + O_2 \rightarrow O_3$	9.29	4×10^9 M^{-1} s^{-1} (Kläning *et al.* 1984)
$O^{\bullet-} + O_2 \rightleftharpoons O_3^{\bullet-}$	9.30	3.6×10^9 M^{-1} s^{-1} (Buxton *et al.* 1988)
$ClO^{\bullet} + O_3^{\bullet-} \rightarrow O_3 + ClO^-$	9.31	1×10^9 M^{-1} s^{-1} (Kläning *et al.* 1984)

and 350 nm, Rao *et al.* (2010) also confirmed that chlorite was only produced at 350 nm. Buxton and Subhani (1972b) explained the absence of chlorite in irradiated solutions of ClO^- at 253.7 and 313 nm by the low yield of $O(^3P)$ and by destruction of any chlorite ion produced from Cl_2O_2 (reaction 9.17). Chlorite can also be oxidized to chlorine dioxide by $^\bullet OH/O^{\bullet-}$ (reactions 9.19 and 9.20). Other studies showed that chlorine dioxide can be oxidized to chlorate by $^\bullet OH/O^{\bullet-}$ (Kläning *et al.* 1985):

$$^\bullet OH + ClO_2 \rightarrow ClO_3^- + H^+ \quad (k = 4.0 \pm 0.4) \times 10^9\ M^{-1}\ s^{-1};\ \text{Kläning } et\ al. 1985) \tag{9.32}$$

$$O^{\bullet-} + ClO_2 \rightarrow ClO_3^- \qquad (k = 2.7 \pm 0.4) \times 10^9\ M^{-1}\ s^{-1};\ \text{Kläning } et\ al. 1985) \tag{9.33}$$

The oxygen atoms $O(^1D)$ and $O(^3P)$ produced through hypochlorite photolysis (reactions 9.5 and 9.7, Table 1) also contribute to the decomposition of hypochlorite. Most of $O(^1D)$ will react with water molecules to generate H_2O_2 (reaction 9.23) which further reacts with hypochlorite to form dioxygen ($^1O_2$) and chloride (reaction 9.24). H_2O_2 has also been detected during electrochemical oxidation of hypochlorite solutions at pH 9.5 by Macounová *et al.* (2015) and its formation has been attributed to the following set of reactions initiated by the hydrolysis of $ClO^\bullet$ to $HO_2^\bullet/O_2^{\bullet-}$ radicals:

$$ClO^\bullet + H_2O \rightarrow HO_2^\bullet + Cl^- + H^+ \tag{9.34}$$

$$ClO^\bullet + OH^- \rightarrow O_2^{\bullet-} + Cl^- + H^+ \tag{9.35}$$

$$O_2^{\bullet-} + HOCl \rightarrow O_2 + Cl^- + {}^\bullet OH \tag{9.36}$$

$$HO_2^\bullet \rightleftharpoons O_2^{\bullet-} + H^+ \tag{9.37}$$

$$HO_2^\bullet + O_2^{\bullet-} + H_2O \rightleftharpoons H_2O_2 + O_2 + OH^- \tag{9.38}$$

$O(^3P)$ atoms can both reduce hypochlorite and chlorite to chloride (reactions 9.26 and 9.28) and oxidize hypochlorite and chlorite to chlorite and chlorate (reactions 9.25 and 9.27), respectively. The distribution of stable photoproducts (Cl^-, ClO_3^- and O_2) will therefore depend on the quantum yields of formation of $O(^1D)$ and $O(^3P)$ which are wavelength dependent (Table 9.1), and on the absolute and relative rate constants of reactions 9.25–9.28.

Buxton and Subhani (1972b) observed the formation of ozone (O_3) and ozonide anion radicals ($O_3^{\bullet-}$) in flash photolysis experiments of O_2-saturated solutions of ClO^-, which was attributed to reactions 9.29–9.30. Ozone can be involved in reactions with ClO^-, ClO_2^- and with chlorine containing free radicals (e.g., $Cl^\bullet$, $ClO^\bullet$) (Siddiqui, 1996; von Sonntag & von Gunten, 2012).

In addition, chlorite and chlorine dioxide can also be photodecomposed to chloride and chlorate as major end-products (Buxton & Subhani 1972a; Karpel Vel Leitner *et al.* 1992a, 1992b).

The photodecomposition pathways of HOCl in water are not known. $^\bullet OH$ and $Cl^\bullet$ generated from the primary step of HOCl photolysis react with HOCl to form $ClO^\bullet$ (reactions 9.39 and 9.40 in Table 9.4). The self-reaction of $ClO^\bullet$ forms Cl_2O_2 which decomposes to Cl^-, ClO_2^-, ClO_3^- and O_2, whereas secondary reactions of $^\bullet OH$ with ClO_2^- result in ClO_2 and ClO_3^-.

As shown in Table 9.4, the rate constants for the reaction of $^\bullet OH$ and $Cl^\bullet$ with free chlorine (HOCl and ClO^-) are not well documented in the literature and the published values for the reaction of $HO^\bullet$ with HOCl differ by several orders of magnitude (from $8.46 \times 10^4\ M^{-1}\ s^{-1}$ to $2 \times 10^9\ M^{-1}\ s^{-1}$).

Table 9.4 Rate constants for the reaction of •OH and Cl• with HOCl and ClO^-.

Reactions		Rate Constant ($M^{-1}\ s^{-1}$)	Reference
$^{\bullet}OH + HOCl \rightarrow ClO^{\bullet} + H_2O$	9.39	1.4×10^8	Zuo *et al.* (1997); pH 0.
		2.0×10^9	Matthew & Anastasio (2006)
		8.46×10^4	Watts & Linden (2007a)
$^{\bullet}OH + ClO^- \rightarrow ClO^{\bullet} + HO^-$	9.11	$(9.0 \pm 0.5) \times 10^9$	Buxton & Subhani (1972a)
		2.7×10^9	Zuo *et al.* (1997)
$Cl^{\bullet} + HOCl \rightarrow ClO^{\bullet} + HCl$	9.40	3.0×10^9	Kläning & Wolff (1985)
$Cl^{\bullet} + ClO^- \rightarrow ClO^{\bullet} + Cl^-$	9.13	8.2×10^9	Kläning & Wolff (1985)

It has also been shown that trace levels of perchlorate (ClO_4^-) can be formed from the photodecomposition of ClO^- at pH > 10 (Kang *et al.* 2006) or of free chlorine ($HOCl + ClO^-$) at initial pH values ranging from 2.6 to 11.4 (Rao *et al.* 2010). As •OH cannot oxidize ClO_3^-, perchlorate production has been attributed to the oxidation of ClO_3^- by Cl• to $ClO_3^{\bullet}$ radicals, which dimerize to give dichlorine hexaoxide Cl_2O_6. The subsequent hydrolysis of Cl_2O_6 results in ClO_4^- and ClO_3^- (Kang *et al.* 2006; Rao *et al.* 2010):

$$ClO_3^- + Cl^{\bullet} \rightarrow ClO_3^{\bullet} + Cl^- \tag{9.41}$$

$$ClO_3^{\bullet} + ClO_3^{\bullet} \rightarrow Cl_2O_6 \tag{9.42}$$

$$Cl_2O_6 + H_2O \rightarrow ClO_4^- + ClO_3^- + 2H^+ \tag{9.43}$$

Rao *et al.* (2010) found that the amount of ClO_4^- formed depends on the initial concentrations of free chlorine species, the background concentrations of Cl^-, ClO_2^- and ClO_3^-, wavelength and pH, but it is independent of light intensity. However, the concentration of ClO_4^- would not exceed 0.1 μg/L in the UV/Cl_2 applications to drinking water treatment ([Cl_2] < 0.1 mM; pH 7) (Rao *et al.* 2010).

9.2.3.3 Reaction quantum yields of chlorine photodecomposition in the absence of organic compounds

Table 9.5 summarizes the overall quantum yield values of photodecomposition of HOCl (Φ-HOCl, acidic pH), ClO^- (Φ-ClO^-, alkaline pH), and of their combination at pH values where the two species co-exist (Φ-Chlorine) as reported in the literature.

Feng *et al.* (2010) determined the overall quantum yield of photodecomposition of free chlorine at 253.7 nm using the expression developed by Bolton and Stefan (2002):

$$\ln\frac{[C]_0}{[C]_F} = k_1' F = \frac{\Phi\,\varepsilon(\lambda)\ln(10)}{10U(\lambda)} F \tag{9.44}$$

$$\Phi_\lambda = \frac{k_1' \times 10 \times U(\lambda)}{\varepsilon(\lambda)\ln(10)} \tag{9.45}$$

Table 9.5 Overall quantum yields of photodecomposition of HOCl (Φ-HOCl), ClO^- (Φ-ClO^-) and their mixture (Φ-Chlorine) in organic-free water.

Chlorine Species	Experimental Conditions			Quantum Yield (Φ)	Quantum Yield	References
	pH	Wavelength (nm)	[Chlorine] (mM)			
ClO^-	11.5	253.7	1	Φ-ClO^-	0.86 ± 0.07	Buxton & Subhani (1972b)
ClO^-	12.0	313	1	Φ-ClO^-	0.43 ± 0.06	Buxton & Subhani (1972b)
ClO^-	12.1	365	7–10	Φ-ClO^-	0.64 ± 0.05	Buxton & Subhani (1972b)
HOCl + ClO^-	5, 7 and 9	240	5.71	Φ-Chlorine	1.21 (pH 5) 1.24 (pH 7) 1.50 (pH 9)	Cooper *et al.* (2007)
HOCl + ClO^-	5, 7 and 9	253.7	5.71	Φ-Chlorine	1.64 (pH 5) 1.51 (pH 7) 0.84 (pH 9)	Cooper *et al.* (2007)
HOCl + ClO^-	5, 7 and 9	265.2	5.71	Φ-Chlorine	1.39 (pH 5) 1.10 (pH 7) 0.92 (pH 9)	Cooper *et al.* (2007)
HOCl + ClO^-	5, 7 and 9	296.7	5.71	Φ-Chlorine	0.78 (pH 5) 0.76 (pH 7) 0.80 (pH 9)	Cooper *et al.* (2007)
HOCl + ClO^-	5, 7 and 9	313	5.71	Φ-Chlorine	0.80 (pH 5) 0.71 (pH 7) 0.80 (pH 9)	Cooper *et al.* (2007)
HOCl + ClO^-	5 and 7	334	5.71	Φ-Chlorine	0.69 (pH 5) 0.61 (pH 7)	Cooper *et al.* (2007)
HOCl + ClO^-	5 and 7	365	5.71	Φ-Chlorine	0.73 (pH 5) 0.55 (pH 7)	Cooper *et al.* (2007)
HOCl	5	253.7	< 1	Φ-HOCl	1.0 ± 0.1	Feng *et al.* (2007)
HOCl	5	253.7	19	Φ-HOCl	4.5 ± 0.2	Feng *et al.* (2007)
ClO^-	10	253.7	0.05–9	Φ-ClO^-	0.9 ± 0.1	Feng *et al.* (2007)
HOCl	4	253.7	0.014–0.056	Φ-HOCl	1.5	Watts & Linden (2007a)
HOCl	4	MP UV (200–350)	0.014–0.056	Φ-HOCl	3.7	Watts & Linden (2007a)
ClO^-	10	253.7	0.014–0.056	Φ-ClO^-	1.2	Watts & Linden (2007a)
ClO^-	10	MP lamp (200–350)	0.014–0.056	Φ-ClO^-	1.7	Watts & Linden (2007a)
HOCl + ClO^-	7.1–7.9	253.7	0.014–0.056	Φ-Chlorine	1.3–1.7	Watts & Linden (2007a)

(*Continued*)

Table 9.5 Overall quantum yields of photodecomposition of HOCl (Φ-HOCl), ClO^- (Φ-ClO^-) and their mixture (Φ-Chlorine) in organic-free water. (*Continued*)

Chlorine species	Experimental conditions			Quantum yield (Φ)	Quantum yield	References
	pH	Wavelength (nm)	[Chlorine] (mM)			
$HOCl + ClO^-$	7.1–7.9	MP UV (200–350)	0.014–0.056	Φ-Chlorine	1.2–1.7	Watts & Linden (2007a)
HOCl	5	253.7 nm	1.41	Φ-ClO^-	1.0 ± 0.1	Jin *et al.* (2011)
ClO^-	10	253.7 nm	1.41	Φ-ClO^-	1.15 ± 0.08	Jin *et al.* (2011)
ClO^-	10	303 ± 8 nm	0–4.23	Φ-ClO^-	0.87 ± 0.01	Chan *et al.* (2012)
HOCl	5	MP lamp	0.15	Φ-HOCl	1.06 ± 0.01	Wang *et al.* (2012)
ClO^-	10	MP lamp	0.15	Φ-ClO^-	0.89 ± 0.08	Wang *et al.* (2012)
HOCl	5	253.7 nm	0.01–0.1	Φ-HOCl	1.45 ± 0.06	Fang *et al.* (2014)
ClO^-	10	253.7 nm	0.01–0.1	Φ-ClO^-	0.97 ± 0.05	Fang *et al.* (2014)

where

$[C]_0$ and $[C]_t$ are the concentrations (M) of free chlorine before and after exposure to UV light, respectively,
F is the fluence at the wavelength λ (J m^{-2}),
k'_1 is the fluence-based first-order rate constant (m^2 J^{-1}),
Φ (λ) is the overall quantum yield of photodecomposition of free chlorine at wavelength λ,
ε (λ) is the molar absorption coefficient (M^{-1} cm^{-1}) of free chlorine at wavelength λ,
U (λ) is the molar photon energy (J $einstein^{-1}$) at wavelength λ.

When irradiated with the polychromatic radiation emitted by the medium pressure (MP) UV lamps, the free chlorine species can be photodegraded by all radiations absorbed in the 200–375 nm range (Figure 9.2). Under MP-UV irradiation, an apparent quantum yield of photodecomposition of free chlorine ($\Phi_{300-375\ nm}$) can be determined from the photolysis *pseudo*-first order rate constant (k_1, s^{-1}) and the specific rate of light absorption by free chlorine species summed over all wavelengths ($\Sigma\ k_s(\lambda)$, einstein mol^{-1} s^{-1}) using the expressions developed by Schwazenbach *et al.* (1993):

$$\Phi_{200-375nm} = \frac{k_1}{\sum k_S(\lambda)} \tag{9.46}$$

$$k_S(\lambda) = \frac{E_p^0(\lambda)\varepsilon(\lambda)[1 - 10^{-a(\lambda)z}]}{a(\lambda)z} \tag{9.47}$$

where

E_P^0 is the incident photon irradiance (10^{-3} einstein cm^{-2} s^{-1}),
a (λ) represents the solution absorption coefficient (cm^{-1}) at wavelength λ,
z is the depth of solution layer (cm).

Despite the disparity of the published values (Table 9.2), most quantum yields for the decomposition of HOCl ($pH \approx 5$) in dilute aqueous solution ($[Cl_2]_{0,T} < 1$ mM) are in the range 0.90–1.64 at radiation

wavelengths in the range 240 to 265 nm. If each $^{\bullet}OH$ and $Cl^{\bullet}$ generated from the primary step of photolysis of HOCl (reaction 9.8) decomposes another molecule of HOCl, the overall quantum yield of photodecomposition of HOCl should be equal to $3\Phi_{primary}$ (if no free chlorine is generated by subsequent reactions), where $\Phi_{primary}$ represents the primary quantum yield of photolysis of HOCl. The highest overall quantum values reported in Table 9.5 for the photodecomposition of HOCl in the range 240–365 nm ($1.45 < \Phi < 1.64$) seem to be consistent with the primary quantum yield value of photolysis of HOCl at 266 nm ($\Phi_{primary} \approx 0.5 \pm 0.05$) determined by Thomsen *et al.* (2001). For radiation wavelengths longer than 290 nm, the published overall quantum yields of photolysis of HOCl at monochromatic radiation are in the range 0.69–0.80 (Table 9.5). Similar experiments conducted with free chlorine solution at pH ≈ 9 (ClO^- present as the predominant free chlorine species) or with aqueous solution of hypochlorite (pH > 11) show that the overall quantum yields of photodecomposition of ClO^- are roughly equal to 0.75 ± 0.10.

Under polychromatic irradiation (MP UV lamp; 200–350 nm), overall quantum yields close to unity were determined by Wang *et al.* (2012) at pH 5 and 10, whereas higher values were obtained by Watts and Linden (2007a) at pH 4 ($\Phi = 3.7$) and at pH 7.1–7.9 ($\Phi = 1.2$–1.7) (Table 9.5).

Cooper *et al.* (2007) examined the rates of photodecomposition of free chlorine ($[Cl_2]_{0,T} = 5.1$ mM) at various wavelengths (from 240 to 365 nm) and at various pH (pH 5, 7 and 9). The authors isolated *quasi*-monochromatic radiation from a Xe-Hg lamp using narrow band cut-off filters (10 nm band-width). The data obtained at pH 5 and 7 show a decrease of the quantum yields with increasing wavelength.

Feng *et al.* (2007) showed that the quantum yield of photodecomposition of HOCl (pH 5) at 253.7 nm increased linearly when the concentration of HOCl increased from 70 to 1350 mg chlorine/L ($\Phi = 1.0 \pm 0.1$ for [HOCl] < 70 mg/L and $\Phi = 4.5 \pm 0.2$ for [HOCl] = 1350 mg/L) whereas the quantum yield of ClO^- photolysis (pH 10) did not vary with the concentration of chlorine ($\Phi = 0.9 \pm 0.1$ for $3.5 < [ClO^-] < 640$ mg/L). The increase in the quantum yield of HOCl photodecomposition with the concentration of HOCl has been attributed to chain reactions initiated by $^{\bullet}OH$ and $Cl^{\bullet}$ radicals (Table 9.4). However, the concentration-independent quantum yield reported by Feng *et al.* (2007) for the photodecomposition of ClO^- remains unexplained providing that $^{\bullet}OH$ and $Cl^{\bullet}$ can also decompose ClO^- ($k > 1 \times 10^9$ M^{-1} s^{-1}; Table 9.4).

9.2.3.4 Reaction quantum yields of chlorine photodecomposition in the presence of organic compounds

Addition of methanol was found to accelerate the photodecomposition of chlorine at sunlight wavelengths, especially at low pH (Nowell & Crosby, 1985). Feng *et al.* (2007) also demonstrated that addition of methanol increased the photodecomposition rate of HOCl at 253.7 nm. As shown in Figure 9.5, the quantum yield of photodecomposition of HOCl in the absence and in the presence of 120 mM of methanol were equal to 1.0 ± 0.1 and ~55, respectively. In another study, the quantum yield of HOCl photolysis at pH 5 and 253.7 nm increased from (1.0 ± 0.1) to (16.3 ± 0.3) when the concentration of methanol increased from 0 to 86.5 mM (Jin *et al.* 2011). By contrast, addition of methanol (0–50 mM) did not affect the rate of photodecomposition of ClO^- (pH = 10) as reported by Feng *et al.* (2007) and Jin *et al.* (2011), i.e. (1.20 ± 0.20) at $20 < [CH_3OH]_0 < 50$ mM) and (1.15 ± 0.08) at $0 < [CH_3OH]_0 < 61.8$ mM, respectively.

The increase of the quantum yield of HOCl in the presence of methanol has been explained by chain reactions involving organic radicals as also suggested by Oliver and Carey (1977):

$$RH + {}^{\bullet}OH \rightarrow R^{\bullet} + H_2O \tag{9.48}$$

$$RH + Cl^{\bullet} \rightarrow R^{\bullet} + H^+ + Cl^- \tag{9.49}$$

$$R^{\bullet} + HOCl \rightarrow ROH + Cl^{\bullet} \quad (9.50)$$

$$R^{\bullet} + HOCl \rightarrow RCl + {}^{\bullet}OH \quad (9.51)$$

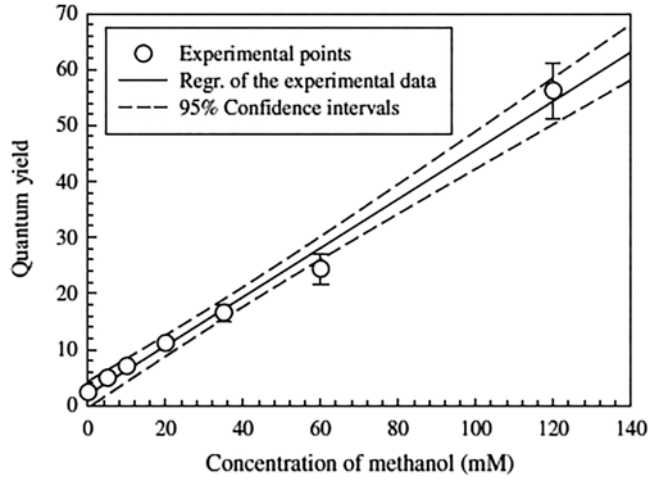

Figure 9.5 Quantum yield of HOCl photolysis (253.7 nm, pH 5) as a function of methanol concentration (Feng *et al.* 2007).

This accelerating effect on the rate of photodecomposition of free chlorine was also observed with more complex molecules like those constituting the natural organic matter (NOM) present in drinking water (Ormeci *et al.* 2005). By dissolving a mixture of humic acid and alginic acid in deionized water (pH ~ 7.2) followed by chlorination for 5 hours to minimize the background chlorine demand during the photolysis experiments, Feng *et al.* (2010) showed that the quantum yields of free chlorine photolysis at 253.7 nm increased linearly with TOC concentration ($\Phi = 1.0 \pm 0.1$ for TOC < 0.4 mg/L; $\Phi = 4.9 \pm 0.4$ for TOC ~ 6.8 mg/L).

Feng *et al.* (2007) determined similar fluence-based rate constants (~2.9×10^{-5} m^2 J^{-1}) for 71 mg/L (1 mM) free chlorine decomposition at pH 5 and pH 10 in deionized water, under exposure to the 253.7 nm radiation. That would correspond to UV doses of ~2.4×10^4 J m^{-2} and ~8×10^4 J m^{-2} required to decompose 50% and 90% of free chlorine, respectively. At a UV dose of 400 J m^{-2} typically used for UV disinfection of drinking water, the decomposition of free chlorine would be nearly 1% (pH independent), when the initial concentration of free chlorine is lower than 71 mg/L.

Lower UV doses (2×10^3–6×10^3 J m^{-2}) are needed to reduce the free chlorine concentration by 50% in surface water or in drinking water containing about 2–4 mg/L TOC (Ormeci *et al.* 2005).

Wang *et al.* (2012) determined the fluence-based rate constants (m^2 J^{-1}) for photodecomposition of free chlorine species under polychromatic radiation emitted from a MP lamp as $(15.0 \pm 0.1) \times 10^{-6}$, $(33.7 \pm 0.4) \times 10^{-6}$ and $(58.7 \pm 1.5) \times 10^{-6}$ at pH 5, 7.5, and 10, respectively. These rate constants are up to one order of magnitude larger than those determined for H_2O_2 photolysis under the same pH and UV radiation conditions. Fluence-based rate constants for free chlorine and monochloramine photodegradation at pH 6 and 9 under monochromatic (253.7 nm) and polychromatic (200–400 nm) radiation as function of chlorine concentration and water quality were reported by Watts and Linden (2007a).

9.3 REACTIVITY AND FATE OF CHLORINE RADICALS

9.3.1 Equilibria involving the Cl•, $Cl_2^{\bullet-}$ and •OH species

As chloride is always present in free chlorine solutions, Cl• and •OH generated from the photolysis of HOCl and ClO^- can react with chloride to give $Cl_2^{\bullet-}$, HClOH• and $ClOH^{\bullet-}$. The chlorine-containing free radicals and •OH are involved in very fast equilibria. The rate constants for various reactions have been reported in the literature and are summarized in Table 9.6. Of note, the reactions given in Table 9.6 do not lead to a decrease of the total concentration of radicals.

Table 9.6 Rate constants for various equilibrium reactions involving Cl• and •OH in the presence of chloride.

Reaction		Rate constants
$Cl^\bullet + Cl^- \rightarrow Cl_2^{\bullet-}$	9.52	4.1×10^9 M^{-1} s^{-1} (Jayson *et al.* 1973) 6.5×10^9 M^{-1} s^{-1} (Kläning & Wolff, 1985) $(8.5 \pm 0.7) \times 10^9$ M^{-1} s^{-1} (Buxton *et al.* 1998) $(7.8 \pm 0.8) \times 10^9$ M^{-1} s^{-1} (Yu & Barker, 2003) $(7.8 \pm 0.8) \times 10^9$ M^{-1} s^{-1} (Yu, 2004)
$Cl_2^{\bullet-} \rightarrow Cl^\bullet + Cl^-$	9.53	$(1.1 \pm 0.4) \times 10^5$ s^{-1} (Jayson *et al.* 1973) $(6.0 \pm 0.5) \times 10^4$ s^{-1} (Buxton *et al.* 1998) $(5.2 \pm 0.3) \times 10^4$ s^{-1} (Yu & Barker, 2003) $(5.7 \pm 0.4) \times 10^4$ s^{-1} (Yu, 2004)
$Cl^\bullet + H_2O \rightarrow HClOH^\bullet$	9.54	$(2.5 \pm 0.2) \times 10^5$ s^{-1} (McElroy, 1990)
$HClOH^\bullet \rightarrow Cl^\bullet + H_2O$	9.55	$<1 \times 10^3$ s^{-1} (McElroy, 1990)
$Cl^\bullet + H_2O \rightarrow ClOH^{\bullet-} + H^+$	9.56	7.2×10^4 s^{-1} (Jayson *et al.* 1973) 1.6×10^5 s^{-1} (Kläning & Wolff, 1985) $(2.5 \pm 0.2) \times 10^5$ s^{-1} (McElroy, 1990) $(1.8 \pm 0.6) \times 10^5$ s^{-1} (Yu, 2004)
$ClOH^{\bullet-} + H^+ \rightarrow Cl^\bullet + H_2O$	9.57	$(2.1 \pm 0.7) \times 10^{10}$ M^{-1} s^{-1} (Jayson *et al.* 1973) 2.1×10^{10} M^{-1} s^{-1} (Kläning & Wolff, 1985) $(2.6 \pm 0.6) \times 10^{10}$ M^{-1} s^{-1} (Yu & Barker, 2003) $(2.4 \pm 0.4) \times 10^{10}$ M^{-1} s^{-1} (Yu, 2004)
$^\bullet OH + Cl^- \rightarrow ClOH^{\bullet-}$	9.58	$(4.3 \pm 0.4) \times 10^9$ M^{-1} s^{-1} (Jayson *et al.* 1973) $(4.2 \pm 0.2) \times 10^9$ M^{-1} s^{-1} (Yu, 2004)
$ClOH^{\bullet-} \rightarrow {}^\bullet OH + Cl^-$	9.59	$(6.1 \pm 0.8) \times 10^9$ s^{-1} (Jayson *et al.* 1973) $(6.0 \pm 1.1) \times 10^9$ s^{-1} (Yu, 2004)
$Cl_2^{\bullet-} + H_2O \rightarrow HClOH^\bullet + Cl^-$	9.60	1.3×10^3 s^{-1} (McElroy, 1990)
$HClOH^\bullet + Cl^- \rightarrow Cl_2^{\bullet-} + H_2O$	9.61	5×10^9 M^{-1} s^{-1} (McElroy, 1990)
$Cl_2^{\bullet-} + HO^- \rightarrow ClOH^{\bullet-} + Cl^-$	9.62	4.5×10^7 M^{-1} s^{-1} (Grigorev *et al.* 1987)
$ClOH^{\bullet-} + Cl^- \rightarrow Cl_2^{\bullet-} + HO^-$	9.63	1.0×10^5 M^{-1} s^{-1} (Grigorev *et al.* 1987)
$Cl^\bullet + OH^- \rightarrow ClOH^{\bullet-}$	9.64	1.8×10^{10} M^{-1} s^{-1} (Kläning & Wolff, 1985)
$ClOH^{\bullet-} \rightarrow {}^\bullet OH + Cl^-$	9.65	23 s^{-1} (Kläning & Wolff, 1985)
$HClOH^\bullet \rightarrow ClOH^{\bullet-} + H^+$	9.66	1.0×10^8 s^{-1} (McElroy, 1990)
$Cl_2^{\bullet-} + H_2O \rightarrow ClOH^{\bullet-} + H^+ + Cl^-$	9.67	$<1 \times 10^2$ (Yu & Baker, 2003)

Not all reactions in Table 9.6 are well-known or well-understood, and discrepancies still exist between reported rate constants and measured equilibrium constants (Yu, 2004). Such uncertainties impact severely the accuracy of the kinetic models for the UV/Chlorine AOP reported in the literature, as well as the calculations of the concentrations of reactive radicals (•OH and Cl-based radicals) in this process. Armstrong *et al*. (2015) recommend the following values of equilibrium constants and uncertainties for the reactions involving Cl-based radicals and •OH:

$$Cl^{\bullet} + Cl^{-} \rightleftharpoons Cl_2^{\bullet-} \qquad K = (1.4 \pm 0.2) \times 10^5\,M^{-1} \qquad (9.52–9.53)$$

$$Cl^{\bullet} + H_2O \rightleftharpoons ClOH^{\bullet-} + H^{+} \qquad K = 5.0 \times 10^{-6}\,M \text{ (uncertainty within a factor of two)} \qquad (9.56–9.57)$$

$$^{\bullet}OH + Cl^{-} \rightleftharpoons ClOH^{\bullet-} \qquad K = (0.70 \pm 0.13)\,M^{-1} \qquad (9.58–9.59)$$

$$^{\bullet}OH + Cl^{-} + H^{+} \rightleftharpoons Cl^{\bullet} + H_2O \qquad K = 9.1 \times 10^4\,M^{-2} \text{ (uncertainty within a factor of two)} \qquad (9.68)$$

$$Cl_2^{\bullet-} + H_2O \rightleftharpoons {}^{\bullet}OH + H^{+} + 2Cl^{-} \qquad K = (6.1 \pm 0.7) \times 10^{-11}\,M^3 \qquad (9.69)$$

Reactions 9.52–9.69 show that the types and concentrations of radicals in organic-free water will depend on pH and on the concentration of chloride. For example, based on the above reported bimolecular rate constants and equilibrium constants, one can conclude that $Cl^{\bullet}$ can be converted into $Cl_2^{\bullet-}$ in the presence of chloride at concentrations higher than ~1 mM under acidic pH or into •OH at neutral pH. However, more studies are required to understand and to validate the contribution of each reactive radical species to the degradation of micropollutants *via* UV/Chlorine process.

9.3.2 Termination reactions of •OH, Cl• and $Cl_2^{\bullet-}$ in water

Termination reactions involving •OH, $Cl^{\bullet}$ and $Cl_2^{\bullet-}$ decrease the concentrations of free radicals and lead to the formation of free chlorine (reactions 9.71–9.74 in Table 9.7) and hydrogen peroxide (reaction 9.70 in Table 9.7). H_2O_2 can then reduce free chlorine to chloride and O_2 (reactions 9.77 and 9.78; Held *et al*. 1978).

Table 9.7 Termination reactions involving •OH, $Cl^{\bullet}$ and $Cl_2^{\bullet-}$ and subsequent reactions.

Reactions		Rate Constants ($M^{-1}\,s^{-1}$)	Reference
$^{\bullet}OH + {}^{\bullet}OH \rightarrow H_2O_2$	9.70	5.5×10^9	Buxton *et al.* (1988)
$Cl^{\bullet} + Cl^{\bullet} \rightarrow Cl_2$	9.71	8.8×10^7	Wu *et al.* (1980)
$Cl_2^{\bullet-} + Cl_2^{\bullet-} \rightarrow Cl_2 + 2\,Cl^{-}$	9.72	$\log(k) = 8.8 + 1.6\,I^{0.5}/(I^{0.5} + 1)$ $k = 6.3 \times 10^8\,M^{-1}\,s^{-1}$ for I = 0	Alegre *et al.* (2000)
$Cl_2^{\bullet-} + {}^{\bullet}OH \rightarrow HOCl + Cl^{-}$	9.73	1×10^9	Wagner *et al.* (1986)
$Cl_2^{\bullet-} + Cl^{\bullet} \rightarrow Cl_2 + Cl^{-}$	9.74	2.1×10^9	Yu *et al.* (2004)
$Cl_2 + H_2O \rightarrow HOCl + HCl$	9.1		
$HOCl \rightleftharpoons ClO^{-} + H^{+}$	9.2		
$^{\bullet}OH + HOCl/ClO^{-} \rightarrow ClO^{\bullet} + H_2O/HO^{-}$	9.39/9.11	Table 9.4	
$Cl^{\bullet} + HOCl/ClO^{-} \rightarrow ClO^{\bullet} + HCl/Cl^{-}$	9.40/9.13	Table 9.4	
$Cl_2^{\bullet-} + ClO^{-} \rightarrow ClO^{\bullet} + 2\,Cl^{-}$	9.75	5.4×10^8 ($I = 5$ M)	Zuo *et al.* (1997)
$H_2O_2 \rightleftharpoons HO_2^{-} + H^{+}$	9.76	$pK_a = 11.7$	
$H_2O_2 + ClO^{-} \rightarrow Cl^{-} + {}^1O_2 + H_2O$	9.77	3.4×10^3	Held *et al.* (1978)
$HO_2^{-} + HOCl \rightarrow Cl^{-} + {}^1O_2 + H_2O$	9.78	4.4×10^7	Held *et al.* (1978)

The role of radical – radical termination reactions on the decomposition pathways of free chlorine in the UV/Cl_2 process is relatively minor because the concentrations of free radicals are much lower than the concentrations of free chlorine species and therefore most of the $^{\bullet}OH$, $Cl^{\bullet}$ and $Cl_2^{\bullet-}$ will be consumed by the molecular chlorine species or by other radical scavengers present in water.

9.3.3 Reactivity of $Cl^{\bullet}$ and $Cl_2^{\bullet-}$ towards organic and inorganic compounds

9.3.3.1 Methods for determination of $Cl^{\bullet}$ and $Cl_2^{\bullet-}$ rate constants

$Cl^{\bullet}$ and $Cl_2^{\bullet-}$ are strong oxidants with $E°(Cl^{\bullet}/Cl^{-}) = 2.43$ V and $E°(Cl_2^{\bullet-}/2Cl^{-}) = 2.13$ V *vs* NHE (Armstrong *et al*. 2015). $Cl^{\bullet}$ and $Cl_2^{\bullet-}$ react with organic and inorganic compounds by H-atom abstraction, electron transfer or addition to unsaturated bonds. The rate constants for the reactions of $Cl^{\bullet}$ and $Cl_2^{\bullet-}$ with solutes in water are very scarce.

The bimolecular rate constants of $Cl^{\bullet}$ and $Cl_2^{\bullet-}$ with solutes are usually determined from pulse radiolysis or laser flash photolysis experiments by monitoring the decay of transient absorbance at 340 nm. Both $Cl^{\bullet}$ and $Cl_2^{\bullet-}$ display an absorption band with molar absorption coefficients at 340 nm of ~3700 and ~8800 M^{-1} cm^{-1}, respectively (Thomsen *et al*. 2001; Yu *et al*. 2004).

$Cl^{\bullet}$ can be generated directly by laser flash photolysis of chloroacetone (Buxton *et al*. 2000, reaction 9.79), and indirectly, by pulse radiolysis of aqueous solutions of sodium chloride (reactions 9.80, 9.56–9.59). Chlorine atoms can be also generated during flash photolysis of sodium persulfate solution in the presence of chloride ions (reactions 9.81–9.82):

$$CH_3C(O)CH_2Cl + h\nu \rightarrow CH_3C(O)CH_2^{\bullet} + Cl^{\bullet} \quad (9.79)$$

$$H_2O \rightsquigarrow H^{\bullet}, {}^{\bullet}OH, e_{aq}^{-}, H^{+}, H_2O_2, H_2 \quad (9.80)$$

$$^{\bullet}OH + Cl^{-} \rightleftharpoons ClOH^{\bullet-} \quad (9.58–9.59)$$

$$ClOH^{\bullet-} + H^{+} \rightleftharpoons Cl^{\bullet} + H_2O \quad (9.56–9.57)$$

$$S_2O_8^{2-} + h\nu \rightarrow 2SO_4^{\bullet-} \quad (9.81)$$

$$SO_4^{\bullet-} + Cl^{-} \rightleftharpoons Cl^{\bullet} + SO_4^{2-} \quad (9.82)$$

Chlorine and dichlorine radicals oxidize the organic or inorganic solutes, S:

$$Cl^{\bullet} + S \rightarrow \text{Products} \quad (9.83)$$

$$Cl_2^{\bullet-} + S \rightarrow \text{Products} \quad (9.84)$$

The system is selected such that the substrate S decays exclusively through $Cl^{\bullet}$ and $Cl_2^{\bullet-}$ radicals:

$$-d[S]/dt = (k_1[Cl^{\bullet}] + k_2[Cl_2^{\bullet-}])[S] \quad (9.85)$$

where k_1 and k_2 are the second-order rate constants (M^{-1} s^{-1}) for the reaction of $Cl^{\bullet}$ and $Cl_2^{\bullet-}$ with S, respectively.

If [S] ≫ [$Cl^{\bullet}$] and ([S] ≫ [$Cl_2^{\bullet-}$], the degradation of S follows *pseudo*-first order kinetics with an apparent rate constant k_{app} (s^{-1}):

$$k_{app} = \alpha_1 k_1 + \alpha_2 k_2, \ i.e., \quad k_{app} = \frac{1}{1 + K[Cl^-]} k_1 + \frac{K[Cl^-]}{1 + K[Cl^-]} k_2 \tag{9.86}$$

where, α_1 and α_2 are the molar fractions of $Cl^\bullet$ and $Cl_2^{\bullet-}$ radicals, respectively, and $K = [Cl_2^{\bullet-}]/([Cl^-][Cl^\bullet]) = 1.4 \times 10^5\ M^{-1}$ (Buxton *et al.* 1998).

Laser flash photolysis of chloroacetone represents the best method to generate Cl atoms for the determination of $Cl^\bullet$ rate constants because $Cl_2^{\bullet-}$ is not present at the beginning of the reaction (Buxton *et al.* 2000). Determination of rate constants for $Cl^\bullet$ and $Cl_2^{\bullet-}$ reactions from laser photolysis of $Na_2S_2O_8$/NaCl solutions is more complicated because chloride concentration must be adjusted in order to minimize reaction of $SO_4^{\bullet-}$ with S, thus to have a selective degradation of S by $Cl^\bullet$ or by $Cl_2^{\bullet-}$. Literature data show that some kinetic constants for the reaction of $Cl_2^{\bullet-}$ with organic compounds were significantly overestimated due to an incomplete conversion of $Cl^\bullet$ to $Cl_2^{\bullet-}$ (Wicktor *et al.* 2003). Furthermore, the determination of rate constants for reactions of $Cl_2^{\bullet-}$ requires high chloride concentrations (0.5–1 M), and ionic strength corrections.

9.3.3.2 Reactions of $Cl^\bullet$ with organic compounds

Table 9.8 provides rate constants for the reaction of $Cl^\bullet$ with selected aliphatic (Gilbert *et al.* 1988; Buxton *et al.* 2000; Wicktor *et al.* 2003; Mertens & von Sonntag, 1995; Zhu *et al.* 2005) and aromatic compounds (Alegre *et al.* 2000; Mártire *et al.* 2001). An excellent database on the rate constants for the reactions of selected inorganic radicals, including $Cl_2^{\bullet-}$, with inorganic and organic compounds was compiled by Neta *et al.* (1988).

Rate constants for the reactions of $Cl^\bullet$ with most aliphatic compounds (alcohols, aldehydes, ketones and acids) are in the range of 10^7 and $10^{10}\ M^{-1}\ s^{-1}$ and are of the same order of magnitude as those of hydroxyl radical. $Cl^\bullet$ atoms react with aromatic compounds at near diffusion-controlled rates ($k \sim (1–2) \times 10^{10}\ M^{-1}\ s^{-1}$).

$Cl^\bullet$ reacts with oxygenated aliphatic compounds more likely by H-abstraction from a C—H bond. This mechanism is supported by ESR spectroscopy (Gilbert *et al.* 1988), and by the correlation of the rate constant with the bond dissociation enthalpy for the weakest C—H bond (Wicktor *et al.* 2003). H-abstraction from O—H group *via* an electron transfer mechanism has also been proposed (Gilbert *et al.* 1988):

$$(CH_3)_3COH + Cl^\bullet \rightarrow [Cl^- + (CH_3)_3C(+)OH] \rightarrow H^+ + Cl^- + (CH_3)_3CO^\bullet \rightarrow (CH_3)_2CO + CH_3^\bullet \tag{9.87}$$

$Cl^\bullet$ reacts by direct addition to the C=C bond of unsaturated aliphatic compounds. For example, $Cl^\bullet$ adds to the C=C double bond of tetrachloroethene to form a pentachloroethyl radical which is rapidly converted into a peroxyl radical in the presence of oxygen (Mertens & von Sonntag, 1995):

$$Cl^\bullet + CCl_2{=}CCl_2 \rightarrow CCl_3{-}CCl_2^\bullet \tag{9.88}$$

$$CCl_3{-}CCl_2^\bullet + O_2 \rightarrow CCl_3{-}CCl_2OO^\bullet \tag{9.89}$$

$$CCl_3{-}CCl_2OO^\bullet \rightarrow \text{Products (trichloroacetic acid, } CO_2 \text{ and HCl)} \tag{9.90}$$

Table 9.9 gives the identified oxidation by-products of benzene, benzoic acid, toluene, and chlorobenzene from the reactions of these compounds with $Cl^\bullet$ and $Cl_2^{\bullet-}$ generated by laser and

conventional flash photolysis of $Na_2S_2O_8$ aqueous solutions containing chloride ions (Alegre *et al.* 2000; Mártire *et al.* 2001). Absorption spectra of transient species showed that the addition of $Cl^{\bullet}$ to aromatic rings to form chlorocyclohexadienyl radicals (Cl-CHD) is the predominant mechanism. The disproportionation reactions of Cl-CHD radicals lead to chlorobenzoic acid. In air saturated solutions, the Cl-CHD radicals decompose to form both chlorinated and oxidation by-products (Table 9.9).

Table 9.8 Rate constants for reactions of $Cl^{\bullet}$ and $Cl_2^{\bullet-}$ with selected organic compounds in water.

Organic Compound	$Cl^{\bullet}$ (M^{-1} s^{-1})	$Cl_2^{\bullet-}$ (M^{-1} s^{-1})
Methanol	$(1.0 \pm 0.2) \times 10^{9a}$; $(1.0 \pm 0.1) \times 10^{9b}$	3.5×10^{3c}; $(0.3 \pm 1.3) \times 10^{4b}$ $(5.1 \pm 0.8) \times 10^{4d}$
Ethanol	$(1.7 \pm 0.7) \times 10^{9a}$; $(2.2 \pm 0.7) \times 10^{9b}$	4.5×10^{4c}; $(1.2 \pm 0.2) \times 10^{5d}$
2-propanol	$(1.5 \pm 0.1) \times 10^{9a}$; $(3.2 \pm 0.7) \times 10^{9b}$	1.2×10^{5c}; $(1.9 \pm 0.3) \times 10^{5d}$
Tert-butanol	$(6.2 \pm 0.5) \times 10^{8a}$; $(1.5 \pm 0.1) \times 10^{9b}$	$(2.6 \pm 0.5) \times 10^{4d}$
Diethyl ether	$(1.3 \pm 0.1) \times 10^{9b}$	$(4.0 \pm 0.2) \times 10^{5d}$; $(3.6 \pm 0.2) \times 10^{5b}$
Methyl-*tert*-butyl ether (MTBE)	$(1.3 \pm 0.1) \times 10^{9b}$	$(7 \pm 1) \times 10^{4d}$; $(1.6 \pm 1.5) \times 10^{4b}$
Tetrahydrofuran	$(2.6 \pm 0.4) \times 10^{9}$	$(5.3 \pm 0.6) \times 10^{5b}$
Formic acid ($pK_a = 3.75$)	$(1.3 \pm 0.3) \times 10^{8}$ (pH 1)^a; $(4.2 \pm 0.5) \times 10^{9a}$; $(2.8 \pm 0.3) \times 10^{9}$(pH 1)^b	6.7×10^{3} (pH 1)^c; $(8.0 \pm 1.4) \times 10^{4}$ (pH 4)^d
Acetic acid ($pK_a = 4.75$)	$(3.2 \pm 0.2) \times 10^{7}$(pH 1)^a; $(3.7 \pm 0.4) \times 10^{9a}$; $(1.0 \pm 0.2) \times 10^{8}$ (pH 1)^b	$<10^{4}$ (pH 7)^c; $(1.5 \pm 0.8) \times 10^{3}$ (pH 0.4)^d
Hydrated formaldehyde	$(1.4 \pm 0.1) \times 10^{9}$(pH 1)^a; $(3.2 \pm 0.2) \times 10^{7}$ (pH 1)^a; $(1.4 \pm 0.3) \times 10^{9b}$	
Acetone	$<5 \times 10^{6a}$; $(7.8 \pm 0.7) \times 10^{7b}$	$1.4 \times 10^{3c,d}$
Dichloromethane	$(9.3 \pm 0.3) \times 10^{6b}$	
Trichloromethane	$(2.3 \pm 0.5) \times 10^{8b}$	
Tetrachloroethene	2.8×10^{8e}	
Chlorpromazine		5×10^{9i}
Dimethylsulfoxide (DMSO)	$(6.3 \pm 0.6) \times 10^{9f}$	1.6×10^{7f}
Dimethylsulfone	$(8.2 \pm 1.6) \times 10^{5f}$	
Benzene	$(0.6–1.2) \times 10^{10g}$	$<1 \times 10^{5h}$
Toluene	$(1.8 \pm 0.3) \times 10^{10h}$	$<1 \times 10^{6h}$
Chlorobenzene	$(1.8 \pm 0.3) \times 10^{10h}$	$<1 \times 10^{6h}$
Benzoic acid ($pK_a = 4.2$)	$(1.8 \pm 0.3) \times 10^{10h}$	2×10^{6} (pH 7)^c; $<10^{6}$ (pH 4)^h
p-Chlorobenzoic acid ($pK_a = 4.0$)		3×10^{6} (pH 7)^c
p-Hydroxybenzoic acid ($pK_{a1} = 4.6$; $pK_{a2} = 9.2$)		2.8×10^{8} (pH 7)^c
Phenol		2.5×10^{8c}; 5×10^{8i}

[a]Buxton *et al.* (2000); [b]Wicktor *et al.* (2003); [c]Hasegawa & Neta (1978); [d]Jacobi *et al.* (1999); [e]Mertens & von Sonntag (1995); [f]Zhu *et al.* (2005); [g]Alegre *et al.* (2000); [h]Mártire *et al.* (2001); [i]Willson (1973).

Table 9.9 By-products from the degradation of aromatic compounds by chlorine atoms.

Parent Compound	Identified Oxidation By-products	Reference
Benzene	Chlorobenzene (10%) 2,4-Hexadiene-aldehyde	Alegre *et al.* (2000)
Chlorobenzene	Phenol 2-Chlorophenol Trichlorophenols	Mártire *et al.* (2001)
Toluene	1-Chloro-2-methylbenzene, 1-Chloro-4-methylbenzene, Benzaldehyde, benzyl alcohol Benzyl chloride, biphenyl	Mártire *et al.* (2001)
Benzoic acid	3-Chlorobenzoic acid and 4-chlorobenzoic acid (estimated yield: 30%) Chlorobenzene (yield < 0.4%)	Mártire *et al.* (2001)

In the case of chlorobenzene, cyclohexadienyl radicals may also be formed by charge transfer from the aromatic ring to $Cl^{\bullet}$ to give an unstable cation radical which hydrolyses to give hydroxycyclohexadienyl radicals (HO-CHD) (Figure 9.6). HO-CHD radicals undergo disproportionation reactions to yield chlorophenol and unstable chloroxyclohexadienes which decompose to phenol or chlorobenzene. The mechanism of formation of tri- and tetrachlorophenols involve peroxyl radicals as intermediate species, which decompose to endoperoxides and further to chlorophenols.

9.3.3.3 Reactions of $Cl_2^{\bullet-}$ with organic compounds

Literature data show that $Cl_2^{\bullet-}$ is 2–5 orders of magnitude less reactive than $Cl^{\bullet}$ (Table 9.8). Rate constants for the reaction of $Cl_2^{\bullet-}$ with aliphatic compounds are in the range 10^3–10^5 M^{-1} s^{-1} for saturated alcohols, ketones and acids, 10^5–10^6 M^{-1} s^{-1} for amino-acids, 10^6–10^8 M^{-1} s^{-1} for unsaturated aliphatic compounds (e.g., fumaric acid, acrylic acid and allyl alcohol). Rate constants for $Cl_2^{\bullet-}$ reactions with aromatic compounds range from ~10^6 M^{-1} s^{-1} for benzoic acid derivatives to 10^7–10^9 for phenol, aniline and anisole derivatives. $Cl_2^{\bullet-}$ reacts with organic solutes by H-abstraction from aliphatic compounds and aromatic rings, with the NH_2 group of amino acids, with the unsaturated bonds in aliphatic compounds by $Cl^{\bullet}$ addition, and by one electron transfer from aromatic compounds containing electron-rich substituents like OH, NH_2 or OCH_3 groups (Hasegawa & Neta, 1978). For example, $Cl_2^{\bullet-}$ can abstract one electron from phenol to produce a phenol cation radical which evolves to a phenoxyl radical. The subsequent reaction of $Cl_2^{\bullet-}$ with phenoxyl radical has been hypothesized to explain the formation of chlorophenols (Vione *et al.* 2015):

$$H - Ph - OH + Cl_2^{\bullet-} \rightarrow H - Ph^{\bullet+} - OH + 2\ Cl^- \quad (9.91)$$

$$H - Ph^{\bullet+} - OH \rightleftharpoons H - Ph - O^{\bullet} + H^+ \quad (9.92)$$

$$H - Ph - O^{\bullet} + Cl_2^{\bullet-} \rightarrow Cl - Ph - OH + Cl^- \quad (9.93)$$

The lifetime of $Cl_2^{\bullet-}$ is much longer than that of $Cl^{\bullet}$, thus, it accumulates in solution at higher concentrations than those of $Cl^{\bullet}$. Therefore, the bimolecular reactions of $Cl_2^{\bullet-}$ may not be negligible in the UV/Chlorine process applications.

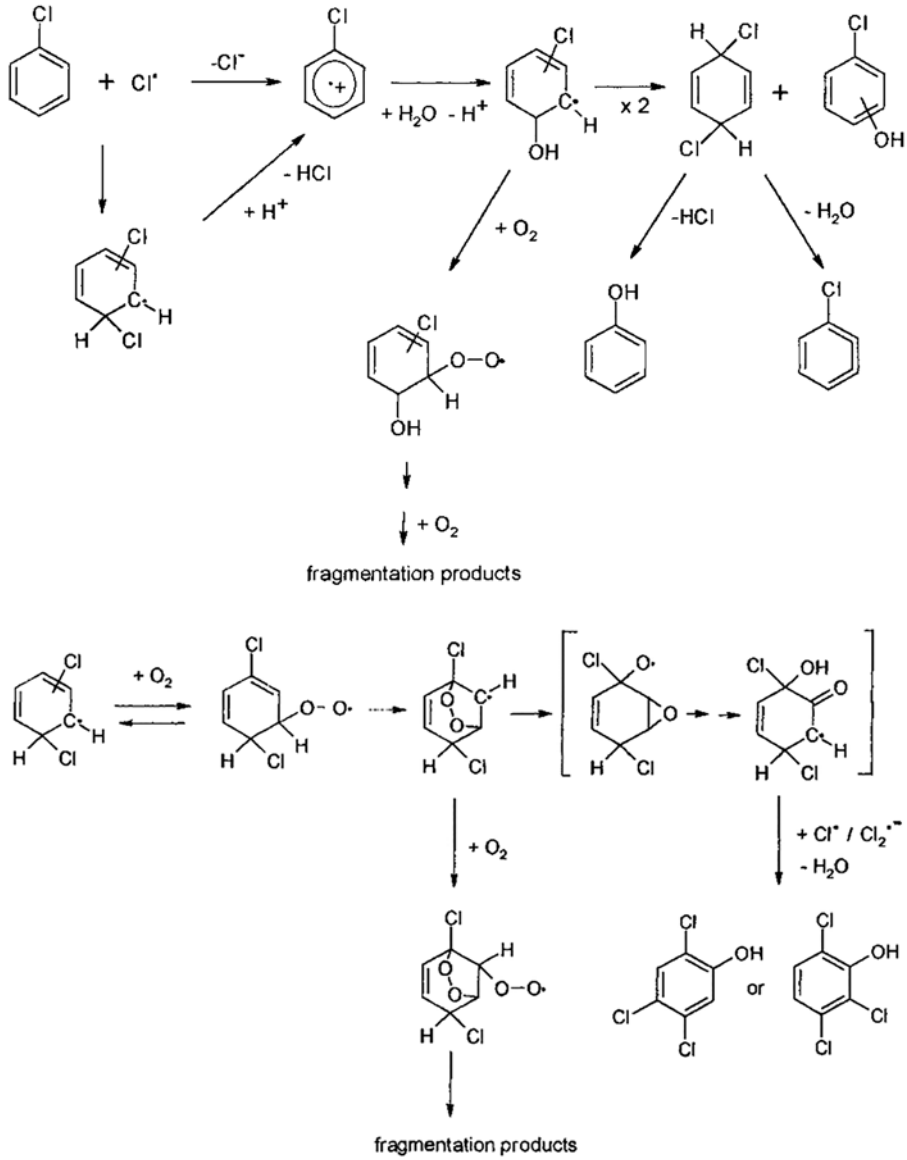

Figure 9.6 Degradation pathways of chlorobenzene by Cl•. Adapted with permission from Mártire *et al.* (2001). Copyright 2016 American Chemical Society.

9.3.3.4 Reactions of Cl• and $Cl_2^{\bullet-}$ with inorganic compounds present in natural waters

Reduced forms of inorganic compounds such as Fe^{2+}, Mn^{2+}, NO_2^- and H_2S which can be present in groundwater under anoxic and anaerobic conditions can be oxidized by Cl• and $Cl_2^{\bullet-}$ as well as by molecular chlorine. Bicarbonate and carbonate ions which are present in groundwater and surface waters at concentrations ranging from 0.5 to 5 mM are well-known •OH scavengers. The few rate constants

reported in literature indicate that these ions can also scavenge $Cl^{\bullet}$ and $Cl_2^{\bullet-}$ and that $Cl^{\bullet}$ and $Cl_2^{\bullet-}$ can react faster than $^{\bullet}OH$ with the bicarbonate ion which is the predominant species at neutral pH (Table 9.10).

Table 9.10 Rate constants for the reactions of $Cl^{\bullet}$, $Cl_2^{\bullet-}$ and $^{\bullet}OH$ with bicarbonate and carbonate ions.

Reactions		Rate Constant ($M^{-1}\ s^{-1}$)	References
$HCO_3^- + Cl^{\bullet} \rightarrow CO_3^{\bullet-} + HCl$	9.94	2.2×10^8	Mertens & von Sonntag (1995)
$CO_3^{2-} + Cl^{\bullet} \rightarrow CO_3^{\bullet-} + Cl^-$	9.95	5.0×10^8	Mertens & von Sonntag (1995)
$HCO_3^- + Cl_2^{\bullet-} \rightarrow CO_3^{\bullet-} + H^+ + 2\ Cl^-$	9.96	8.0×10^7	Matthew & Anastasio (2006)
$CO_3^{2-} + Cl_2^{\bullet-} \rightarrow CO_3^{\bullet-} + 2\ Cl^-$	9.97	1.6×10^8	Matthew & Anastasio (2006)
$HCO_3^- + {}^{\bullet}OH \rightarrow CO_3^{\bullet-} + H_2O$	9.98	8.5×10^6	Buxton *et al.* (1988)
$CO_3^{2-} + {}^{\bullet}OH \rightarrow CO_3^{\bullet-} + HO^-$	9.99	3.9×10^8	Buxton *et al.* (1988)

During the application of the UV/Cl_2 AOP, the highly reactive hydroxyl radicals and chlorine atoms generated from HOCl/ClO^- photolysis are involved in pH-dependent equilibria and reactions with water constituents (e.g. chloride ion, bicarbonate ion, dissolved organic matter, chemical pollutants, etc.) as well as with the free chlorine species (HOCl/ClO^-). Some of these reactions are shown in Tables 9.4, 9.6 and 9.7, and a simplified reaction scheme is given in Figure 9.7, where S_i represents any radical scavenger in the water matrix other than the target pollutant and free chlorine species.

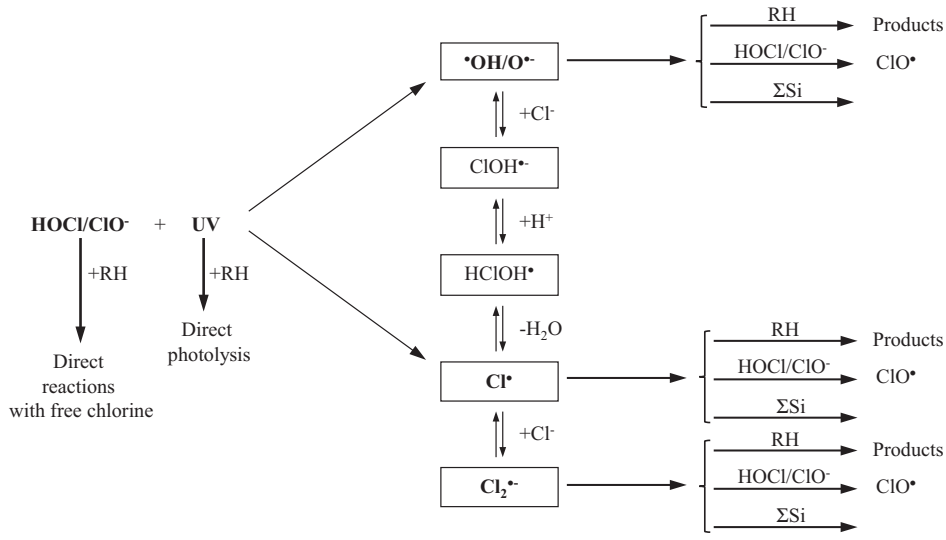

Figure 9.7 Simplified reaction scheme showing the different degradation pathways of an organic solute (RH) by the UV/Cl_2 process (ΣSi represents free radical scavengers) (De Laat, 2016).

The individual contribution of $^{\bullet}OH$, $Cl^{\bullet}$ and $Cl_2^{\bullet-}$ reactions to the overall oxidation of a given pollutant RH will depend on parameters that affect the equilibrium reactions involving these free radicals such as pH and chloride ion concentration (reactions in Table 9.6), on the steady-state concentrations of free radicals and on the rate constant values for the reactions of $^{\bullet}OH$, $Cl^{\bullet}$ and $Cl_2^{\bullet-}$ with RH.

9.4 UV/Cl_2 PROCESS FOR CONTAMINANT REMOVAL FROM WATER

9.4.1 Degradation pathways of organic compounds

The degradation pathways of organic pollutants during the UV/Cl_2 AOP can follow parallel reactions e.g. direct photolysis if the organic compounds absorb the radiation, oxidation *via* free radicals ($^{\bullet}OH$ and $Cl^{\bullet}$ and to a lesser extent $Cl_2^{\bullet-}$ and other radical species formed in the system), and dark ("thermal") reactions of free chlorine with the organic pollutants. Chlorination reactions can occur before, inside, and after the UV reactor. The relative contribution of direct photolysis, dark chlorination, and free radical reactions to the degradation of organic pollutants depends on many parameters among which the chemical and photochemical properties of organic compounds (e.g., quantum yields and molar absorption coefficients at the irradiation wavelengths, rate constants for the reactions of organic pollutants with free chlorine and with oxidizing radicals), UV system (lamp type and spectral power distribution, fluence rate, mixing efficiency), water composition (dissolved organic carbon, alkalinity, other water matrix constituents which can compete with the target pollutant for photons or/and for the reactive radical species), UV/Cl_2 process operating conditions (pH, concentration of free chlorine).

Some studies on the UV/Cl_2 process showed that organic compounds resistant to both molecular chlorine oxidation and UV photolysis (LP and MP lamps, solar radiation-simulating lamps) could be degraded by the combination of chlorine and UV radiation, thus demonstrating indirectly the generation of highly reactive radicals ($^{\bullet}OH$, $Cl^{\bullet}$) during photolysis of HOCl or ClO^-. These degradation reactions have been observed for ethanol and *n*-butanol (Oliver & Carey, 1977), ethylene glycol dimethyl ether and related substrates, acetic and propionic acids (Ogata *et al*. 1978; Ogata *et al*. 1979), 1-chlorobutane and n-octanol (Nowell & Hoigné, 1992b) and aromatic compounds containing electron-withdrawing groups such as nitrobenzene and benzoic acid (Oliver & Carey, 1977; Ogata & Tomizawa, 1984; Nowell & Crosby, 1985). More recently, *p*-chlorobenzoic acid (pCBA) has been used in UV/Cl_2 experiments as a probe compound to quantify the steady-state concentrations of $^{\bullet}OH$ (Watts & Linden, 2007a; Jin *et al*. 2011). Methanol has also been used in UV/Cl_2 experiments to estimate hydroxyl radical yield factor, $\eta = \Delta[^{\bullet}OH]/\Delta[\text{Free chlorine}]$ (Jin *et al*. 2011).

The observed by-products indicate that the degradation mechanisms of organic compounds by UV/Cl_2 AOP involve hydroxylation, oxidation, and halogenation reactions. For example, the oxidation of nitrobenzene by UV/Cl_2 and by UV/H_2O_2 yields 2-, 3- and 4-nitrophenol as initial by-products (Nowell & Crosby, 1985; Watts *et al*. 2007b) but in the case of UV/Cl_2 other by-products (e.g. chlorophenols) are rapidly formed (Watts *et al*. 2007b).

In a study on the herbicide chlortoluron degradation by UV(253.7 nm)/Cl_2 AOP ($[\text{Chlortoluron}]_0 = 5\ \mu M$; $[\text{Chlorine}]_0 = 25–100\ \mu M$), Guo *et al*. (2016) showed that the attack of $^{\bullet}OH$ on chlortoluron ($k = (2.18 \pm 0.83) \times 10^9\ M^{-1}s^{-1}$) was the predominant degradation pathway. The authors identified ten aromatic degradation by-products. Among the identified intermediates, two were also formed through direct photolysis (C—Cl bond scission) followed by hydroxylation of the aromatic ring. The other products indicated that the UV/Cl_2 AOP leads to hydroxylation and chlorination of the aromatic ring and of methyl groups at the amide moiety. Post-chlorination experiments ($[\text{Chlortoluron}]_0 = 100\ \mu M$; ($[\text{Chlorine}]_0 = 500\ \mu M$) showed that UV/Cl_2 enhanced the formation of C-DBPs (1,1-dichloroacetone, 1,1,1-trichloroacetone, chloroform, chloroacetaldehyde) and of N-DBPs (dichloroacetonitrile and trichloronitromethane) compared to UV radiation alone.

Qin *et al*. (2014) studied the oxidation of antiprotozoal agent ronidazole (RNZ) by UV/Cl_2 ($[RNZ]_0 = 0.1$ mM; $[Cl_2]_{T,0} = 1$ mM; pH 7; 253.7 nm) and identified two chlorinated by-products which were also formed by chlorination alone and five hydroxylated by-products, four of which were also formed during UV photolysis. Post-chlorination ($[\text{post-}Cl_2]_0 = 1$ mM; pH 7; 7 days) showed that UV/Cl_2 generated

chloroform and trichloronitromethane (TCNM) precursors (such as amines and imines) through the •OH-induced degradation of heterocyclic ring of RNZ.

Deng *et al.* (2014) showed that the UV(253.7 nm)/Cl_2 process promoted the formation of TCNM precursors (methylamine and dimethylamine) during the treatment of aqueous solutions of polyamine. TCNM concentrations decreased under extended UV exposure through direct photolysis. The UV/Cl_2-enhanced degradation of polyamine to methylamine and dimethylamine and probably to other TCNM precursors has been attributed to the contribution of free radicals (•OH and Cl•) and of reactive species generated from photodegradation of chloramine intermediates. The addition of *tert*-butanol (free radical scavenger) completely inhibited the formation of TCNM from methylamine and partially decreased the formation of TCNM from dimethylamine and polyamine. Based on experimental data, the authors proposed two different reaction schemes for the formation of TCNM from methylamine and dimethylamine. The higher levels of TCNM formed from methylamine by UV/Cl_2 as compared to the dark chlorination, were explained by the OH and Cl radical-enhanced rate of formation of nitromethane (CH_3NO_2) from chloramines. Other mechanisms leading to TCNM from dimethylamine involve methyl-imine as an intermediate. TCNM formation *via* the UV/Cl_2 process likely involves photo-enhanced chlorination reactions (Deng *et al.* 2014).

Xiang *et al.* (2016) showed that the degradation of the anti-inflammatory drug ibuprofen (IBP) by UV(253.7 nm)/Cl_2 AOP generated significantly more total organic chlorine ([TOCl] = 31.6 μM) than dark chlorination ([TOCl] = 0.2 μM) after 30 min reaction time. Aliphatic chlorinated by-products (chloroform, chloral hydrate, 1,1-dichloro-2-propanone, 1,1,1-trichloropropanone, dichloroacetic and trichloroacetic acids) accounted for 17.4% to the TOCl. Based on the identified hydroxylated and chlorinated by-products, the authors proposed the degradation pathways for ibuprofen by UV/Cl_2 AOP presented in Figure 9.8.

The chlorinated products shown in brackets were identified for the first time. The analyses showed that the primary steps of the degradation of IBP lead to the formation of six hydroxylated derivatives and one monochlorinated by-product at pH 6. Similar experiments conducted at pH 0 where only Cl• is formed from photolysis of Cl_2, demonstrated that degradation of IBP yielded monochlorinated byproducts without formation of hydroxylated intermediates. From these data, the authors concluded that the formation of hydroxylated compounds can be attributed to •OH attack only. Further degradation reactions lead to the formation of several aromatic intermediates *via* hydroxylation, decarboxylation, demethylation and chlorination reactions and to the formation aliphatic by-products *via* ring opening reactions (Figure 9.8).

In a comparative study of the degradation of herbicide atrazine (ATZ) by UV alone, UV/Cl_2 and UV/H_2O_2 AOPs ($[ATZ]_0$ = 5 μM; $[Chlorine]_0$ or $[H_2O_2]$ = 0 or 70 μM; pH 7; 253.7 nm), Kong *et al.* (2016) identified five, eleven, and ten atrazine by-products in UV alone, UV/Cl_2 and UV/H_2O_2, respectively. As the identified by-products of atrazine in the UV/Cl_2 process did not reveal the addition of Cl atom to atrazine structure, the authors proposed that oxidation by •OH and Cl• rather than chlorine substitution was the degradation pathway. Quantification of the three primary by-products of atrazine (desethyl-atrazine (DEA), desisopropyl-atrazine (DIA) and desethyl-desisopropyl-atrazine (DEIA)) at the beginning of the reaction showed that the DEA:DIA yield ratios were ~4 and ~1 for UV/Cl_2 and UV/H_2O_2, respectively. This was attributed to different reaction mechanisms of •OH and Cl• with atrazine.

Wang *et al.* (2016a) conducted an extensive study on UV(253.7 nm)/Cl_2–based degradation of the antiepileptic drug carbamazepine (CBZ), which included by-product identification and mechanistic pathways, kinetic modeling, and process economics (electrical energy per order, E_{EO}). No significant direct photolysis was observed, and direct (thermal) chlorination accounted for only 5% of the overall degradation yield of CBZ by the UV/Cl_2 process. The degradation rate constants were determined for

various experimental conditions, including pH (4.5–10.5), chloride and bicarbonate concentrations (0–50 mM), free chlorine dose (0.03–0.63 mM), and UV irradiance. The authors concluded that chloride ion effect was negligible; instead, bicarbonate ion concentration reduced the observed rate constant. The kinetic model is similar to that developed by Fang *et al.* (2014), but some key radical rate constants used in the two works are largely different; e.g., $k_{Cl^{\bullet},HCO_3^-} = 2.2 \times 10^8$ M^{-1} s^{-1} (Fang *et al.* 2014), $k_{Cl^{\bullet},HCO_3^-} = 2.9 \times 10^9$ M^{-1} s^{-1} (Wang *et al.* 2016a); $k_{Cl^{\bullet},TBA} = 3.0 \times 10^8$ M^{-1} s^{-1} (Fang *et al.* 2014), $k_{Cl^{\bullet},TBA} = 1.9 \times 10^9$ M^{-1} s^{-1} (Wang *et al.* 2016a). Although no chlorinated byproducts were identified in the product study, the authors did not exclude the Cl atom reactions and determined the relative contribution of •OH and Cl• to the overall rate constant (k_{obs}), as a function of pH.

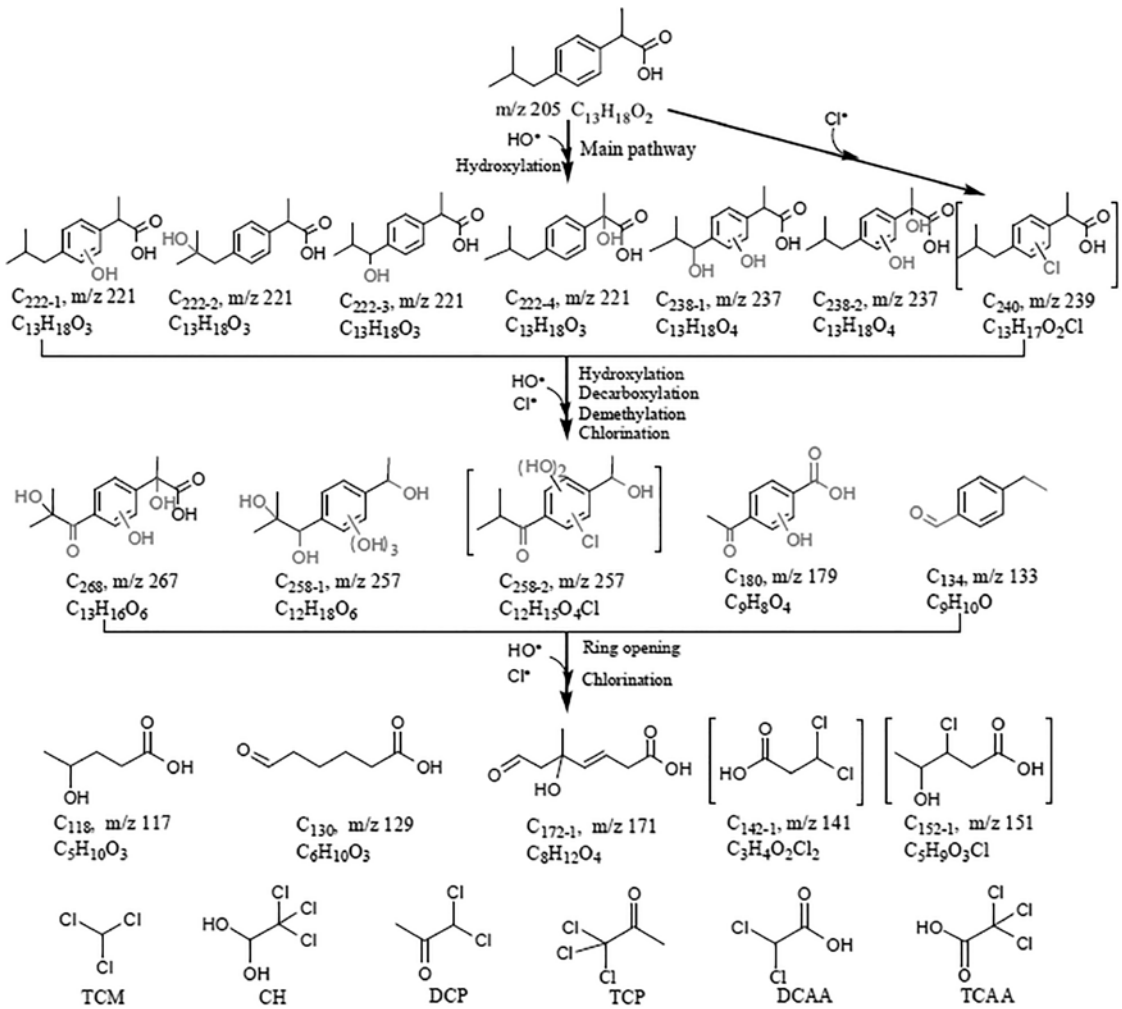

Figure 9.8 Proposed pathways for the degradation of ibuprofen by UV/Cl_2 AOP. Reprinted with permission from Xiang *et al.* (2016). Copyright 2016 Elsevier.

Competition kinetics experiments with nitrobenzene and benzoic acid as chemical probes allowed the determination of $k_{Cl^{\bullet},CBZ} = (5.6 \pm 1.6) \times 10^{10}$ M^{-1} s^{-1}, which is larger than typical diffusion rate coefficients. The authors recognized that more investigations are required in order to properly understand the $Cl^{\bullet}$ reactivity, i.e., transient kinetics in complex systems. The E_{EO} data were calculated from collimated beam experiments in deionized water and in wastewater effluent samples for a chlorine dose of 0.28 mM (~20 mg/L). The authors included the energy requirements associated with both chlorine and UV power consumption, and were found as 0.32 and 0.44 kWh/m^3/order for CBZ removal in deionized water (pH 7) and wastewater effluent (3.1 mg/L TOC; 62.2 mg/L IC; 7.9 mg-N/L; 24 mg/L NO_3^-; pH 7), respectively.

9.4.2 Kinetic modeling of UV/Cl_2 AOP

As compared to the UV/H_2O_2 AOP, the photochemical and chemical reactions involved in the UV/Cl_2 process are much less elucidated, and many rate constants are either unknown or not well documented. Some studies on micropollutant degradation with the UV/Cl_2 AOP have attempted kinetic modeling of the experimental data. However, the key input parameters, including the apparent photolysis quantum yield of free chlorine species and radical yields, rate constants for the reactions of radicals with the free chlorine species, as well as the radical species considered in the oxidative degradation mechanisms vary from one model to another.

Fang *et al.* (2014) investigated the degradation of benzoic acid by UV(253.7 nm)/Cl_2 process under various experimental conditions, including pH and initial concentrations of benzoic acid, free chlorine, chloride ion, bicarbonate ion, *tert*-butanol and Suwannee River Natural Organic Matter. Benzoic acid was not degraded by either UV alone or 'dark' chlorination. The degradation with the UV/Cl_2 process followed first-order kinetics with respect to the concentration of benzoic acid. The authors developed a complex kinetic model which accounted for HOCl and ClO^- photolysis to $^{\bullet}OH$ /$O^{\bullet-}$ and $Cl^{\bullet}$ radicals, pH and chloride-dependent equilibria between the highly reactive species ($^{\bullet}OH$, $O^{\bullet-}$, $Cl^{\bullet}$, $Cl_2^{\bullet-}$, HClOH and $ClOH^{\bullet-}$, Table 9.6), radical ($^{\bullet}OH$, $Cl^{\bullet}$) reactions with free chlorine species (HOCl, ClO^-) yielding the oxychlorine radical $ClO^{\bullet}$, and reactions of radical species with benzoic acid and water matrix constituents, such as bicarbonate and chloride ions, and Suwannee River NOM. In order to elucidate the role of each radical species in the degradation of benzoic acid, Fang *et al.* (2014) used chemical probes, such as nitrobenzene (apparently non-reactive towards $Cl^{\bullet}$) and *tert*-butanol (reactive with both to $^{\bullet}OH$ and $Cl^{\bullet}$).

The kinetic model simulated reasonably well the degradation of benzoic acid under a variety of experimental conditions, some of which are exemplified in the next section. Computer simulations showed that the degradation of benzoic acid could mainly be attributed to $^{\bullet}OH$ and $Cl^{\bullet}$ given that the rate constants of $Cl_2^{\bullet-}$ and $O^{\bullet-}$ with benzoic acid are several orders of magnitude smaller than those of $^{\bullet}OH$ and $Cl^{\bullet}$ and the fraction of hydroxyl radicals present as $O^{\bullet-}$ can be neglected at pH < 9. The model was also used to determine the relative contributions of $^{\bullet}OH$, $O^{\bullet-}$, $Cl^{\bullet}$ and $Cl_2^{\bullet-}$ radicals to the degradation of benzoic acid. From the theoretical expression and experimental value of the *pseudo*-first order rate constant of benzoic acid decay in the presence of NOM, a rate constant of $k_{Cl^{\bullet},NOM} = 1.3 \times 10^4$ $(mg\ C/L)^{-1}$ s^{-1} was computed for the reaction of $Cl^{\bullet}$ with NOM. This value is smaller than the frequently reported rate constant of $^{\bullet}OH$ with NOM ($k_{^{\bullet}OH,NOM} = 2.5 \times 10^4$ $(mg\ C/L)^{-1}$ s^{-1} which indicates that NOM is a stronger scavenger of $^{\bullet}OH$ than of $Cl^{\bullet}$. However, the computed $k_{Cl^{\bullet},NOM}$ rate constant must be validated experimentally.

Fang *et al.*'s kinetic model appears to be the most comprehensive model to-date for the UV/Cl_2 AOP, although it does not consider the fate of oxychlorine radical $ClO^{\bullet}$ which is formed with high yields in this process and could impact the real-time oxidant and radical concentrations in the UV/Cl_2 process. This

kinetic model was recently used by Aghdam *et al.* (2016) for the UV/Cl_2-based degradation of N,N′-diethyl-*meta*-toluamide (DEET), an insect repellent. In this study, the authors estimated the rate constant for the chlorine atom reaction with DEET as 8×10^9 M^{-1} s^{-1}, which is almost twice the $^{\bullet}OH$ rate constant (4.95×10^9 M^{-1} s^{-1}, Song *et al.* 2009). It was reported that the contribution of $Cl^{\bullet}$ to the overall degradation of DEET at pH 6 and 7 was approx. 30 and 45%, respectively. The basics of Fang *et al.*′s kinetic model were employed in other recent UV/Cl_2 studies to estimate the contribution of direct UV photolysis and $^{\bullet}OH$ and $Cl^{\bullet}$ species to the ibuprofen degradation (Xiang *et al.* 2016) and to model carbamazepine degradation (Wang *et al.* 2016a).

Qin *et al.* (2014) proposed a kinetic model for the UV(253.7 nm)/Cl_2 degradation of ronidazole (RNZ) in deionized water in the absence of radical scavengers other than the oxidant species and target compound. The authors state that in the UV/Cl_2 process the dominant oxidant is the $^{\bullet}OH$, and used a quantum yield of ~1.0 for both HOCl and ClO^- photolysis. The model accounts for 'dark' chlorination of RNZ, but disregards the $Cl^{\bullet}$ reactions with the oxidant species and RNZ. Both Fang *et al.*′s (2014) and Qin *et al.*′s (2014) UV/Cl_2 kinetic models used the $k_{HO^{\bullet},HOCl} = 2 \times 10^9$ M^{-1} s^{-1} (Matthew & Anastasio, 2006).

Wang *et al.* (2012) built a numerical model in MatLab® to simulate the TCE photodegradation with the UV/Cl_2 process in deionized water exposed to polychromatic radiation from a MP lamp. The authors determined the experimental fluence rate-based rate constants and compared those to the model-computed data. The model accounted for TCE direct photolysis and TCE reaction with $Cl^{\bullet}$ formed from TCE photolysis, but did not include the reactions of $Cl^{\bullet}$ formed from HOCl and ClO^- photolysis with either the oxidant species or TCE. The authors used the observed $^{\bullet}OH$ yields in their study (0.79 and 1.18, for HOCl and ClO^-, respectively), which were different from those reported in other studies (Jin *et al.* 2011; Chan *et al.* 2012; Watts & Linden, 2007a). The $ClO^{\bullet}$ reactions were not considered in the model. Wang *et al.*′s kinetic model used $k_{HO^{\bullet},HOCl} = 8.46 \times 10^4$ M^{-1} s^{-1} (Watts & Linden, 2007a), which is almost five orders of magnitude smaller than that used with the models discussed above. For the input kinetic parameters used in their model, Wang *et al.* found a good agreement between the experimental and computed fluence based-rate constants of TCE degradation by UV (polychromatic)/Chlorine process.

The UV/Cl_2 AOP kinetic models discussed above use different values for the same key input parameters (e.g., quantum yields, $^{\bullet}OH$ and $Cl^{\bullet}$ rate constants) – all of which are in the published literature. Large discrepancies are between such key parameters reported in the literature, which reflects rather limited current understanding of the fundamentals of the UV/Cl_2 process and of the fate and contribution of $Cl^{\bullet}$ and $ClO^{\bullet}$ species to the reaction mechanisms, as well as the need for more research on the UV/Cl_2 process.

9.4.3 The impact of selected parameters on UV/Cl_2 process performance

The oxidation rates of organic micropollutants in aqueous solutions follow *pseudo*-first-order decay with respect to the concentration of the organic solute (Nowell & Hoigné 1992b; Wang *et al.* 2012; Fang *et al.* 2014; Qin *et al.* 2014; Guo *et al.* 2016; Xiang *et al.* 2016) and are proportional to the fluence rate (Qin *et al.* 2014; Guo *et al.* 2016). The degradation rate of a target micropollutant by UV/Cl_2 AOP depends on various parameters including radiation wavelength, pH, chlorine dose, concentration of radical scavengers, and UV water absorption coefficient. The degradation rates also depend on pollutant chemical properties such as reactivity towards free radicals (in particular $^{\bullet}OH$ and $Cl^{\bullet}$) and free chlorine, and on micropollutant photostability (molar absorption coefficient and photolysis quantum yield at the radiation wavelength).

9.4.3.1 Effect of pH

The UV/Cl_2 process is more efficient in mild acidic conditions (pH ~ 5) than at neutral pH and in alkaline media (pH > 7). The decrease of the efficiency of the UV/Cl_2 AOP with increasing pH was reported in buffered solutions prepared in deionized water. Some examples include the oxidation of *p*-chlorobenzoic acid (LP and MP lamps; Watts & Linden, 2007a), nitrobenzene (Watts *et al.* 2007b), benzoic acid (Fang *et al.* 2014; Figure 9.9), trichloroethene (MP lamp; Wang *et al.* 2012), 1,4-dioxane ($\lambda = 253.7$ nm; Kishimoto & Nishimura, 2015), ronidazole ($\lambda = 253.7$ nm; Qin *et al.* 2015), chlortoluron ($\lambda = 253.7$ nm; Guo *et al.* 2016), ibuprofen ($\lambda = 253.7$ nm; Xiang *et al.* 2016), atrazine ($\lambda = 253.7$ nm; Kong *et al.* 2016) and carbamazepine ($\lambda = 253.7$ nm; Wang *et al.* 2016a). Similar trends were observed for the oxidation of micropollutants in natural waters as reported for 2-methylisoborneol (Rosenfeldt *et al.* 2013; Wang *et al.* 2015a), trichloroethene (Wang *et al.* 2011), geosmin and caffeine (Wang *et al.* 2015a), and chlorinated volatile organic compounds (Boal *et al.* 2015).

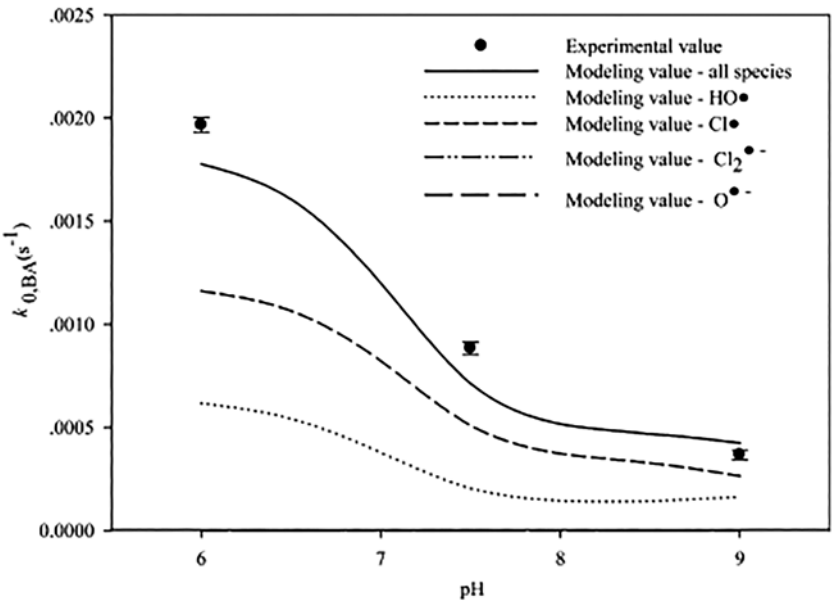

Figure 9.9 The pH effect on the *pseudo*-first-order rate constant of benzoic acid degradation by UV/Cl_2 AOP ([Benzoic acid]$_0$ = 5 μM, [Free chlorine]$_0$ = 70 μM). Reprinted with permission from Fang *et al.* (2014). Copyright 2016 American Chemical Society.

The efficiency of the UV/Cl_2 process is optimal at slightly acidic pH where HOCl is the predominant free chorine species. Watts and Linden (2007b) and Watts *et al.* (2010) attributed the higher efficiency of the UV/Cl_2 process at pH ≈ 5 to higher photo-generation rates of free radicals from HOCl than from ClO^- and to a much lower scavenging rate of $^{\bullet}OH$ by HOCl ($k = 8.5 \times 10^4$ M^{-1} s^{-1}) than by ClO^- ($k = 8 \times 10^9$ M^{-1} s^{-1}). As illustrated in Figure 9.10, Fang *et al.* (2014) could simulate reasonably well the effect of pH (6 < pH < 9) on the apparent first-order rate constant of degradation of benzoic acid by using rate constants of 2×10^9 and 8×10^9 M^{-1} s^{-1} for the reaction of $^{\bullet}OH$ with HOCl and ClO^-, respectively. Simulation curves for the degradation of benzoic acid by $^{\bullet}OH$ and $Cl^{\bullet}$ also confirmed that the decrease of the rate of degradation of benzoic acid with increasing pH can be attributed to a decrease of the quantum

yields of radical formation and to an increase in the scavenging capacity of free chlorine for both •OH and Cl•. In the pH range of 6 to 9, the contribution of $Cl_2^{\bullet-}$ and $O^{\bullet-}$ to the oxidation of benzoic acid can be neglected. The need for chemicals (acids and bases) for pH adjustment in the full-scale applications of the UV/Cl_2 AOP to decontamination of natural waters would increase considerably the operating costs and complexity.

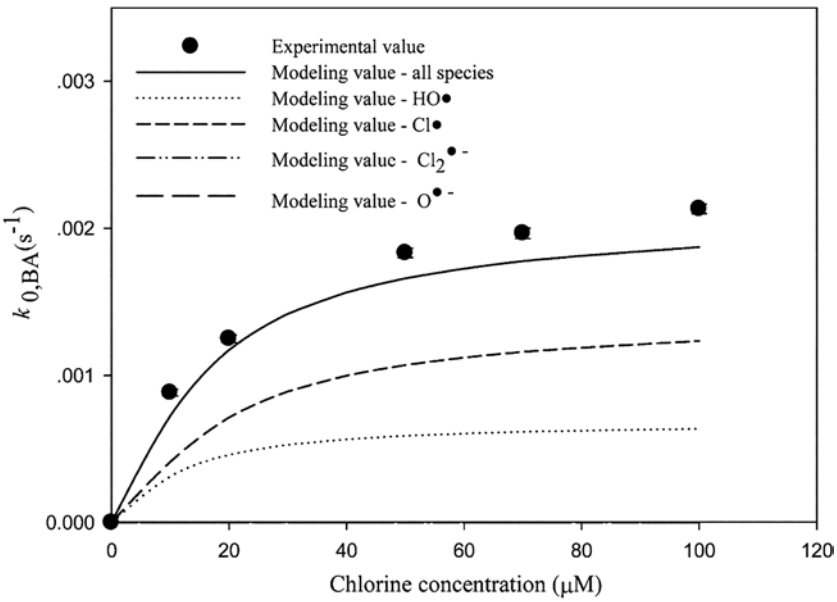

Figure 9.10 *Pseudo*-first-order rate constants for the degradation of benzoic acid by UV/Cl_2 as a function of chlorine dose; $[\text{Benzoic acid}]_0 = 5$ μM, pH 6.0. Reprinted with permission from Fang *et al.* (2014). Copyright 2016 American Chemical Society.

9.4.3.2 Effect of free chlorine dose

In the UV/Cl_2 AOP, increasing free chlorine dosage will increase the photo-generation rates of oxidizing radicals and the consumption rates of free radicals by residual free chlorine. Therefore, there exists an optimum dose of free chlorine for a given UV/Cl_2 application, which is related to water quality and process conditions.

Laboratory scale UV (253.7 nm)/Cl_2 experiments showed that the *pseudo*-first order rate constants for the degradation of nitrobenzene ($[\text{Nitrobenzene}]_0 = 5$ μM; $[\text{Free chlorine}]_0 = 30$–$150$ μM, pH 5; Watts *et al*. 2007b), chlortoluron ($[\text{Chlortoluron}]_0 = 5$ μM; $[\text{Free chlorine}]_0 = 25$–$100$ μM, pH 7; Guo *et al*. 2016) and carbamazepine ($[\text{Carbamazepine}]_0 = 8.5$ μM; $[\text{Free chlorine}]_0 = 30$–$630$ μM, pH 7; Wang *et al*. 2016a) increased linearly with increasing concentration of free chlorine. In these cases, the optimum chlorine dose was higher than the chlorine doses tested by the authors. On the other hand, the experimental and modeling results obtained by Fang *et al*. (2014) for the degradation rates of benzoic acid show two kinetic regimes (Figure 9.10), with faster rate increase at low chlorine doses than at higher chlorine doses. This effect can be explained by the higher •OH and Cl• scavenging capacity of the oxidant (free chlorine) at large doses than and low doses.

Xiang *et al*. (2016) also showed that the degradation rate of ibuprofen ($[Ibuprofen]_0 = 10$ μM; $[Free\ chlorine]_0$= 0–100 μM; pH 6; 253.7 nm) increased more gradually with increasing chlorine dose at chlorine dose higher than 70 μM.

Depending on the chemical and photochemical properties of the organic micropolluant, the chlorine dose would impact the contribution of direct photolysis reactions (for compounds which can be photolyzed at the irradiation wavelength) or of direct oxidation reactions with chlorine (for compounds very reactive towards molecular chorine) to the overall micropollutant degradation rates.

9.4.3.3 Effect of chloride ion concentration

Chloride is present in free chlorine solutions and in natural waters. Chloride reacts reversibly with $^{\bullet}OH$ and $Cl^{\bullet}$ to produce $HClOH^{\bullet}/ClOH^{\bullet-}$ and $Cl_2^{\bullet-}$ radicals (reactions 9.52–9.68), thus the presence of chloride may affect the degradation rates of organic micropollutants by the UV/Cl_2 AOP. However, the experimental data obtained at pH 6 for benzoic acid ($[Cl^-]$: 0–20 mM; Fang *et al*. 2014) and for ibuprofen ($[Cl^-]$: 0–10 mM; Xiang *et al*. 2016), and at pH 7 for atrazine ($[Cl^-]$: 0–10 mM; Kong *et al*. 2016) and carbamazepine ($[Cl^-]$: 0–50 mM; Wang *et al*. 2016a) show that the degradation rates of these micropollutants were not significantly affected by the chloride ion concentration under the tested conditions. The modeling data obtained by Fang *et al*. (2014) for the oxidation of benzoic acid at pH 6 showed that an increase of the chloride concentration from 0 to 20 mM did not change the contribution of $^{\bullet}OH$ and $Cl^{\bullet}$ to the degradation of benzoic acid but slightly increased the contribution of $Cl_2^{\bullet-}$.

9.4.3.4 Effect of alkalinity

As for all the other AOPs which are operated at neutral pH, the degradation rates of micropollutants by the UV/Cl_2 process also decrease in the presence of increasing alkalinity. Fang *et al*. (2014) showed that the *pseudo*-first order rate constants of degradation of benzoic acid decreased by a factor of 2.6 when the concentration of bicarbonate increased from 0 to 4 mM. Similar experiments conducted by Xiang *et al*. (2016) for the degradation of ibuprofen showed that the rate constant decreased only by a factor of 1.25 when the concentration of bicarbonate increased from 0.2 to 4 mM. As shown in Table 9.10, bicarbonate reacts much faster with $Cl^{\bullet}$ than with $^{\bullet}OH$. Therefore, the inhibiting effect of alkalinity on the efficiency of the UV/Cl_2 AOP would be more pronounced for micropollutants which have large second-order reaction rate constants with $Cl^{\bullet}$, and whose radical degradation mechanism is dominated by $Cl^{\bullet}$ rather than by $^{\bullet}OH$. In natural waters, the alkalinity exerts a buffering capacity and the water pH could be within the 6.8–8.2 range. In that range the free chlorine speciation varies significantly, and that impacts the UV/Cl_2 process performance.

9.4.3.5 Effect of natural organic matter (NOM)

Natural organic matter (NOM) can affect the efficiency of UV/Cl_2 AOP in various ways. NOM absorbs UV light (absorption coefficient at 253.7 nm ≈ 3 L m^{-1} (mg DOC)$^{-1}$), thus, acts as an inner filter reducing the photolysis rate of free chlorine to oxidizing radicals ($^{\bullet}OH$ and $Cl^{\bullet}$). It has also been shown that NOM can significantly increase the overall quantum yields of photodecomposition of free chlorine through radical chain reactions which are undesired in AOP applications (Ormeci *et al*. 2005; Feng *et al*. 2010). NOM competes with the target organic micropollutants for the $^{\bullet}OH$ and $Cl^{\bullet}$, thus lowering the steady-state concentrations of oxidizing radicals and the degradation rates of organic micropollutants. The rate constants for the reaction of $^{\bullet}OH$ with NOM extracts are in the range 1.2×10^4–3.8×10^4 L (mg DOC)$^{-1}$ s^{-1}

(Westerhoff *et al.* 2007). The direct reaction of free chlorine with NOM (water chlorine demand) may also lead to an instant consumption of free chlorine and to the formation of chlorination by-products (Westerhoff *et al.* 2004).

In their detailed study on the degradation of benzoic acid by the UV/Cl_2 AOP, Fang *et al.* (2014) showed that the *pseudo*-first order rate constant decreased from 2×10^{-3} s^{-1} to 1.2×10^{-3} s^{-1} when the concentration of NOM (Suwannee River NOM isolate, SW NOM) increased from 0 to 10 mg C/L. The authors estimated the $Cl^{\bullet}$ rate constant for the reaction with SW NOM as $k_{Cl\bullet,NOM} = 1.3 \times 10^4$ $(mg\ C/L)^{-1}$ s^{-1}, which is roughly half of that for the $^{\bullet}OH$ reaction.

9.4.4 UV/Cl_2 versus UV/H_2O_2

Similarly to the UV/H_2O_2 process, the UV/Cl_2 AOP may only be used to treat water that absorbs weakly the UV radiation wavelengths emitted by LP lamps (253.7 nm) or MP lamps (200–400 nm). The potential applications of these two AOPs therefore concern the decontamination of groundwater, drinking water sources, and tertiary wastewater effluents for direct or indirect potable reuse. Literature is available on bench-scale studies comparing the UV/Cl_2 and UV/H_2O_2 AOP efficiencies, most of which conducted in deionized water. Comparative studies on pilot- and full-scale UV/Cl_2 and UV/H_2O_2 at water treatment facilities are very limited, and were published almost exclusively in conference proceedings rather than in peer-reviewed journals. Selected examples from the published literature are discussed in this section.

9.4.4.1 Oxidation of nitrobenzene

A lab-scale comparative study on the degradation of a probe compound (nitrobenzene, NB, $k_{\bullet OH} = 3.9 \times 10^9$ M^{-1} s^{-1}) by the UV/Cl_2 and UV/H_2O_2 processes has been performed by Watts *et al.* (2007b) under identical experimental conditions ($[NB]_0 = 5$ µM in deionized water; [Free chlorine]$_0$ or $[H_2O_2]_0 = 0.03$–0.35 mM), using a *quasi*-collimated beam apparatus with LP lamps (253.7 nm). The data showed that the degradation rates of NB ($[Oxidant]_0 = 0.11$ mM) increased in the following order: UV/Cl_2 (pH 7) < UV/H_2O_2 (pH 5 and 7) < UV/Cl_2 (pH 6) < UV/Cl_2 (pH 5). The degradation rate of NB by UV/H_2O_2 at pH 6 was faster than that by UV/Cl_2 at pH 7 at oxidant dose > 0.22 mM. Similar experiments performed with a reservoir water (TOC = 4.32 mg/L; Alkalinity = 80 mg $CaCO_3$/L; $UV_{253.7\ nm} = 0.21$ cm^{-1}) and a post-sand filtered water (TOC = 2.2 mg/L; Alkalinity = 77.5 mg $CaCO_3$/L; $UV_{253.7\ nm} = 0.05$ cm^{-1}) showed that the degradation rates of NB ($[NB]_0 = 5$ µM) by the two AOPs (pH 5, 7 and 9.5) were much slower than in deionized water because of the presence of photon absorbers and of radical scavengers in the natural waters. Data obtained with sand-filtered water showed that the UV/Cl_2 AOP at pH 5 was the most efficient process and that a 90% removal of NB was achieved with a chlorine dose of 7.7 mg/L and a UV dose of about 1200 mJ cm^{-2}.

9.4.4.2 Removal of volatile organic compounds (VOCs)

Middleton Water Supply Region of Waterloo (ON, Canada) uses the UV/Cl_2 process with TrojanUVSwift™ECT 16L30 reactors for groundwater remediation. The primary contaminant is trichloroethene (TCE, ~5 µg/L), but very low levels of 1,4-dioxane are occasionally detected in the water. Wang *et al.* (2011) performed a series of tests at this water facility to examine the UV/Cl_2 treatment performance at various flowrates (50, 55, 80, and 95 L/s) and to compare the UV/Cl_2 and UV/H_2O_2 processes at one flowrate (55 L/s). The oxidant concentrations were fixed for all tests, i.e., 9 mg/L (127 µM) free chlorine and 8 mg/L (235 µM) H_2O_2; TCE concentration in the groundwater was within the 4–6 µg/L range. Groundwater contained very low TOC (~0.65 mg/L), relatively high alkalinity

(~288 mg/L as $CaCO_3$), and pH was 7.55. The authors reported TCE data for both direct photolysis (no oxidant) and UV-AOPs. Free chlorine was almost completely removed in the UV reactor (0.06 mg Cl_2/L residual) in all tests. Depending on the flowrate, 50 to 70% TCE was destroyed by UV alone. At 55 L/s, ~64% TCE was removed by direct photolysis, whereas ~90% and 75% removal was achieved with the UV/Cl_2 and the UV/H_2O_2 processes, respectively. A 90% removal yield was determined for the UV/H_2O_2 process at a flowrate of 30 L/s. The cost estimates for the same TCE treatment level were 13 and 18 cents per m^3 water treated by UV/Cl_2 and UV/H_2O_2 process, respectively. No process optimization (e.g., oxidant dose) was attempted in this study, such that the outcomes may not reflect correctly the AOP performance.

Bench-scale experiments conducted by Wang *et al.* (2012) using a MP collimated beam apparatus (UV doses up to 2000 mJ cm^{-2}), TCE (1.1 μM) in ultra-pure water, and identical initial concentrations of free chlorine and H_2O_2 (0.15 mM) showed that UV/Cl_2 was 2.3-fold more efficient for TCE removal than the UV/H_2O_2 process at pH 5.5, whereas the UV/H_2O_2 process became more efficient than UV/Cl_2 at pH 7.5 (4-fold) and pH 10. In the UV/Cl_2 process at pH 7.5 and pH 10, direct photolysis contributed approx. 71–74% to the overall rate constant, with less than ~30% contribution of the radical-induced degradation. The comparison of the two AOPs is based on the fluence-based rate constants calculated for each set of conditions. Identification of TCE degradation by-products was not undertaken in these two studies but it is conceivable to assume that the routes of degradation of TCE by UV/Cl_2 are as complex as those observed with the UV/H_2O_2 process (Li *et al.* 2007).

Boal *et al.* (2015) reported comparative studies on UV/Cl_2 and UV/H_2O_2 AOPs at two Aerojet Rocketdyne (Sacramento County, CA, USA) groundwater extraction and treatment (GET) plants. The two GET facilities use different treatment technologies to meet the water remediation goals. Both water facilities implemented the UV/H_2O_2 AOP with Calgon Carbon RAYOX™ Medium Pressure Ultraviolet (MP-UV) reactors (Calgon Carbon Corporation, Pittsburgh, Pennsylvania) to remove NDMA and VOCs (TCE, 1,2-DCE, 1,1-DCE, and vinyl chloride) from contaminated groundwater. One facility operates at low flowrate and high chemical dose (LFHC), whereas the other plant operates at high flowrate and low chemical dose (HFLC). The UV-AOP effluent from the HFLC facility is passed through GAC filters to enhance the UV/H_2O_2 treatment prior to groundwater recharge. The Electrical Energy Dose was 5.89 kWh/kgal (1.56 kWh/m^3) and 0.97 kWh/kgal (0.26 kWh/m^3) at the LFHC and HFLC facility, respectively. Hypochlorite for the UV/Cl_2 process was produced with a MIOX VAULT H25 on-site generation system. The UV/H_2O_2 process was tested without any pH adjustment and concentration ranges of 6.5–8.2 mg/L (LFHC plant) and 6.6–6.9 mg/L (HFLC plant). The H_2O_2 residual ranged from 3.3 to 3.5 mg/L (LFHC), and from 5.3 to 6.0 mg/L (HFLC). UV/Cl_2 tests were conducted at chlorine doses ranging from 0.8 to 7.7 mg/L at LFHC facility, and 0.9 to 5.7 mg/L at HFLC plant. NDMA was removed below method detection limit (MDL) of 2 ng/L in all tests at both water treatment plants, except in the 7.8 mg/L H_2O_2 run (23 ng/L). VOCs were all below MDL in the UV/H_2O_2 tests. In the UV/Cl_2 process, at LFHC facility, the VOCs were below MDL in all tests except for the 0.8 mg/L chlorine test where TCE (0.53 μg/L) approached the MDL (0.5 μg/L), and 1,1-DCE residual was 0.66 μg/L. At the HFLC plant, where the water pH was 7.7, all VOCs except TCE were removed under all free chlorine dose conditions.

The data showed that the optimum chlorine dose for TCE removal was about 2.5 mg/L at the LFHC plant (pH ~ 7.0), and no benefit was observed from increasing the chlorine dose from 3.6 mg/L to 5.7 mg/L at the HFLC plant (pH 7.69). The process economics indicated that the chemical costs for the UV/Cl_2 AOP were approximately one-fourth to one-half of the costs of the UV/H_2O_2 AOP which is the current process used at the two facilities. Table 9.11 summarizes the key outcomes from this study.

The UV/Cl_2 and UV/H_2O_2-effluents were not acutely toxic to the aquatic organism *Ceriodaphnia dubia*, except one UV/Cl_2 effluent from LFHC facility which affected 10% of the organisms.

Table 9.11 NDMA and VOC treatment data for the UV/H_2O_2 and UV/Cl_2 processes and associated treatment costs at the two facilities (Boal *et al.* 2015).

	LFHC Facility			HFLC Facility		
	Raw Water	**UV/H_2O_2**	**UV/Cl_2**	**Raw Water**	**UV/H_2O_2**	**UV/Cl_2**
Oxidant dose (mg/L)		6.5–8.2	2.8		6.6–6.9	3.6
Effluent oxidant (mg/L)		3.3–3.5	<0.02		5.3–6.0	<0.02
Electrical Energy Dose (kWh/1000 gallons)		5.89	5.89		0.97	0.97
pH	7.06			7.69		
Alkalinity (mg/L $CaCO_3$)	86			130		
NDMA (ng/L)	930–1300	<2; 23	<2	27–37	<2	<2
TCE (μg/L)	12–14	<0.5	<0.5	8–9.7	<0.5	1.8
1,1-DCE (μg/L)	16–19	<0.5	<0.5	<0.5	<0.5	<0.5
1,2 DCE (μg/L)	0.8–0.9	<0.5	<0.5	<0.5–0.55	<0.5	<0.5
Treatment cost ($/kgal)		0.067*	0.017*		0.073**	0.038**

*Treatment including only oxidant costs (7.4 mg/L H_2O_2; 2.5 mg/L Cl_2)
**Treatment including oxidant costs (7.4 mg/L H_2O_2; 3.0 mg/L Cl_2) and GAC costs.

9.4.4.3 Removal of emerging contaminants

Xiang *et al*. (2016) compared the degradation rates of ibuprofen (IBP) in deionized water by UV/Cl_2 and UV/H_2O_2 AOPs under identical experimental conditions ($[IBP]_0$ = 10 μM; $[Free\ chlorine]_0$ or $[H_2O_2]$ = 100 μM; pH 6.0; UV (253.7 nm) fluence rate = 1.05 mW/cm^2). The data showed that the degradation rate of IBP at pH 6 was 3.3 times faster for the UV/Cl_2 than for the UV/H_2O_2 process, which was attributed to the difference in photochemical characteristics of the two oxidants: $\varepsilon_{HOCl} \approx 60\ M^{-1}\ cm^{-1}$; $\varepsilon_{H2O2} = 19.6\ M^{-1}\ cm^{-1}$ and $\Phi_{HOCl} \approx 1–1.5$; $\Phi_{H2O2} \approx 1.0$.

Watts and Linden (2009) observed similar removal yields of tris(2-butylethyl) phosphate (TBEP, $[TBEP]_0$ = 50 μg/L) with the UV/Cl_2 and UV/H_2O_2 processes. The experiments were performed in simulated surface water (2 mg/L DOC; 30 mg/L bicarbonate; 0.3 mg/L nitrate) at pH 6.8, with oxidant doses of 6.1 mg/L and 3.4 mg/L for H_2O_2 and free chlorine, respectively, and UV fluence up to 1000 mJ cm^{-2}.

Sichel *et al*. (2011) compared the degradation yields of eight emerging contaminants (ECs) treated with the UV/Cl_2 and UV/H_2O_2 processes (Table 9.12). The treatment was performed in a flow-through mode using a low-pressure lamp UV reactor powered at 40, 80 or 200 W. The matrix was tap water as-is or enriched in dissolved organic carbon, which was spiked with a mixture of ECs at environmental levels (μg/L). The initial concentrations of free chlorine were 1 or 6 mg/L, whereas the H_2O_2 concentration was 5 mg/L. This concentration of H_2O_2 was selected to be similar to that used in the first full-scale application of the UV/H_2O_2 process at a drinking water treatment plant in Europe (Andijk, The Netherlands; Kruithof *et al*. 2007). The MP-UV (Trojan UVSwiftECT™ 16L30) reactors in Andijk are operated with 6 mg/L H_2O_2 and an electrical energy dose (E_{ED}) of approximately 0.5 kWh/m^3 to remove a wide range of organic micropollutants from surface water.

For an electrical energy consumption of 0.32 kWh/m^3, the addition of 1 mg Cl_2/L significantly increased the removals of all ECs as compared to UV alone. At a lower energy consumption (0.16 kWh/m^3), the UV/Cl_2 process ($[Cl_2]_{inlet}$ = 6.1 ± 0.1 mg/L; $[Cl_2]_{outlet}$ = 5.4 ± 0.2 mg/L) was found to be more efficient than the UV/H_2O_2 process ($[H_2O_2]$ = 5.2 mg/L). The electrical energy required to achieve 90%

reduction of ECs with the UV/H_2O_2 process under the conditions used in Sichel *et al.*'s work varied from 0.17 to 1.00 kWh/m^3, depending on the treated contaminant. The authors estimated 30–75% energy reduction and up to 30–50% operational process cost savings for the UV/Cl_2 process as compared to the UV/H_2O_2 process.

Table 9.12 Degradation yields of emerging contaminants (tap water, pH 7) under various treatment conditions. Data estimated from the figures given in Sichel *et al.* (2011).

	Cl_2 Alone 15 min Contact Time	**UV Alone**	**UV/Cl_2**	**UV/H_2O_2**	**UV/Cl_2**	**UV/H_2O_2**	**E_{EO}(kWh/m^3/order) UV/H_2O_2**
[Cl_2] (mg/L)	6	0	1	0	6	0	
[H_2O_2] (mg/L)	0	0	0	5	0	5	
E_{ED} (kWh/m^3)	0	0.32	0.32	0.32	0.16	0.16	
17α-ethinylestradiol		8	100	92			
Benzotriazole	1	11	94	71	71	25	0.52
Tolyltriazole	4	18	94	63	70	29	0.59
Desethylatrazine	17	13	21	48	23	19	1.00
Carbamazepine	4	3	48	58	90	32	0.62
Sulfamethoxazole	100	55	100	92	100	64	0.29
Diclofenac	32	61	100	100	100	88	0.17
Iopamidole	4	31	92	81	96	58	0.42

E_{ED} = Electrical Energy Dose
E_{EO} = Electrical energy per order

Yang *et al.* (2016) reported the removal yields for ten pharmaceuticals and personal care products (PPCP) treated with UV/Cl_2 and UV/H_2O_2 processes (253.7 nm radiation) in sand-filtered water samples collected from three water treatment facilities. The water quality parameters varied greatly; e.g., 3.5, 1.1, and 1.9 mg/L TOC; 0.013, 0.027, and 3.14 mg/L NH_3-N (important parameter in UV/Cl_2 process); 3.5, 47.4, 14.1 mg/L HCO_3^-. The transmittance (94–95% $T_{1\ cm,253.7\ nm}$) and pH (7.6–7.9) were *quasi*-similar in the three waters. The pH was adjusted to 7 in all tests. The authors observed ~100% degradation yields for triclosan, 2-ethylhexyl-4-methoxycinnamate (EHMC), ciprofloxacin, tetracycline, benzophenone-3 (BP3), and trimethoprim with chlorine alone (3 mg/L) and UV/chlorine (3 mg/L) at the same reaction time, in the high-TOC, low ammonia, and low alkalinity water. 90–98% degradation was determined in the same water with the UV/H_2O_2 (5 mg/L) process for triclosan, sulfamethoxazole, EHMC, and ciprofloxacin. Less than 20% removal was observed for caffeine for all processes used with this water. Among the three waters tested, the lowest removal yields with the UV/Cl_2 (5 mg/L) process were observed in the water with the highest ammonia content. The UV/Cl_2 process outperformed the UV/H_2O_2 process in two of the three waters, and showed similar performance in ammonia-rich water. The authors indicated that both $^{\bullet}OH$ and $Cl^{\bullet}$ were the oxidizing radicals in the UV/Cl_2 process. Approx. 20% increase in total THM level was observed UV/Cl_2- and UV/H_2O_2-treated water (high ammonia, moderate alkalinity sample) upon 24h-incubation time and a free chlorine residual of ~1 mg/L, but the t-THMs did not exceed 40 μg/L. Chloral hydrate increased by ~30% post-UV/Cl_2 process applied to high-TOC water, relative to untreated and UV/H_2O_2-treated water samples.

9.4.4.4 Removal of taste and odor-causing compounds (T&O) from drinking water sources

A pilot-scale study was performed at Richard Miller Water Treatment Plant of Greater Cincinnati Water Works to compare the efficiency of the UV/Cl_2 and UV/H_2O_2 AOPs for the removal of 2-methylisoborneol (MIB) (Rosenfeldt *et al.* 2013). MIB was spiked at 30 ng/L to the pretreated water (0.78 mg/L TOC; 68 mg/L alkalinity as $CaCO_3$). The data showed that the MP UV/Cl_2 (1 or 5 mg/L) AOP was able to remove 80–90% MIB at pH 6, and 45–70% MIB at pH 7.5 at a UV dose of 250 mJ cm^{-2}. The authors observed that the UV/Cl_2 process outperformed the UV/H_2O_2 AOP at both low and high oxidant concentrations when pH was in the acidic range. Operating costs (UV + chemicals, $/1000 gal of treated water) for 1-log removal of MIB were lower for the UV/Cl_2 AOP at pH 6 (0.07–0.14 and 0.11–0.15 for chlorine doses of 2 and 5 mg/L, respectively) than for the UV/H_2O_2 AOP at pH 6 or 7.5 (0.26 and 0.18–0.19 for H_2O_2 doses of 2 and 5 mg/L, respectively). The costs for the UV/H_2O_2 process would increase to $0.30/kgal and $0.27-$0.28 per kgal of treated water for 2 and 5 mg/L H_2O_2, respectively, if the costs associated with the removal of H_2O_2 residual are considered.

A recent study compared the UV/Cl_2 and the UV/H_2O_2 AOPs with respect to the removal of geosmin, MIB and caffeine from drinking water at full-scale UV installation (Wang *et al.* 2015a). The tests were conducted at Cornwall Water Purification Plant (Ontario, Canada) which uses the UV/H_2O_2 AOP with MP-UV reactors (Trojan UVSwiftECT™ 8L24) to control T&O-causing compounds occurring in the surface water during the seasonal algal blooming events. Pre-treated (pre-chlorination, coagulation, flocculation, sand/anthracite filtration) St. Lawrence River water (pH 7.9; 1.5 mg/L TOC; 92 mg/L alkalinity as $CaCO_3$; 0.3 mg/L chlorine residual) was passed through one MP-UV reactor at a flowrate of 100 L/s (estimated UV dose of 2000 ± 150 mJ cm^{-2}; 83.5 kW reactor power; $E_{ED} = 0.23$ kWh/m^3). In the first set of tests, geosmin and MIB were spiked to the water upstream to the UV reactor at ≈ 400 ng/L), and the oxidant doses were either 2, 6 or 10 mg/L free chlorine (UV/Cl_2) or 1.0, 2.9 or 4.8 mg/L H_2O_2 (UV/H_2O_2). The second set was scheduled during a T&O event (~18 ng/L geosmin in water) and only the UV/Cl_2 AOP was tested. Water pH was adjusted to 6.5, 7.5 and 8.5 in both sets. The MIB and geosmin treatment data from the first set are shown in Figure 9.11.

Wang *et al.* (2015a) calculated the electrical energy per order (E_{EO}) for all treatment conditions illustrated in Figure 9.11. The lowest E_{EO} were observed at pH 6.5 and for the highest oxidant dose tested in both AOPs. The E_{EO} values at pH 6.5 for geosmin were 0.16 and 0.23 kWh/m^3/order for the UV/Cl_2 (10 mg/L) AOP and UV/H_2O_2 (4.8 mg/L), respectively. At pH 7.5 and 8.5, the geosmin E_{EO} values increased for both AOPs at all oxidant doses. The reported E_{EO} values at pH 6.5 for MIB were 0.22 and 0.31 kWh/m^3/order for the UV/Cl_2 (10 mg/L) and UV/H_2O_2 (4.8 mg/L), respectively; similar E_{EO} – pH patterns as for geosmin were observed.

In addition to the full-scale tests described above, the authors performed pilot-scale tests on caffeine treatment under oxidant dose conditions similar to full-scale. Post-filtered Lake Simcoe water from Keswick WTP (ON, Canada) – 3.5 mg/L TOC, 123 mg/L alkalinity as $CaCO_3$, 0.04 cm^{-1} (254 nm) absorption coefficient – was treated in a 40L completely mixed batch reactor (Rayox®, Calgon Carbon Corporation, Pittsburgh, PA) equipped with 1 kW MP lamp. Larger caffeine E_{EO} data were reported for pilot- than full-scale tests, which is explained by the difference in the water quality used in the two treatment settings. The authors concluded that caffeine could be a good surrogate to estimate the treatment of T&O compounds with UV/Cl_2 and UV/H_2O_2 processes, and recommended pilot- or full-scale tests be conducted at water utilities to confirm site-specific performance of UV/Cl_2 process prior to implementation.

9.4.4.5 UV/Chlorine AOP for Water Reuse: Terminal Island Water Reclamation Plant (TIWRP) Case Study

In recent years, the UV/Cl_2 AOP has been evaluated at pilot- and full-scale as a potential cost-effective advanced treatment of tertiary wastewater effluents in water reuse applications. The City of Los Angeles

Department of Public Works (DPW) Bureau of Sanitation (LASAN) is expanding the TIWRP Advanced Water Purification Facility (AWPF) capacity for advanced treatment of tertiary effluent from 15.77 m^3/min (6 MGD) to 31.55 m^3/min (12 MGD) (Aflaki *et al.* 2015). The advanced treated water will be used for groundwater recharge and to supply the local industries and irrigation facilities, thus, replacing and reducing the potable water consumption for industrial purposes. The AWPF Expansion will include an additional microfiltration (MF) system, a reverse osmosis (RO) system followed by an AOP for disinfection and removal of the organic micropollutants passing through RO membranes, a tertiary effluent equalization tank (7570 m^3 (2MG)) upstream of AWTP, and a series of upgrades to the existing pumping and chemical dosing facilities.

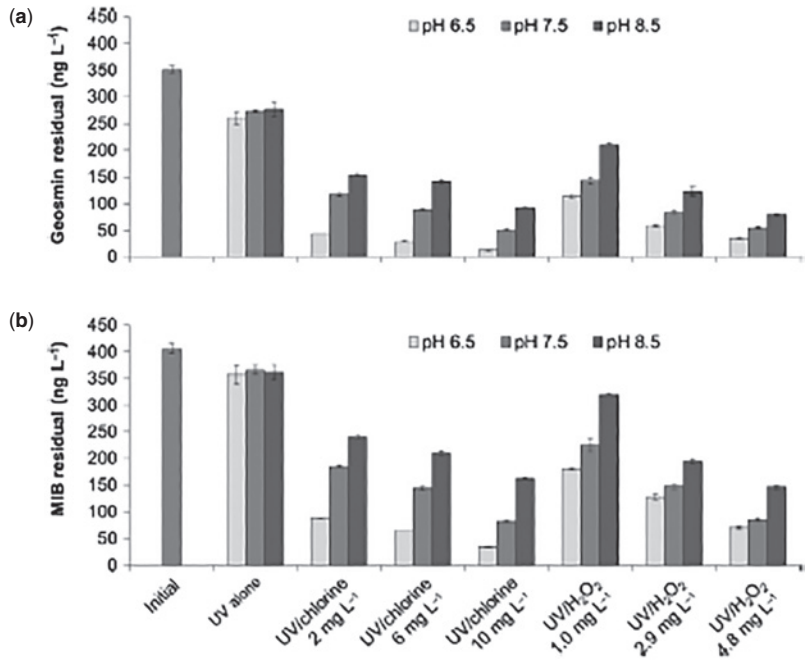

Figure 9.11 Geosmin (a) and MIB (b) removal in the 1st full-scale test at the Cornwall Water Purification Plant (ON, Canada). Reprinted with permission from Wang *et al.* (2015a). Copyright 2016 Elsevier.

Advanced treatment of tertiary effluents is currently practiced in (indirect or direct) potable water reuse applications at water utilities around the world, with UV/H_2O_2 as an AOP for microorganism (viruses, bacteria and protozoa) control and NDMA, 1,4-dioxane, and other micropollutant treatment (see Chapter 14 for extended information). NDMA levels in tertiary effluents at TIWRP are below CA notification limit of 10 ng/L, such that this compound was not the primary consideration for AOP implementation at AWPF. LASAN's AOP investment decision for the TIWRP AWPF Ultimate Expansion project was based on 18-month extensive bench- and pilot-scale studies, which allowed LASAN to select the best AOP technology for this specific project and the AOP system scale-up approach for full compliance with California Department of Drinking Water (DDW) and Groundwater Replenishment Reuse Regulations (GRRR). CA DWW, GRRRs of 2014 require 12-log virus-, 10-log *Giardia lamblia*, and 10-log *Cryptosporidium parvum* inactivation, <10 ng/L NDMA, and ≥0.5-log 1,4-dioxane removal (or equivalent treatment) in RO-AOP treated water, and were used by LASAN to set design criteria for the bench- and pilot-scale tests.

Four AOPs were investigated at bench-scale on RO product water: UV/H_2O_2, UV/Cl_2, O_3/H_2O_2, and H_2O_2/O_3/UV. The UV/H_2O_2 and UV/Cl_2 AOPs were tested with both low- and medium-pressure mercury vapor lamps, whereas the O_3/H_2O_2 process was tested for both H_2O_2 injection before O_3 and H_2O_2 injection after ozone. Specifics on these preliminary tests are available in Aflaki *et al.* (2015). The bench-scale data showed that all tested AOPs met the microorganism removal criteria set by LASAN for each AOP, THMs and HAAs were not formed as a result of UV/Cl_2 AOP, chlorate was not detected in the AOP effluents, and bromate was formed in O_3/H_2O_2 AOP only under specific pH and [O_3]:[H_2O_2] molar ratio conditions, which were further adjusted in the pilot trials.

Pilot testing was considered absolutely required in order to (*a*) confirm the bench-scale results, (*b*) establish a correct relationship between bench-, pilot- and, thereafter, full-scale data, (*c*) establish relationship between chemical dose and speciation and hydraulic conditions, (*d*) refine design criteria and costs for each AOP, (*e*) assess byproduct formation under refined chemical and hydraulic conditions, (*f*) determine scalable conditions/criteria and select the AOP for full-scale system.

Pilot-scale testing was conducted for 12 months using WEDECO MiPRO AOP pilot system designed to operate all abovementioned AOPs, with fully automated PLC and operator interface, remote monitoring and data-logging and online water quality monitoring instrumentation. Neither bench- nor pilot-scale data are available in Aflaki *et al.* (2015) except some UV (253.7 nm)/Cl_2 process data which are shown in Figure 9.12. The O_3/H_2O_2 AOP removed effectively 1,4-dioxane, but failed to remove NDMA from 30 ng/L (spiked to RO product water for the purpose of these studies) to below 10 ng/L. MP UV-based AOPs met all design criteria, but was not considered due to high life cycle costs as compared to LP UV (see Aflaki *et al.* 2015 for life cycle cost comparison). Both LP – UV/Cl_2 and -UV/H_2O_2 were effective for 1,4-dioxane and NDMA treatment, but higher H_2O_2 concentrations were required.

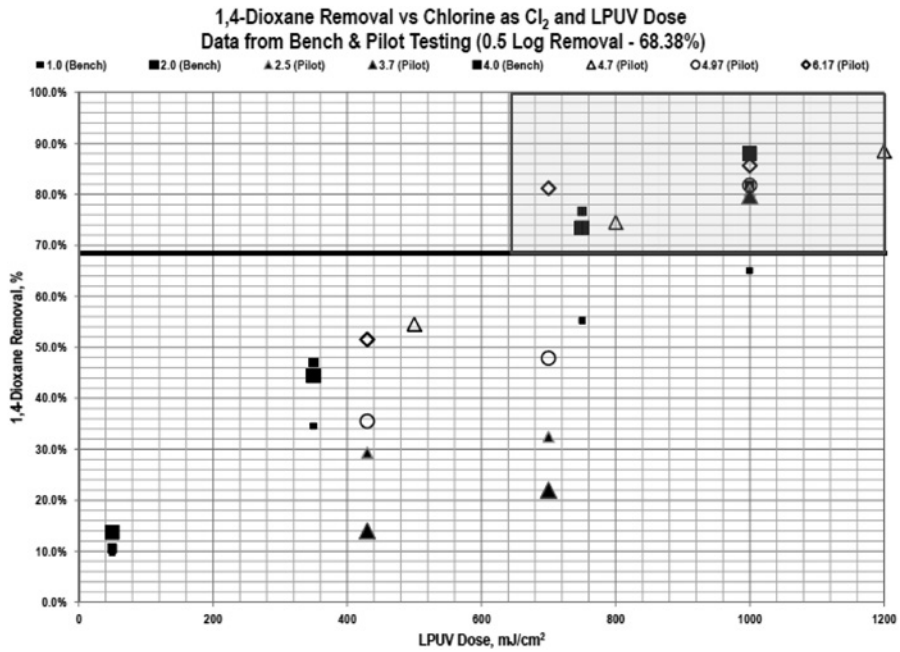

Figure 9.12 Selected UV(253.7 nm)/Chlorine pilot test data (courtesy of Dr. R. Aflaki).

Under all chemical dose and UV dose conditions shown in the squared area in Figure 9.12, LP-UV/chlorine achieved more than 0.5-log 1,4-dioxane (>68.38%) removal in RO product water.

The LP-UV/Cl_2 process was the most cost-effective among tested AOPs. In addition to meeting the performance criteria and low life cycle cost, the selection of the UV/Cl_2 AOP over the UV/H_2O_2 AOP presents the following advantages: NaOCl is already used in the existing plant as secondary disinfectant; lower dosage of oxidant; the chlorine residual is used for water disinfection in the distribution network; insignificant DBP formation; easy-to-understand, -to operate, and -to monitor process.

The LP-UV/Chlorine AOP was selected for full-scale implementation at TIWRP AWPF. Chemical cost savings of $3.3 M over 20 year-operation is expected based on H_2O_2 and free chlorine cost calculations.

The AOP design basis are: flowrate of 3 to 12 MGD, TOC < 0.25 mg/L, *%T*(1 cm, 254 nm) > 96%, California groundwater recharge regulations.

The AOP design criteria are: 6-log virus inactivation, 0.5-log 1,4-dioxane removal, <10 ng/L NDMA, UV dose of 920 mJ cm^{-2}, free chlorine dose of 2–4 mg/L. The project was awarded to Xylem/Wedeco, with the startup in late 2016. Two Wedeco K143 Series LP UV reactors with 17 rows of lamps (one UV intensity sensor per row) and 12 lamps (600 W/ lamp) per row in each reactor will be installed and operated at TIWRP AWPF. The K143 reactor is modular allowing for more rows for linear expansion. The system is equipped with real-time monitoring of transmittance, flowrate, and intensity, which allows real-time UV dose calculations and operational adjustments to the UV dose set point. Of note, the UV dose is the design criterion and the process performance monitoring parameter. Online monitoring instrumentation of pH, free and total chlorine will ensure optimal oxidant dosing and treatment performance. The LASAN's TIWRP AWPF will be the first advanced treatment facility in the world to install the LP-UV/chlorine AOP for water reuse.

9.4.4.6 Solar radiation-based UV/Cl_2 for remediation of oil sands process-affected water

The possibility of using the solar-driven UV/Cl_2 AOP in water and wastewater treatment has been investigated by Chan *et al.* (2012) for the degradation of methylene blue (MB) and cyclohexanoic acid (CHA), and by Shu *et al.* (2014) for detoxification of oil sands process-affected water remediation (OSPW). These two studies were carried out under actual sunlight on the campus of the University of Alberta (Edmonton, AB, Canada). Chan *et al.* (2012) demonstrated that chlorination under sunlight UV led to MB photobleaching (0.039 mM MB; 1.37 mM ClO^-) and to CHA degradation (0.23 mM CHA; 1.55 mM ClO^-). Shu *et al.* (2014) studied the solar UV radiation-induced photolysis of free chlorine as a means to degrade naphthenic acids (NAs) and fluorophore organic compounds, and to decrease the acute toxicity of OSPW. The main characteristics of the OSPW were as follows: pH 8.3–8.6; 277 NTU; 47 mg/L TOC; 683 ± 32 mg/L bicarbonate; 451 mg/L Cl^-; approx. 33 mg/L total NAs. Four experiments were conducted. Upon exposure for up to 7 hours to solar radiation in the presence of either 200 or 300 mg/L NaOCl, up to 84% NAs and fluorophore organic compounds (e.g., petroleum polyaromatic hydrocarbons) were removed from OSPW. The process reduced the acute toxicity of OSPW toward *Vibrio fischeri*, but no change in the toxicity toward goldfish primary kidney macrophages was observed relative to untreated OSPW. The study concluded that the solar-driven UV/Cl_2 AOP is a promising approach to decontamination of OSPW but further studies are needed to optimize the process for toxicity removal.

9.4.5 Byproduct formation in the UV/Cl_2 AOP

Chlorine is widely used for drinking water disinfection. The applied chlorine dose satisfies the water background chlorine demand and ensures 0.3–0.5 mg/L residual in the water distribution network. The reactions of free chlorine with the organic matter present in the water lead to a series of disinfection by-products (DBPs) such as trihalomethanes (THMs), haloacetic acids (HAAs), haloacetonitriles (HANs), haloketones (HKs) and halopicrins (Richardson *et al*. 2007).

Application of UV/Cl_2 AOP to drinking water treatment could generate chlorinated organic (e.g., halogenated NOM, DBPs) and inorganic (chlorite, chlorate, bromate) byproducts. Unlike the drinking water chlorination conditions (0.5–2 mg/L Cl_2; 0.5–4 h contact time in the reservoirs, up to 72 h in the distribution network), the UV/Cl_2 AOP would require high chlorine doses (3–6 mg/L as a practical range) and very short contact time ($\ll$1 min) under high UV energy exposures in the UV reactors. Chlorinated compounds can be formed inside the UV reactors through the reactions of chlorine atoms with NOM. Additionally, the UV radiation and the hydroxyl and chlorine radicals generated from the photolysis of free chlorine change the structure of natural organic matter to DBP precursors prone to chlorination in the reservoirs and water distribution system. Selected publications on byproduct formation as a result of UV/Cl_2 process are discussed in the next few sections. Additional information on the byproduct formation topic is provided in the studies on micropollutant removal with the UV/Cl_2 AOP exemplified in Section *9.4.4*.

9.4.5.1 NOM oxidation and Disinfection byproducts

Zhao *et al*. (2011) examined the formation of halogenated organics (TOX) upon exposure to MP-UV in combination with free chlorine, and compared the data to 'dark' chlorination. The authors used probe compounds and showed that nitrobenzene (NB) and benzoic acid (BA), which are compounds bearing electron-withdrawing groups, were largely converted to chlorinated products upon exposure to MP-UV/Cl_2 (0.28 mM NaOCl, pH 6.5, ~220 mJ cm^{-2}). Increased TOX relative to dark chlorination were observed also in the presence of bromide, with bromine being incorporated into the products. At pH 8.5, no TOX were observed from NB, and lower TOX yields from BA were measured in the absence of bromide. Similar experiments conducted with Suwannee River NOM (5 mg C/L) showed significant conversions of NOM to TOX both under dark chlorination and MP-UV/Cl_2 exposure; however, no significant difference was observed between the levels measured for the two processes. In the presence of bromide, MP-UV/Cl_2 led to slightly lower TOX levels than chlorination alone, at both pHs. Structural changes in NOM were observed in the ESI-tqMS spectra recorded for UV/Cl_2-treated NOM, particularly in polar and ionizable fractions of NOM. Other changes in the solution properties – e.g., UV absorbance – were noted. The study reflects the role of halogen atoms in the transformation of UV exposed organic matter.

Pisarenko *et al.* (2013) investigated the impact of UV/Cl_2 AOP on NOM oxidation and DBP formation on pre-chlorinated Colorado River water collected from a water utility. The water samples (2.6 mg/L TOC; pH 8.1, adjusted to 6.0, 7.5, and 9.0; $UV_{253.7\,nm}$ = 0.045 cm^{-1}) were spiked at various free chlorine levels (0–50 mg/L NaOCl), and further exposed to either monochromatic UV-C (253.7 nm, ~3900 mJ/cm^2) or polychromatic UV-A (310–410 nm; max. at 365 nm, ~7000 mJ cm^{-2} radiation. Chlorine doses and UV fluences used in this study are far larger than those practiced in real water treatment applications. Hydrochloric acid used to adjust pH to 6 and 7.5 raised the chloride concentration and increased the $Cl^{\bullet}$ water demand *via* Cl^- reactions. Insignificant NOM mineralization (TOC loss < 0.3 mg/L) was observed, while ~50% and 40% reduction of UV_{254} absorbance at pH 6 and 7.5, respectively, was achieved with the UV-C/Cl_2 process. Fluorescence excitation-emission matrix and SEC-UV fluorescence data indicated major structural changes in NOM and reduction of aromaticity (chromophoric NOM). At 10 mg/L free

chlorine and pH 7.5, the UV-C/Cl_2 process did not affect the total (four) THM level, increased the total (nine) HAA level and decreased the TOX, relative to the control (dark chlorination). Chloroform was the overwhelming THM with UV-C/Cl_2, whereas chloro-bromo-THMs prevailed in both dark chlorination and UV-A/Cl_2 processes. Dichloro- and trichloroacetic acids were the major HAAs. As free chlorine was almost completely decomposed over the 2-h exposure to either LP or MP radiation, the 2-h 'dark chlorination' where large Cl_2 residual is expected, may have not been a true 'control' for these tests. The high UV doses may have degraded the DBP precursors or/and the DBPs generated in the process.

Wang *et al*. (2015b) undertook full-scale and pilot-scale byproduct formation studies during the application of UV/Cl_2 and UV/H_2O_2 processes for T&O and caffeine treatment. Process details are given in Section *9.4.4.4*. The chlorinated and brominated organic byproducts monitored in these studies were the four THMs, nine HAAs, 1,1-dichloro- and 1,1,1-trichloro-2-propanone (HKs), four haloacetonitriles (HANs), chloropicrin, and adsorbable organic halides (AOX), whereas the inorganic byproducts monitored included chlorite, chlorate, perchlorate, and bromate. The inorganic byproducts from this work are discussed in Sections *9.4.5.2* and *9.4.5.3*. No change in t-THMs relative to untreated water (18 μg/L) was observed in any UV/Cl_2- and UV/H_2O_2-effluents from full-scale tests (Cornwall WTP). That is, THMs were not formed during the short residence time (30 s) in the UV reactor (~1800 mJ cm^{-2}). In Lake Simcoe water (pilot), which was not pre-chlorinated at the intake, UV/Cl_2-treated samples (60 s) led to more than 100% increase of t-THMs relative to untreated or UV alone-treated waters. Upon 24-h incubation time, THMFP increased by 30–100% in the UV/Cl_2 (10 mg/L)- and UV/H_2O_2(4.8 mg/L)-treated full-scale effluents, with more t-THMs being formed in UV/Cl_2 process at pH 6.5 than in all other samples. Much larger THMFP increase was observed in pilot- than at full-scale tests. HAA9 levels increased in full-scale UV/Cl_2 (pH 6.5 and 7.5) effluents (10–40%) relative to untreated water; no increase was observed for the UV/H_2O_2-treated effluents. The 24-h HAA9FP increased by 40–110%, and 20–90%, in Cornwall and Lake Simcoe water, respectively, for both AOPs. That shows that HAA precursors are formed from radical-induced degradation of dissolved NOM. Dichloro- and trichloroacetic acids accounted for approx. 60% of the t-HAAs.

HKs and chloropicrin were not formed in either UV-AOP at full-scale treatment; up-to 4-fold increase in HANs was observed only in the UV/Cl_2 process at pH 6.5 and 7.5, but the levels were very low (up to 4 μg/L). Similar fold-increase yields were observed for HANFP in both UV/Cl_2 and UV/H_2O_2-treated samples, with levels up to 15 μg/L. Much larger HAN levels were formed in UV/Cl_2-treated Lake Simcoe water at pilot-scale than in UV/Cl_2-treated water at full-scale (Cornwall WTP), and the HANFP at pH 6.5 was determined as ~30 μg/L. Dichloro- and bromodichloro-acetonitriles were the major HAN species. AOX and AOX-FP increased marginally if at all in the UV-AOP effluents at full-scale relative to the original water. Up to ~5-fold increased AOX levels (~100 μg C/L) were quantified in UV/Cl_2-treated Lake Simcoe water relative to untreated water (~20 μg C/L). Since no such patterns were observed in the UV/H_2O_2 tests, the authors suggested that the adsorbable halogenated organics formed in the UV/Cl_2 process resulted from $Cl^{\bullet}$ reactions with NOM and that $Cl^{\bullet}$ species originated from chlorine photolysis.

Iodinated DBPs (I-DBPs) can be formed in iodide-containing waters during the chlorination process. Iodinated X-ray contrast agents (e.g., iopromide, iohexol, iopamidol) are emerging contaminants in waste- and surface waters. Both UV alone and AOP-driven degradation of iodinated compounds results in iodide which is further oxidized to hypoiodous acid (HOI) during the chlorination practices. HOI could generate I-DBPs in reactions with dissolved organic matter. Wang *et al*. (2016b) examined the degradation of iohexol by UV alone and UV/Cl_2 AOP, in both laboratory water and water collected from two WTPs. For a given water matrix, the yield and speciation of the observed I-THMs depended on the process, chlorine concentration, and pH. Post-UV/Cl_2 treatment chlorination resulted in less I-THMs than post-UV (alone) chlorination.

Zhang *et al.* (2015) investigated the role of UV/chlorine for ammonia and DBP reduction. In their study, chlorine was added to ammonia-rich water to a 0.8 Cl_2/N molar ratio, which in the presence of UV (253.7 nm) translated into a UV/chloramine process rather than UV/(free) chlorine AOP. The water samples were collected from a municipal drinking water treatment plant from Harbin, China. Monochloramine absorbs the 253.7 nm radiation much stronger than free chlorine and photolyzes to $Cl^{\bullet}$; nitrite and nitrate are among final degradation products. Free ammonia (0.07 mM) was removed by ~50% upon exposure to UV/chlorine (as NH_2Cl) at 800 mJ cm^{-2}. The authors postulated H-atom abstraction from NH_3 by $Cl^{\bullet}$ followed by a sequence of reactions starting from the aminyl ($NH_2^{\bullet}$) radical. Post-UV/chlorine water chlorination showed a lower Cl_2 demand and generated less THMs and HAAs than untreated water. The process formed more HANs than 'dark' chlorination of untreated water. This study is relevant to water reuse applications where free ammonia can be present in RO permeates, thus, an increased Cl_2 demand would be observed. Chloramine photolysis will occur in UV/Cl_2 water reuse applications, such that more complex chemistry and photochemistry than in the absence of chloramines is expected, and undesirable process byproducts could be formed.

9.4.5.2 Chlorite, chlorate, and perchlorate

Chloride, chlorite, and chlorate are the only reported photodegradation products of free chlorine. Laboratory studies performed in deionized water showed that 9% to 30% (by mass) of chlorine can convert to chlorate at 253.7 nm (Buxton & Subhani, 1972b; Feng *et al.* 2010). In a full-scale study on the degradation of TCE in groundwater by MP–UV/Cl_2 (9 mg/L; pH 7.55; 90% TCE reduction) at Middleton WTP, ON, Canada, Wang *et al.* (2011) showed that the concentration of chlorate in treated water was approximately 0.95 mg/L. This concentration exceeded the WHO drinking water guideline for chlorate of 0.7 mg/L, and was marginally lower than Health Canada drinking water guideline of 1 mg/L. In their full-scale (Trojan UVSwiftECT™ 8L24) studies conducted at the drinking water treatment plant in Cornwall (see test conditions in Section *9.4.4.4*), Wang *et al.* (2015b) showed that 2 to 17% (by mass) of free chlorine photolyzed in the reactor was converted to chlorate. The highest values were measured at pH 8.5 and 10 mg/L Cl_2. Chlorite and perchlorate were not detected. However, chlorite is a product of chlorine photolysis at 365 nm, which is one of the strong lines of MP lamp emission spectrum (Buxton & Subhani, 1972b). As the maximum concentration of chlorate in drinking water has been regulated at 1 mg/L by Health Canada (2012), the formation of chlorate would be the predominant limiting factor for the use of the UV/Cl_2 AOP for water treatment with the purpose of drinking water production. Additionally, chlorate may also be introduced in water with commercial NaOCl solutions (Stanford *et al.* 2011).

9.4.5.3 Bromate

Bromate ion is a potential human carcinogen and its concentration in drinking water is regulated at 10 µg/L. Bromate is typically produced at drinking water treatment plants which use ozonation of natural waters containing bromide ions (von Gunten & Oliveras, 1998). Formation of hydroxyl radicals in the free chlorine photolysis may promote the formation of bromate in UV reactors during the treatment of bromide-rich waters.

Laboratory scale experiments carried out in a batch LP-UV reactor with bromide solutions prepared in deionized water (80 µg/L Br^-; pH ≈ 7.8) and filtered Yangtze River water (56.3 µg/L Br^-; 1.7 mg/L DOC; pH ≈ 7.5) showed that the UV/Cl_2 process (5 mg/L Cl_2) led to bromate formation (Huang *et al.* 2008). The bromate yields increased with the applied UV dose. Bromate levels of ~10 µgL (maximum permissible level in drinking water) were measured at ~200 mJ cm^{-2} in deionized water, and at ~700 mJ cm^{-2} in the

river water. For the highest UV dose tested (~1450 mJ cm^{-2}), residual free chlorine was <0.5 mg/L, and bromate was quantified as ~18 and ~12 µg/L in deionized water and in river water, respectively (0.01–0.14 mole BrO_3^-/mole Br^-). Huang *et al.*'s study showed that bromate formation was much higher in the UV/Cl_2 process than in dark chlorination, and depended also on pH and chlorine dose. Bromate formation in the order of 0.1 to 2 µg/L, with higher levels at lower pH (consistent with Huang *et al.*'s findings), were measured by Wang *et al.* (2015b) in the full-scale study on the UV/Cl_2 AOP at Cornwall, ON, WTP, even at the low concentrations of bromide (2–3 µg/L) present in the surface water. More full-scale studies with water containing various bromide levels (levels as large as 700 µg/L are reported in surface waters treated for drinking water production) are needed in order to assess whether bromate formation in the UV/Cl_2 AOP should be a concern.

9.5 RESEARCH NEEDS

This literature review has shown that the mechanisms for the overall photodecomposition of free chlorine in pure water are very complex and depend on many parameters, among which, pH and radiation wavelength. The kinetic studies available in the public domain provide quantum yield values for the overall photodecomposition of free chlorine species, but there is no comprehensive kinetic model for the UV/Cl_2 AOP which includes all initiation, propagation, and termination reactions occurring in this process. These reactions must be captured in a kinetic model in order to predict correctly the steady state concentrations of the oxidizing species and the micropollutant degradation rates. Fundamental research is needed to elucidate reaction mechanisms, to understand the role of reactive species characteristic to the UV/Cl_2 process such as $Cl^{\bullet}$, $ClO^{\bullet}$, $Cl_2^{\bullet-}$, to determine accurate rate constants for the reactions of $^{\bullet}OH$ and $Cl^{\bullet}$ with HOCl, water constituents and micropollutants targeted in the water sources.

In water reuse, the RO permeates contain chloramines and could contain free ammonia. Chloramines absorb the UV radiation and undergo photolysis with large and pH- and oxygen-dependent quantum yields, with formation of radical species and stable products which interfere with free chlorine chemistry and photochemistry. Should ammonia be present in the water, free chlorine consumption and additional chloramine formation should be expected. The role of chloramines in the UV/Cl_2 AOP is not studied and its implications on process performance are unknown.

Research is needed to clarify the contribution of the various radicals generated during the UV/chlorine process to the degradation of micropolluants, to determine the rate constants for the reactions of $Cl^{\bullet}$ and $Cl_2^{\bullet-}$ with organic and inorganic compounds, to better understand the fate of organic radicals ($R^{\bullet}$, $ROO^{\bullet}$) and the secondary reactions involving HOCl and ClO^-, and to know the impact of water matrix constituents on the efficiency of the UV/Cl_2 process.

The UV/Cl_2 AOP is insufficiently studied with respect to its implications on the treated water quality, including toxicity, mutagenicity, and genotoxicity, and the emerging disinfection byproduct formation.

9.6 CONCLUSIONS

As compared to other AOPs, the studies on the oxidation of organic compounds by UV/Cl_2 process are very recent and scarce. However, pilot- and full-scale studies performed at drinking water and water reuse treatment plants over the past few years indicate that the UV/Chlorine process may represent a promising alternative to the UV/H_2O_2 AOP, particularly from economic and process operating perspectives. For the purpose of potable water production and water reuse, the formation of undesirable by-products (chlorate, bromate, TOX, THMs, HAAs, HANs) must be predicted and controlled to ensure that the treated water quality meets the regulatory standards.

The use of the UV/Cl_2 AOP to treat groundwater or surface water contaminated with organic micropollutants requires chlorine doses of 5 to 10 mg /L and UV doses of 500–2000 mJ cm^{-2}. Given the complexity of reaction mechanisms and the diversity of micropollutant degradation pathways (direct photolysis, reaction with free chlorine, oxidation by radicals), bench-scale research and preliminary pilot trials are needed in order to determine the optimal process conditions (UV dose, chlorine dose, pH), to select and to size the UV equipment for specific applications, and to estimate the treatment costs. The chlorine dosage in the UV/Cl_2 applications must be optimized in order to obtain an acceptable residual concentration of free chlorine for secondary disinfection of treated water in the reservoirs and distribution network, thus, avoiding the use of a quenching reagent for free chlorine.

9.7 ACKNOWLEDGEMENT

Special thanks to Dr. Roshanak Aflaki from City of Los Angeles Department of Public Works, CA, for providing the figure with the TIWRP pilot data adapted from Aflaki *et al.* (2015).

9.8 REFERENCES

Aflaki R., Hammond S., Tag Oh S., Hokanson D., Trussell S. and Bazzi A. (2015). Scaling-up step-by-step and AOP investment decision. Proceedings of the Water Environment Federation's Technical Exhibition and Conference (WEFTEC), September 26–30, 2015, Chicago, IL, USA, pp. 9–21.

Aghdam E., Sun J. and Shang C. (2016). DEET degradation by the UV/chlorine process: kinetics, contributions of radicals and byproduct formation. *IUVA World Congress*, January 31–February 3, 2016, Vancouver, BC, Canada. https://iuva.wildapricot.org/resources/Documents/world%20conference%202016/tuesday/5/Ehsan%20Aghdam%20IUVA.pdf

Alegre M. L., Gerones M., Rosso J. A., Bertolitti S. G., Braun A. M., Martire D. O. and Gonzalez M. C. (2000). Kinetic study of the reactions of chlorine atoms and $Cl_2^{\bullet-}$ radical anions in aqueous solutions. 1. Reaction with Benzene. *Journal of Physical Chemistry A*, **104**(14), 3117–3125.

Allmand A. J., Cunliffe P. W. and Maddison R. E. W. (1925). The photodecomposition of chlorine water and of aqueous hypochlorous acid solutions. Part I. *Journal of the Chemical Society, Transactions*, **127**, 822–840.

Armstrong D. A., Huie R. E., Koppenol W. H., Lymar S. V., Merényi G., Neta P., Ruscic B., Stanbury D. M., Steenken S. and Wardman P. (2015). Standard electrode potentials involving radicals in aqueous solution: inorganic radicals (IUPAC Technical Report). *Pure and Applied Chemistry*, **87**(11–12), 1139–1150.

Boal A. K., Rhodes C. and Garcia S. (2015). Pump-and-treat groundwater remediation using chlorine/ultraviolet advanced oxidation processes. *Groundwater Monitoring & Remediation*, **35**(2), 93–100.

Bolton J. R. and Stefan M. I. (2002). Fundamental photochemical approach to the concepts of fluence (UV dose) and electrical energy efficiency in photochemical degradation reactions. *Research on Chemical Intermediates*, **28**(7), 857–870.

Buxton G. V. and Subhani M. S. (1972a). Radiation chemistry and photochemistry of oxychlorine ions. Part 1. -Radiolysis of aqueous solutions of hypochlorite and chlorite ions. *Journal of the Chemical Society, Faraday Transactions 1: Physical Chemistry in Condensed Phases*, **68**, 947–957.

Buxton G. V. and Subhani M. S. (1972b). Radiation chemistry and photochemistry of oxychlorine ions. Part 2. -Photodecomposition of aqueous solutions of hypochlorite ions. *Journal of the Chemical Society, Faraday Transactions 1: Physical Chemistry in Condensed Phases*, **68**, 958–969.

Buxton G. V., Bydder M. and Salmon G. A. (1998). Reactivity of chlorine atoms in aqueous solution. Part I: the equilibrium $Cl^{\bullet} + Cl^- \rightleftharpoons Cl_2^{\bullet-}$. *Journal of the Chemical Society, Faraday Transactions*, **94**(5), 653–657.

Buxton G. V., Greenstock C. L., Helman W. P. and Ross A. B. (1988). Critical review of rate constants for reactions of hydrated electrons, hydrogen atoms and hydroxyl radicals ($OH^{\bullet}/O^{\bullet-}$) in aqueous solution. *Journal of Physical and Chemical Reference Data*, **17**(2), 513–886.

Buxton G. V., Bydder M., Salmon G.A. and Williams J. E. (2000). The reactivity of chlorine atoms in aqueous solution. Part III: the reaction of $Cl^{\bullet}$ with solutes. *Physical Chemistry Chemical Physics*, **2**, 237–245.

Chan P. Y., El-Din M. G. and Bolton J. R. (2012). A solar-driven UV/chlorine advanced oxidation process. *Water Research*, **46**(17), 5672–5682.

Connick R. E. and Chia, Y. (1959). The hydrolysis of chlorine and its variation with temperature. *Journal of the American Chemical Society*, **81**(6), 1280–1284.

Cooper W. J., Jones A. C., Whitehead R. F. and Zika R. G. (2007). Sunlight-induced photochemical decay of oxidants in natural waters: implications in ballast water treatment. *Environmental Science & Technology*, **41**(10), 3728–3733.

De Laat J. (2016). Personal communication.

De Laat J. and Berne F. (2009). La déchloramination des eaux de piscines par irradiation UV. Etude bibliographique. Theoretical and practical aspects of the dechloramination of swimming pool water by UV irradiation. *European Journal of Water Quality*, **40**(2), 129–149.

Deborde M. and von Gunten U. (2008). Reactions of chlorine with inorganic and organic compounds during water treatment – Kinetics and mechanisms: a critical review. *Water Research*, **42**(1–2), 13–51.

Deng L., Huang C. H. and Wang Y. L. (2014). Effects of combined UV and chlorine treatment on the formation of trichloronitromethane from amine precursors. *Environmental Science & Technology*, **48**(5), 2697–2705.

Fang J., Fu Y. and Shang C. (2014). The roles of reactive species in micropollutant degradation in the UV/Free chlorine system. *Environmental Science & Technology*, **48**(3), 1859–1868.

Feng Y., Smith, D. W. and Bolton J. R. (2007). Photolysis of aqueous free chlorine species (HOCl and OCl) with 254 nm ultraviolet light. *Journal of Environmental Engineering and Science*, **6**(3), 277–284.

Feng Y., Smith, D. W. and Bolton J. R. (2010). A potential new method for determination of the fluence (UV dose) delivered in UV reactors involving the photodegradation of free chlorine. *Water Environment Research*, **82**(4), 328–334.

Gilbert B. C., Stell J. K., Peet W. J. and Radford K. J. (1988). Generation and reactions of the chlorine atom in aqueous solution. *Journal of the Chemical Society, Faraday Transactions 1: Physical Chemistry in Condensed Phases*, **84**(10), 3319–3330.

Grigorev A. E., Makarov I. E. and Pikaev A. K. (1987). Formation of Cl_2 in the bulk solution during the radiolysis of concentrated aqueous solutions of chloride. *High Energy Chemistry*, **21**, 99–102.

Guo Z. B., Lin Y. L., Xu B., Huang H., Zhang T. Y., Tian F. X. and Gao Y. (2016). Degradation of chlortoluron during UV irradiation and UV/chlorine processes and formation of disinfection by-products in sequential chlorination. *Chemical Engineering Journal*, **283**, 412–419.

Hasegawa K. and Neta P. (1978). Rate constants and mechanisms of reaction of Cl_2^- radicals. *Journal of Physical Chemistry*, **82**(8), 854–857.

Health Canada (2012). Guidelines for Canadian Drinking Water Quality – Summary Table. Water, Air and Climate Change Bureau. Healthy Environments and Consumer Safety Branch, Health Canada, Ottawa, Ontario, Canada.

Held A. M., Halko D. J. and Hurst J. K. (1978). Mechanisms of chlorine oxidation of hydrogen peroxide. *Journal of American Chemical. Society*, **100**(18), 5732–5740.

Herrmann H. (2007). On the photolysis of simple anions and neutral molecules as sources of O^-/OH, SO_x- and Cl in aqueous solution. *Physical Chemistry Chemical Physics*, **9**(30), 3925–3964.

Huang X., Gao N. and Deng Y. (2008). Bromate ion formation in dark chlorination and ultraviolet/chlorination processes for bromide-containing water. *Journal of Environmental Sciences*, **20**(2), 246–251.

Jacobi H. W., Wicktor F., Herrmann H. and Zellner R. (1999). A laser flash photolysis kinetic study of reactions of the Cl_2^- radical anion with oxygenated hydrocarbons in aqueous solution. *International Journal of Chemical Kinetics*, **31**(3), 169–181.

Jayson G. G., Parsons B. J. and Swallow A. J. (1973). Some simple, highly reactive, inorganic chlorine derivatives in aqueous solution. Their formation using pulses of radiation and their role in the mechanism of the Fricke dosimeter. *Journal of the Chemical Society, Faraday Transactions 1: Physical Chemistry in Condensed Phases*, **69**(0), 1597–1607.

Jin J., El-Din M. G. and Bolton J. R. (2011). Assessment of the UV/chlorine process as an advanced oxidation process. *Water Research*, **45**(4), 1890–1896.

Kang N., Anderson T. A. and Jackson W. A. (2006). Photochemical formation of perchlorate from aqueous oxychlorine anions. *Analytica Chimica Acta*, **567**(1), 48–56.

Karpel Vel Leitner N., De Laat J. and Doré M. (1992a). Photodécomposition du bioxyde de chlore et des ions chlorite par irradiation U.V. en milieu aqueux – Partie I. Sous-produits de réaction. Photodecomposition of chlorine dioxide and chlorite by U.V.-Irradiation—Part I. Photo-products. *Water Research*, **26**(12), 1655–1664.

Karpel Vel Leitner N., De Laat J. and Doré M. (1992b). Photodécomposition du bioxyde de chlore et des ions chlorite par irradiation U.V. en milieu aqueux – Partie II. Etude cinétique. Photodecomposition of chlorine dioxide and chlorite by U.V.-Irradiation—Part II. Kinetic study. *Water Research*, **26**(12), 1665–1672.

Kishimoto N. and Nishimura H. (2015). Effect of pH and molar ratio of pollutant to oxidant on a photochemical advanced oxidation process using hypochlorite. *Environmental Technology*, **36**(19), 2436–2442.

Kläning U. K. and Wolff T. (1985). Laser flash photolysis of HClO, ClO^-, HBrO, and BrO^- in aqueous solution. Reactions of Cl^- and Br^- atoms. *Berichte der Bunsengesellschaft für Physikalische Chemie*, **89**, 243–245.

Kläning U. K., Sehested K. and Wolff T. (1984). Ozone formation in laser flash photolysis of oxoacids and oxoanions of chlorine and bromine. *Journal of the Chemical Society, Faraday Transactions 1*, 80, 2969–2979.

Kläning U. K., Sehested K. and Holcman J. (1985). Standard Gibbs energy of formation of the hydroxyl radical in aqueous solution. Rate constants for the reaction $ClO_2^- + O_3 \rightleftarrows O_3^- + ClO_2$. *Journal of Physical Chemistry*, **89**(5), 760–763.

Kong X., Jiang J., Ma J., Yang Y., Liu W. and Liu Y. (2016). Degradation of atrazine by UV/chlorine: efficiency, influencing factors, and products. *Water Research*, **90**, 15–23.

Kruithof J. C., Kamp P. C. and Martijn B. J. (2007). UV/H_2O_2 Treatment: a practical solution for organic contaminant control and primary disinfection. *Ozone: Science & Engineering: The Journal of the International Ozone Association*, **29**(4), 273–280.

Legrini O., Oliveros, E. and Braun, M. (1993). Photochemical processes for water treatment. *Chemical Reviews*, **93**(2), 671–689.

Li K., Stefan M. I. and Crittenden J. C. (2007). Trichloroethene degradation by UV/H_2O_2 advanced oxidation process: product study and kinetic modelling. *Environmental Science & Technology*, **41**(5), 1696–1703.

Macounová K. M., Simic N., Ahlberg E. and Krtil P. (2015). Electrochemical water-splitting based on hypochlorite oxidation. *Journal of the American Chemical Society*, **137**(23), 7262–7265.

Mártire D. O., Rosso J. A., Bertolotti S., Le Roux G. C., Braun A. M. and Gonzalez M. C. (2001). Kinetic Study of the reactions of chlorine atoms and $Cl_2^{\bullet-}$ radical anions in aqueous solutions. II. Toluene, benzoic acid and chlorobenzene. *Journal of Physical Chemistry A*, **105**(22), 5385–5392.

Matthew B. M. and Anastasio C. (2006). A chemical probe technique for the determination of reactive halogen species in aqueous solution: part 1 – Bromide solutions. *Atmospheric Chemistry and Physics*, **6**(9), 2423–2437.

McElroy W. J. (1990). A laser photolysis study of the reaction of SO_4^- with Cl^- and the subsequent decay of Cl_2^- in aqueous solution. *Journal of Physical Chemistry*, **94**, 2435–2441.

Mertens M. and von Sonntag C. (1995). Photolysis ($\lambda = 254$ nm) of tetrachloroethene in aqueous solutions. *Journal of Photochemistry and Photobiology A: Chemistry*, **85**(1), 1–9.

Morris J. C. (1966). The acid ionization constant of HOCl from 5 to 35°. *Journal of Physical Chemistry*, **70**(12), 3798–3805.

Neta P., Huie R. E. and Ross A. B. (1988). Rate constants for reactions of inorganic radicals in aqueous solution. *Journal of Physical Chemistry and Reference Data*, **17**(3), 1027–1284.

Nowell L. H. and Crosby D. G. (1985). Photodegradation of water pollutants in chlorinated water. In: Water Chlorination: Chemistry, Environmental Impact and Health Effects, R. Jolley W. Davis S. Katz M. Jr, Roberts and V. Jacobs (eds), Lewis Publishers Inc., Chelsea, Michigan, pp. 1055–1062.

Nowell L. H. and Hoigné, J. (1992a). Photolysis of aqueous chlorine at sunlight and ultraviolet wavelengths I. Degradation rates. *Water Research*, **26**(5), 593–598.

Nowell L.H. and Hoigné, J. (1992b). Photolysis of aqueous chlorine at sunlight and ultraviolet wavelengths II. Hydroxyl radical production. *Water Research*, **26**(5), 599–605.

Ogata Y. and Tomizawa K. (1984). Photoreaction of benzoic acid with sodium hypochlorite in aqueous alkali. *Journal of the Chemical Society, Perkin Transactions 2*, 6, 985–988.

Ogata Y., Takagi K. and Susuki T. (1978). Photolytic oxidation of ethylene glycol, dimethyl ether and related compounds by aqueous hypochlorite. *Journal of the Chemical Society, Perkin Transactions 2*, **6**, 562–567.

Ogata Y., Suzuki T. and Takagi K. (1979). Photolytic oxidation of aliphatic acids by aqueous sodium hypochlorite. *Journal Chemical Society, Perkin Transactions 2*, **12**, 1715–1719.

Oliver B. G. and Carey J. H. (1977). Photochemical production of chlorinated organic in aqueous solutions containing chlorine. *Environmental Science & Technology*, **11**(9), 893–895.

Ormeci B., Ducoste J. J. and Linden K. G. (2005). UV disinfection of chlorinated water: impact on chlorine concentration and UV dose delivery. *Journal of Water Supply: Research and Technology-AQUA*, **54**(3), 189–199.

Oturan M. A. and Aaron J.-J. (2014). Advanced oxidation processes in water/wastewater treatment: principles and applications. A Review. *Critical Reviews in Environmental Science and Technology*, **44**(23), 2577–2641.

Pisarenko A. N., Stanford B. D., Snyder S. A., Rivera S. B. and Boal A. K. (2013). Investigation of the use of chlorine based advanced oxidation in surface water: oxidation of natural organic matter and formation of disinfection byproducts. *Journal of Advanced Oxidation Technologies*, **16**(1), 137–150.

Qin L., Lin Y. L., Xu B., Hu C. Y., Tian F. X., Zhang T. Y., Zhu W. Q., Huang H. and Gao N. Y. (2014). Kinetic models and pathways of ronidazole degradation by chlorination, UV irradiation and UV/chlorine processes. *Water Research*, **65**, 271–281.

Rao B., Estrada N., McGee S., Mangold J., Gu B. and Jackson W. A. (2010). Perchlorate production by photodecomposition of aqueous chlorine solutions. *Environmental Science & Technology*, **46**(21), 11635–11643.

Richardson S. D., Plewa M. J., Wagner E. D., Schoeny R. and Demarini D. M. (2007). Occurrence, genotoxicity, and carcinogenicity of regulated and emerging disinfection by-products in drinking water: a review and roadmap for research. *Mutation Research*, **636**(1–3), 178–242.

Rosenfeldt E., Boal A. K., Springer J., Stanford B., Rivera S., Mashinkunti R. D. and Metz D. H. (2013). Comparison of UV-mediated advanced oxidation. *Journal of the American Water Works Association*, **105**(7), 29–33.

Schwarzenbach R.P., Gschwend P.M. and Imboden D.M. (1993). Chapter 13 in Environmental Organic Chemistry. Wiley-Interscience: John Wiley and Sons, New York.

Shu Z., Li C., Belosevic M., Bolton J. R. and El-Din G. M. (2014). Application of a solar UV/solar advanced oxidation process to oil sands process-affected water remediation. *Environmental Science & Technology*, **48**(16), 9692–9701.

Sichel C., Garcia C. and Andre K. (2011). Feasibility studies: UV/chlorine advanced oxidation treatment for the removal of emerging contaminants. *Water Research*, **45**(19), 6371–6380.

Siddiqui M. S. (1996). Chlorine-ozone interactions: formation of chlorate. *Water Research*, **30**(9), 2160–2170.

Song W., Cooper W. J., Peake B. M., Mezyk S. P., Nickelsen M. G. and O'Shea K. E. (2009). Free-radical-induced oxidative and reductive degradation of N,N'-diethyl-*m*-toluamide (DEET): kinetic studies and degradation pathway. *Water Research*, **43**(3), 635–642.

Stanford B. D., Pisarenko, A. N., Snyder, S. A. and Gordon, G. (2011). Perchlorate, bromate, and chlorate in hypochlorite solutions: guidelines for utilities. *Journal of the American Water Works Association*, **103**(6), 71–83.

Thomsen C. L., Madsen D., Poulsen J. Aa., Thøgersen J., Knak Jensen S. J. and Keiding S. R. (2001). Femtosecond photolysis of aqueous HOCl. *The Journal of Chemical Physics*, **115**(20), 9361–9369.

Vione D., Maurino V., Minero C., Calza P. and Pelizzetti E. (2005). Phenol chlorination and photochlorination in the presence of chloride ions in homogeneous aqueous solution. *Environmental Science & Technology*, **39**(13), 5066–5075.

Von Gunten U. and Oliveras Y. (1998). Advanced oxidation of bromide-containing waters: bromate formation mechanisms. *Environmental Science & Technology*, **32**(1), 63–70.

von Sonntag C. and von Gunten, U. (2012). Chemistry of Ozone in Water and Wastewater Treatment. IWA Publishing, London, UK.

Wagner I., Karthäuser J. and Strehlow H. (1986). On the decay of the dichloride anion Cl_2^- in aqueous solution. *Berichte der Bunsengesellschaft für Physikalische Chemie*, **90**(10), 861–867.

Wang D., Walton T., McDermott L. and Hofmann R. (2011). Control of TCE using UV combined with hydrogen peroxide or chlorine. Proceedings of IOA-IUVA World Congress & Exhibition, 23–27 May, 2011, Paris, France, pp. 152–158.

Wang D., Bolton J. R. and Hofmann R. (2012). Medium pressure UV combined with chlorine advanced oxidation for trichloroethylene destruction in a model water. *Water Research*, **46**(15), 4677–4686.

Wang D., Bolton J. R., Andrews S. A. and Hofmann R. (2015a). UV/chlorine control of drinking water taste and odour at pilot and full-scale. *Chemosphere*, **136**, 239–244.

Wang D., Bolton J. R., Andrews S. A. and Hofmann R. (2015b). Formation of disinfection by-products in the ultraviolet/chlorine advanced oxidation process. *Science of the Total Environment*, **518**–519, 49–57.

Wang W. L., Wu Q. Y., Huang N., Wang T. and Hu H. Y. (2016a). Synergistic effect between UV and chlorine (UV/chlorine) on the degradation of carbamazepine: influence factors and radical species. *Water Research*, **98**, 190–198.

Wang Z., Lin, Y. L., Xu, B., Xia, S. J., Zhang, T. Y. and Gao N. Y. (2016b). Degradation of iohexol by UV/chlorine process and formation of iodinated trihalomethanes during post-chlorination. *Chemical Engineering Journal*, **283**, 1090–1096.

Watts, M. J. and Linden K. G. (2007). Chlorine photolysis and subsequent OH radical production during UV treatment of chlorinated water. *Water Research*, **41**(13), 2871–2878.

Watts M. J. and Linden K. G. (2009). Advanced oxidation kinetics of aqueous trialkyl phosphate flame retardants and plasticizers. *Environmental Science & Technology*, **43**(8), 2937–2942.

Watts M. J. Rosenfeldt E. J. and Linden K. G. (2007). Comparative OH radical oxidation using UV-Cl_2 and UV-H_2O_2 processes. *Journal of Water Supply: Research and Technology-AQUA*, **56**(8), 469–477.

Watts M. J., Hofmann R. and Rosenfeldt E. J. (2012). Low-pressure UV/Cl2 for advanced oxidation oxidation of taste and odor. *Journal of American Water Works Association*, **104**(1), E58–E65.

Westerhoff P., Chao P. and Mash H. (2004). Reactivity of natural organic matter with aqueous chlorine and bromine. *Water Research*, **38**(6), 1502–1513.

Westerhoff P., Mezyk S. P., Cooper W. J. and Minakata D. (2007). Electron pulse radiolysis determination of hydroxyl radical rate constants with Suwannee River fulvic acid and other dissolved organic matter isolates. *Environmental Science & Technology*, **41**(13), 4640–4646.

Wicktor F., Donati A., Herrmann H. and Zellner R. (2003). Laser based spectroscopic and kinetic investigations of reactions of the Cl atom with oxygenated hydrocarbons in aqueous solution. *Physical Chemistry Chemical Physics*, **5**(12), 2562–2572.

Willson R. L. (1973). Free-radical chain oxidation by carbon tetrachloride and related compounds: model pulse-radiolysis studies. *Biochemical Society Transactions*, **1**, 929–931.

Wu D., Wong D. and Di Bartolo B. (1980). Evolution of Cl_2^- in aqueous NaCl solutions. *Journal of Photochemistry*, **14**(4), 303–310.

Xiang Y., Fang J. and Shang C. (2016). Kinetics and pathways of ibuprofen degradation by the UV/chlorine advanced oxidation process. *Water Research*, **90**, 301–308.

Yang X., Sun J., Fu W., Shang C., Li Y., Chen Y., Gan W., and Fang J. (2016). PPCP degradation by UV/chlorine treatment and its impact on DBP formation potential in real waters. *Water Research*, **98**, 309–318.

Yu X. Y. and Barker J. R. (2003). Hydrogen peroxide photolysis in acidic solutions containing chloride ions. I. Chemical mechanism. *Journal of Physical Chemistry A*, **107**(9), 1313–1324.

Yu X. Y., Bao Z. C. and Barker J. R. (2004). Free radical reactions involving $Cl^{\bullet}$, $Cl_2^{-\bullet}$, and $SO_4^{-\bullet}$ in the 248 nm photolysis of aqueous solutions containing $S_2O_8^{2-}$ and Cl^-. *Journal of Physical Chemistry A*, **108**(2), 295–308.

Zhang X., Li W., Blatchley III E. R., Wang X. and Ren P. (2015). UV/chlorine process for ammonia removal and disinfection by-product reduction: comparison with chlorination. *Water Research*, **68**, 804–811.

Zhao Q., Shang C., Zhang X., Ding G. and Yang X. (2011). Formation of halogenated organic byproducts during medium-pressure UV and chlorine coexposure of model compounds, NOM and bromide. *Water Research*, **45**(19), 6545–6554.

Zhu L., Nicovich J. M. and Wine P. H. (2005). Kinetics studies of aqueous reactions of Cl atoms and Cl_2^- radicals with organic sulfur compounds of atmospheric interest. *Journal of Physical Chemistry A*, **109**(17), 3903–3911.

Zuo Z., Katsumura Y., Ueda K. and Ishigure K. (1997). Reactions between some inorganic radicals and oxychlorides studied by pulse radiolysis and laser photolysis. *Journal of the Chemical Society, Faraday Transactions*, **93**(10), 1885–1891.

Chapter 10

Sulfate radical ion – based AOPs

Nathalie Karpel Vel Leitner

10.1 INTRODUCTION

As extensively discussed in the other chapters, the information on $HO^{\bullet}$-based processes from fundamental and applied research was acquired over more than a century. It started in 1894 with Fenton's discovery on metal-activated hydrogen peroxide decomposition resulting in tartaric acid oxidation. The process was further investigated in the 1930's by Haber and Weiss who proved the involvement of hydroxyl radical as the reactive species. But it was in 1977 when the UV/H_2O_2 AOP emerged based on Koubek's publication on the destruction of a number of organic acids through UV photolysis of H_2O_2. Ever since, the use of this process for water decontamination was extensively investigated such that today it is implemented at several water treatment plants around the world.

The 'history' of sulfate radical anion ($SO_4^{\bullet-}$) is more recent and covers about half a century of research, with an increasing interest into sulfate radical-driven oxidation particularly during the last decade when a significant number of laboratory scale studies have been reported in the scientific literature.

The sulfate radical-based processes have been studied extensively in the academic settings, but their industrial implementations are rare. Only a few niche applications were implemented to-date for soil and groundwater remediation with persulfate or sulfate radicals generated through persulfate activation on site; this technology is known as *In Situ* Chemical Oxidation (ISCO).

This chapter gives an overview on the state-of-the-art in research and applications of sulfate radical-based AOPs. The mechanisms of sulfate radical generation and the reactions with organic and inorganic compounds are also described.

10.2 METHODS FOR SULFATE RADICAL GENERATION

Several processes are described in the published literature on the generation of sulfate radical. Those could be homogeneous or heterogeneous, chemical and/or thermal, photochemical, or physical processes. The most common sulfate radical anion generation means are based on persulfate activation. Persulfate ($S_2O_8^{2-}$) is a strong oxidant ($E^0 = 2.1$ eV) which is relatively stable during storage and handling, but can be

activated by various agents in order to generate highly reactive sulfate radicals which are characterized by a higher oxidative potential (2.6 eV) than that of persulfate ion. In practice, persulfate (peroxodisulfate, PDS) can be converted to sulfate radicals through three main processes: direct UV photolysis, thermal-, and metal-activation. The activation of peroxymonosulfate (Oxone, PMS) is also an efficient process for $SO_4^{\bullet-}$ generation.

10.2.1 Mild-thermal and base activation of persulfate

Persulfate heated in the range of 30–90°C was found to be effective for the destruction of various contaminants in water, among which, volatile organic compounds (VOCs) (Huang *et al.* 2005), hydroperfluorocarboxylic acids (Hori *et al.* 2010), and compounds inert toward $HO^{\bullet}$. Under thermal activation, PDS converts into the powerful oxidizing sulfate radicals.

The scission of the O—O bond in $S_2O_8^{2-}$ molecule (reaction 10.1) can be slowly initiated at 30°C and can be extremely rapid at 90°C with an activation energy of about 29 kcal mol^{-1} in neutral solutions (Kolthoff & Miller, 1951).

$$S_2O_8^{2-} \xrightarrow{\text{heat}} 2SO_4^{\bullet-} \tag{10.1}$$

It has been reported also (Furman *et al.* 2010) that alkaline pH conditions catalyze hydrolysis of persulfate to hydroperoxide anion and sulfate ion. The reduction of another persulfate molecule by the hydroperoxide ion leads to sulfate radical and sulfate anion. The net reaction (10.2) for base-activation of persulfate generates also superoxide radical anion ($O_2^{\bullet-}$).

$$2S_2O_8^{2-} + 2H_2O \xrightarrow{OH^-} 3SO_4^{2-} + SO_4^{\bullet-} + O_2^{\bullet-} + 4H^+ \tag{10.2}$$

Until now, alkali would be the most commonly used activators of persulfate for treatment of contaminated groundwater by *in situ* chemical oxidation (ISCO; Siegrist *et al.* 2011).

10.2.2 Photochemical processes

10.2.2.1 Persulfate photolysis

Under UV irradiation, free $SO_4^{\bullet-}$ radicals are formed through homolytic cleavage of peroxide bond in the peroxydisulfate dianion (reaction 10.3).

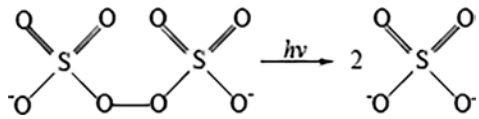

(10.3)

This reaction is a clean source of sulfate radicals with high and pH-independent quantum yields. With similar absorption spectra, the molar absorption coefficients of persulfate ion (20–22 M^{-1} cm^{-1}; Heidt, 1942; Mark *et al.* 1990) and hydrogen peroxide (18.6 M^{-1} cm^{-1} at pH 7.5; Hochanadel, 1962) at 254 nm are comparable.

The quantum yield of sulfate radical formation from persulfate photolysis within the 248–254 nm wavelength range is 1.4 ± 0.3 (Herrmann, 2007; Mark *et al.* 1990; Figure 10.1), much larger than that of $HO^{\bullet}$ formation from hydrogen peroxide photolysis (1.0; Hochanadel, 1962).

The rate constant for the reaction of the generated radical with the oxidant (i.e., $SO_4^{\bullet-} + S_2O_8^{2-}$ *vs* $HO^{\bullet} + H_2O_2$) is smaller in the $S_2O_8^{2-}$/UV system ($k_{SO_4^{\bullet-}/S_2O_8^{2-}} = (6.1 \pm 0.6) \times 10^5$ L mol^{-1} s^{-1}; McElroy & Waygood, 1990) than in the UV/H_2O_2 process ($k_{HO^{\bullet}/H_2O_2} = 2.7 \times 10^7$ L mol^{-1} s^{-1}; Buxton *et al.* 1988).

The low competition for radicals from the oxidant would favor the efficiency of the $S_2O_8^{2-}$/UV process over the UV/H_2O_2 process, under conditions where the water matrix and target contaminants display the same 'radical scavenging capacity' in the two processes.

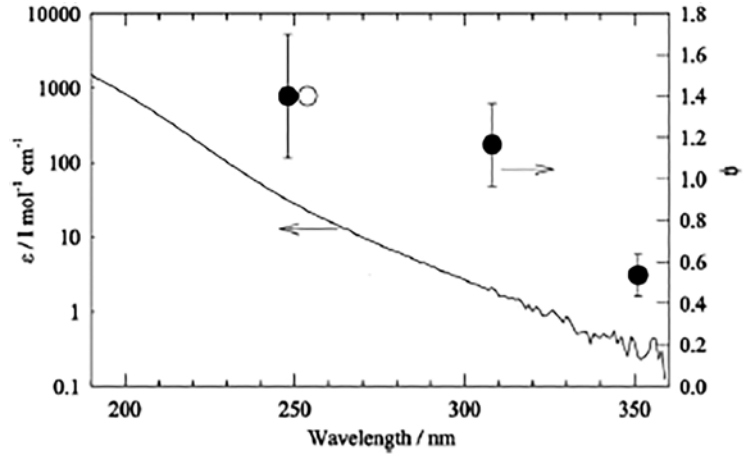

Figure 10.1 UV-absorption spectrum of $S_2O_8^{2-}$ and $SO_4^{\bullet-}$ quantum yields [(o) Mark *et al*., 1990; (•) Herrmann, 2007] for the photolysis of $S_2O_8^{2-}$ in aqueous solution. Reproduced with permission from Herrmann (2007). Copyright The Royal Society of Chemistry, 2016.

10.2.2.2 Peroxomonosulfate photolysis

The molar absorption coefficient of peroxomonosulfate (PMS) in monoprotonated form (HSO_5^-) at $\lambda = 254$ nm was determined as 13.8–14 M^{-1} cm^{-1} at pH 6–7 (Herrmann, 2007; Guan *et al*. 2011) with a higher value for the dissociated form SO_5^{2-} ($\varepsilon = 149.5$ M^{-1} cm^{-1}). PMS photolyzes at 253.7 nm yielding $HO^\bullet$ and $SO_4^{\bullet-}$ radicals through the cleavage of peroxo bond. The apparent quantum yield for $SO_4^{\bullet-}$ in UV/PMS system at 254 nm was calculated as 0.52 ± 0.01 at pH 7, and the apparent quantum yield for total radical formation was estimated to be 1.04 based on the assumption that $HO^\bullet$ and $SO_4^{\bullet-}$ were produced equally (Guan *et al*. 2011); therefore, the total radical yield in UV/PMS process is similar to $HO^\bullet$ yield from the UV/H_2O_2 process.

$$HSO_5^-/SO_5^{2-} + h\nu \rightarrow SO_4^{\bullet-} + HO^\bullet \quad (10.4)$$

The rate of PMS photolysis with the $HO^\bullet$ and $SO_4^{\bullet-}$ formation increases with pH over the pH range of 8–10 (Guan *et al*. 2011).

10.2.3 Transition metal-activated decomposition of persulfate salts

Many transition metals, especially divalent metals which are commonly encountered in soil and groundwater, may act as electron donors to catalyze the decomposition of persulfate through one-electron transfer reaction with generation of sulfate radicals:

$$S_2O_8^{2-} + M^{n+} \rightarrow M^{(n+1)+} + SO_4^{\bullet-} + SO_4^{2-} \quad (10.5)$$

Similarly to Fenton's reagent (ferrous ion-activated hydrogen peroxide decomposition), persulfate is activated by Fe^{2+}:

$$Fe^{2+} + S_2O_8^{2-} \rightarrow SO_4^{\bullet-} + SO_4^{2-} + Fe^{3+} \quad (10.6)$$

However Fe(II) may not be an ideal activating agent since it can also act as a radical and PDS scavenger (reactions 10.7 and 10.8) resulting in a decrease in contaminant destruction efficiency (Liang *et al.* 2004a).

$$SO_4^{\bullet-} + Fe^{2+} \rightarrow Fe^{3+} + SO_4^{2-} \quad k = 4.6 \times 10^9 \text{ L mol}^{-1}\text{ s}^{-1}\,(22°C) \quad (10.7)$$

$$S_2O_8^{2-} + 2\,Fe^{2+} \rightarrow 2\,Fe^{3+} + 2\,SO_4^{2-} \quad (10.8)$$

By minimizing the undesired effects of competing reactions, sequential addition of Fe^{2+} in small increments resulted in an increased pollutant removal efficiency (Liang *et al.* 2004a; Killian *et al.* 2007).

Also, the use of chelated ferrous ion is far superior to the use of free ferrous ion as an activator. Persulfate activation by Fe(II) in the presence of added chelating agents such as EDTA and citric acid, prevents the $SO_4^{\bullet-}$ scavenging by Fe^{2+} (Liang *et al.* 2004b; Rastogi *et al.* 2009; Liang *et al.* 2009). The availability of ferrous ion was found to be controlled by the molar ratio of chelate/Fe^{2+}.

Oh *et al.* (2010) showed that zero-valent iron (Fe^0) can activate persulfate through a mechanism which does not involve aqueous Fe^{2+}. The suggested mechanism involved the heterogeneous activation of persulfate ion *via* electron transfer from Fe^0.

$$Fe^0_{(s)} + 2S_2O_8^{2-}{}_{(aq)} \rightarrow Fe^{2+}{}_{(aq)} + 2\,SO_4^{\bullet-}{}_{(aq)} + 2\,SO_4^{2-}{}_{(aq)} \quad (10.9)$$

However, Fe^0 could also serve as a slow-releasing source of dissolved ferrous ions (reaction 10.10) which would subsequently activate PDS to produce $SO_4^{\bullet-}$.

$$Fe^0 + S_2O_8^{2-} \rightarrow Fe^{2+} + 2\,SO_4^{2-} \quad (10.10)$$

In this system, the recycling of ferric ion at the zero valent iron surface could avoid the accumulation of ferrous ion and reduce the precipitation of iron hydroxides.

Similarly to PDS activation, variant valence transition metal ions can activate PMS to form sulfate (majority) but also hydroxyl radicals:

$$M^{n+} + HSO_5^- \rightarrow M^{(n+1)+} + OH^- + SO_4^{\bullet-} \quad (10.11)$$

$$HSO_5^- + M^{n+} \rightarrow M^{(n+1)+} + SO_4^{2-} + HO^{\bullet} \quad (10.12)$$

The transition metal efficiency for the activation of PMS and the distribution of the two primary radical species formed ($SO_4^{\bullet-}$ *vs* $HO^{\bullet}$) depends on the nature and speciation of the metal, but $SO_4^{\bullet-}$ formation would be favored in most cases (Anipsitakis & Dionysiou, 2004).

10.2.4 Miscellaneous processes

10.2.4.1 Peroxymonosulfate/ozone combination

Recently, the simultaneous generation of hydroxyl radical and sulfate radical in the reaction of ozone with deprotonated peroxymonosulfate (SO_5^{2-}) has been demonstrated by Yang *et al.* (2015). In the proposed

reaction mechanism, the formation of an adduct ($^{-}O_3SO_5^{-}$) between the reacting species was suggested by the authors (reactions 10.13–10.18).

$$SO_5^{2-} + O_3 \rightarrow {}^{-}O_3SO_5^{-} \quad (10.13)$$

$${}^{-}O_3SO_5^{-} \rightarrow SO_5^{\bullet-} + O_3^{\bullet-} \quad (10.14)$$

$${}^{-}O_3SO_5^{-} \rightarrow SO_4^{2-} + 2O_2 \quad (10.15)$$

$$O_3^{\bullet-} \rightleftharpoons O^{\bullet-} + O_2 \quad (10.16)$$

$$O^{\bullet-} + H_2O \rightleftharpoons HO^{\bullet} + OH^{-} \quad (10.17)$$

$$SO_5^{\bullet-} + O_3 \rightarrow SO_4^{\bullet-} + 2O_2 \quad (10.18)$$

10.2.4.2 Photocatalysis in presence of persulfate

It was observed that like in the case of H_2O_2, the $S_2O_8^{2-}$ or HSO_5^{-} addition was beneficial in the photocatalysis oxidation and mineralisation of dyes. The sulfate radical formed and reactions of persulfate with the photogenerated conduction band electrons (reaction 10.19) can exert a dual function: as strong oxidant with production of additional oxidizing species and as electron scavenger, thus inhibiting the electron-hole recombination at the semiconductor surface (Konstantinou & Albanis, 2004; Madhavan *et al.* 2006).

$$S_2O_8^{2-} + e^{-}_{CB} \rightarrow SO_4^{\bullet-} + SO_4^{2-} \quad (10.19)$$

Most results demonstrate that peroxydisulfate significantly enhances the photocatalytic activity. However, an excessive dosage of persulfate may result in the saturation of reaction rate due to adsorption of the SO_4^{2-} end-product onto the TiO_2 surface (Syoufian & Nakashima, 2007).

10.2.4.3 Persulfate activation by reaction with species from water molecules

Pulse radiolysis of water was used for the determination of many rate constants (Neta *et al.* 1988). The radiolysis of water forms short-lived intermediates i.e. hydrated electrons, hydrogen atoms and hydroxyl radicals. Numerous kinetic studies involving the sulfate radical have used the reduction of peroxydisulfate ions with the hydrated electron (reaction 10.20) as a means of radical generation.

$$S_2O_8^{2-} + e^{-}_{aq} \rightarrow SO_4^{\bullet-} + SO_4^{2-} \quad k = 1.2 \times 10^{10}\ \mathrm{L\,mol^{-1}\,s^{-1}} \quad \text{(Buxton } \textit{et al.}\ 1988) \quad (10.20)$$

Recently, Criquet and Leitner (2011, 2012) showed that the oxidizing properties of the sulfate radicals formed in the reaction of peroxydisulfate ions with the hydrated electrons during electron beam irradiation of aqueous solutions containing carboxylic acids are responsible for enhancing the degradation and mineralization of these compounds.

In sonochemical systems, acoustic cavitation is also known to generate OH and H radicals due to thermal decomposition of water. Thus, these species, especially the reductive $H^{\bullet}$ can react with peroxydisulfate ions to produce the sulfate radicals in ultrasound/$S_2O_8^{2-}$ processes. In addition, peroxydisulfate ions can also be decomposed into sulfate radicals by the heat generated within the bubbles formed in such sonochemical systems (Neppolian *et al.* 2010).

Additional persulfate activation processes and techniques for organic contaminant treatment (e.g. activation by electrochemistry or by activated carbon) are covered in a recent review by Matzek and Carter (2016).

10.3 PROPERTIES AND STABILITY OF SULFATE RADICAL IN PURE WATER

10.3.1 Oxidation-reduction potential

In aqueous solutions, the standard oxidation-reduction potentials (E^0) of ozone ($E^0 = 2.07$ V), hydrogen peroxide ($E^0 = 1.78$ V), permanganate ($E^0 = 1.70$ V) and persulfate (~2.01 V), are close. The sulfate radical has an even higher redox potential ($E^0 = 2.6$ V). Once formed, the sulfate radical is a short-lived but very strong oxidizing agent. $SO_4^{\bullet-}$ is the strongest oxidant among the sulfur-oxygen radicals $SO_n^{\bullet-}$ (with n = 3, 4, and 5 and redox potentials of 0.63, 2.5–3.1, and 1.1 V respectively at pH 7; Neta *et al*. 1988; Antoniou *et al*. 2010a).

Table 10.1 summarizes the radical rate constants of a few classes of organic compounds. It is clear that the reactivity of $SO_4^{\bullet-}$ is generally lower than that of the $HO^{\bullet}$ except in the case of aromatics.

Table 10.1 Rate constants (k/L mol^{-1} s^{-1}) for the reaction of $HO^{\bullet}$ and $SO_4^{\bullet-}$ radicals with selected carboxylic acids, methyl ether, alcohols, aromatics and amines in aqueous solution at 292 K.

Compound	$HO^{\bullet}$	$SO_4^{\bullet-}$
(a) HCO_2^-	4.3×10^9	1.1×10^8
(a) HCOOH	1.3×10^8	4.6×10^5
(a) CH_3COO^-	7.5×10^7	3.7×10^6
(a) CH_3COOH	1.8×10^7	1.4×10^4
(a) $CH_3CO_2CH_3$	1.2×10^8	5.0×10^4
(b) methanol	9.7×10^8	3.2×10^6
(b) ethanol	$1.2–2.8 \times 10^9$	$1.6–7.7 \times 10^7$
(b) propanol	2.8×10^9	6×10^7
(b) *tert*-butyl alcohol	$3.8–7.6 \times 10^8$	$4–9.1 \times 10^5$
Aromatics		
(b) Benzene	7.8×10^9	$2.4–3 \times 10^9$
(b) Nitrobenzene	$3.0–3.9 \times 10^9$	$<10^6$
(b) Phenol	6.6×10^9	8.8×10^9
(b) Benzoic acid	4.2×10^9	1.2×10^9
(b) Anisole	7.8×10^9	4.9×10^9
(c) 4-Chlorotoluene	5.5×10^9	1.1×10^9
(c) 4-Bromotoluene	2.9×10^9	1.0×10^9
Amines and Amino acids		
(d) Alanine	7.7×10^7	$(4.9 \pm 0.1) \times 10^6$
(d) Glycine	1.7×10^7	$(3.7 \pm 0.1) \times 10^6$
(d) Tryptophan		2.0×10^9
(d) Tyrosine		5.8×10^8

(a) Buxton *et al.* (2001); (b) cited in Liang and Su (2009); (c) Choure *et al.* (1997); (d) Bosio *et al.* (2005).

10.3.2 pH dependence

In pure water, the sulfate radical concentration can decrease due to the recombination and the reaction with the oxidant:

$$SO_4^{\bullet-} + SO_4^{\bullet-} \rightarrow S_2O_8^{2-} \quad 2k = (8.9 \pm 0.3) \times 10^8\,M^{-1}\,s^{-1} \quad \text{(McElroy \& Waygood, 1990)} \qquad (10.21)$$

$$S_2O_8^{2-} + SO_4^{\bullet-} \rightarrow S_2O_8^{\bullet-} + SO_4^{2-} \quad k < 1 \times 10^4 - 7 \times 10^5\ M^{-1}\,s^{-1} \quad \text{(Chitose } \textit{et al.}\text{ 1999)} \qquad (10.22)$$

In aqueous solution, the sulfate radicals can also participate in pH-dependent reactions to produce hydroxyl radicals (Liang & Su, 2009):

$$SO_4^{-\bullet} + H_2O \rightarrow H^+ + SO_4^{2-} + OH^{\bullet} \quad \text{(over the entire pH range)} \quad k[H_2O] < 2 \times 10^{-3}\ s^{-1} \qquad (10.23)$$

$$SO_4^{\bullet-} + OH^- \rightarrow SO_4^{2-} + OH^{\bullet} \quad \text{(predominant in alkaline media)} \quad k = (6.5 \pm 1.0) \times 10^7\ M^{-1}\,s^{-1} \qquad (10.24)$$

While the contribution of reaction 10.23 is small in most reaction systems (Norman *et al.* 1970), in alkaline solutions, the reaction of sulfate radical with hydroxide ion occurs very rapidly (reaction 10.24).

Therefore, the dominant radical species ($SO_4^{\bullet-}$ *vs* $OH^{\bullet}$) changes depending on the solution pH. Figure 10.2 exemplifies the relative distribution of sulfate and hydroxyl radicals in water as a function of pH.

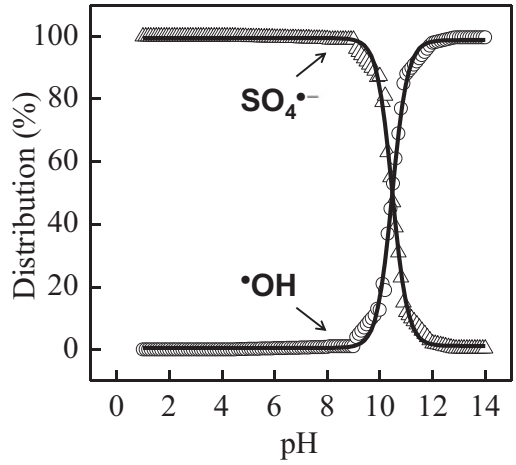

Figure 10.2 Effect of pH on the distribution of radical species in pure water. Adapted from Fang *et al.* (2012); courtesy of Dr. Guodong Fang, 2016.

Dogliotti and Hayon (1967) monitored the absorbance of sulfate radical ion at 455 nm during the flash photolysis of persulfate solutions of varying pH; virtually no absorption was measured at pH > 10.8, which indicates the total conversion of $SO_4^{\bullet-}$ into $OH^{\bullet}$ in strong alkaline media (Figure 10.3).

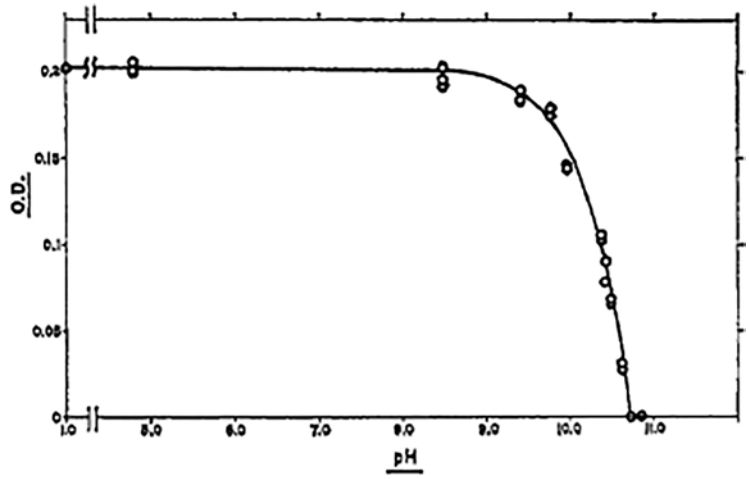

Figure 10.3 Variation of optical density of $SO_4^{\bullet-}$ transient at 455 nm with pH in the flash photolysis of 10^{-2} M persulfate solutions. Reprinted with permission from Dogliotti and Hayon (1967). Copyright 2016 American Chemical Society.

The water pH impacts the effectiveness of contaminant removal with $SO_4^{\bullet-}$ based AOTs through the following parameters:

- rate of generation of radical species, which can depend on the oxidant speciation for certain activating systems; thus when considering the elimination of benzoic acid in the UV/PMS system, Guan *et al.* (2011) concluded that the production of $SO_4^{\bullet-}$ and $OH^{\bullet}$ increases with pH in the range 8–11 due to the increase of the form SO_5^{2-} which has a higher molar absorption coefficient than the form HSO_5^-. This observation has similarity with the UV/H_2O_2 system whereas it does not apply in the case of the $S_2O_8^{2-}$/UV process (see § 10.2.2).
- relative distribution of radical species in water (e.g. $SO_4^{\bullet-}$ *vs* $OH^{\bullet}$; Figure 10.2; or other like $Cl^{\bullet}/Cl_2^{\bullet-}$ *vs* $OH^{\bullet}$; see § 10.6 and Chapter 9);
- ionization state of some organic compounds, i.e. protonated or deprotonated, given that these forms display different reactivity towards the oxidizing radical species;
- radical scavenging capacity of the water matrix and its pH-dependence (e.g. reactions with bicarbonates/carbonates, dissolved organic matter).

The overall pH impact on the contaminant degradation yield would be dictated by the combination of all the above conditions.

It should also be noted that in unbuffered or low alkalinity waters, an acidification is usually observed in the PDS-activated AOPs due to HSO_4^- formed as a primary stable reaction product and to the presence of acid transformation products and protons.

10.4 REACTION MECHANISMS WITH ORGANIC MOLECULES IN PURE WATER

The sulfate radical anion reacts with organic compounds of various classes following three basic processes: hydrogen atom abstraction, one-electron transfer, or addition to unsaturated bonds.

Hydrogen atom abstraction:

$$RH + SO_4^{\bullet -} \rightarrow R^{\bullet} + HSO_4^{-} \quad (10.25)$$

One electron oxidation:

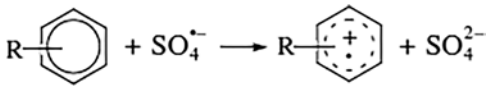

(10.26)

Addition to an unsaturated bond:

$$H_2C{=}CHR + SO_4^{\bullet -} \rightarrow {}^{-}OSO_2OCH_2{-}C^{\bullet}HR \quad (10.27)$$

Sulfate radical is more selective than the HO radical in the reactions with organic and inorganic compounds. Mechanisms of $SO_4^{\bullet -}$ reactions differ somewhat from those of hydroxyl radical reactions; for example, sulfate radical reacts more readily by electron transfer than $HO^{\bullet}$ but slower by H-abstraction and addition. Thus, the products of sulfate radical-based oxidation may be different than those of OH radical-induced oxidations. The following sub-sections provide examples of reactions of sulfate radical anion with various classes of organic compounds.

10.4.1 Hydrogen-abstraction reactions

10.4.1.1 Alkanes and alcohols

The reactions of alcohols, alkanes and ethers with $SO_4^{\bullet -}$ proceed *via* H-abstraction. The rate constants for H-abstraction reactions of $SO_4^{\bullet -}$ are about one to two orders of magnitude smaller than those of $HO^{\bullet}$ reactions.

In the absence of oxygen, the radicals formed in the H-abstraction reactions can be involved in chain reactions as described by Mendez-Diaz *et al*. (2010):

$$SO_4^{\bullet -} + RH_2 \rightarrow SO_4^{2-} + H^+ + RH^{\bullet} \quad (10.28)$$

$$RH^{\bullet} + S_2O_8^{2-} \rightarrow R + SO_4^{2-} + H^+ + SO_4^{\bullet -} \quad (10.29)$$

$$SO_4^{\bullet -} + RH \rightarrow R^{\bullet} + SO_4^{2-} + H^+ \quad (10.30)$$

$$2\,R^{\bullet} \rightarrow RR \text{ (dimer)} \quad (10.31)$$

$$SO_4^{\bullet -} + H_2O \rightarrow HSO_4^{-} + HO^{\bullet} \quad (10.32)$$

$$HO^{\bullet} + S_2O_8^{2-} \rightarrow HSO_4^{-} + SO_4^{\bullet -} + \tfrac{1}{2}O_2 \quad (10.33)$$

Levey and Hart (1975) suggested the following chain mechanism for the oxidation of alcohols by sulfate radical:

$$SO_4^{-\bullet} + R_2CHOH \rightarrow HSO_4^{-} + R_2C^{\bullet}OH \quad (10.34)$$

$$R_2C^{\bullet}OH + S_2O_8^{2-} \rightarrow HSO_4^{-} + SO_4^{\bullet -} + R_2C{=}O \quad (10.35)$$

In the presence of oxygen, organic peroxyl radicals ($ROO^{\bullet}$) are formed. Mark *et al.* (1990) provided a detailed mechanism of *tert*-butanol (*tert*-butyl alcohol, TBA) oxidation in the presence of oxygen *via* a bimolecular decay of *tert*-butanol-derived peroxyl radical with formation of carbonyl compounds:

$$SO_4^{\bullet-} + (CH_3)_3COH \rightarrow SO_4^{2-} + H^+ + {}^{\bullet}CH_2C(CH_3)_2OH \quad (10.36)$$

$${}^{\bullet}CH_2C(CH_3)_2OH + O_2 \rightarrow {}^{\bullet}O_2CH_2C(CH_3)_2OH \quad (10.37)$$

$$2\,{}^{\bullet}O_2CH_2C(CH_3)_2OH \rightarrow HOC(CH_3)_2CH_2O_4CH_2C(CH_3)_2OH \quad (RO_4R) \quad (10.38)$$

$$RO_4R \rightarrow HOC(CH_3)_2CH_2OH + O_2 + HOC(CH_3)_2CHO \quad (10.39)$$

$$RO_4R \rightarrow 2\,HOC(CH_3)_2CHO + H_2O_2 \quad (10.40)$$

$$RO_4R \rightarrow 2\,CH_2O + 2\,{}^{\bullet}C(CH_3)_2OH + O_2 \quad (10.41)$$

$${}^{\bullet}C(CH_3)_2OH + O_2 \rightarrow HO_2^{\bullet} + (CH_3)_2CO \quad (10.42)$$

This reaction mechanism is similar to that known from $HO^{\bullet}$ attack on TBA.

10.4.2 Electron transfer reactions

10.4.2.1 Carboxylic acids

Hydroxyl radicals have been reported to react with substituted acetates by hydrogen abstraction (electrophilic attack) from the substituted methyl group ($-CR_1R_2H$):

$$HO^{\bullet} + R_1{-}CHR_2COO^- \rightarrow H_2O + R_1{-}C^{\bullet}R_2COO^- \quad (10.43)$$

Oxidation of carboxylic acids by $HO^{\bullet}$ results in minor decarboxylation.

Unlike the $OH^{\bullet}$ reaction, the H-abstraction reaction of $SO_4^{\bullet-}$ with aliphatic carboxylic acids is not the predominant degradation pathway of these compounds. Instead, electron-transfer reaction with the carboxylate ion appears to be more favored, and leads to decarboxylation (Madhavan *et al.* 1978). For instance, the sulfate radicals are known to react by an electron transfer mechanism with the carboxylate group of acetate and halogenated acetates, yielding carboxy radicals. The carboxy radicals undergo further decarboxylation to the $C^{\bullet}R_1R_2H$ radicals (reactions 10.44, 10.45 where R_1, R_2: CH_3, H, Br, Cl, F, NH_3^+; Chawla & Fessenden, 1975; Madhavan *et al.* 1978; Bosio *et al.* 2005):

$$SO_4^{\bullet-} + R_1CHR_2COO^- \rightarrow SO_4^{2-} + R_1CHR_2COO^{\bullet} \quad (10.44)$$

$$R_1CHR_2COO^{\bullet} \rightarrow {}^{\bullet}CR_1R_2H + CO_2 \quad (10.45)$$

Criquet and Leitner (2009) compared acetate and TOC removal in the H_2O_2/UV and $S_2O_8^{2-}$/UV processes and observed similar acetate decay patterns, but greater TOC abatement during the UV/persulfate process. The authors explained the better performance of mineralization through the decarboxylation reaction *via* sulfate radicals (reaction 10.46) and the oxidation of intermediates (methanol, formaldehyde

and formate ions). Unlike the UV/persulfate process, the H_2O_2/UV-induced degradation of acetate results in the formation of glyoxylate, glycolate, and oxalate ions.

$$SO_4^{\bullet-} + CH_3COO^- \rightarrow SO_4^{2-} + {}^{\bullet}CH_3 + CO_2 \quad (10.46)$$

Acetate, malonate, propionate, and succinate ions undergo decarboxylation with a minimum 80% efficiency (Madhavan *et al.* 1978). Similarly to the OH radical, the sulfate radical reacts slower with protonated species than with deprotonated species.

10.4.2.2 Aminoacids and amines

Studies by Madhavan *et al.* (1978) and Bosio *et al.* (2005) on amino acids (and peptides) degradation by sulfate radicals showed high decarboxylation yields, which points to the carboxyl group as the favored attack site for $SO_4^{\bullet-}$. Peptides are much more reactive than their parent amino acids, and the aromatic moieties confer a higher reactivity. In oxygen-depleted conditions, the carbon-centered radical is involved in the reaction with the oxidant (PDS) as exemplified below for glycine:

$$H_2N{-}CH_2CO_2^- + SO_4^{\bullet-} \rightarrow H_2N{-}C^{\bullet}H_2 + CO_2 + SO_4^{2-} \quad (10.47)$$

$$H_2NC^{\bullet}H_2 + S_2O_8^{2-} \rightarrow HN{=}CH_2 + H^+ + SO_4^{2-} + SO_4^{\bullet-} \quad (10.48)$$

Oxidation of amine-based molecules by sulfate radicals would also proceed through electrophilic attack at the nitrogen atoms with formation of N-centered radicals *via* one electron transfer, as in the case of cytidine (Aravindakumar *et al.* 2003). Thus, the aniline-derivative oxidation with $SO_4^{\bullet-}$ starts with one-electron transfer to the sulfate radical with formation of a N-centered radical cation ($R\text{-}NH_2^{\bullet+}$) which hydrolyzes rapidly to hydroxylamine derivatives (R-NHOH), and not through radical addition to the aromatic ring as commonly observed in $OH^{\bullet}$ oxidation (Mahdi-Ahmed *et al.* 2012).

10.4.2.3 Aromatics

In the reaction of sulfate radical with electron-rich aromatic compounds, the electron transfer from the aromatic ring to $SO_4^{\bullet-}$ is the preferred reaction pathway. Zemel and Fessenden (1978) studied the products of the reactions of $SO_4^{\bullet-}$ with some benzene derivatives using ESR and optical absorption spectrometry. All reactions are consistent with the oxidation of the benzene ring to an intermediate cationic species:

$$C_6H_4(R_1R_2) + SO_4^{\bullet-} \rightarrow {}^{\bullet+}C_6H_4(R_1R_2) + SO_4^{2-} \quad (10.49)$$

This high selectivity of the electron transfer reaction from the aromatic ring to sulfate radical was confirmed by Neta *et al.* (1977), who observed a linear correlation between the rate constants for the reaction of $SO_4^{\bullet-}$ with a number of substituted benzenes and the Hammett substituent constant σ which reflects the electron charge distribution on the ring. The authors determined the bimolecular rate constants using pulse radiolysis.

The radical cation formed reacts rapidly with water molecule to form the hydroxycyclohexadienyl radical, which is the same intermediate formed upon reaction of $HO^{\bullet}$ with aromatic rings. Parallel reactions also occur depending on the substituents on the aromatic ring, i.e. either loss of a proton (from hydroxyl or methyl group) or loss of CO_2 from the carboxyl functional groups (Zemel & Fessenden, 1978).

Thus, with a very short lifetime, the cation radical intermediate species resulting from sulfate radical reaction with benzoate ion can follow two pathways, i.e., decarboxylation to a phenyl radical, and hydrolysis and protonation to hydroxycyclohexadienyl radical (Zemel & Fessenden, 1978). The branching ratio of the two pathways is 70:30 (Figure 10.4), indicating that the loss of CO_2 from the oxidized form is the most important pathway (70%) in benzoic acid degradation *via* $SO_4^{\bullet-}$, whereas the decarboxylation yield resulting from the hydroxyl radical reaction with benzoate ion represents less than 10% of the overall degradation mechanism. Similar results were reported by Criquet and Leitner (2015) in a recent study on the degradation of *p*-hydroxybenzoic acid by sulfate radicals generated by electron beam irradiation. Benzoquinone was the main transformation product detected in the presence of persulfate with no polyhydroxybenzoic acids being formed, whereas polyhydroxylated derivatives of *p*-hydroxybenzoic acid were found in the $OH^{\bullet}$ radical-based ionizing radiation system in absence of persulfate.

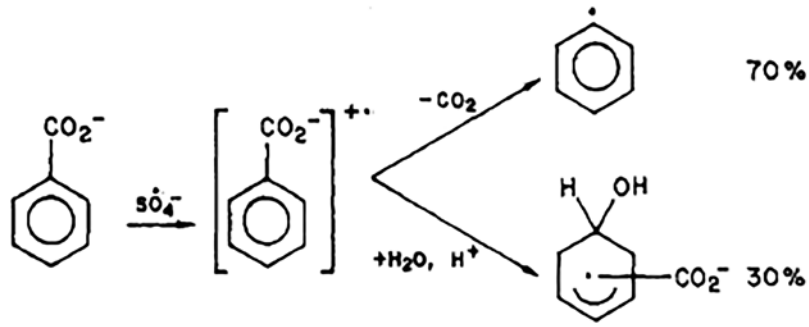

Figure 10.4 Mechanism of reaction of $SO_4^{\bullet-}$ with benzoate proposed by Zemel and Fessenden (1978). Reprinted with permission. Copyright 2016 American Chemical Society.

Indeed, the primary radical cation produced in the reaction of the sulfate radical with aromatics follows various paths to more stable intermediate radicals. Zemel and Fessenden (1978) studied the products of the reaction of $SO_4^{\bullet-}$ with three toluate isomers and concluded on the following pathways:

- *o*-toluate gives mainly the *o*-carboxybenzyl radical by loss of H^+ from the methyl group;
- *m*-toluate would lead to the formation of a mixture of OH adducts (hydroxycyclohexadienyl radicals) through hydroxylation *via* reaction of primary radical cation with water molecules with no trace of *m*-carboxybenzyl radicals;
- *p*-toluate: 25–35% and 25–45% of primary radical cation evolve to *p*-carboxybenzyl and two methyl-substituted hydroxycyclohexadienyl radicals, respectively, the other 20–50% would decarboxylate to *p*-methylphenyl radical.

Figure 10.5 presents the evolution of the primary radical cation to the intermediate radicals.

Even though the radical intermediates generated through sulfate radical reactions with aromatics are often different than those formed in the hydroxyl-radical mediated degradation reactions of organic contaminants, many transformation products are identical. For example, Anipsitakis *et al.* (2006) identified catechol, hydroquinone, and quinone from the sulfate radical attack of phenol which are also common transformation products found in $OH^{\bullet}$-based AOTs. The authors explained these results by the formation of the dihydroxycyclohexadienyl radical (the same as that involved in the attack of aromatic rings by the OH radical) from the primary radical cation produced in the initial reaction of the sulfate radical on phenol.

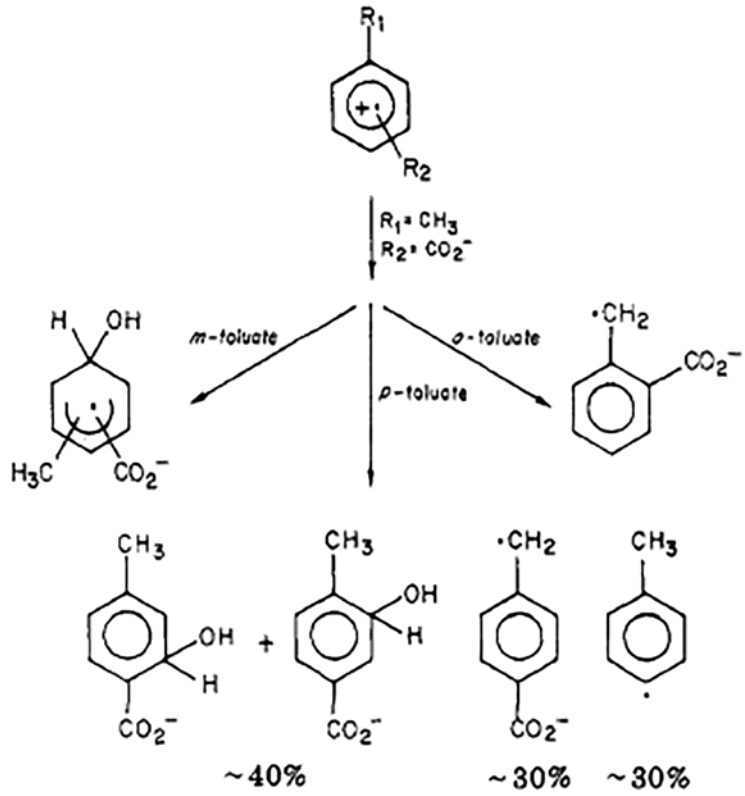

Figure 10.5 Product yields in the reaction of $SO_4^{\bullet-}$ with three isomeric toluate ions. Adapted with permission from Zemel and Fessenden (1978). Copyright 2016 American Chemical Society.

10.4.3 Addition to unsaturated bonds

Norman *et al.* (1970) suggested that the sulfate radical anion reacts with the unsaturated structure of 3,3-dimethylacrylic acid or its anion either by addition to the double bond followed by heterolysis (reactions 10.50 and 10.51) or by electron transfer (reaction 10.52):

$$(CH_3)_2C{=}CH{-}COOH + SO_4^{\bullet-} \rightarrow (CH_3)_2C(OSO_2O^-){-}C^{\bullet}H{-}COOH \rightarrow (CH_3)_2C^+{-}C^{\bullet}H{-}COOH + SO_4^{2-} \quad (10.50)$$

$$(CH_3)_2C{=}CH{-}COOH + SO_4^{\bullet-} \rightarrow (CH_3)_2C^{\bullet}{-}C(OSO_2O^-)H{-}COOH \rightarrow (CH_3)_2C^{\bullet}{-}C^+H{-}COOH + SO_4^{2-} \quad (10.51)$$

$$(CH_3)_2C{=}CH{-}COOH + SO_4^{\bullet-} \rightarrow (CH_3)_2C^+{-}C^{\bullet}H{-}COOH + SO_4^{2-} \quad (10.52)$$

The radical cations resulted from the two pathways hydrolyze to form the hydroxylated radicals ($(CH_3)_2C(OH){-}C^{\bullet}H{-}COOH$ and $(CH_3)_2C^{\bullet}{-}C(OH)H{-}COOH$), which are similar to those arising from the initial $HO^{\bullet}$ attack.

Similarly, when sulfate radicals are involved in the oxidation of trichloroethylene (TCE), an electron-transfer mechanism from olefin to $SO_4^{\bullet-}$ was proposed (Liang *et al*. 2009), followed by decomposition of the radical cation in the aqueous medium to form the hydroxyalkyl radical (analogous to the one formed directly by OH radical addition):

$$Cl_2C{=}CHCl + SO_4^{\bullet-} \rightarrow Cl_2C^{\bullet}{-}C^{+}HCl + SO_4^{2-} \quad (10.53)$$

$$Cl_2C^{\bullet}{-}C^{+}HCl + H_2O \rightarrow (OH)CHCl{-}C^{\bullet}Cl_2 + H^{+} \quad (10.54)$$

10.5 SULFATE RADICAL-BASED TREATMENT OF WATER MICROPOLLUTANTS

There is an abundant literature on the potential use of sulfate radical-based advanced oxidation systems for the degradation of many organic contaminants of concern over their impact on environment, aquatic wildlife, and human health, given their occurrence and persistence. A compilation of these studies has been published recently (Zhang *et al*. 2015). Many studies at laboratory scale were focused on the elimination of contaminants frequently detected in aquatic environment and drinking water sources and transformation product formation. Only selected classes of micropollutants will be exemplified in this section. Table 10.2 presents the $SO_4^{\bullet-}$ second order rate constants for the reactions with a series of environmental contaminants, as collected from the recently published literature. The kinetic data as well as the full-studies indicate that sulfate radical-based AOTs are effective at degrading the studied contaminants at comparable or higher rates than those determined in hydroxyl radical-based AOTs.

Table 10.2 Bimolecular rate constants for $SO_4^{\bullet-}$ reactions with relevant environmental micropollutants.

Micropollutant (P)	$k_{SO_4^{\bullet-},P}$ /10^9 M^{-1} s^{-1}	Reference
	Pesticides	
Atrazine	3 (pH5)	Manoj *et al.* (2007)
Atrazine	3.5 ± 0.08 (pH7-8)	Lutze *et al.* (2015a)
Atrazine	2.59	Khan *et al.* (2014)
Deisopropyl-atrazine	2.0 ± 0.57 (pH7-8)	Lutze *et al.* (2015a)
Desethyl-atrazine	0.96 ± 0.017 (pH7-8)	Lutze *et al.* (2015a)
Desethyl-desisopropyl-atrazine	0.15 ± 0.008 (pH7-8)	Lutze *et al.* (2015a)
Terbuthylazine	3.0 ± 0.05 (pH7-8)	Lutze *et al.* (2015a)
Propazine	2.2 ± 0.05 (pH7-8)	Lutze *et al.* (2015a)
Desethyl-terbuthylazine	0.36 ± 0.023 (pH7-8)	Lutze *et al.* (2015a)
1,3,5-triazine	0.081 (pH5)	Manoj *et al.* (2007)
2,4,6-trimethoxy-1,3,5-triazine	0.051 (pH5)	Manoj *et al.* (2007)
2,4-dioxohexahydro-1,3,5-triazine	0.046	Manoj *et al.* (2007)
Amitrol	0.377 ± 0.017 (pH7)	Orellana-Garcia *et al.* (2015)
	0.258 ± 0.028 (pH3)	
	0.292 ± 0.013 (pH12)	

(*Continued*)

Table 10.2 Bimolecular rate constants for $SO_4^{\bullet-}$ reactions with relevant environmental micropollutants. (*Continued*)

Micropollutant (P)	$k_{SO_4^{\bullet-},P}$ /10^9 M^{-1} s^{-1}	Reference
Glyphosate	0.16 ± 0.01 (pH4-5)	Diaz Kirmser *et al.* (2010)
Paraquat	1.2 ± 0.3 (pH4-5)	Diaz Kirmser *et al.* (2010)
Clomazone	0.94 ± 0.04 (pH4.4)	Gara *et al.* (2009)
	Algal toxins and T&O causing compounds	
Cylindrospermopsin	4.5 (pH 7.4)	He *et al.* (2013)
2-methylisoborneol (2-MIB)	0.42 ± 0.06 (pH 4-7)	Xie *et al.* (2015)
Geosmin	0.76 ± 0.06 (pH 7.0)	Xie *et al.* (2015)
	Polychlorinated biphenyls (pH 5)	
2-Monochlorobiphenyl	0.21	Fang *et al.* (2012)
4-Monochlorobiphenyl	0.199	Fang *et al.* (2012)
2,4-Dichlorobiphenyl	0.089	Fang *et al.* (2012)
2,4′-Dichlorobiphenyl	0.0688	Fang *et al.* (2012)
2,2′-Dichlorobiphenyl	0.0265	Fang *et al.* (2012)
4,4′-Dichlorobiphenyl	0.131	Fang *et al.* (2012)
2,4,4′-Trichlorobiphenyl	0.025	Fang *et al.* (2012)
	Pharmaceuticals	
Amoxicillin*	3.48 ± 0.05 (pH 7.4)	Rickman and Mezyk (2010)
Penicillin G*	2.08 ± 0.04 (pH 7.4)	Rickman and Mezyk (2010)
Penicillin V*	2.89 ± 0.05 (pH 7.4)	Rickman and Mezyk (2010)
Piperacillin*	1.74 ± 0.11 (pH 7.4)	Rickman and Mezyk (2010)
Cefaclor*	2.44 ± 0.04 (pH 7.4)	Rickman and Mezyk (2010)
Sulfamethoxazole	12.5 ± 3.1 (pH7)	Mahdi-Ahmed *et al.* (2012)
Diclofenac	9.2 ± 2.6 (pH7)	Mahdi-Ahmed *et al.* (2012)
Carbamazepine	1.92 ± 0.01 (pH3)	Matta *et al.* (2011)
	2.63	Rao *et al.* (2013)
Ciprofloxacin	1.2 ± 0.1 (pH7)	Mahdi-Ahmed and Chiron (2014)
Atenolol	13 (pH7)	Liu *et al.* (2013a)
	22	Liu *et al.* (2013b)
Iopromide	(1.5 ± 0.5) × 10^4 M^{-1} s^{-1}	Chan *et al.* (2010)

**Beta-lactam antibiotics*

Usually, $SO_4^{\bullet-}$ rate constants have been determined by competition kinetics, laser flash photolysis, pulse radiolysis or by solving equations of the reaction system based on the radical steady-state assumption. In a recent study, Xiao *et al*. (2015) developed a Quantitative Structure Activity Relationship (QSAR) model for $SO_4^{\bullet-}$ reactivity prediction. An empirical relationship with two descriptors, i.e. E_{LUMO} (Energy of the

Lowest Unoccupied Molecular Orbital) and E_{HOMO} (Energy of the Highest Occupied Molecular Orbital) energy gap and the ratio of oxygen atoms to carbon atoms, was proposed to provide a reliable mean to predict $k_{SO_4^{\bullet-}}$ of trace organic compounds.

10.5.1 Pesticides

The rate constants of $SO_4^{\bullet-}$ with many substituted triazine pesticides and their metabolites were determined by Manoj *et al.* (2007) and Lutze *et al.* (2015a). The rate constants for $SO_4^{\bullet-}$ reactions (Table 10.2) are smaller than those for the $OH^{\bullet}$ reactions with similar triazines except that for atrazine. The degradation products of $SO_4^{\bullet-}$ reaction with atrazine were identified, and potential degradation pathways were proposed (Lutze *et al.* 2015a; Khan *et al.* 2014). From transient absorption spectra, intermediate species were assigned to carbon centered radicals, OH-adducts and N-centered radicals. Among various possible mechanisms, dealkylation appears to predominate, with the removal of ethyl group being favored over the removal of the isopropyl substituent (Lutze *et al.* 2015a).

Degradation studies on other pesticides, such as diuron, amitrol, endosulfan, clomazone, paraquat, and glyphosate focused on kinetic aspects and on the role of experimental parameters (temperature, pH, oxidant dose, initial pollutant concentration, alkalinity and inorganic anions, organic matter) (Tan *et al.* 2012; Orellana-Garcia *et al.* 2015; Shah *et al.* 2013; Diaz Kirmser, 2010; Gara *et al.* 2009). Along with other environmental chemical pollutants, pesticides were proven to interfere with the endocrine system, and can produce adverse developmental, reproductive, neurological, cardiovascular, metabolic, and immune effects in humans (Schug *et al.* 2011).

10.5.2 Pharmaceuticals

The reactions of sulfate radical with pharmaceuticals of various structures and biochemical activities are also well represented in the literature. Such studies include antimicrobial agents (sulfamethoxazole, sulfamethazine, ciprofloxacin, β-lactam antibiotics), anti-inflammatory drugs and analgesics (ibuprofen, diclofenac), X-ray contrast media (iopromide), antiepileptic drugs (carbamazepine), and β-blockers (atenolol) (Ghauch *et al.* 2013; Mahdi-Ahmed *et al.* 2012; Gao *et al.* 2012; Mahdi-Ahmed & Chiron, 2014; Rickmann & Mezyk, 2010; Roshani & Leitner, 2011; Chan *et al.* 2010; Deng *et al.* 2013; Matta *et al.* 2011; Rao *et al.* 2013; Liu *et al.* 2013a, 2013b). The successful reduction of most of these pollutants in water (initial concentration range: 20–500 μM) was achieved and the impact of various water quality and process parameters on the performance of sulfate radical-induced oxidation as well as on the yield of $SO_4^{\bullet-}$ generation were addressed in these and other literature studies.

The reactivity of aniline-based pharmaceuticals toward sulfate radical anion was studied using diclofenac and sulfamethoxazole as probe compounds (Mahdi-Ahmed *et al.* 2012). It was reported that these compounds react with sulfate radical anion at diffusion-controlled kinetics, with second order rate constants in the $9 \times 10^9 - 13 \times 10^9$ M^{-1} s^{-1} range. It was suggested that selective oxidative reaction started with the formation of a N-centered radical through one-electron transfer from the amino group of pharmaceutical to sulfate radical anion. This was followed by a sequence of degradation reactions involving decarboxylation, hydroxylation, and bond cleavage.

10.5.3 Algal toxins and taste-and-odor (T&O) causing compounds

Algal toxins (powerful neurotoxins and hepatotoxins) and T&O compounds are currently treated in surface water for drinking water production using the UV/H_2O_2 AOP. To the best of our knowledge only few studies

explored the potential use of sulfate radical-based AOPs for the degradation of these compounds. He *et al.* (2013) found comparable second-order rate constants of the cyanobacterial toxin cylindrospermopsin with hydroxyl and sulfate radicals (5.1×10^9 M^{-1} s^{-1} and 4.5×10^9 M^{-1} s^{-1}, respectively). The other few studies (Antoniou *et al.* 2010a, 2010b) have shown that sulfate radical-based AOPs are capable at degrading the cyanotoxin microcystin-LR (1 μM) at comparable and/or higher rates than selected hydroxyl radical-based AOPs, and that a complex mixture of intermediate products are formed from sulfate radical attack on different sites of the MC-LR structure (benzene ring, diene bonds, unsaturated C-bond, oxidative bond cleavage).

2-Methylisoborneol (2-MIB) and geosmin are also produced from *Cyanobacteria* during the algae bloom seasons, and, although non-toxic, they affect the water aesthetics (odor). The degradation of 2-MIB and geosmin using the UV/persulfate process has been satisfactorily modeled and accounted for the $SO_4^{\bullet-}$ reactions with carbonate species and the organic matter present in the solution (Xie *et al.* 2015).

10.5.4 Volatile organic compounds (VOCs)

Many studies concerned with the role of various factors such as oxidant/compound molar ratio and water matrix characteristics (e.g., pH, Cl^- and HCO_3^- concentrations, presence of humic acid) on the removal of VOCs, among which methyl *tert*-butyl ether (MTBE), 1,1,1-trichloroethane (TCA), 1,4-dioxane, trichloroethylene, BTEX, whereas other studies focused on degradation intermediates and possible oxidation pathways. One of the earliest studies investigated the UV-light assisted degradation of the industrial solvent 1,4-dioxane (400 μM) in the presence of peroxydisulfate, and showed the formation of ethylene glycol diformate, formic acid, and formaldehyde as intermediates indicating an oxidative ring opening mechanism (Maurino *et al.* 1997). These compounds were also postulated mechanistically and observed experimentally in the 1,4-dioxane degradation *via* OH radical oxidation during the UV/H_2O_2 AOP (Stefan & Bolton, 1998).

In a study comparing H_2O_2/UV and $S_2O_8^{2-}$/UV performance for the degradation of 1,1,1-trichloroethane (TCA; 0.15–0.75 mM), Gu *et al.* (2012) identified 1,1,1,2-tetrachloroethane, carbon tetrachloride, chloroform, tetrachloroethylene, 1,1-dichloroethylene, and tri- and dichloroacetic acids during TCA oxidation in the $S_2O_8^{2-}$/UV process while only monochloroacetic acid and no volatile intermediates were detected in the H_2O_2/UV process. The numerous toxic intermediate produced in the $S_2O_8^{2-}$/UV process determined the authors to conclude that despite the higher efficiency of the $S_2O_8^{2-}$/UV process, the H_2O_2/UV process was more environmentally friendly. However, in the course of TCA removal by the sonolysis-activated persulfate process, Li *et al.* (2013) observed that the concentrations of most intermediates reached a maximum and then gradually decreased to near zero with the released chloride ion accounting for 91% of the total chlorine initially present in the TCA ($(TCA)_0 = 85$ mg/L). Almost all initial TCA-organic chlorine was mineralized as chloride ion except for that bound in carbon tetrachloride and 1,1,1,2-tetrachloroethane indicating that sufficient oxidation time (energy) can overcome the release of toxic intermediates from the process. Moreover, the chloride ions can be oxidized by sulfate radicals to chlorine radicals such that chlorine radical reactions would play an important role in the mechanism of TCA degradation (Figure 10.6).

The ability of thermally activated persulfate oxidation to degrade 59 VOCs in their mixture (0.6–2 μM for each VOC) including chlorinated ethenes, BTEX and trichloroethanes, was investigated by Huang *et al.* (2005). The authors found that compounds with "C=C" bonds or with aromatic rings substituted with reactive functional groups were readily degraded, whereas the saturated hydrocarbons and halogenated alkanes were much more resistant to oxidation.

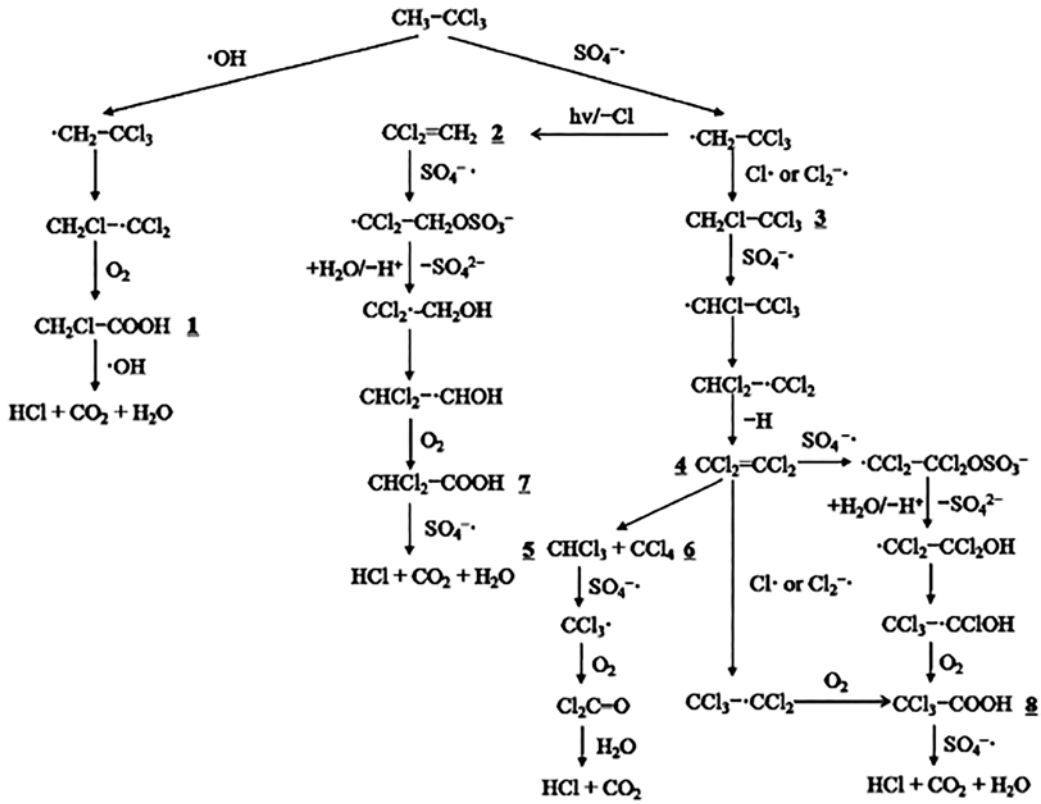

Figure 10.6 Proposed TCA oxidation pathway in UV/H_2O_2 and UV/$S_2O_8^{2-}$ processes. Reprinted with permission from Gu *et al.* (2012). Copyright 2016 American Chemical Society.

10.5.5 Perfluorinated compounds

Perfluorinated acids, especially perfluorocarboxylic acids (PFCAs), hydroperfluorocarboxylic acids (H-PFCAs), perfluoroether carboxylic acids and perfluorooctane sulfonate (PFOS) raised a particular interest, given the widespread contamination of water and soil with these toxic pollutants as well as their resistance to treatment *via* $OH^{\bullet}$-based AOPs. On May 19, 2016, the US EPA has issued the health advisory levels of 70 ng/L (ppt) for PFOS and perfluorooctanoic acid (PFOA) in order to provide Americans, including the most sensitive populations, with a margin of protection from a lifetime exposure to these contaminants from drinking water (https://www.epa.gov/ground-water-and-drinking-water/drinking-water-health-advisories-pfoa-and-pfos). These advisory levels were determined based on the agency's assessment of the latest peer-reviewed science on the health risks from exposure to these chemicals.

The effective decomposition of perfluorocarboxylic acids (PFCAs, $C_nF_{2n+1}COOH$; 0.5 μM-1.35 mM) bearing C_4-C_8 perfluoroalkyl groups with $SO_4^{\bullet-}$ radical anions formed from activated persulfate processes was demonstrated (Hori *et al.* 2005, 2010; Lee *et al.* 2009; Liu *et al.* 2012). Fluoride and CO_2 were reported as the major products during the breakdown of fluorinated chains, along with shorter-chain PFCAs through the loss of CF_2 units, with no formation of CF_4 and CF_3H fluorocarbons responsible for ozone layer depletion.

The mechanism of PFCA decomposition induced by $SO_4^{\bullet-}$ was studied and reported in the literature. Reactions 10.55–10.61 exemplify succinctly the degradation of PFOA (Lee *et al.* 2009; Hori *et al.* 2010). Decarboxylation with formation of unstable perfluoroalkyl radicals ($C_nF_{2n+1}^{\bullet}$; reactions 10.55, 10.56) which hydrolyze to perfluorinated alcohols ($C_nF_{2n+1}OH$; reaction 10.57) are the first steps of $SO_4^{\bullet-}$-induced degradation of PFCAs. The perfluorinated alcohol eliminates HF to form $C_{n-1}F_{2n-1}COF$ (reaction 10.60). Liu *et al.* (2012) suggested that the perfluoroalkyl radical could react with $SO_4^{\bullet-}$ to form the unstable intermediate adduct ($C_nF_{2n+1}OSO_3^-$), which hydrolyzes to the corresponding alcohol ($C_nF_{2n+1}OH$; reactions 10.58, 10.59). Hydrolysis of the acid fluoride ($C_{n-1}F_{2n-1}COF$) would generate a PFCA shortened by one CF_2 unit (i.e. $C_{n-1}F_{2n-1}COOH$; reaction 10.61). The shortened PFCAs would undergo a similar mechanism, essentially leading to shorter and shorter PFCAs through the loss of CF_2 units and mineralization to CO_2 and F^-. Short-chain PFCA species were found to degrade and mineralize more easily than long chains (Lee *et al.* 2009). The $SO_4^{\bullet-}$ generated from persulfate ($S_2O_8^{2-}$) was quantitatively converted into sulfate ion (SO_4^{2-}).

$$SO_4^{\bullet-} + C_7F_{15}COOH \rightarrow SO_4^{2-} + C_7F_{15}COOH^{\bullet+} \quad (10.55)$$

$$C_7F_{15}COOH^{\bullet+} \rightarrow C_7F_{15}^{\bullet} + CO_2 + H^+ \quad (10.56)$$

$$C_7F_{15}^{\bullet} + H_2O \rightarrow C_7F_{15}OH + H^{\bullet} \quad (10.57)$$

$$C_7F_{15}^{\bullet} + SO_4^{\bullet-} \rightarrow C_7F_{15}OSO_3^- \quad (10.58)$$

$$C_7F_{15}OSO_3^- + H_2O \rightarrow C_7F_{15}OH + HSO_4^- \quad (10.59)$$

$$C_7F_{15}OH \rightarrow C_6F_{13}COF + F^- + H^+ \quad (10.60)$$

$$C_6F_{13}COF + H_2O \rightarrow C_6F_{13}COOH + F^- + H^+ \quad (10.61)$$

The $S_2O_8^{2-}$/UV process was successfully applied to the decomposition of perfluorononanoic acid (3.25 μM) contained in a floor wax wastewater (Hori *et al.* 2005).

The decomposition mechanism of hydroperfluorocarboxylic acids (H-PFCAs; $HC_nF_{2n}COOH$) differs from that of PFCAs. H-PFCAs did not form shorter-chain H-PFCAs (Hori *et al.* 2010). Perfluorodicarboxylic acids with various chain lengths were found to be the reaction intermediates. The reaction mechanism for H-PFCAs degradation can be explained by nucleophilic substitution by $SO_4^{\bullet-}$ at the carbon atom attached to the ω-H atom of the H-PFCAs which releases F^-, followed by formation of perfluorodicarboxylic acids ($HOOCC_{n-1}F_{2n-2}COOH$) which react with $SO_4^{\bullet-}$ to give shorter-chain perfluorodicarboxylic acids (Hori *et al.* 2010). The initial decomposition rates of H-PFCAs were higher than those for the corresponding PFCAs (Hori *et al.* 2010).

The literature concludes that sulfate radical-based processes are promising options for the removal of these persistent micropollutants from wastewater effluents and drinking water sources.

10.6 REACTIONS WITH WATER MATRIX CONSTITUENTS IN SULFATE RADICAL-DRIVEN OXIDATIONS

10.6.1 Reactions with inorganic compounds

10.6.1.1 Carbonate / bicarbonate ions

Bicarbonate ion (HCO_3^-) is an important water matrix constituent over the pH range characteristic to natural waters (6.8–8.2), and is a known 'scavenger' of OH radical, thus, impacting the micropollutant

treatment performance. The rate constants for the reactions of $HO^{\bullet}$ and $SO_4^{\bullet-}$ with bicarbonate ion reported in the literature are 8.5×10^6 M^{-1} s^{-1} and 1.6×10^6 M^{-1} s^{-1}, respectively, whereas the rate constants for the reactions with carbonate ion are 3.9×10^8 M^{-1} s^{-1} and 6.1×10^6 M^{-1} s^{-1}, for $HO^{\bullet}$ and $SO_4^{\bullet-}$, respectively (Buxton *et al.* 1988; Zuo *et al.* 1999). The sulfate radical reactions with these species are electron transfer reactions.

$$HCO_3^- + SO_4^{\bullet-} \rightarrow CO_3^{\bullet-} + SO_4^{2-} + H^+ \quad (10.62)$$

$$CO_3^{2-} + SO_4^{\bullet-} \rightarrow CO_3^{\bullet-} + SO_4^{2-} \quad (10.63)$$

Yang *et al.* (2014) showed that the presence of 2.3 mM bicarbonate did not have a significant impact on the degradation kinetics of benzoic acid, 3-cyclohexene-1-carboxylic acid, and cyclohexanecarboxylic acid through the $S_2O_8^{2-}$/UV process. The three compounds were selected as model compounds for the aromatic, alkene, and alkane constituents of naphthenic acids, and were dosed at 10–100 µM. Lutze *et al.* (2015b) observed a significant decrease in the atrazine and *p*-nitrobenzoic acid removal rates with the $S_2O_8^{2-}$/UV process in the presence of HCO_3^- in river Ruhr water samples. However, the authors ascribed the main loss in oxidation capacity to the presence of chloride ions rather than to the scavenging of $SO_4^{\bullet-}$ by HCO_3^-. Moreover, Bennedsen *et al.* (2012) observed that the effectiveness of various persulfate activation processes for the dyestuff *p*-nitrosodimethylaniline removal was impacted differently by the presence of carbonate and hydrogen carbonate anions. Results showed that carbonates (10–100 mM) could enhance the bleaching rate in the alkaline persulfate activation system and should not be strictly considered as radical scavengers. Reactive carbonate radicals produced by oxidation with sulfate radicals may play an important role in the system.

10.6.1.2 Reaction with chloride ion

Sulfate radical-based AOPs are more sensitive to the presence of chloride ions in the water matrix than the $HO^{\bullet}$-based AOPs since the reaction of $SO_4^{\bullet-}$ with Cl^- is pH-independent, whereas the OH radical reaction with chloride ion is acid-catalyzed. Sulfate radicals react moderately fast with Cl^- ($k = (3.6 \pm 0.1) \times 10^8$ $M^{-1}s^{-1}$; Zuo *et al.* 1997), and the reaction kinetics depend on the ionic strength of the medium (Yu *et al.* 2004). The reaction yields chlorine atoms ($Cl^{\bullet}$), which further react with Cl^- ($k = 7.8 \pm 0.8) \times 10^9$ M^{-1} s^{-1}; Yu & Barker, 2003) to form the dichlorine radical anion ($Cl_2^{\bullet-}$), and an equilibrium is established between all species (reactions 10.64, 10.65). The equilibrium constant ($K = (1.4 \pm 0.2) \times 10^5$ M^{-1}; Yu & Barker, 2003) implies that $Cl_2^{\bullet-}$, not $Cl^{\bullet}$ will be the predominant chlorine radical species in water matrices containing chloride ions. The fast reacting species are involved in reactions with pH and chloride concentration-dependent product patterns (Yu *et al.* 2004; selected reactions 10.66–10.68; for details see also Chapter 9). The $HO^{\bullet}$ is formed at neutral pH from $Cl^{\bullet}/Cl_2^{\bullet-}$ reaction with water. Thus, at moderate to high Cl^- concentrations (mM range) the sulfate radical-based process may be converted into a conventional hydroxyl radical-based AOP (Lutze *et al.* 2015b).

$$Cl^- + SO_4^{\bullet-} \rightleftharpoons Cl^{\bullet} + SO_4^{2-} \quad (10.64)$$

$$Cl^{\bullet} + Cl^- \rightleftharpoons Cl_2^{\bullet-} \quad (10.65)$$

$$Cl^{\bullet}/Cl_2^{\bullet-} + H_2O \rightarrow ClOH^{\bullet-} + H^+ / + Cl^- \quad (10.66)$$

$$ClOH^{\bullet-} \rightleftharpoons OH^{\bullet} + Cl^{-} \quad (10.67)$$

$$Cl_2^{\bullet-} + Cl_2^{\bullet-} \rightarrow Cl_2 + 2\,Cl^{-} \quad (10.68)$$

At pH 3 a significant formation of chlorate was also observed in $S_2O_8^{2-}$/UV experiments on chloride oxidation in pure water (Lutze *et al.* 2015b).

In natural waters, considering the rate constants for the reactions of chloride and bicarbonate ions with sulfate radical, the scavenging of $SO_4^{\bullet-}$ by chloride will predominate.

Following a complex reaction system, bicarbonate ion scavenges $Cl^{\bullet}$ and $Cl_2^{\bullet-}$ (reactions 10.69 and 10.70; $k = 2.2 \times 10^8$ M^{-1} s^{-1} and $k = 8.0 \times 10^7$ M^{-1} s^{-1} respectively; Mertens & von Sonntag, 1995; Matthew & Anastasio, 2006) which are the key radical intermediates in the formation of OH radicals, thus impacting the conversion of $SO_4^{\bullet-}$ into $HO^{\bullet}$. The resulting carbonate radical anion is much less reactive toward organic compounds than the OH radical.

$$Cl^{\bullet} + HCO_3^{-} \rightarrow CO_3^{\bullet-} + Cl^{-} + H^{+} \quad (10.69)$$

$$Cl_2^{\bullet-} + HCO_3^{-} \rightarrow CO_3^{\bullet-} + 2\,Cl^{-} + H^{+} \quad (10.70)$$

The overall oxidation efficiency and reaction pathways are affected differently by Cl^- and HCO_3^- depending on the $SO_4^{\bullet-}$-based AOP, the target compounds and the experimental conditions (Bennedsen *et al.* 2012).

10.6.1.3 Reaction with bromide ion

The reaction between Br^- and $SO_4^{\bullet-}$ ($k_{Br^-,SO_4^{\bullet-}} = 3.5 \times 10^9$ M^{-1} s^{-1}, Neta *et al.* 1988) forms bromine atoms ($Br^{\bullet}$) (reaction 10.71). The rate constant $k_{Br^-,SO_4^{\bullet-}}$ is one order of magnitude larger than $k_{Cl^-,SO_4^{\bullet-}}$ ($(3.6 \pm 0.1) \times 10^8$ $M^{-1}s^{-1}$; Zuo *et al.* 1997).

$$Br^{-} + SO_4^{\bullet-} \rightarrow Br^{\bullet} + SO_4^{2-} \quad (10.71)$$

Once $Br^{\bullet}$ is formed, it quickly reacts with bromide ion to produce dibromine anion radical ($Br_2^{\bullet-}$). $Br^{\bullet}$ and $Br_2^{\bullet-}$ can go through a series of reactions with Br^- and H_2O to form $BrOH^{\bullet-}$ and HOBr/BrO^- (Wang *et al.* 2014; Lutze *et al.* 2014). In ultrapure water at pH 7, 5.8 to 100% conversion of an initial concentration of 20 μM bromide into bromate by UV/persulfate was observed for persulfate dosages of 20 to >300 μM (Fang & Shang, 2012). The formation of bromate via sulfate radical-initiated reactions resembles the well described mechanism of the hydroxyl radical-based bromate formation. Hypobromous acid is a requisite intermediate in the formation of bromate (Figure 10.7; Fang & Shang, 2012).

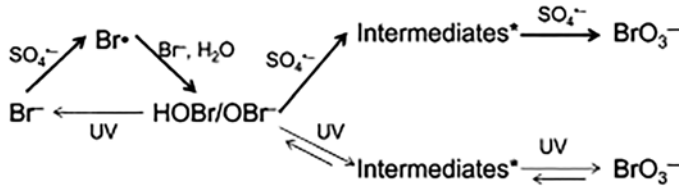

Figure 10.7 Proposed pathways of bromate formation from bromide oxidation by UV/Persulfate. Reprinted with permission from Fang and Shang (2012). Copyright 2016 American Chemical Society.

Bromide is present in water sources worldwide at concentrations in the 0–2.3 mg L^{-1} range, such that the conversion to bromate could constitute a disadvantage of sulfate radical-based AOPs if considered to treat bromide-containing drinking waters. It has been shown (Fang & Shang, 2012) that for controlling the bromate formation, elevated pH (>8) may be an option for degradation of micropollutants *via* AOPs which are not negatively impacted by alkaline conditions.

10.6.2 Reactions in natural waters

The $SO_4^{\bullet-}$-based treatment efficiency depends upon the competing reactions that scavenge the free radicals. In natural waters, the reactions of sulfate radical with bicarbonate and chloride ions compete with those of target micropollutants, and could limit the sulfate radical process efficiency. The dissolved organic matter present in all natural waters will also have a significant impact on the performance of sulfate radical-based AOPs.

10.6.2.1 Reactions with dissolved organic matter

The rate constants for the reactions of sulfate and hydroxyl radicals with humic acids differ significantly. A value of 6.8×10^3 L mg-C^{-1} s^{-1} for the rate constant of humic acids with sulfate radicals was reported recently by Lutze *et al.* (2015a). The rate constants cited in the literature for the reaction of $HO^{\bullet}$ with NOM are in the range $(2.2–6.7) \times 10^4$ L mg-C^{-1} s^{-1} (Westerhoff *et al.* 1999) thus, higher than that for $SO_4^{\bullet-}$. The lower reactivity of $SO_4^{\bullet-}$ toward organic matter compared with $HO^{\bullet}$ was explained by the fact that H-abstraction reactions involving $SO_4^{\bullet-}$ are slower than those exerted by $^{\bullet}OH$ (Lutze *et al.* 2015a). Thus, saturated moieties of the organic matter react faster with $HO^{\bullet}$. For water treatment purposes, this will lead to a weaker $SO_4^{\bullet-}$ scavenging capacity of the dissolved organic matter, which would contribute to an increased degradation efficiency of pollutants by the sulfate radical-based processes compared to $^{\bullet}OH$–based AOPs, and could counterbalance the lower reactivity of some compounds toward sulfate radical anion. Moreover, since the dissociated forms of acids usually react faster than their protonated forms, the scavenging of sulfate radicals is expected to decrease with decreasing pH. Thus, in the presence of humic acids, many compounds are degraded more efficiently by sulfate radicals than by hydroxyl radicals. As a consequence, sulfate radical based technologies would be promising for the removal of contaminants from wastewater treatment plant effluents because of the higher selectivity of sulfate radical anion over hydroxyl radical, limiting radical scavenging by natural organic matter and allowing for higher abatement rates.

10.6.2.2 Chlorinated transformation byproducts

Both enhancing and inhibitory effects of chloride ion on the degradation of pollutants in sulfate radical-driven processes are reported in the published literature. Figure 10.8 summarizes the key reactions in the UV/persulfate process in the presence of chloride ion and the pH-dependent species involved in those reactions. The distribution of radicals in the system depicted in Figure 10.8 depends on:

(i) scavenging of the reactive sulfate radicals;
(ii) formation of reactive halogen radicals;
(iii) sulfate radical reactions leading to the less selective HO radicals.

Using a model freshwater matrix with added salts, Yang *et al.* (2014) reported that the degradation yields of benzoic acid and cyclohexanecarboxylic acid (10–100 μM) were higher with the UV/$S_2O_8^{2-}$ AOP

than with the UV/H_2O_2 process because of the higher quantum efficiency of $S_2O_8^{2-}$ than H_2O_2 photolysis at 253.7 nm, i.e. 0.7 and 0.5, respectively. However in simulated saline water, the authors observed that the UV/$S_2O_8^{2-}$ AOP was more inhibited by high concentrations of Cl^- (540 mM) than the UV/H_2O_2 AOP because of the more favorable oxidation of Cl^- by $SO_4^{\bullet-}$ than $HO^\bullet$ at pH 7. However, the reactive halogen species formed in the UV/$S_2O_8^{2-}$/Cl^- system are also capable of oxidizing organics. The contribution of chlorine reactive species to the contaminant degradation will depend on the structural characteristics of those compounds, as Cl species are more selective in their reactions than the sulfate and hydroxyl radicals (Yang *et al.* 2014), on the chloride concentration, and on the sulfate radical generation system (Yuan *et al.* 2011; Wang *et al.* 2011). Reactive halogen species would react efficiently with the electron-rich moieties of the organic compounds (Yang *et al.* 2014).

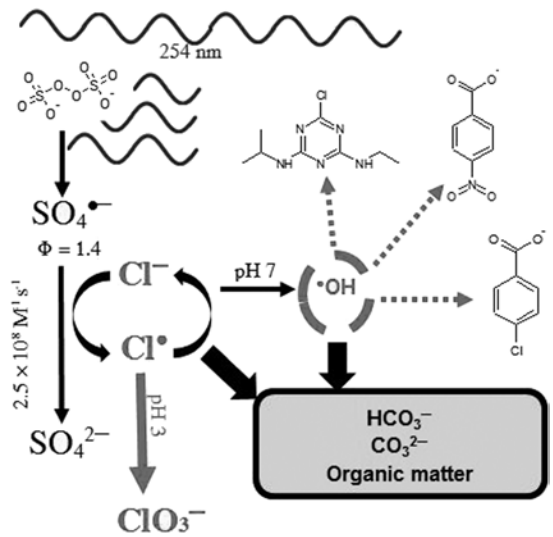

Figure 10.8 Simplified reaction scheme of sulfate radical interactions with chloride ion in the UV/persulfate process. Reprinted from Lutze *et al.* (2015b). Copyright 2016 with permission from Elsevier.

In the presence of high concentrations of chloride, some undesirable chlorinated compounds can be formed. Anipsitakis *et al.* (2006) reported the formation of chlorinated intermediates (maximum concentration 46 μM) in cobalt-activated peroxomonosulfate oxidation of phenol and 2,4-dichlorophenol (3–30 mM). The authors observed that chloride from either the cobalt counterion (2–15 mM) or the substrate oxidation itself is involved in the production of chlorine radicals and free chlorine species from reaction with sulfate radicals, which are responsible for the formation of the detected chlorinated intermediates. In a study on the degradation of an azo dye (0.1–0.2 mM) by the sulfate radical-based cobalt/peroxymonosulfate process, Yuan *et al.* (2011) also identified some chlorinated aromatic compounds (Figure 10.9). The authors reported a dual effect of chloride (0.2–200 mM) (i) inhibition of sulfate radical-induced oxidation due to scavenging by chloride, and (ii) accelerated degradation of the azo dye *via* chlorine radical/active chlorine species (HOCl) formed in reaction of Cl^- with sulfate radical and peroxomonosulfate, respectively. From a kinetic model of the sulfate radical generation system based on persulfate decomposition, Fang *et al.* (2012) calculated that the total radical concentration was significantly higher (fifty times) in the presence

of 100 mM Cl^- (pH < 6) than that without Cl^-. These aspects could have significant impact on the selection of sulfate radical-based advanced oxidation process for detoxification of chloride-rich wastewaters (like in the textile industry).

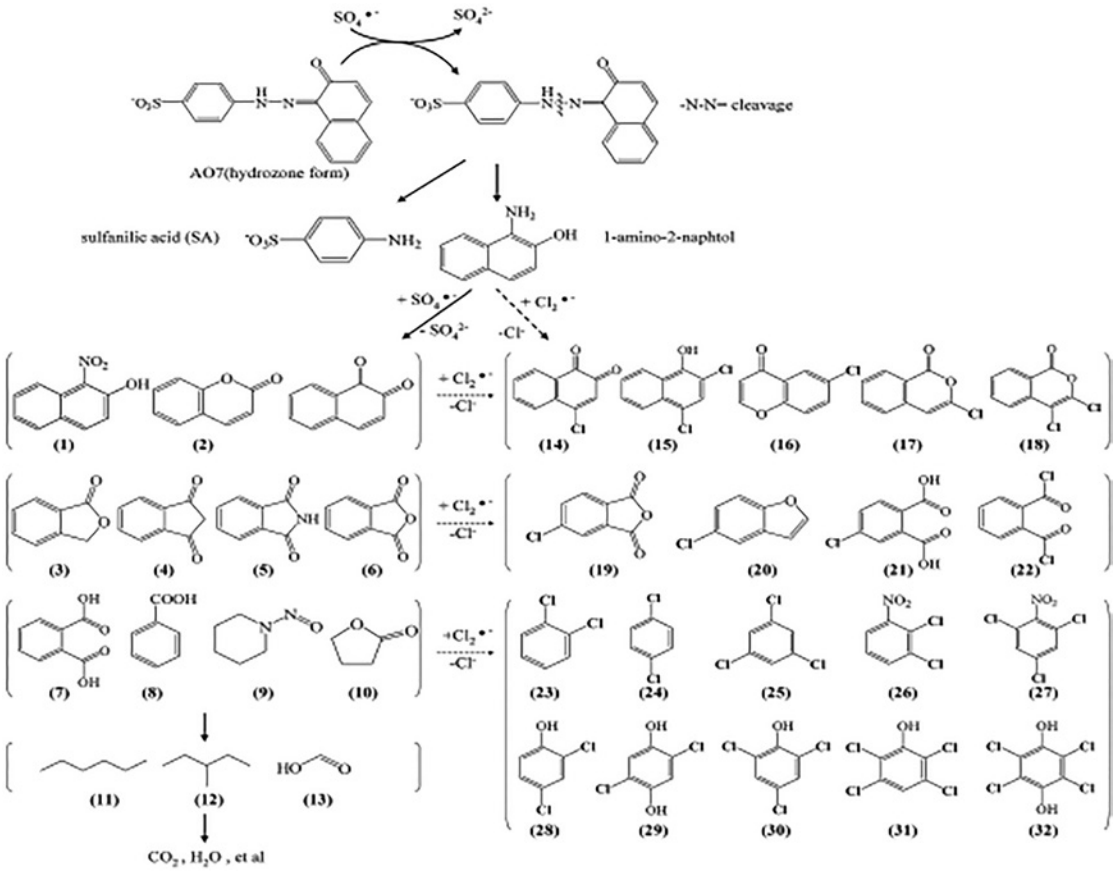

Figure 10.9 Byproducts identified (numbered in parentheses) and proposed reaction pathways for $SO_4^{\bullet-}$ radical-based oxidation of Acid Orange 7 in the presence of chloride ions. Reprinted with permission from Yuan *et al.* (2011). Copyright Elsevier 2016.

10.6.2.3 Brominated by-products

Water matrix constituents such as natural organic matter (NOM) are not only diminishing the oxidation efficiency by consumption of oxidants but can also affect the reaction mechanisms. Significantly reduced bromate formation was observed in real waters as compared to laboratory water. This inhibition was attributed to the role of NOM and inorganic compounds as competitors by reacting with the key intermediates in bromate formation (i.e., HOBr/BrO^- and $Br^{\bullet}$; Fang & Shang, 2012). The effect of NOM in the control of bromate formation was also explained by formation of superoxide in the reaction of sulfate radicals with aromatic moieties of organic matter (Lutze *et al.* 2014). In general, the superoxide radical anion is a mild reducing agent, but it reduces hypobromous acid/hypobromite efficiently (reactions

10.72 and 10.73; $k_{O_2^{\bullet-},\,HOBr} = 3.5 \times 10^9\ M^{-1}\,s^{-1}$ and $k_{O_2^{\bullet-},\,BrO^-} < 2 \times 10^8\ M^{-1}\,s^{-1}$, Schwarz & Bielski, 1986) yielding bromine atoms and bromide ions.

$$HOBr/Br^- + O_2^{\bullet-} \rightarrow O_2 + OH^- + Br_2^{\bullet-} \quad (10.72)$$

$$BrO^-/Br^- + O_2^{\bullet-} + H_2O \rightarrow O_2 + 2\,OH^- + Br_2^{\bullet-} \quad (10.73)$$

The chain reactions involving reactive bromine species in the presence of bromide can be terminated by reactions with NOM. These reactions may lead to the formation of bromine-containing by-products of potential health risk concern (Wang *et al.* 2014). Wang *et al.* (2014) studied the formation of total organic bromine (TOBr) and brominated disinfection byproducts (Br-DBPs) from isolated natural organic matter oxidation by sulfate radicals generated from PMS activation in the presence of bromide ion (2.5–6.5 μM). Bromoform and dibromoacetic acid were identified as major Br-DBPs (3.5–6 and 2–7 μg mg^{-1} C, respectively) at pH 7.5. However, it was found that the sulfate radical AOP produced much less TOBr than the bromination process.

10.6.2.4 Sulfate ion as a byproduct

In sulfate radical-based AOPs, sulfate ions will be formed as the end-product, which leads to an increase in salt content in the media. The release of sulfate ion in waters from using oxidants such as persulfate or peroxymonosulfate might affect the quality of the water. However, the SO_4^{2-} is practically inert and is not considered to be a pollutant. The US EPA has listed sulfate ion under the National Secondary Drinking Water Standards with a maximum concentration of 250 mg/L (1.43 mM), based on aesthetic reasons. The literature studies on UV/persulfate process for contaminant treatment indicate that the concentration of the sulfate ion released from the process is very low and below the secondary drinking water standard. Furthermore, when the degradation of concentrated pollutants is pursued, the high concentration of sulfate ions from the oxidant can be reduced or eliminated by implementing technologies available for sulfate ion removal (e.g. ion exchange resins).

10.7 COMMERCIAL APPLICATIONS

The sulfate radical-based processes have received an increasing interest from the academic communities. Most of the published literature on sulfate radical-based AOPs reports laboratory studies. Optimization of process efficiency is rarely within the scope of those studies. Industrial implementations are limited.

10.7.1 Total organic carbon (TOC) analyzers

The oldest application concerns TOC analyzers, and dates back to late 1960s when Ehrhardt (1969) first described a new method combining the radiation from a mercury vapor high pressure arc lamp and persulfate solutions for measurement of dissolved organic carbon in sea water by oxidation into carbon dioxide. In that publication, PDS was only considered as an oxygen donor to enable the complete oxidation of dissolved organic carbon. TOC analyzers were developed later on the principle of persulfate activated by UV (253.7 nm) and more recently a heated-UV-persulfate TOC system was commercialized.

10.7.2 *In Situ* chemical oxidation (ISCO)

Over the past few decades, there has been an increasing interest in sodium persulfate as an oxidant for the destruction of a broad range of soil and groundwater contaminants, conceptually developed as an *In Situ*

Chemical Oxidation (ISCO) process. Persulfate is widely used in ISCO remediation of contaminated environment with organic pollutants, such as chlorinated solvents, BTEXs, PAHs (Siegrist *et al.* 2011). The remediation of groundwater contamination using ISCO involves injecting oxidants (with potentially co-amendments) directly into the contaminated source zone.

The common methods for persulfate activation into sulfate radicals in ISCO technology are highly alkaline media, heat, and the environmental friendly transition metal iron.

10.7.3 Other applications

Some recent presentations report the UV/persulfate process implementation for urea, isopropyl alcohol, acetone, atrazine, and chloroform destruction in high purity water production for microelectronics industry (Knapp, 2009; Feng, 2011; Coulter *et al.* 2014). The data emphasize the process efficiency relative to UV (and $VUV_{185\ nm}$) oxidation process commonly used in Ultrapure Water (UPW) production. In particular, the combination with persulfate (Siemens Vanox™ AOP) has been proven to be effective for urea oxidation, one of contaminants poorly treated by $HO^{\bullet}$ and not effectively removed with conventional UPW treatment processes. With such treatment options, the TOC is removed to very low levels (usually to less than 1 microgram/L) and the water can be recycled (as ultrapure water) in the microelectronics industry. The UV/persulfate process was also found superior to UV(253.7 nm)/VUV(184.9 nm) AOP for trace TOC removal in water contaminated with isopropyl alcohol (IPA) a common cleaning agent and its major degradation byproduct, acetone. The hydroxyl radicals formed through water photolysis at 184.9 nm are effective at the removal of IPA ($k_{OH,IPA} = 1.9 \times 10^9\ M^{-1}\ s^{-1}$, Buxton *et al.* 1988), but are not very reactive towards acetone ($k_{OH,acetone} = 1.1 \times 10^8\ M^{-1}\ s^{-1}$, Buxton *et al.* 1988).

10.8 FUTURE RESEARCH NEEDS

The sulfate radical-based AOPs are still at the research stage, with only a few, limited niche applications (e.g., soil decontamination), and virtually no full-scale implementation.

The following could be identified as future research needs at laboratory scale:

- In view of the complexity of the reaction systems involving sulfate radicals in natural waters and wastewaters ($SO_4^{\bullet-}$ interaction with chlorides and bicarbonates, contribution of the $^{\bullet}OH$ and $Cl_2^{\bullet-}$ in the oxidation process, impact of organic matter, etc.), the simulation of the impact of various parameters by kinetic modeling is necessary for a better understanding of the system and process optimization (pollutant removal, oxidant dosage and consumption, byproduct mitigation strategies). Depending on the application areas, this approach would help with the quantification of by-products and would allow assessments on the potential risk of formation of undesirable compounds (halogenated organics, bromate, chlorate, etc.). This would also allow a better knowledge of the classes of compounds which may be degraded by the use of the sulfate radical-based AOPs, as well as the impact of water matrix constituents on the process efficiency with respect to the reactive species (e.g., $SO_4^{\bullet-}$, $^{\bullet}OH$, $Cl^{\bullet}$, $Cl_2^{\bullet-}$) and their reactivity toward the target micropollutants.
- Systematic approach to the role of various physico-chemical characteristics of water (pH, organic and mineral composition, and UV light absorption properties) on the sulfate radical-based AOP treatment performance for various classes of micropollutants, as well as to the process optimization and comparison with the OH radical-based AOPs are needed.
- Research on oxidant dose optimization is rare and removal of oxidant residual from the treated water is not represented in the published literature.

Practical implementation of sulfate radical-based AOPs would require extensive pilot work, reactor design and scale-up kinetic and computational fluid dynamics models. Life cycle assessment and cost studies of water treatment with sulfate-based AOPs would be also required, should the sulfate radical-based AOP become a competitive process for water remediation.

10.9 CONCLUSIONS

Although the first works date back more than half a century, the sulfate radical-based processes have attracted increasing interest over the past decade as evidenced by the increasing number of publications. At laboratory scale, persulfate and peroxomonosulfate are commonly used with UV light or transition metals in order to initiate the sulfate radical oxidation mechanisms. The reactive sulfate radicals, often associated with formed hydroxyl radicals, are of interest due to their high selectivity and reactivity toward numerous micropollutants and their intermediate oxidation products. $SO_4^{\bullet-}$-based oxidation may complement more common $HO^{\bullet}$-based AOPs. However, the technology should be carefully optimized in practice considering the organic and inorganic water constituents to maximize the contaminant removal efficiency and to minimize the risk of formation of potential harmful transformation products.

10.10 ACKNOWLEDGEMENTS

Special thanks to Dr Mihaela Stefan (Trojan Technologies, London, ON, Canada) for her valuable comments on the manuscript and warm support throughout this work.

10.11 REFERENCES

Anipsitakis G. P. and Dionysiou D. D. (2004). Radical generation by the interaction of transition metals with common oxidants. *Environmental Science & Technology,* **38**, 3705–3712.

Anipsitakis G. P., Dionysiou D. D. and Gonzalez M. A. (2006). Cobalt-mediated activation of peroxymonosulfate and sulfate radical attack on phenolic compounds. Implications of chloride ions. *Environmental Science & Technology*, **40**, 1000–1007.

Antoniou M. G., de la Cruz A. A. and Dionysiou D. D. (2010a). Degradation of microcystin-LR using sulfate radicals generated through photolysis, thermolysis and e- transfer mechanisms. *Applied Catalysis B: Environmental*, **96**, 290–298.

Antoniou M. G., de la Cruz A. A. and Dionysiou D. D. (2010b). Intermediates and reaction pathways from the degradation of Microcystin-LR with sulfate radicals. *Environmental Science & Technology*, **44**, 7238–7244.

Aravindakumar, C. T., Schuchmann, M. N., Rao, B. S. M., von Sonntag, J. and von Sonntag, C. (2003). The reactions of cytidine and 2′-deoxycytidine with $SO_4^{\bullet-}$ revisited. Pulse radiolysis and product studies. *Organic & Biomolecular Chemistry*, **1**, 401–408.

Bennedsen L. R., Muff J. and Sogaard E. G. (2012). Influence of chloride and carbonates on the reactivity of activated persulfate. *Chemosphere*, **86**, 1092–1097.

Bosio G. Criado S., Massad W., Nieto F. J. R., Gonzalez M. C., Garcia N. A. and Martire D. O. (2005). Kinetics of the interaction of sulfate and hydrogen phosphate radicals with small peptides of glycine, alanine, tyrosine and tryptophan, *Photochem. Photobiol. Sci.*, **4**, 840–846.

Buxton G. V., Greenstock C. L., Helman W. P. and Ross A. B. (1988). Critical review of rate constants for reactions of hydrated electrons, hydrogen atoms and hydroxyl radicals ($^{\bullet}OH/^{\bullet}O^{-}$) in aqueous solution. *Journal of Physical and Chemical Reference Data*, **17**, 513–886.

Buxton G. V., Wang J. and Salmon G. A. (2001). Rate constants for the reactions of $NO_3^{\bullet}$, $SO_4^{\bullet-}$ and $Cl^{\bullet}$ radicals with formate and acetate esters in aqueous solution. *Physical Chemistry Chemical Physics*, **3**, 2618–2621.

Chan T. W., Graham N. J. D. and Chu W. (2010). Degradation of iopromide by combined UV irradiation and peroxydisulfate. *Journal of Hazardous Materials*, **181**, 508–513.

Chawla O. P. and Fessenden R. W. (1975). Electron Spin resonance and pulse radiolysis studies of some reactions of $SO_4^{\bullet-}$. *Journal of Physical Chemistry*, **79**, 2693–2700.

Chitose N., Katsumura Y., Domae M., Zuo Z. and Murakami T. (1999). Radiolysis of aqueous solutions with pulsed helium ion beams – 2. Yield of $SO_4^{\bullet-}$ formed by scavenging hydrated electron as a function of $S_2O_8^{2-}$ concentration. *Radiation Physics and Chemistry*, **54**, 385–391.

Choure S. C., Bamatraf M. M. M., Rao B. S. M., Das R., Mohan H. and Mittal J. P. (1997). Hydroxylation of chlorotoluenes and cresols: a pulse radiolysis, laser flash photolysis, and product analysis study. *Journal of Physical Chemistry*, **101**, 9837–9845.

Coulter B., Sundstrom G., Hall C. and Doung S. (2014). An advanced oxidation process update for removal of low organic levels. http://www.evoqua.com/en/brands/IPS/productinformationlibrary/aop-removal-low-organics-presentation.pdf

Criquet J. and Leitner N. K. V. (2009). Degradation of acetic acid with sulfate radical generated by persulfate ion photolysis. *Chemosphere*, **77**, 194–200.

Criquet J. and Leitner N. K. V. (2011). Radiolysis of acetic acid aqueous solutions-Effect of pH and persulfate addition. *Chemical Engineering Journal*, **174**, 504–509.

Criquet J. and Leitner N. K. V. (2012). Electron beam irradiation of citric acid aqueous solutions containing persulfate. *Separation and Purification Technology*, **88**, 168–173.

Criquet J. and Leitner N. K. V. (2015). Reaction pathway of the degradation of the p-hydroxybenzoic acid by sulfate radical generated by ionizing radiations. *Radiation Physics and Chemistry*, **106**, 307–314.

Deng J., Shao Y., Gao N., Xia S., Tan C., Zhou S. and Hu X. (2013). Degradation of the antiepileptic drug carbamazepine upon different UV-based advanced oxidation processes in water. *Chemical Engineering Journal*, **222**, 150–158.

Diaz Kirmser E. M., Martire D. O., Gonzalez M. C. and Rosso J. A. (2010). Degradation of the herbicides Clomazone, Paraquat, and Glyphosate by thermally activated peroxydisulfate. *Journal of Agricultural and Food Chemistry*, **58**, 12858–12862.

Dogliotti L. and Hayon E. (1967). Flash photolysis of persulfate in aqueous solutions. Study of the sulfate and ozonide radical anions. *Journal of Physical Chemistry*, **71**, 2511–2516.

Ehrhardt M. (1969). A new method for the automatic measurement of dissolved organic carbon in sea water. *Deep-Sea Research*, **16**, 393–397.

Fang G.-D., Dionysiou D. D., Wang Y., Al-Abed S. R. and Zhou D.-M. (2012). Sulfate radical-based degradation of polychlorinated biphenyls: effects of chloride ion and reaction kinetics. *Journal of Hazardous Materials*, **227–228**, 394–401.

Fang J. Y. and Shang C. (2012). Bromate formation from bromide oxidation by the UV/persulfate process. *Environmental Science & Technology*, **46**, 8976–8983.

Feng J. (2011). UV oxidation with persulfate for High-Purity Water in microelectronics and pharmaceutical applications. CD Conference Proceedings: Ultrapure Water Asia Conference. Singapore Water Week, Singapore, July 6–7, 2011.

Furman O. S., Teel A. L. and Watts R. J. (2010). Mechanism of base activation of persulfate. *Environmental Science & Technology*, **44**, 6423–6428.

Gao Y.-Q., Gao N.-Y., Deng Y., Yang Y.-Q. and Ma Y. (2012). Ultraviolet (UV) light-activated persulfate oxidation of sulfamethazine in water. *Chemical Engineering Journal*, **195–196**, 248–253.

Gara P. M. D., Bosio G. N., Arce V. B., Poulsen L., Ogilby P. R., Giudici R., Gonzalez M. C. and Martire D. O. (2009). Photoinduced degradation of the herbicide Clomazone model reactions for natural and technical systems. *Photochemistry and Photobiology*, **85**, 686–692.

Ghauch A., Ayoub G. and Naim S. (2013). Degradation of sulfamethoxazole by persulfate assisted micrometric Fe^0 in aqueous solution. *Chemical Engineering Journal*, **228**, 1168–1181.

Gu X., Lu S., Qiu Z., Sui Q., Miao Z., Lin K., Liu Y. and Luo Q. (2012). Comparison of photodegradation performance of 1,1,1-Trichloroethane in aqueous solution with the addition of H_2O_2 or $S_2O_8^{2-}$ oxidants. *Industrial & Engineering Chemistry Research*, **51**, 7196–7204.

Guan Y.-H., Ma J., Li X.-C., Fang J.-Y. and Chen L.-W. (2011). Influence of pH on the formation of sulfate and hydroxyl radicals in the UV/peroxymonosulfate system. *Environmental Science & Technology*, **45**, 9308–9314.

He X., de la Cruz A. A. and Dionysiou D. D. (2013). Destruction of cyanobacterial toxin cylindrospermopsin by hydroxyl radicals and sulfate radicals using UV-254 nm activation of hydrogen peroxide, persulfate and peroxymonosulfate. *Journal of Photochemistry and Photobiology A-Chemistry*, **251**, 160–166.

Heidt L. J. (1942). The photolysis of persulfate. *Journal of Chemical Physics*, **10**(5), 297–302.

Herrmann H. (2007). On the photolysis of simple anions and neutral molecules as sources of O^-/OH, SO_x^- and Cl in aqueous solution. *Physical Chemistry Chemical Physics.*, **9**, 3935–3964.

Hochanadel C. J. (1962). Photolysis of dilute hydrogen peroxide solution in the presence of dissolved hydrogen and oxygen. Evidence relating to the nature of the hydroxyl radical and the hydrogen atom produced in the radiolysis of water. *Radiation Research*, **17**, 286–301.

Hori H., Yamamoto A., Hayakawa E., Taniyasu S., Yamashita N. and Kutsuna S. (2005). Efficient decomposition of environmentally persistent perfluorocarboxylic acids by use of persulfate as a photochemical oxidant. *Environmental Science & Technology*, **39**, 2383–2388.

Hori H., Murayama M., Inoue N., Ishida K. and Kutsuna S. (2010). Efficient mineralization of hydroperfluorocarboxylic acids with persulfate in hot water. *Catalysis Today*, **151**, 131–136.

Huang K. C., Zhao Z., Hoag G. E., Dahmani A. and Block P. A. (2005). Degradation of volatile organic compounds with thermally activated persulfate oxidation. *Chemosphere*, **61**, 551–560.

Khan J. A., He X., Shah N. S., Khan H. M., Hapeshi E., Fatta-Kassinos D. and Dionysiou D. D. (2014). Kinetic and mechanism investigation on the photochemical degradation of atrazine with activated H_2O_2, $S_2O_8^{2-}$ and HSO_5^-. *Chemical Engineering Journal*, **252**, 393–403.

Killian P. F., Bruell C. J., Liang C. and Marley M. C. (2007). Iron(II) activated persulfate oxidation of MGP contaminated soil. *Soil & Sediment Contamination*, **16**, 523–537.

Knapp A. G. (2009). Advanced oxidation for the removal of organic contaminants in industrial waters. CD Conference Proceedings: Ultrapure Water Conference. Portland, OR, November 4–5, 2009.

Kolthoff I. M. and Miller I. K. (1951). The chemistry of persulfate. I. The kinetics and mechanism of the decomposition of the persulfate ion in aqueous medium. *Journal of the American Chemical Society*, **73**, 3055–3059.

Konstantinou I. K. and Albanis T. A. (2004). TiO_2-assisted photocatalytic degradation of azo dyes in aqueous solution: kinetic and mechanistic investigations A review. *Applied Catalysis B.*, **49**, 1–14.

Lee Y. C., Lo S. L., Chiueh P. T. and Chang D. G. (2009). Efficient decomposition of perfluorocarboxylic acids in aqueous solution using microwave-induced persulfate. *Water Research*, **43**, 2811–2816.

Levey G. and Hart E. J. (1975). γ-Ray and electron pulse radiolysis studies of aqueous peroxodisulfate and peroxodiphosphate ions. *Journal of Physical Chemistry*, **79**, 1642–1646.

Li B., Li L., Lin K., Zhang W., Lu S. and Luo Q. (2013). Removal of 1,1,1-Trichloroethane from aqueous solution by a sono-activated persulfate process. *Ultrasonics Sonochemistry*, **20**, 855–863.

Liang C. and Su H. W. (2009). Identification of sulfate and hydroxyl radicals in thermally activated persulfate. *Industrial & Engineering Chemistry Research*, **48**, 5558–5562.

Liang C., Bruell C. J., Marley M. C. and Sperry K. L. (2004a). Persulfate oxidation for *in situ* remediation of TCE. I. Activated by ferrous ion with and without a persulfate-thiosulfate redox couple. *Chemosphere*, **55**, 1213–1223.

Liang C., Bruell C. J., Marley M. C. and Sperry K. L. (2004b). Persulfate oxidation for *in situ* remediation of TCE. II. Activated chelated by ferrous ion. *Chemosphere*, **55**, 1225–1233.

Liang C., Liang C.-P. and Chen C.-C. (2009). pH dependence of persulfate activation by EDTA/Fe(III) for degradation of trichloroethylene. *Journal of Contaminant Hydrology*, **106**, 178–182.

Liu C. S., Higgins C. P., Wang F. and Shih K. (2012). Effect of temperature on oxidative transformation of perfluorooctanoic acid (PFOA) by persulfate activation in water. *Separation and Purification Technology*, **91**, 46–51.

Liu X., Zhang T., Zhou Y., Fang L. and Shao Y. (2013a). Degradation of atenolol by UV/peroxymonosulfate: kinetics, effect of operational parameters and mechanism. *Chemosphere*, **93**, 2717–2724.

Liu X., Fang L., Zhou Y., Zhang T. and Shao Y. (2013b). Comparison of UV/PDS and UV/H_2O_2 processes for the degradation of atenolol in water. *Journal of Environmental Sciences*, **25**, 1519–1528.

Lutze H. V., Bakkour R., Kerlin N., von Sonntag C. and Schmidt T. C. (2014). Formation of bromate in sulfate radical based oxidation: mechanistic aspects and suppression by dissolved organic matter. *Water Research*, **53**, 370–377.

Lutze H. V., Bircher S., Rapp I., Kerlin N., Bakkour R., Geisler M., von Sonntag C. and Schmidt T. C. (2015a). Degradation of chlorotriazine pesticides by sulfate radicals and the influence of organic matter. *Environmental Science & Technology*, **49**, 1673–1680.

Lutze H. V., Kerlin N. and Schmidt T. C. (2015b). Sulfate radical-based water treatment in presence of chloride: formation of chlorate, inter-conversion of sulfate radicals into hydroxyl radicals and influence of bicarbonate. *Water Research*, **72**, 349–360.

Madhavan J., Muthuraaman B., Murugesan S., Anandan S. and Maruthamuthu P. (2006). Peroxomonosulphate, an efficient oxidant for the photocatalysed degradation of a textile dye, acid red 88. *Solar Energy Materials & Solar Cells*, **90**, 1875–1887.

Madhavan V., Levanon H. and Neta P. (1978). Decarboxylation by $SO_4^{\bullet-}$ radicals. *Radiation Research*, **76**, 15–22.

Mahdi-Ahmed M. and Chiron S. (2014). Ciprofloxacin oxidation by UV-C activated peroxymonosulfate in wastewater. *Journal of Hazardous Materials*, **265**, 41–46.

Mahdi-Ahmed M., Barbati S., Doumenq P. and Chiron S. (2012). Sulfate radical anion oxidation of diclofenac and sulfamethoxazole for water decontamination. *Chemical Engineering Journal*, **197**, 440–447.

Manoj P., Prasanthkumar K. P., Manoj V. M., Aravind U. K., Manojkumar T. K. and Aravindakumar C. T. (2007). Oxidation of substituted triazines by sulfate radical anion ($SO_4^{\bullet-}$) in aqueous medium: a laser flash photolysis and steady state radiolysis study. *Journal of Physical Organic Chemistry*, **20**, 122–129.

Mark G., Schuchmann M. N., Schuchmann H. P. and von Sonntag C. (1990). The photolysis of potassium peroxodisulphate in aqueous solution in the presence of *tert*-butanol: a simple actinometer for 254 nm radiation. *Journal of Photochemistry and Photobiology A-Chemistry*, **55**, 157–168.

Matta R., Tlili S., Chiron S. and Barbati S. (2011). Removal of carbamazepine from urban wastewater by sulfate radical oxidation. *Environmental Chemistry Letters*, **9**, 347–353.

Matthew B. M. and Anastasio C. (2006). A chemical probe technique for the determination of reactive halogen species in aqueous solution: Part 1- Bromide solutions. *Atmospheric Chemistry and Physics*, **6**, 2423–2437.

Matzek L. W. and Carter K. E. (2016). Activated persulfate for organic chemical degradation: a review. *Chemosphere*, **151**, 178–188.

Maurino V., Calza P., Minero C., Pelizzetti E. and Vincenti M. (1997). Light-assisted 1,4-Dioxane degradation. *Chemosphere*, **35**, 2675–2688.

McElroy W. J. and Waygood S. J. (1990). Kinetics of the reactions of the $SO_4^{\bullet-}$ radical with $SO_4^{\bullet-}$, $S_2O_8^{2-}$, H_2O and Fe^{2+}. *Journal of the Chemical Society Faraday Transactions*, **86**, 2557–2564.

Mendez-Diaz J., Sanchez-Polo M., Rivera-Utrilla J., Canonica S. and von Gunten, U. (2010). Advanced oxidation of the surfactant SDBS by means of hydroxyl and sulphate radicals. *Chemical Engineering Journal*, **163**, 300–306.

Mertens M. and von Sonntag C. (1995). Photolysis ($\lambda = 254$ nm) of tetrachloroethene in aqueous solutions. *Journal of Photochemistry and Photobiology A-Chemistry*, **85**, 1–9.

Neppolian B., Doronila A. and Ashokkumar M. (2010). Sonochemical oxidation of arsenic(III) to arsenic(V) using potassium peroxydisulfate as an oxidizing agent. *Water Research*, **44**, 3687–3695.

Neta P., Madhavan V., Zemel H. and Fessenden R. W. (1977). Rate constants and mechanism of reaction of $SO_4^{\bullet-}$ with aromatic compounds. *Journal of the American Chemical Society*, **99**, 163–164.

Neta P., Huie R. E. and Ross A. B. (1988). Rate constants for reactions of inorganic radicals in aqueous solution. *Journal of Physical and Chemical Reference Data*, **17**, 1027–1247.

Norman R. O. C., Storey P. M. and West P. R. (1970). Electron spin resonance studies. Part XXV. Reactions of the sulphate radical anion with organic compounds. *Journal of the Chemical Society (B)*, 1087–1095.

Oh S.-Y., Kang S.-G. and Chiu P. C. (2010). Degradation of 2,4-dinitrotoluene by persulfate activated with zero-valent iron. *Science of the Total Environment*, **408**, 3464–3468.

Orellana-Garcia F., Alvarez M. A., Lopez-Ramon M. V., Rivera-Utrilla J. and Sanchez-Polo M. (2015). Effect of $HO^{\bullet}$, $SO_4^{\bullet-}$ and $CO_3^{\bullet-}$ /$HCO_3^{\bullet}$ radicals on the photodegradation of the herbicide amitrole by UV radiation in aqueous solution. *Chemical Engineering Journal*, **267**, 182–190.

Rao Y. F., Chu W. and Wang Y. R. (2013). Photocatalytic oxidation of carbamazepine in triclinic-WO_3 suspension: role of alcohol and sulfate radicals in the degradation pathway. *Applied Catalysis A*, **468**, 240–249.

Rastogi A., Al-Abed S. R. and Dionysiou D. D. (2009). Effect of inorganic, synthetic and naturally occurring chelating agents on Fe(II) mediated advanced oxidation of chlorophenols. *Water Research*, **43**, 684–694.

Rickman K. A. and Mezyk S. P. (2010). Kinetics and mechanisms of sulfate radical oxidation of β-lactam antibiotics in water. *Chemosphere*, **81**, 359–365.

Roshani B. and Leitner N. K. V. (2011). The influence of persulfate addition for the degradation of micropollutants by ionizing radiation. *Chemical Engineering Journal*, **168**, 784–789.

Schug T. T., Janesick A., Blumberg B. and Heindel J. J. (2011). Endocrine disrupting chemicals and disease susceptibility. *Journal of Steroid Biochemistry and Molecular Biology*, **127**(3–5), 204–215.

Schwarz H. A. and Bielski B. H. J. (1986). Reactions of hydroperoxo and superoxide with iodine and bromine and the iodide (I_2^-) and iodine atom reduction potentials. *Journal of Physical Chemistry*, **90**, 1445–1448.

Shah N. S., He X., Khan H. M., Khan J. A., O'Shea K. E., Boccelli D. L. and Dionysiou D. D. (2013). Efficient removal of endosulfan from aqueous solution by UV-C/peroxides: a comparative study. *Journal of Hazardous Materials*, **263**, 584–592.

Siegrist R. L., Crimi M. and Simpkin T. J. (2011). *In Situ* Chemical Oxidation for Groundwater Remediation. Springer, New York.

Stefan M. I. and Bolton J. R. (1998). Mechanism of the degradation of 1,4-Dioxane in dilute aqueous solution using the UV/Hydrogen peroxide process. *Environmental Science & Technology*, **32**(11), 1588–1595.

Syoufian A. and Nakashima K. (2007). Degradation of methylene blue in aqueous dispersion of hollow titania photocatalyst: optimization of reaction by peroxydisulfate electron scavenger. *Journal of Colloid and Interface Science*, **313**, 213–218.

Tan C., Gao N., Deng Y., An N. and Deng J. (2012). Heat-activated persulfate oxidation of diuron in water. *Chemical Engineering Journal*, **203**, 294–300.

Wang P., Yang S., Shan L., Niu R. and Shao X. (2011). Involvements of chloride ion in decolorization of Acid Orange 7 by activated peroxydisulfate or peroxymonosulfate oxidation. *Journal of Environmental Sciences*, **23**, 1799–1807.

Wang Y., Le Roux J., Zhang T. and Croue J. P. (2014). Formation of brominated disinfection byproducts from natural organic matter isolates and model compounds in a sulfate radical-based oxidation process. *Environmental Science & Technology*, **48**, 14534–14542.

Westerhoff P., Aiken G., Amy G. and Debroux J. (1999). Relationships between the structure of natural organic matter and its reactivity towards molecular ozone and hydroxyl radicals. *Water Research*, **33**, 2265–2276.

Xiao R., Ye T., Wei Z., Luo S., Yang Z. and Spinney R. (2015). Quantitative Structure-Activity Relationship (QSAR) for the oxidation of trace organic contaminants by sulfate radical. *Environmental Science & Technology*, **49**, 13394–13402.

Xie P., Ma J., Liu W., Zou J., Yue S., Li X., Wiesner M. R. and Fang J. (2015). Removal of 2-MIB and geosmin using UV/persulfate: contributions of hydroxyl and sulfate radicals. *Water Research*, **69**, 223–233.

Yang Y., Pignatello J. J., Ma J. and Mitch W. A. (2014). Comparison of halide impacts on the efficiency of contaminant degradation by sulfate and hydroxyl radical-based advanced oxidation processes (AOPs). *Environmental Science & Technology*, **48**, 2344–2351.

Yang Y., Jiang J., Lu X., Ma J. and Liu Y. (2015). Production of sulfate radical and hydroxyl radical by reaction of ozone with peroxymonosulfate: a novel Advanced Oxidation Process. *Environmental Science & Technology*, **49**, 7330–7339.

Yu X.-Y. and Barker J. R. (2003). Hydrogen peroxide photolysis in acidic aqueous solutions containing chloride ions. I. Chemical mechanism. *Journal of Physical Chemistry A*, **107**, 1313–1324.

Yu X.-Y., Bao Z.-C. and Barker J. R. (2004). Free radical reactions involving $Cl^{\bullet}$, $Cl_2^{\bullet-}$, and $SO_4^{\bullet-}$ in the 248 nm photolysis of aqueous solutions containing $S_2O_8^{2-}$ and Cl^-. *Journal of Physical Chemistry A*, **108**, 295–308.

Yuan R., Ramjaun S. N., Wang Z. and Liu J. (2011). Effects of chloride ion on degradation of Acid Orange 7 by sulfate radical-based advanced oxidation process: implications for formation of chlorinated aromatic compounds. *Journal of Hazardous Materials*, **196**, 173–179.

Zhang B.-T, Zhang Y., Teng Y. and Fan M. (2015). Sulfate radical and its application in decontamination technologies. *Critical Reviews in Environmental Science and Technology*, **45**, 1756–1800.

Zemel H. and Fessenden R. W. (1978). The mechanism of reaction of $SO_4^{\bullet-}$ with some derivatives of benzoic acid. *Journal of Physical Chemistry*, **82**, 2670–2676.

Zuo Z., Katsumura Y., Ueda K. and Ishigure K. (1997). Reactions between some inorganic radicals and oxychlorides studied by pulse radiolysis and laser photolysis. *Journal of the Chemical Society Faraday Transactions*, **93**, 1885–1891.

Zuo Z., Cai Z., Katsumura Y., Chitose N. and Muroya Y. (1999). Reinvestigation of the acid-base equilibrium of the (bi)carbonate radical and pH dependence of its reactivity with inorganic reactants. *Radiation Physics and Chemistry*, **55**, 15–23.